# Enabling Technologies for the Subsurface Exploration of the Solar System

Ryan Timoney

Submitted for the degree of
Doctor of Philosophy
From the University of Glasgow


University of Glasgow

University of Glasgow
School of Engineering
Glasgow, G12 8QQ

# Declaration

"I herewith declare that, except where explicit reference is made to the contribution of others, that this dissertation is the result of my own work and has not been submitted for any other degree at the University of Glasgow or any other institution."

Printed Name: Ryan Timoney

Date: 26.9.2019

*"Far better it is to dare mighty things, to win glorious triumphs, even though checkered by failure, than to rank with those poor spirits who neither enjoy nor suffer much, because they live in the gray twilight that knows not victory nor defeat."*

Theodore Roosevelt (1858-1919)

# Abstract

Future robotic exploration missions within the Solar System, focussing on either scientific discovery or the emerging field of In-Situ Resource Utilisation (ISRU), shall require the development of technologies which are capable of exploring to ever-greater depths beneath the planetary surface. In order to achieve these ambitious goals, advances in the existing state of the art in robotic sampling are required.

This Ph.D. presents findings on the development of novel solutions within this field. The development of the Ultrasonic Planetary Core Drill (UPCD), a system based upon the ultrasonic-percussive drill technique, was designed with a Mars Sample Return (MSR) objective at the core of the development. Breakthroughs in autonomous control and the robotic assembly of drill strings were required in order to meet the requirements set. The system was tested at Coal Nunatak, Antarctica, in December 2016.

A rotary-percussive drilling system for use in extracting subglacial bedrock samples from Earth's Polar Regions was developed. Making use of technologies devised in the UPCD project, this collaboration with the British Antarctic Survey (BAS) required a low resource approach to the problem in order to ensure compatibility with existing BAS systems and logistical constraints.

Building upon technologies developed and confidence generated in previous systems, the subglacial bedrock was industrialised into what became the Percussive Rapid Access Isotope Drill (P-RAID). This system underwent initial field trials at the Skytrain Ice Rise, Antarctica in January 2019 with the intention to further develop the system for full deployment.

# Acknowledgements

This thesis is the culmination of everything that I have worked for since I was first struck by the notion that pursuing a career in aerospace engineering could be a worthwhile and enjoyable pursuit. Moreover, it's the sum of countless hours of dedication (devotion, even) to a cause which I believe to be of enormous value: the continued exploration of our Solar System.

While at times the undertaking of a Ph.D. can feel a little like a solitary affair, the reality couldn't be further from the truth. This thesis is for my mother, Marie, who has supported me without a shadow of a doubt from the start. If ever I've questioned my ability to achieve whatever it is that I have set out to accomplish, she has been there to offer her unfaltering support. I have also been exceptionally fortunate to have the wisdom of my father, Stephen, throughout my life. He quickly identified the areas in which I have excelled and those which have brought me joy and has been there to knit those together ever since. There is no doubt in my mind that, without his guidance, this thesis would never have been a reality. To my sister, Alyssa, who does a terrible job of hiding her admiration for what I have achieved. Your joyful spirit is infectious and being around you makes all problems fade away.

I would like to thank my supervisor, Dr. Patrick Harkness for creating a stream of exciting opportunities which have taken me to the ends of the Earth and everywhere in between in pursuit of my research. Dr. Kevin Worrall is worthy of a special mention for both his technical expertise in the areas of electronics, programming and all related wizardry, and for putting up with me during the many, many weeks spent in our tent during Antarctic field trials. The memories accrued over the course of this Ph.D. will last a lifetime.

Special thanks goes to Dr. David Firstbrook for both his academic support and his excellent company during our many international conference trips, and Dr. Gilles Bailet for his personal and professional guidance, and for always keeping my best interests at heart.

Finally, I would like to thank those closest to me for putting up with my long absences abroad over the past few years and my often single-minded approach to my work. Your love, support and patience has given me the strength to achieve everything that I have.

# Contents

Chapter 1 ..... 1

Introduction ..... 1

1.1 Overview ..... 1

1.2 Aims and Objectives ..... 2

1.3 Thesis Structure ..... 3

Chapter 2 ..... 5

Drilling in Extreme Environments ..... 5

2.1 Terrestrial Drilling in Extreme Environments ..... 5

2.2 Historical Planetary Drilling Missions ..... 7

2.3 Future Drilling Missions ..... 14

2.3.1 Future Technologies ..... 17

2.4 Subglacial Bedrock Sampling Systems ..... 18

Chapter 3 ..... 23

Theory of Drilling in Extreme Environments ..... 23

3.1 Drilling Process ..... 23

3.2 Challenges of Planetary Drilling ..... 24

3.3 Drilling Techniques ..... 29

3.3.1 Rotary Drilling ..... 29

3.3.2 Rotary - Percussive Drilling ..... 32

3.3.3 Cutting Fluids ..... 35

3.4 Drilling Power ..... 36

3.5 Spoil Removal Techniques ..... 37

..... 39

Chapter 4 ..... 42

Development of the Ultrasonic Planetary Core Drill (UPCD) ..... 42

4.1 Ultrasonic-Percussive Drilling Technique Overview ..... 42

4.1.1 Ultrasonic Actuator ..... 42
4.1.2 Free Mass and Percussive Power ..... 45
4.2 UPCD Development Overview ..... 46
4.3 UPCD Mechanical Architecture ..... 47
4.4 Drill Tool Design ..... 48
4.5 Sample Caching Carousel ..... 51
4.6 Drill Bit Terrain Clamp ..... 52
4.7 Concept of Operations Overview ..... 53
4.8 Drill String Connections ..... 53
4.8.1 Making and Breaking Drill Strings ..... 53
4.8.2 Threaded Connection Operations ..... 54
4.8.3 Practical Limitations of Threaded Interfaces ..... 57
4.8.4 Bayonet Connection Interfaces ..... 58
4.8.5 Bayonet Connection Operations ..... 59
4.9 Concept of Operations Trade-off Study ..... 62
4.10 Transmission of Percussion ..... 70
4.10.1 Test Procedure ..... 71
4.10.2 Experimental Results ..... 73
4.10.3 Discussion ..... 78
4.10.4 Conclusions ..... 79
4.11 Laboratory Dry Drilling Performance ..... 81
4.11.1 Test Setup ..... 81
4.11.2 Experimental Results and Discussion ..... 82
4.12 Mission Applicability ..... 86
4.13 Antarctic Field Campaign ..... 87
4.13.1 Coal Nunatak Field Site ..... 88
4.13.2 Drilling Operations at Coal Nunatak ..... 92
4.13.3 Conclusions ..... 101
4.14 Drill Control ..... 101

4.14.1 Baseline Bang-Bang Algorithm ..... 101
4.14.2 Advanced Thermal Control ..... 104
4.14.3 Sensing Refreeze Faults ..... 107
4.14.4 Experimental Setup ..... 109
4.14.5 Experimental Results ..... 112
4.14.6 Conclusions ..... 115
4.15 Chapter Conclusions ..... 116
Chapter 5 ..... 117
Development of the Subglacial Bedrock Sampler ..... 117
5.1 Subglacial Exploration ..... 117
5.2 Challenges Facing Subglacial Bedrock Sampling ..... 118
5.2.1 Logistical Challenges ..... 118
5.3 Technical Challenges ..... 119
5.4 BAS Rapid Access Isotope Drill (RAID) Redevelopment ..... 121
5.5 Subglacial Bedrock Sampler Design Methodology ..... 124
5.5.1 Analogies to Planetary Exploration and Design Implications ..... 124
5.6 Rock Cutting Methods ..... 125
5.7 Spoil Removal Techniques ..... 128
5.8 Subglacial Bedrock Sampler Design ..... 129
5.8.1 Subglacial Bedrock Sampler Architecture ..... 129
5.9 Percussive Mechanism Design ..... 130
5.10 Multi-Motor Auger Gearbox ..... 137
5.11 Laboratory Drilling Performance ..... 139
5.11.1 Experimental Setup ..... 139
5.11.2 Experimental Results and Discussion ..... 141
5.11.3 Core Quality ..... 151
5.11.4 System Capability and Robustness Discussion ..... 154
5.11.5 Drill Performance Discussion ..... 155
5.12 TVAC Testing Campaign ..... 158

5.12.1 Mars Environmental Testing ..... 158
5.12.2 FH Aachen Test Campaign ..... 161
5.12.3 Experimental Setup ..... 162
5.12.4 Experimental Procedure ..... 166
5.12.5 Experimental Results and Discussion ..... 167
5.12.6 Discussion ..... 175
5.13 Chapter Conclusions ..... 177
Chapter 6 ..... 178
Percussive Rapid Access Isotope Drill (P-RAID) ..... 178
6.1 Modification of the Subglacial Bedrock Sampler ..... 178
6.2 Skytrain Ice Rise Campaign – January 2019 ..... 186
6.3 Chapter Conclusions ..... 189
Chapter 7 ..... 190
Conclusions and Future Work ..... 190
7.1 Summary of Drilling System Applications ..... 190
7.2 Chapter Overview ..... 191
7.3 Future Work ..... 195
7.4 Publications ..... 196
7.4.1 Book Sections ..... 196
7.4.2 Articles ..... 196
7.4.3 Conference or Workshop Proceedings ..... 197
7.4.4 Press Publications ..... 198
Appendix ..... 199
Subglacial Bedrock Sampler Test Campaign ..... 199
Portland Limestone Figures ..... 199
Locharbriggs Sandstone Figures ..... 204
Chapter 8 ..... 206
Bibliography ..... 206

# Table of Figures

Figure 1: Apollo 15 drilling operations. (NASA Image AS15-92-12407) ..... 8

Figure 2: Hole produced by the RAT tool on Opportunity. Note the pristine rock exposed by the RAT process. Image courtesy of NASA/JPL-Caltech. ..... 9

Figure 3: ISAD with sample in its scoop upon the cessation of a trenching and sampling operation. Image courtesy of Honeybee Robotics. ..... 10

Figure 4: MSL rotary-percussive drilling system layout [11] ..... 11

Figure 5: MSL first full-depth drill hole of target "John Klein". ..... 11

Figure 6: SD2 drilling system schematic [12]. ..... 13

Figure 7: Telemetry from SD2 drill position showing a complete deployment and retraction of the drill bit to 560 mm [13]. ..... 13

Figure 8: $HP^3$ mole cut-away schematic [14]. ..... 14

Figure 9: ExoMars rover deploying 2 m drillstring [15]. ..... 15

Figure 10: NASA Mars 2020 'adaptive caching' strategy. Courtesy: NASA/JPL-Caltech ..... 16

Figure 11: ProSEED drilling system sample capture mechanisms. Standard drilling configuration (L), Russian sampling mechanism (middle) and European sampling tube deployed (R) [20]. ..... 17

Figure 12: Surface-driven drilling rig [24]. ..... 19

Figure 13: U.S. IDP Winkie drill system. Courtesy: U.S. IDP. ..... 20

Figure 14: 8 m core obtained using ASIG drill system. Courtesy: U.S. IDP. ..... 21

Figure 15: IDP RAID drill schematic. Courtesy: U.S. IDP .....22

Figure 16: Full faced rotary drill bit and borehole (L) and coring bit and borehole (R) [25]. .....24

Figure 17: Example of auger choking caused by excessive input of fluffy, fine grained cuttings. .....26

Figure 18: NASA InSight solar array deployment on Mars. Courtesy: NASA/JPL-Caltech.....28

Figure 19: Schematic of the rotary drilling process whereby the application of Weight on Bit and Torque/RPM act to break the formation and remove spoil [25]. .....29

Figure 20: Mechanics of a rotary drill bit assuming a sharp cutting face. .....30

Figure 21: Mechanics of a rotary drill bit assuming partially blunted cutting face. The forward force, $F_s$, is split and consists of $F_s^c$ at the sharp edge and $F_s^f$ at the surface which has been worn flat. .....31

Figure 22: Example of the Coulomb-Mohr failure criterion used to predict brittle rock failures. .....33

Figure 23: Energy conversion of compressive wave travelling through hard materials (left) and soft material (right) [28]. .....35

Figure 24: Schematic of typical one and two scroll augers [32]. .....38

Figure 25: Plot of auger starting speeds for a range of friction coefficients. .....39

Figure 26: Augering over a range of rotational speeds. .....40

Figure 27: Evacuation of simulated borehole using a differential pressure of 3300 Pa at an ambient pressure of 670 Pa [34].....41

Figure 28: Ultrasonic-Percussive Drilling Schematic [36]. ..... 43

Figure 29: Typical ultrasonic horn geometries [37]. ..... 44

Figure 30: Full wavelength ultrasonic actuator with waveform overlaid. ..... 45

Figure 31: Damage to the anvil-bit (L) and the horn tip (R) caused by free mass. ..... 45

Figure 32: UPCD Mechanical Architecture. ..... 47

Figure 33: Full-wavelength UPCD drill tool [41]. ..... 49

Figure 34: Experimental results of the effective impulse for the full and half-wave transducers at 5, 10 and 15 N values of weight on bit. Results for forces above 250 N (a), 500 N (b), 750 N (c) and 1 kN (d) [41]. ..... 50

Figure 35: Experimental Rate of Progress for full and half -wavelength transducers for various teeth and weight on bit levels [41]. ..... 50

Figure 36: Sample Caching Carousel Architecture. Diameter of carousel is 240 mm for reference. ..... 51

Figure 37: Drill Bit Exchange Clamp Architecture ..... 52

Figure 38: ExoMars type threaded connections. [42]. ..... 56

Figure 39: Mars Exploration Rover, Spirit coated in extremely fine dust.. ..... 58

Figure 40: Drill bit disconnection procedure. Drill string in typical drilling configuration (L) and disconnection event (R) [43]. ..... 61

Figure 41: CCM drill bits. Two Extension Bits shown (top and centre) and Cutting Bit (lower). ..... 63

Figure 42: UPCD assembly colour coded to match ConOps Diagrams ..... 66

Figure 43: Continuous Core Method (CCM) ConOps .....67

Figure 44: Discrete Core Method (DCM) ConOps .....69

Figure 45: Percussion transmission test items. Control (L) and Bayonet-connected bit (R). .....71

Figure 46: UPCD Horizontal Test Rig. Bit diameter of 20 mm, for reference. .....72

Figure 47: Locharbriggs sandstone - Bayonet interface drill bit - 20 W.....74

Figure 48: Locharbriggs sandstone - Control drill bit - 20 W.....75

Figure 49: Locharbriggs sandstone - Bayonet interface drill bit - 25 W.....75

Figure 50: Locharbriggs sandstone – Control drill bit – 25 W .....76

Figure 51: Locharbriggs sandstone - Bayonet interface drill bit - 30 W.....76

Figure 52: Locharbriggs sandstone - Control drill bit - 30 W.....77

Figure 53: Comparison of drilling rates through different sandstones using a Control drill bit and a Bayonet interface drill bit at different power levels. .....77

Figure 54: Locharbriggs (top), Blaxter (middle) and Clashach (bottom) sandstone specimens post-testing. .....80

Figure 55: UPCD drill into dry Locharbriggs sandstone under laboratory conditions ...81

Figure 56: UPCD drilling run in Locharbriggs sandstone using new teeth and standard UPCD drilling bit. Ultrasonic reference power level set at 10 W.....82

Figure 57: UPCD drilling run in Locharbriggs sandstone using once-used teeth and standard UPCD drilling bit. Ultrasonic power level set at 10 W. .....83

Figure 58: UPCD drilling run in Locharbriggs sandstone using twice-used teeth and standard UPCD drilling bit. Ultrasonic power level set at 10 W. ..... 83

Figure 59: UPCD drilling run in Locharbriggs sandstone using new teeth and standard UPCD drilling bit. Ultrasonic reference power level set at 16 W. ..... 84

Figure 60: UPCD drilling run in Locharbriggs sandstone. ..... 85

Figure 61: Coal Nunatak field test site. ..... 90

Figure 62: Frost polygon features at the field site (top). Similar features have been found at both the Phoenix and Viking landing sites on Mars (bottom). ..... 91

Figure 63: Extent of the near-surface melting at the Coal Nunatak field site ..... 93

Figure 64: Aborted drill run in sticky terrain. ..... 94

Figure 65: UPCD operating in trench carved into the ice pack. ..... 95

Figure 66: Assembly and Disassembly of complete drill string in Antarctic ice pack. .. 97

Figure 67: Position of Drill Tool during drilling operations in ice pack. ..... 99

Figure 68: Total power consumption of the UPCD system during drilling operations into the ice pack. ..... 100

Figure 69: Partially melted ice core recovered from drilling operations. ..... 100

Figure 70: Measured RMS voltage, power and current of the ultrasonic transducer. . 102

Figure 71: Control algorithm used in UPCD. (a) Timer output, (b) integrator's output, (c) sample held condition, (d) motion compared with reference level. [45]. ..... 103

Figure 72: Figure detailing the relationship between the moisture content within ice-cemented terrain and the strength of the ‘composite’ mixture created (L) and a plot detailing the effect of reduced temperatures on the strength of pure ice (R).....104

Figure 73: Freeze-in event at shallow depth. .....106

Figure 74: Bit glaze and auger blocking event.....106

Figure 75: UPCD drilling run in 10% saturated regolith.. .....108

Figure 76: Drill bit instrumented with thermocouples (brown sensors) and electrodes (yellow sensors) for use in the thermal control system.....108

Figure 77: Instrumented UPCD hardware. Thermal control hardware includes the addition of downhole thermocouples and electrodes, and a slip ring assembly to transfer these signals from the rotating bit. .....110

Figure 78: Temperature – resistance plots for 10% water/weight (top) and 20% water/weight (bottom) simulated permafrost mixes. .....111

Figure 79: Frozen 10% water/weight permafrost core obtained during experimentation. .....112

Figure 80: Experimental results from test run in 10% water/weight sample (top) and fully saturated (20% water/weight) sample (bottom).....113

Figure 81: Results from an experimental test run in fully saturated simulant. .....115

Figure 82: Schematic of subglacial layering [62]. .....119

Figure 84: RAID Cutting Face. Outer diameter of 80 mm, for reference. .....122

Figure 85: The Rapid Access Isotope Drill (RAID) in service.. .....123

Figure 86: Typical motion of the spring-cam actuated mechanism. T.....127

Figure 87: Subglacial Bedrock Sampler prototype assembly CAD (L) and following a series of successful tests in the BAS Cold Chamber Facility designed to replicate Antarctic field conditions (R). ..... 130

Figure 88: Example of barrel cam wear. ..... 131

Figure 89: Cycloidal barrel cam geometries. 1-Drop, 2-Drop and 4-Drop (L-R). ..... 134

Figure 90: Hammer motor torque requirements for single, double and quad drop cycloidal barrel cams with a vertical displacement of 17 mm. ..... 136

Figure 91: Hammer motor torque requirement for 4-Drop cam compared to cam geometry. ..... 137

Figure 92: Subglacial Bedrock Sampler laboratory test rig. ..... 140

Figure 93: Portland limestone experimental run using small drill bit and rotation-only drilling. 20/10 N WoB. ..... 142

Figure 94: Portland limestone experimental run using small drill bit, 2-drop cam and 500 RPM hammer velocity. 12/8 N WoB. ..... 143

Figure 95: Portland limestone experimental run using small drill bit, 4-drop cam and 500 RPM hammer velocity. 12/8 N WoB. ..... 144

Figure 96: Portland limestone experimental run using medium drill bit, 4-drop cam and 500 RPM hammer velocity. 12/8 N WoB. ..... 145

Figure 97: Locharbriggs sandstone experimental run using small drill bit and rotation-only drilling. 40/30 N WoB. ..... 146

Figure 98: Locharbriggs sandstone experimental run using small drill bit, 2-drop cam and 500 RPM hammer velocity. 12/8 WoB. ..... 147

Figure 99: Locharbriggs sandstone experimental run using small drill bit, 4-drop cam and 500 RPM hammer velocity. 12/8 WoB. .....148

Figure 100: Locharbriggs sandstone experimental run using medium drill bit, 4-drop cam and 500 RPM hammer velocity. 12/8 WoB. .....149

Figure 101: Locharbriggs sandstone experimental run using medium drill bit, 4-drop cam and 1500 RPM hammer velocity. 12/8 WoB. .....150

Figure 102: Locharbriggs sandstone captured during a laboratory experimental campaign using the medium drill bit geometry. .....152

Figure 103: Limestone core captured during a laboratory experimental campaign using the medium drill bit geometry. .....152

Figure 104: Core samples obtained from experimental drilling campaign. .....153

Figure 105: Regolith temperatures profile over the course of one Martian day at Phoenix landing site. Results from a number of excavated trenches accessed by the Thermal and Electrical Conductivity Probe (TECP) instrument attached to the robotic arm of the lander. .....159

Figure 106: Phase diagram for $H_2O$ with Mars ambient pressure and temperature ranges noted.....160

Figure 107: Aachen TVAC Facility with subglacial bedrock sampler prototype in the foreground during preparations. .....162

Figure 108: Passive cooling system used for pre-cooling saturated regolith simulants to cryogenic temperatures. .....164

Figure 109: Test rig prior to chamber insertion. .....165

Figure 110: Drilling system fully integrated into TVAC chamber and awaiting pump down. .....167

Figure 111: Drilling run in fully saturated cryogenic BP simulant. 2-drop cam profile, 17 mm height. Small bit geometry. Percussive motor speed set to 2000 RPM. Manual control (no autonomy). ..... 168

Figure 112: Drilling run in fully saturated freezer temperature BP simulant. 4-drop cam profile, 11 mm height. Autonomous control. ..... 168

Figure 113: Spoil pattern produced due to a transition from auger-dominated spoil removal to sublimation induced gas blasting..... 170

Figure 114: Spoil ejected by gas blasting distributed at the base of the test rig - a substantial distance from the borehole. ..... 171

Figure 115: Drilling run in fully saturated cryogenic BP simulant. 2-Drop cam profile, 17 mm height. Autonomous control. Run conducted at ambient pressure outside of chamber..... 172

Figure 116: Production of muddy spoil during the drilling process at ambient pressure conditions..... 173

Figure 117: Borehole comparison following cryogenic drilling runs at ambient atmospheric pressure (top) and in-vacuum at pressures of ~1 mBar (bottom)..... 174

Figure 118: P-RAID Design Cutaway. Length of assembly detailed is 3 m, outer diameter of 80 mm..... 179

Figure 119: Ball Transfer Units (BTU) roller assembly. ..... 180

Figure 120: Sonde with drill bit shown adjacent to the outer casing assembly. ..... 180

Figure 121: P-RAID system with drill bit stowed (L) and deployed (R) from within the outer casing of the assembly. Length of assembly 4 m, outer diameter of 80 mm. ..... 181

Figure 122: Core catching device installation. Diameter of catcher 20 mm, length 25 mm. ..... 182

Figure 123: Limestone borehole following a successful drill run (top). The core generated during drilling was captured within the drill bit (bottom). .....184

Figure 124: Toothed drill crown next to the drill bit. Crown interfaces with the drill bit as a continuation of the auger scroll in order to allow a seamless transit of spoil. Bit diameter of 40 mm, length of bit 450 mm. .....185

Figure 125: P-RAID system during fit checks at Skytrain Ice Rise. Note, the drill bit is fully deployed. Total assembled length of 5 m. .....187

Dedicated to the memory of my grandad, James McNally, for imparting upon me the value of free thought and intellect from a young age.

# Chapter 1

# Introduction

## 1.1 Overview

Never before has one species achieved such a breadth of exploration in a more condensed timeframe. There are few statements of such magnitude which can be made without a trace of hyperbole, but surely this remains virtuous. Between the Wright Brothers achievement of powered flight at Kill Devil Hills in 1903 until the landing of Eagle upon the Sea of Tranquillity in 1969, not 66 years had passed. While the latter accomplishment was one catalysed by human-made political tensions, it was and remains the greatest technological achievement accomplished by, and for the good of all mankind.

The dawn of the Space Age allowed mankind an insight into our Solar System which had previously been limited by astronomical distances and optical physics. Led by advances in in engineering, robotic spacecraft set out to explore the Venusian clouds, Martian deserts, Jovian storms and Saturnian rings from above, unshrouding past mysteries and discovering many afresh in the process.

While much of the Solar System has now been mapped from above, mankind cannot rest assured that its task has been completed. Like Earth's great oceans, great expanses lie unexplored beneath the surface of our planetary neighbours. Robotic missions have to date scratched the surface of these worlds in efforts led by geological curiosity and the promise of astrobiological potential, but the majority remains untouched. Recent discoveries have shed new light on the deep subsurface environments of worlds such as Mars, and developments in our knowledge of the 'Ocean Worlds' of Europa, Ganymede, Enceladus and Titan make these locations enticing targets. Furthermore, our imminent return to the Moon is, in part, fuelled by the subsurface resource potential of our closest neighbour. Resource prospecting missions which directly sample the near subsurface are required in the search for icy deposits postulated at the lower latitudes and in the so-called Permanently Shadowed Regions (PSR) which may enable the establishment of a permanent human outpost while fuelling our most ambitious exploration goals. It is therefore clear that developments which seek to further the state of the art of the technologies required to

accomplish these lofty goals shall maximise the scientific return available for our generation of planetary scientists and create yet more questions for the next.

## 1.2 Aims and Objectives

Robotic drilling systems have proven to be an essential tool in both the subsurface exploration of our terrestrial planetary neighbours and of the extreme environments on Earth, such as those found within the Polar Regions. This work seeks to evaluate the capability of multiple rotary-percussive drilling techniques: the ultrasonic-percussive technique and the spring-cam hammer technique, and build upon the existing state of the art by creating robust, useable architectures which will allow these systems to be implemented in future missions. To this end, the following aims are summarised:

1) Development of a sample acquisition and caching system driven by the use of the ultrasonic-percussive technique, suitable for Mars Sample Return-type mission architectures.

2) Development of a system of robust autonomous drill string assembly which is more robust than conventional threaded connections in a planetary setting.

3) Advancement of low resource drilling autonomy to include control systems compatible with common planetary drilling approaches. A fault-resistant system for core drilling in volatile-rich environments may be required for drilling on Mars.

4) Testing of the ultrasonic-percussive drilling system in a suitable Mars-analogue environment, such as Coal Nunatak, Antarctica.

5) Development of a drilling system breadboard, inspired by planetary drilling techniques and making use of the spring-cam hammer actuator, capable of extracting bedrock from the subglacial rock-ice interface in the Polar Regions.

6) Analysis of the performance of the system during laboratory dry drilling, in a cold chamber and also in a thermal-vacuum chamber used to emulate Mars atmospheric conditions.

7) Industrialisation of the subglacial bedrock sampling breadboard for deployment in Antarctica.

## 1.3 Thesis Structure

**Chapter 2**

An examination of the state of the art in planetary drilling, focussing upon past and present missions and the depths achieved by the systems utilised. Strengths of each system shall be identified alongside elements of the system, or the challenges with which it was tasked, which proved troublesome. An overview of existing technologies used within the field of terrestrial subglacial bedrock sampling is provided.

**Chapter 3**

Drilling theory is discussed alongside the challenges which complicate the planetary drilling process. Rotary and rotary-percussive drilling techniques are evaluated, as are the options available for spoil removal from the borehole. Common metrics such as drilling power and specific energy are introduced alongside minimum acceptable auger speed.

**Chapter 4**

The ultrasonic-percussive drilling technique is introduced, with the technique explained. The objectives of the Ultrasonic Planetary Core Drill (UPCD) project are discussed alongside the challenges facing the development. The design process of key elements of the architecture is provided alongside the process of developing a Concept of Operations based upon the bayonet interface. An overview of a series of experiments which were performed in order to evaluate the suitability of the bayonet in transmitting percussion is provided. An in-depth discussion of the problem of autonomous drill control is seen alongside the solution implemented in both dry and volatile-rich terrain. Results are provided from laboratory testing and an Antarctic field test campaign.

**Chapter 5**

The challenges faced in the development of a subglacial bedrock sampling system are discussed, highlighting the constraints imposed by operations in the Polar Regions. Trade-off studies were performed in order to evaluate the most suitable technologies to be used. The technology development process is detailed focussing on the development of the spring-cam element at the heart of the system. A multi-parameter laboratory campaign is detailed alongside testing in a thermal-vacuum chamber carried out at FH Aachen, Germany.

**Chapter 6**

An overview of the Percussive Rapid Access Isotope Drill (P-RAID) is detailed. Discussion is provided on the constraints imposed by integration with the RAID drill developed by the British Antarctic Survey and key elements of the design which facilitate its use in the Polar Regions. Breakthroughs in the implementation of core catching are introduced. Findings from a field campaign to the Skytrain Ice Rise, Antarctica, are detailed.

**Chapter 7**

Conclusions from the core chapters are explored, highlighting key achievements. Possible area of future work are discussed which seek to build upon the work accomplished within this thesis.

# Chapter 2

# Drilling in Extreme Environments

## 2.1 Terrestrial Drilling in Extreme Environments

Commercial energy prospecting activities (namely, oil and gas exploitation) have a rich heritage of utilising more conventional drilling techniques and technologies, but a recent depletion of resources from regions considered to be readily accessible has pushed industrial operations into territories once deemed inaccessible. These 'extreme environments' may be classified as such through a combination of factors which ensure that the implementation of drilling activities is particularly arduous and/or hazardous. Such factors may include extremes of temperature at the drill site (-50 to +200°C may be expected), geographic isolation, volatility of the terrain to be drilled (or dynamic properties of the terrain associated with a reaction to the drilling process), uncertainty in the target terrain composition, extreme pressures brought about by deep sea operations and operation within an ecologically sensitive region.

Perhaps the most appealing targets for commercial energy exploitation are those found within the Arctic Circle. While drilling activities in the northern polar regions of Earth have been ongoing for decades, these activities have traditionally been limited to onshore or near-shore operations. While the exploitation of energy resources within these regions are fraught with geo-political limitations governed by territorial disputes, and ongoing concerns surrounding the potential for ecological damage to an already-fragile region, the economic potential conferred through commercial drilling operations is tempting. In fact, studies suggest that the northern Arctic may contain as much as 90bn barrels of technically recoverable oil and 44bn barrels of natural gas [1]. While appealing, the conditions present at these sites ensures that the task of extraction is not without challenges. Winter conditions in these regions often approach temperatures in the region of -50°C, ensuring that human operations in support of drilling campaigns are placed at risk of exposure. Extremes of temperature may also result in the formation of thick sea ice which requires careful consideration when designing rigs. Furthermore, sea ice may prevent a significant challenge to winter operations and logistical support, requiring the use of icebreakers and ice-hardened

vessels to support those operating on the rigs. Deepwater operations may also be essential with depths in the range 300 – 3000 m foreseeable. While such depths are commonplace in offshore drilling, ice hardening and low temperature protection are required, with dynamic features designed to prevent against damage from movable floating ice masses. Perhaps most pertinent is the need to prevent the fragile polar regions from ecological damage in the event of an oil spill. As the unique biodiversity in this region is already heavily threatened by climate change, the minimisation of further human-made disruption is clearly a priority. In summary, a number of key challenges such as extreme temperatures, isolation as brought about by the presence of sea ice, a dynamically changing environment and a need for ecological sensitivity makes the operation of drilling rigs within this region particularly difficult.

Drilling for gaseous hydrates presents another challenge within the field of energy prospecting. Offshore extraction of hydrates presents multiple challenges including uncertainty in the composition of the media to be drilled. Furthermore, instabilities in the target terrain brought about by the sampling process itself means that drilling operations must be considered a dynamic process prone to drill well instability [2]. This instability may also lead to the uncontrolled release of gas which may prove to be hazardous to the rig and those manning it. As an aide

In order to mitigate against the risks imposed through the operation of terrestrial drilling hardware in extreme environments, industrial operators are striving to automate existing technologies. Studies suggest that it may be possible to improve the efficiency of production operations while enhancing health and safety statistics and lowering costs [3] [4]. Operational automation, whereby humans are removed from the loop with regard to the tripping of drill strings, and the monitoring of drilling progress may be enabled by advances in real-time drilling autonomy inspired by developments in technologies for drilling on planetary surfaces. Given that planetary drilling systems require levels of autonomy, reliability and fault tolerance which can prevent or mitigate the severity of faults arising within a timeframe on the order of seconds, such systems may prove to be a trustworthy baseline for industrial automation where human lives are endangered. In such circumstances, latency incurred through teleoperation alone may prove to be unacceptable with catastrophic results ensuring that autonomy enabled by machine learning or equivalent may be the most robust solution.

## 2.2 Historical Planetary Drilling Missions

Faced with the challenge of unravelling the rich history of our Solar System, mankind has expanded its horizons beyond terrestrial or orbital studies of our planetary neighbours through the use of robotic and manned missions destined for the surface of our extraterrestrial neighbours. Though much can be learned from surface exploration alone, the incentive to explore the environment beneath is clear. Sheltered from the effects of radiation or aeolian processes, the subsurface of these celestial bodies are akin to a time capsule, acting to pristinely preserve geological, chemical and perhaps biological histories.

The *Luna* series of missions, developed by the Soviet Union in the 1960s, marks the first attempt at deploying extraterrestrial drilling hardware. Luna 16, launched 1970, successfully returned 0.1 kg of lunar regolith to Earth via an autonomous robotic drilling system. The system achieved a depth of 0.35 m after approximately 7 minutes of operation before drilling was halted by a hard rock. Further successes include Luna 20 (1972), which was able to extract 0.03 kg of material from a depth of 0.25 m, while Luna 24 (1976) achieved 0.2 kg of regolith from a depth of 1.6 m [5].

The Apollo 15 mission of 1971 saw the first application of a human-operated drilling system. Astronauts Scott and Irwin attempted to drill through the lunar regolith by hand in order to extract core samples and emplace heat probes for thermal sensing (Figure 1). The drill in question, designed by Martin Marietta Corp., was of the rotary-percussive type with a fibreglass drill string consisting of multiple bits screwed together to provide a total depth capability of approximately three metres. While core samples were acquired during multiple drilling operations, poor alignment of the bits at the mating interfaces prevented the astronauts from achieving depths greater than approximately two metres. The alignment issue prevented drilled cuttings from flowing past the interface, resulting in a choking of the auger at these points. The volume of accumulated cuttings on the auger flutes acted to induce exceptionally high frictional forces upon withdrawal, complicating the extraction process and, in one particular case, injuring Scott. Future missions featured a modification of the drill string with the inclusion of a titanium interface piece between the drill bit sections in order to provide a smooth continuation of the auger helix.

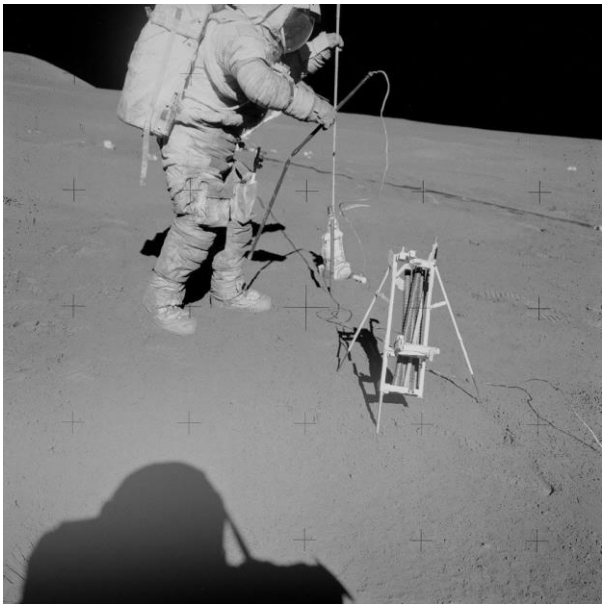

**Figure 1: Apollo 15 drilling operations. (NASA Image AS15-92-12407)**

The launch of the Mars Exploration Rovers (MER), Spirit and Opportunity, in 2003, saw the advent of the subsurface exploration of Mars. Tasked with furthering our knowledge of the geological history of the planet, each rover was equipped with a Rock Abrasion Tool (RAT) developed by Honeybee Robotics. The purpose of the RAT was to remove a few millimetres of weathered material from rock targets of interest and, in doing so, exposing the pristine interior for study [6]. Though a relatively low resource, simple device with a mass of approximately 0.5 kg, consuming no more than 10 W of total power during standard operation, the RAT proved to be a robust piece of hardware. In the case of Opportunity, its RAT device operated for approximately 15 years until the demise of the rover in 2019. Figure 2 depicts the result of a typical RAT ‘drilling’ operation: a hole of approximately 45 mm diameter and 5 mm deep. While the RAT may not be classed as a drilling system in the true sense, it was designed with many of the same requirements due to the uncertainty of the target terrain. This led to a system capable of abrading even the hardest surfaces which could be encountered in modest timeframes.

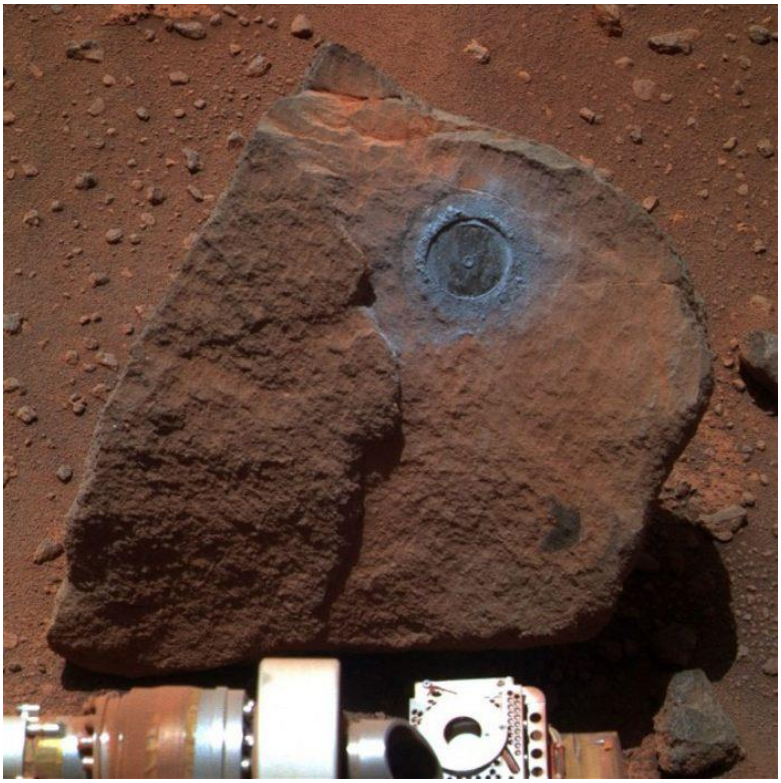

**Figure 2: Hole produced by the RAT tool on Opportunity. Note the pristine rock exposed by the RAT process. Image courtesy of NASA/JPL-Caltech.**

The 2007 NASA Phoenix mission extracted heritage from the Viking Landers 1 and 2 which were equipped with a robotic arm-mounted scoop for the task of trench excavation and the transfer of regolith to a series of on-board ovens for in-situ chemical and biological analysis. This mission to the northern latitudes of Mars was tasked with building upon past landed missions in order to assess habitability and further establish the history of water on the planet. Benefiting from a more northerly landing location than its predecessors of 68° N , and making use of a 2.4 m robotic arm mounting, the Icy Soil Acquisition Device (ISAD) was required to excavate multiple trenches in order to expose near-surface ice which had been postulated to exist at a depth of approximately 5 cm [7]. Having established that ice-cemented regolith and ice lenses held potential to be extremely hard and thus difficult to excavate at the cryogenic temperatures of Mars' northern regions, a rasp device was added to the underside of the scoop to break up any consolidated icy material which may have been found within the trenches. Figure 3 shows the ISAD in operation on the surface of Mars with a sample of regolith in the scoop portion of the device. Developed by Honeybee Robotics at a late stage in the preparation of the mission, the rasp was limited in its operation as a low torque/high speed device due to a restriction in the total power available to the device. This required a current limitation on the rasp motor of 1 A which was capable of rotating the 6.35 mm bit at 5300 RPM, producing 0.054 Nm of output torque [8]. The rasp operated by

preloading the back end of the ISAD against the terrain, resulting in rasped material being ejected into the rear orifice of the scoop. Robotic manipulation of the device then allowed the contents of the scoop to be delivered to the instrument package.

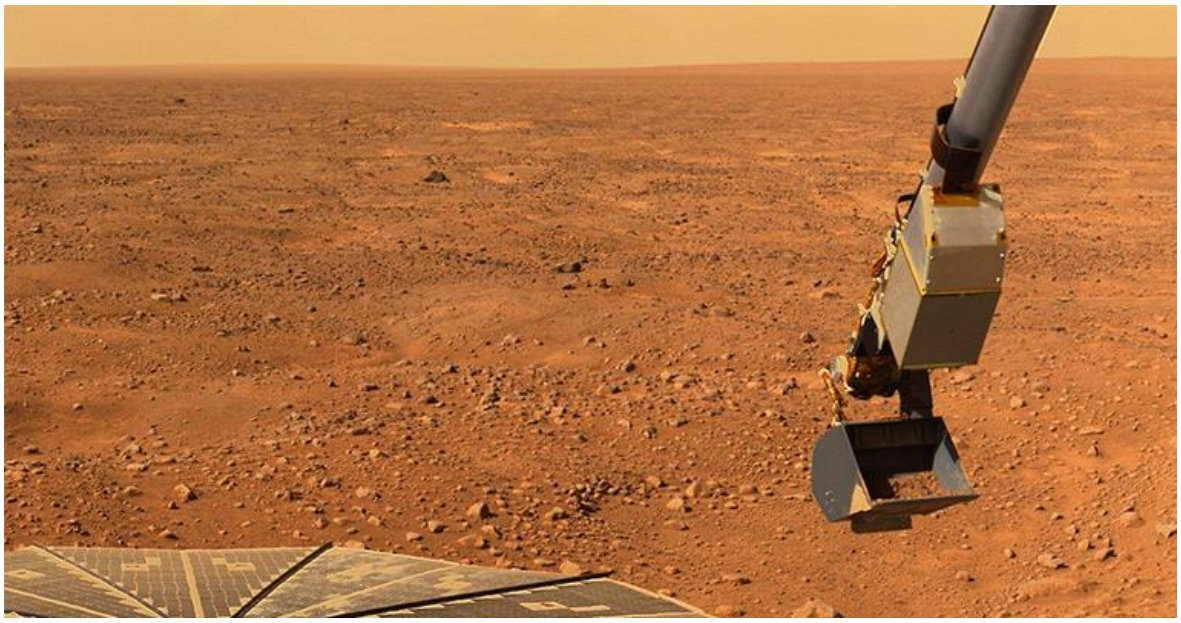

**Figure 3: ISAD with sample in its scoop upon the cessation of a trenching and sampling operation. Image courtesy of Honeybee Robotics.**

Prior to deployment, the rasp tool was tested on simulated permafrost terrain in the laboratory with a uniaxial compressive strength (UCS) of 45 MPa in order to ensure that the system was capable of penetrating even the hardest terrain type foreseeable. While the device was proven capable of excavating icy material as required, the thermal energy imparted to the terrain by the drilling process meant that, in the worst case, approximately 30% of the water content by weight was lost due to sublimation [9]. Ultimately, the ISAD was used to excavate 12 trenches in total, delivering 31 samples (including those containing water ice) to the on-board instrument suite for analysis [10].

The first deployment of a drilling system (in its truest sense) to the surface of Mars was as part of the NASA Mars Science Laboratory (MSL) mission, launched in 2009. Tasked with assessing the habitability, the history of water, the climate and the geology at its landing site, Gale Crater - a near-equatorial landing site (5.4° S) - the roving laboratory was equipped with a rotary-percussive drilling system designed to deliver powdered samples to various instruments on-board. Capable of delivering percussive strikes of between 0.05 – 0.8 J at a maximum rate of 30 Hz, thus generating a maximum of 24 W of net percussive power, the percussive actuator was of the sprung voice coil type. Figure 4 details a basic outline of the drill system including the sample delivery pathway [11].

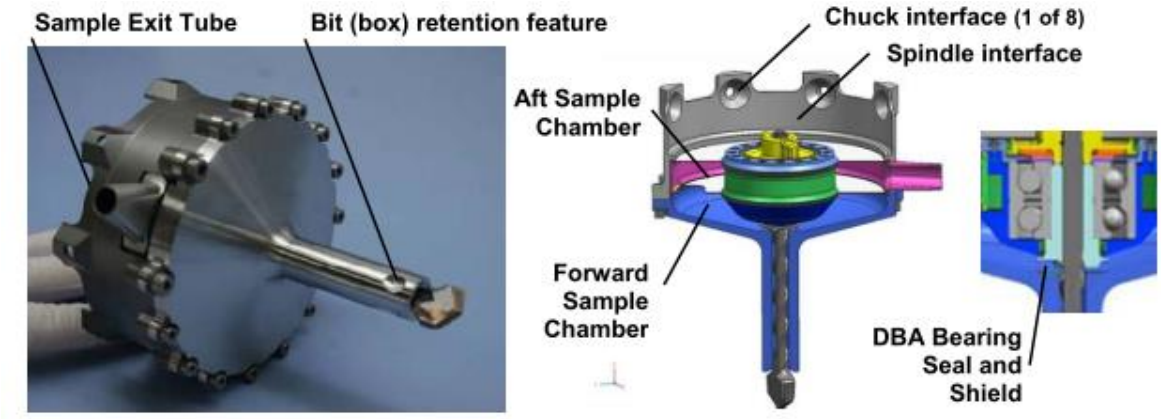


**Figure 4: MSL rotary-percussive drilling system layout** *[11]*.

As of 2018, MSL has drilled at 16 locations on Mars. Each drill hole has a diameter of 16 mm and may be in the region of 50 – 60 mm deep. Figure 5 depicts an image of the first use of the drilling system on Mars in to a rock target known as "John Klein".

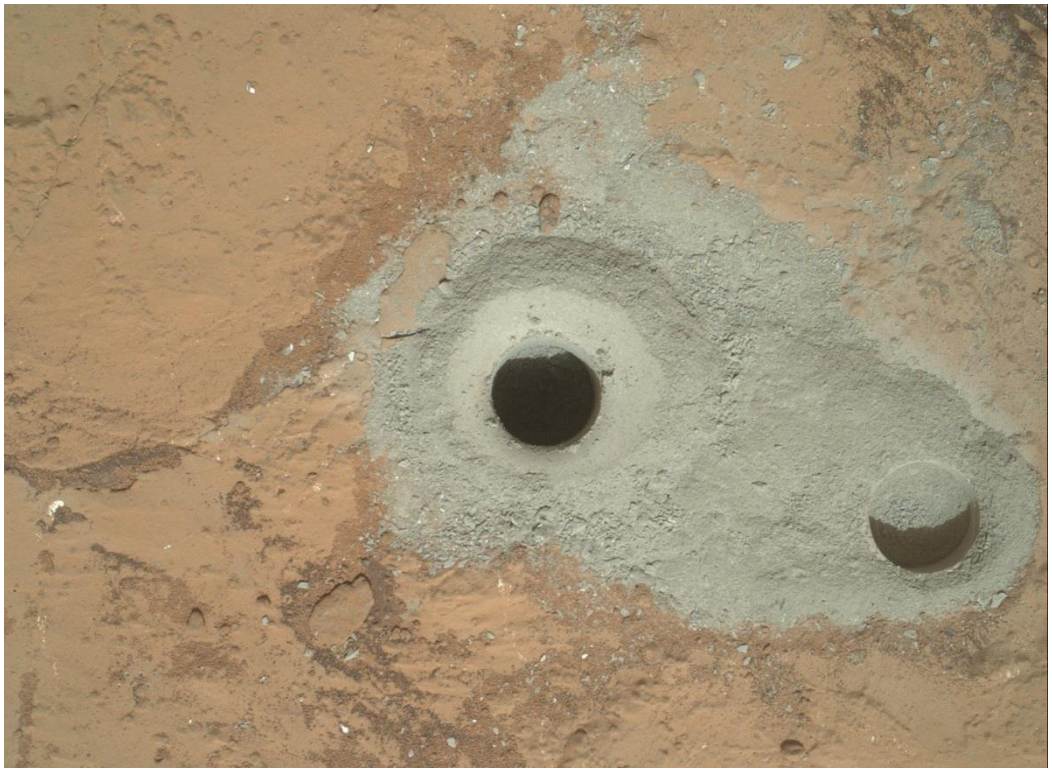

**Figure 5: MSL first full-depth drill hole of target "John Klein". Note, the preparatory drill hole on the right hand side of the image drilled to a shallower depth. Image courtesy NASA/JPL-Caltech.**

While the MSL drilling system initially functioned well, delivering 15 samples between 2012 and December 2016, the system then developed a fault in the drill feed system which prevented the drill from making use of the dual finger-like stabilizers during standard operations. While the feed systems issue was eventually rectified, the motor fault attributable to the problem deemed a return to the previous method of drilling operations too risky. To

this end, a new method of drilling was developed which saw the progression of the drill bit during operations controlled by the arm itself. Obtaining fine motion control using this method required the development of new control software which made use of a force sensor in the robotic arm in order to establish a means of obtaining feedback for further progression.

The Philae lander, part of the ESA Rosetta mission to comet 67P/Churyumov-Gerasimenko touched down on its target in 2014. Unfortunately, the initial contact made with its target resulted in the spacecraft bouncing off the surface twice. This was likely caused by a failure in both of the arresting systems. These bouncing events meant that the final resting place of the lander was not as expected. In fact, the lander was eventually located on its side in a deep, shadowed crack some distance from the point of initial contact. Equipped with a drilling system named SD2, the rotary drilling device was designed to sample to depths of 230 mm beneath the cometary surface, collecting samples in the region of 10 – 40 $mm^3$ for delivery to on-board ovens for chemical analysis [12]. A schematic of the drilling system is detailed in Figure 6. Assisted by the use of anchors on the feet of the lander, SD2 was designed with the capability of drilling with 100 N of weight on bit, utilising approximately 15 W of electrical power and 5 kg total mass. Although the probability of success was deemed to be low due to the off-nominal orientation of the lander, the drill was eventually deployed on the cometary surface. As detailed in Figure 7 feedback received from the spacecraft shows the deployment of the drilling system to the maximum extent achievable (factoring in the drilling platform above the surface of the comet) of 560 mm. Furthermore, the drill was successfully retracted back to the home location and the sample release operation was carried out into an oven (despite there being no guarantee of a sample ever having been achieved). Despite the lack of a positive result from an analysis standpoint, the nominal behaviour of the system after 10 years of spaceflight is a testament to the robustness of the system and proves that such complex mechanisms can survive the trials of long term interplanetary spaceflight [13].

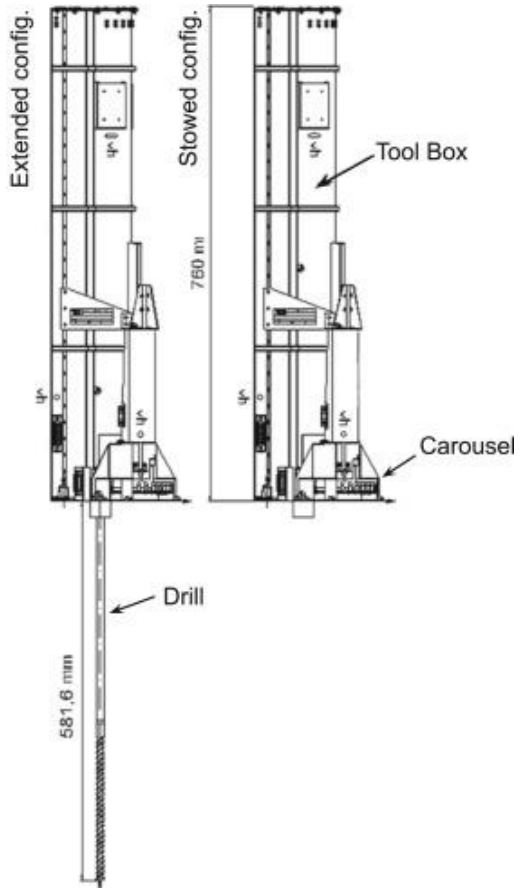


**Figure 6: SD2 drilling system schematic** *[12]***.**

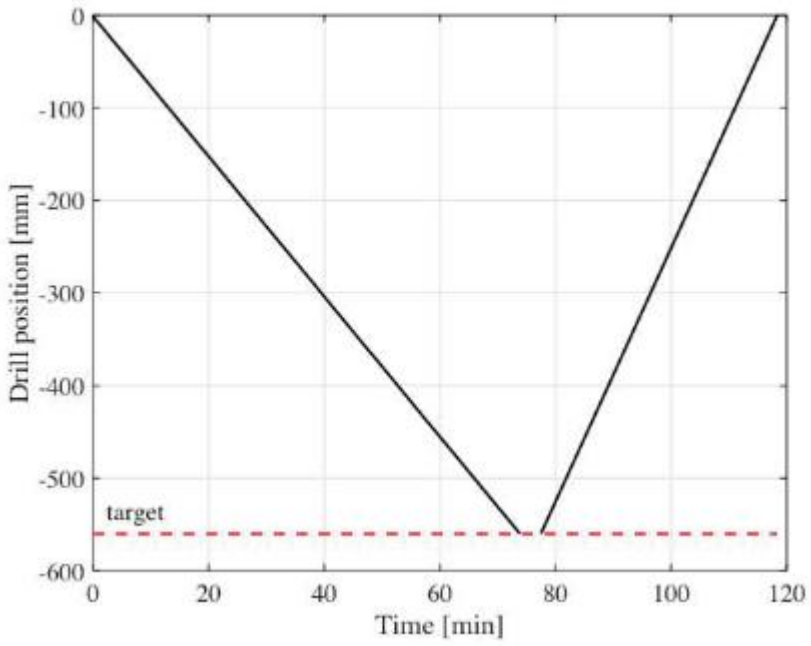


**Figure 7: Telemetry from SD2 drill position showing a complete deployment and retraction of the drill bit to 560 mm** *[13]***.**

The HP$^3$ mole, a DLR-led addition to the NASA InSight mission to the Elysium Planitia region on Mars, seeks to implant a heat probe at depths of up to 5 m beneath the Martian subsurface. The probe, depicted schematically in Figure 8 [14], makes use of cam-hammer driven percussive mechanism to advance to depth, relying on friction between the mole and the borehole to react the force of the recoil. The system was designed to operate with an average power in the region of 5 W. While moles such as HP$^3$ do not directly sample the terrain which is excavated during penetration, they may prove to be a robust option for penetrating loose or lightly consolidated terrain efficiently.

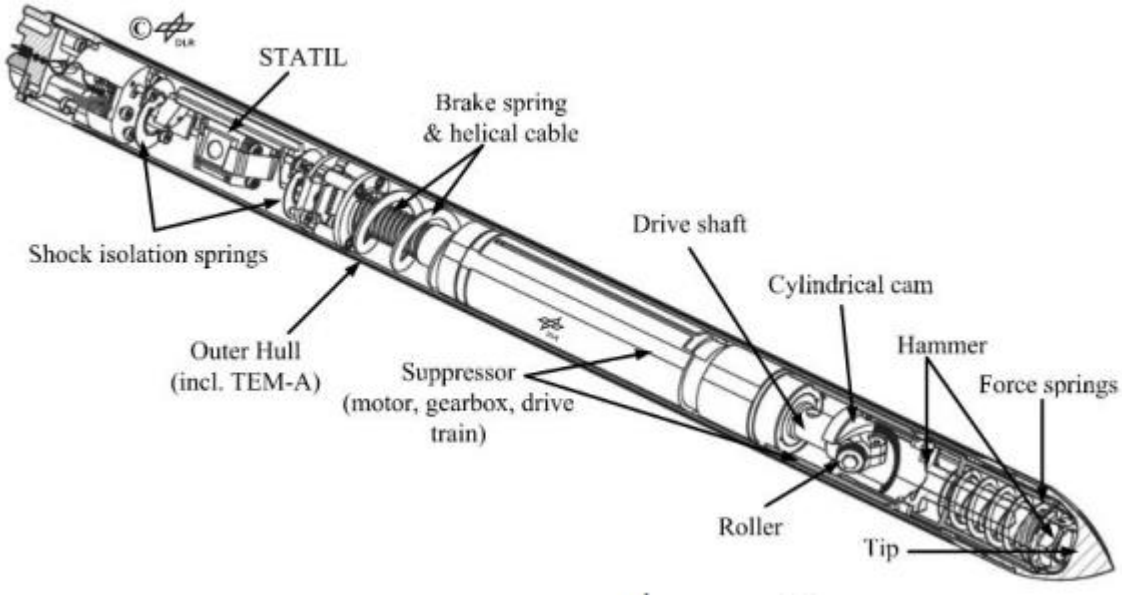


**Figure 8: HP$^3$ mole cut-away schematic** *[14]*.

## 2.3 Future Drilling Missions

The upcoming launch of ExoMars2020, a robotic rover mission to the surface of Mars, shall initiate the dawn of a new era of subsurface exploration on the planet. As the first mission with an astrobiological focus since the Viking era, the rover shall deploy a rotary drilling system to the clay-rich region of Oxia Planum (18° N) in order to obtain discrete cores at depths of up to 2 m beneath the surface. Uniquely, the system will robotically construct a drill string made up of a cutting bit and three additional extension bits in order to reach the targeted depth [15]. The desired depth of 2 m is deep enough to ensure the preservation of any target organic biomarkers against radiation or oxidants. Figure 9 portrays the deployment of the drilling system. The cutting bit is of an interesting design in that during standard drilling operations it operates as a full faced bit. When a core sample to be obtained

at a predetermined depth, a central piston is retracted via an electromechanically-driven ball screw mechanism within the bit which reveals an internal orifice of 10 mm diameter which can be used to collect cores. When a core of sufficient length (~ 30 mm) has been drilled, another mechanism within the bit is actuated which acts to shear the core at the base, simultaneously securing the core within the bit. The core sample is then robotically deposited in to a crushing system in order to pulverise the sample for acceptance by the on-board instrument suite.

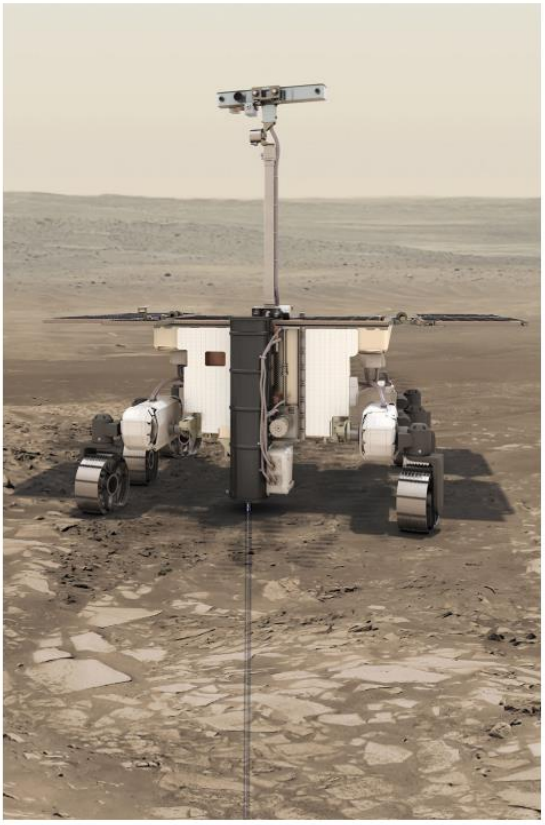

**Figure 9: ExoMars rover deploying 2 m drillstring** *[15]***.**

The complete drill system has a mass of 21 kg and is capable of drilling with a maximum power use of 80 W, using no more than 450 N of weight on the drill bit. Designed for the worst case, it is capable of extracting samples of material which are as hard as marble with penetration rates of up to 0.3 mm/min, while softer samples may be achieved at rates as high as 20 mm/min using no more than 6 Nm of drilling torque [16].

The as-yet unnamed NASA 'Mars 2020' mission shall be the first of multiple stages in order to accomplish the long term goal of returning a sample from Mars. Making use of the MSL rover architecture, the 2020 mission replaces the drill system used on MSL with a rotary-percussive core drilling system. Tasked with obtaining at least 20 samples from multiple locations, the rover shall seek to obtain samples of up to 70 mm in length [17] as scientifically required [18]. These samples shall then be archived using an 'adaptive caching'

system, whereby the sample tubes are stored in a rack on-board the rover and deposited on to the surface when it is deemed most opportune for the mission, or to reduce risk going forward [19]. As shown in Figure 10, the caching strategy enables the rover to continue exploring areas of scientific interest throughout the mission without the mounting burden of carrying its valuable cargo to these potentially risky locations. This strategy also allows specific sample tubes to be selected for return based upon scientific merit. This may only become apparent upon the accrual of all the samples near the end of the primary sampling portion of the mission.

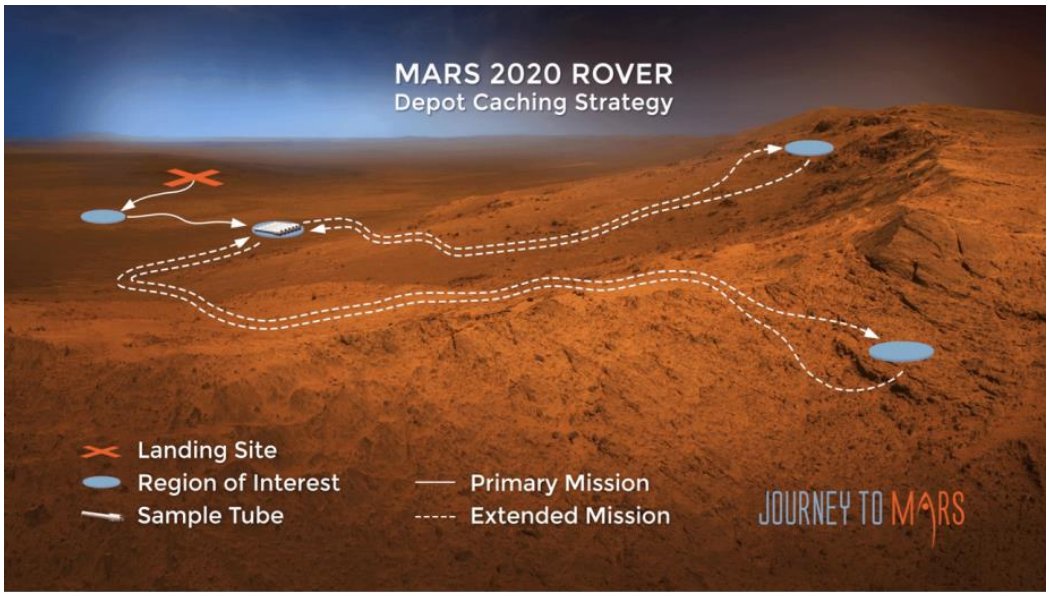


**Figure 10: NASA Mars 2020 'adaptive caching' strategy. Courtesy: NASA/JPL-Caltech**

Luna 27, a joint mission by ESA and Roscosmos, shall deliver a robotic landed platform to the surface of the moon in 2024. Targeting Permanently Shadowed Regions (PSR) at the South Pole-Aitken Basin, the mission seeks to search for volatiles such as frozen water which may be trapped within the lunar regolith. Making use of a drilling rotary-percussive drilling system named ‘ProSEED’, the mission shall capture cuttings samples from a depth of up to 1.2 m. These samples shall then be delivered to an on-board instrument suite, ‘ProSPA’, consisting of two mass spectrometers. In order to provide different quantities of sample to both the Russian and European instruments, the drill system uses a dual sampling system to achieve its goal. The European instrument, requiring only a few $mm^3$ of sample, makes use of a push tube which can be extended beyond the cutting face of the drill bit when sampling is required. The greater quantity of material required by the Russian instrument is achieved through the use of an extendable auger which fully encapsulates drilled cutting upon retraction. Figure 11 depicts the dual sampling system of the ProSEED drill [20].

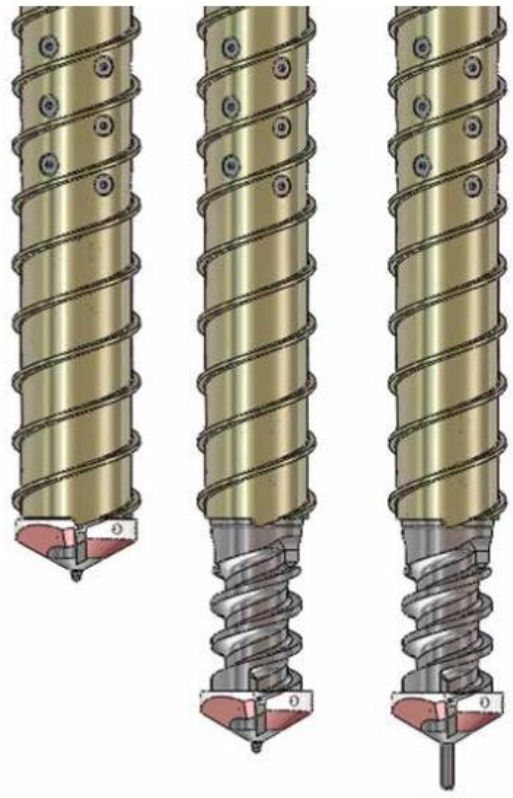

**Figure 11: ProSEED drilling system sample capture mechanisms. Standard drilling configuration (L), Russian sampling mechanism (middle) and European sampling tube deployed (R)** *[20]*.

### 2.3.1 Future Technologies

While the vast majority of the technologies thus far utilised in planetary exploration remain relatively immature in their use within a planetary setting, drilling technologies which may be implementable in the future, such as plasma and laser drilling, are of particular interest for long term applications. Plasma drilling technologies, such as those proposed in [21] [22]. Such systems offer an innovative solution to the task of terrain penetration, achieving the task with minimal mechanical burden and thus minimising risks associated with wear and fatigue. The authors suggest that a system which is of a magnitude compatible with existing rover and lander platforms may be capable of achieving desired penetration rates with as little as 100 W, with larger systems demanding up to 1000 W. While plasma drilling may prove to be an effective means of accessing the subsurface, few details regarding the effect of the drilling process upon the terrain are published. Thus, it is not possible to establish if the spoil produce by the process would be suitable for chemical, geological or biological analysis.

Laser drilling has heritage on Mars in the form of the ChemCam instrument mounted onboard the MSL rover [23]. While not a true drilling system, the ChemCam instrument has proven that laser penetration of rocks on a planetary surface is possible.

Table 1 provides an overview of the drilling systems past and future drilling systems discussed in Chapter 2, taken from the respective literature referenced for each system. A comparison may be made between key parameters such as the type of drilling system implemented, the average total power required to operate the system, the depth targeted, drill system mass, nature of the terrain to be drilled and the type of sample collected (if applicable).

| Drilling Instrument | Type | Ave. Power - W | Target Depth - m | System Mass - kg | Terrain Drilled | Sample Type Collected |
|---|---|---|---|---|---|---|
| Apollo Drill | Rotary-percussive drill | 500 | 2 | ~ 20 | Loose regolith | Cores, regolith |
| Rock Abrasion Tool | Rotary abrasion device | 10 | 0.005 | 0.5 | Consolidated | N/A |
| ISAD | Rotary rasp-like drill | 30 | 0.05 | 0.75 | Ice cemented | Icy regolith |
| MSL Drill | Rotary-percussive drill | 50 | 0.05 | ~ 10 | Consolidated | Powdered cuttings |
| SD2 Drill | Rotary drill | 15 | 0.25 | 5 | Ice cemented | Powdered cuttings |
| HP3 mole | Percussive mole | 5 | 5 | 3 | Loosely consolidated | N/A |
| ExoMars 2020 Drill | Rotary drill | 80 | 2 | 21 | Consolidated | Powdered cuttings, cores |
| Mars 2020 Drill | Rotary-percussive drill | 50 | 0.07 | 10 | Consolidated | Cores |
| ProSEED | Rotary-percussive drill | 180 | 1.2 | 30 | Ice cemented | Powdered cuttings |

**Table 1: Overview of drilling systems. Key parameters extracted from reference literature.**

## 2.4 Subglacial Bedrock Sampling Systems

The scientific exploration of the Polar Regions has seen the extraction of ice samples from a great range of depths, from as shallow as 50 m to as deep as 3 km, in order to answer the key questions relating to many fields of science. The technologies which have been designed to accomplish these task are innumerable and implemented by most every organisation which operates in these regions. While the challenge of extracting ice samples from great depths beneath these frigid terrains is rarely straightforward, it is a challenge for which a number of reliable solutions exist. Although these drilling campaigns may reach the till layer, or even the bedrock beneath the glacier, rarely are attempts made to purposely sample these elements of the glacial lithology.

Technologies for sampling subglacial bedrock are generally classifiable as either surface-driven rigs or wireline drilling systems. Surface-driven rigs are widely used for a number of industrial applications although perhaps the most common of these are found within the fields of energy prospecting, mining and geothermal energy. As such, the ubiquity of this method allows it to be thought of as the most conventional of the drilling techniques. Figure 12 depicts a schematic of a standard surface-driven rig [24]. These rigs typically make use of rotary drilling and copious quantities of cutting fluid, alongside the tripping of hollow drill pipes to achieve the targeted depth. While the heritage brought by the use of such a drilling system ensures that there will be a high degree of confidence in acquiring bedrock samples, the approach requires a vast volume and mass of hardware to achieve. Furthermore, the process of drill pipe tripping is exceptionally time consuming and often comprises the single most intensive portion of the drilling operation. Given the logistical constraints which

may be imposed on Polar Regions exploration efforts, driven primarily by the isolation of such locations, surface-driven drilling rigs may not be suitable for many remote regions of interest.

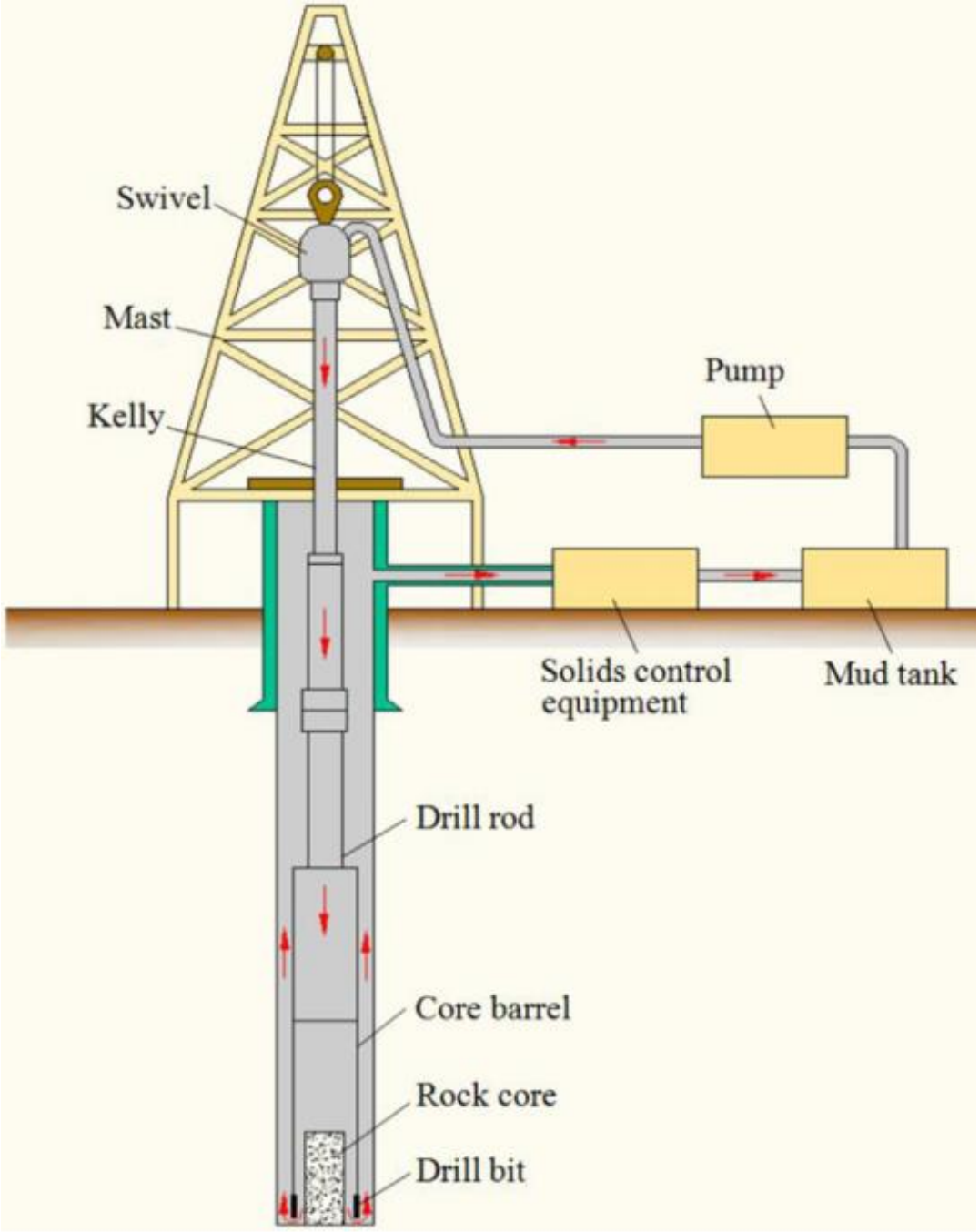


**Figure 12: Surface-driven drilling rig** *[24]*.

While lightweight, portable versions of the technology such as the U.S. Ice Drilling Program (IDP) Winkie drill (Figure 13) do exist, the need for portability reduces the maximum depth achievable to 120 m. The total mass of the Winkie system is approximately 1000 kg and with a power requirement of 2.5 kW, this system does represent a relatively low

resource solution which is capable of achieving rock cores of 32.5 mm. It is of note that the Winkie system requires the use of cutting fluid to achieve its goal.

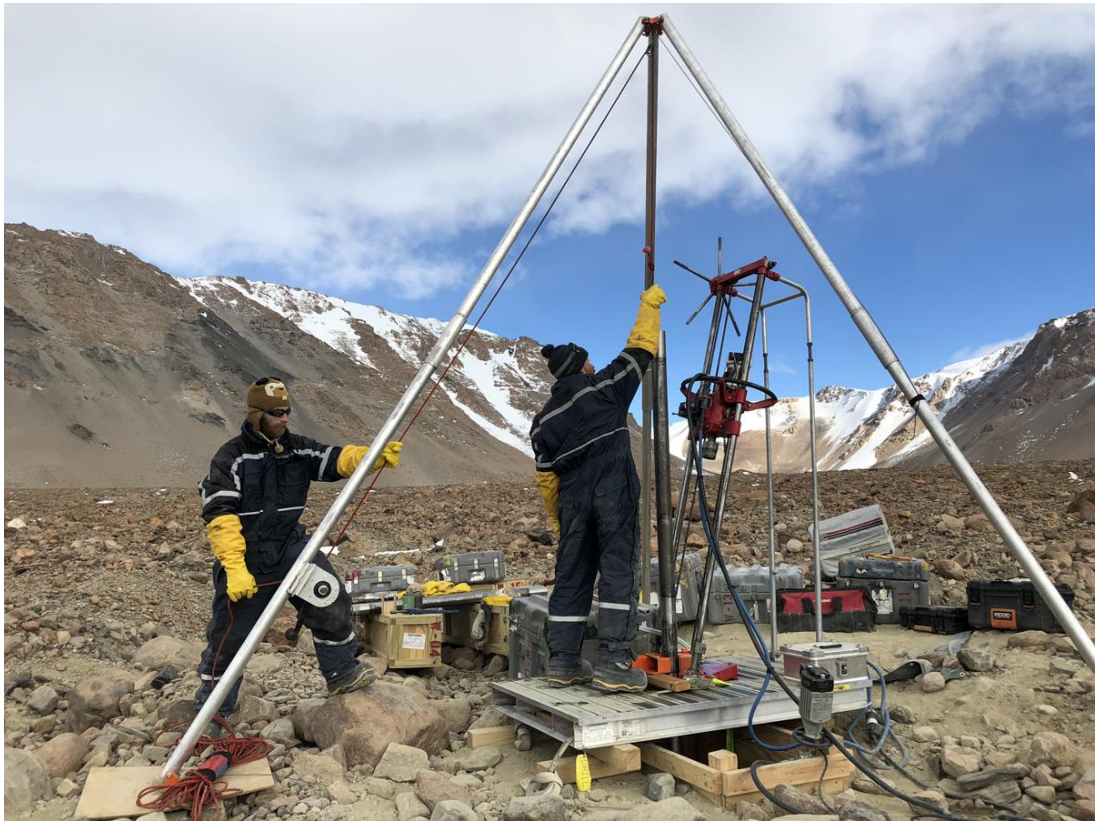

**Figure 13: U.S. IDP Winkie drill system. Courtesy: U.S. IDP.**

An alternative to surface-driven systems exists in the form of the wireline system whereby the cutting bit is suspended on a wire tether which is sent downhole for drilling operations. Such a method negates the need for pipe tripping, thus reducing both the logistical burden and the time taken to reach the required depth. Systems of this type may take multiple forms depending on the depth to be drilled. The IDP Agile Sub-Ice Geological Drill (ASIG) system was designed with the goal of sampling bedrock at a depth of up to 700 m. ASIG is capable of obtaining continuous cores of up to 8 m long, with a diameter of 39 mm, requiring 15,000 kg of hardware and 5 kW of power to do so. Figure 14 shows a core achieved from drilling operations.

In order to achieve bedrock cores from the most extreme depths, the IDP developed the Rapid Access Ice Drill (RAID), not to be confused with that of the British Antarctic Survey (BAS) hardware with the same acronym. Designed to penetrate to depths of up to 3.3 km, the IDP RAID system makes use of a scaled up ASIG architecture in order to sample bedrock cores of at least 25 m with a diameter of 36.5 to 63.5 mm. Capable of operating from start

to finish in 10 days, this system ensures that drilling time is minimised, though the massive weight of the system means that the drill requires intensive logistics and forward planning in order for the complete system to be traversed to the field location. As the Antarctic summer season is short and the continent inaccessible at other times of the year, it may be essential to deploy the system many years before drilling is to take place making use of a tractor traverse or similar. Figure 15 shows a schematic of the RAID system.

**Figure 14: 8 m core obtained using ASIG drill system. Courtesy: U.S. IDP.**

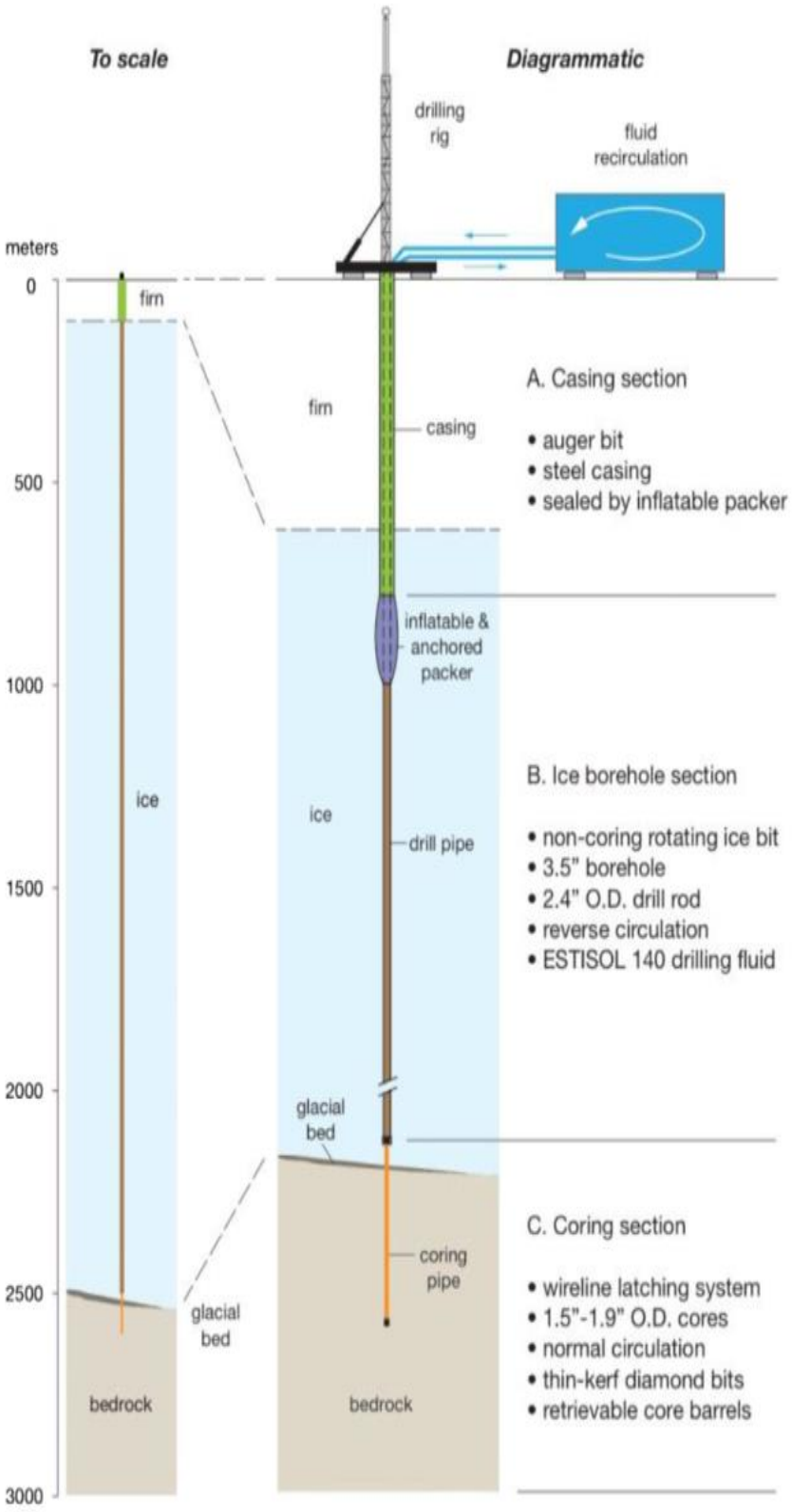


**Figure 15: IDP RAID drill schematic. Courtesy: U.S. IDP**

# Chapter 3

# Theory of Drilling in Extreme Environments

## 3.1 Drilling Process

All missions which seek to explore the subsurface rely upon drilling systems or penetrators to achieve this goal, but the system to be used is dependent upon a number of key factors. If the core priority of the mission is to emplace a probe beneath the surface of the planetary body, or if the act of penetration alone is enough to provide scientific results (such as the mechanical properties of the terrain, for example), then the technologies used will significantly differ from those which may be required when the extraction of samples is the primary objective. In the latter case, the type of samples which are to be extracted may take the form of cores or powdered cuttings.

The extraction of core samples has a number of advantages when compared to sampling powdered cuttings alone but brings challenges. In order to obtain core samples, the drill bit must be designed such that there is a centrally-located annulus in the axial direction of the drill bit which will accumulate consolidated material during drilling operations. As only the terrain in the region between the core annulus and the outer diameter of the drill bit, known as the kerf, is broken during the drilling process, there is a reduction in the amount of work which must be done to reach a given depth when compared to full-faced drilling. While this may prove to be beneficial if the objectives of drilling are to obtain core samples alone or if powered samples are to be obtained from a given depth as efficiently as possible, the volume of powdered cuttings which can be obtained at any depth is reduced. Figure 16 depicts typical rotary drill bit geometries and the boreholes which they generate [25].

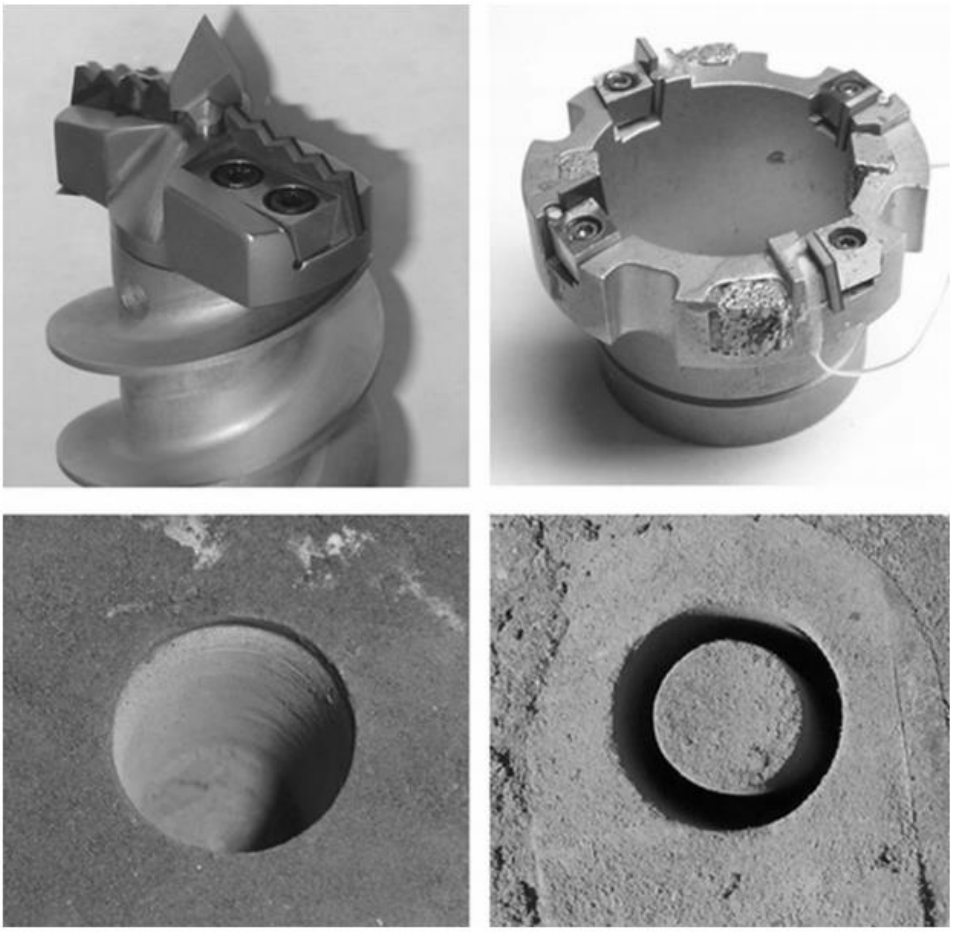

**Figure 16: Full faced rotary drill bit and borehole (L) and coring bit and borehole (R)** *[25]*.

## 3.2 Challenges of Planetary Drilling

As the cadence of landed robotic missions has increased in recent years, the knowledge and know-how accrued has provided mission planners with confidence in the development of ever-more capable systems for deployment on future missions. However, while past mission successes embolden mission planners, the perilous nature of spaceflight is such that past successes cannot be taken for granted. Furthermore, the nature of success is such that future missions may strive to achieve ever more ambitious goals, increasing the risk. This paradigm may also be applicable to the task of subsurface sampling which has seen some early success, though challenges remain as mankind strives to explore to ever greater depths.

The challenge of robotically extracting samples of a planetary subsurface invariably requires a degree of precise robotic manipulation in order to accomplish the task. While teleoperation may be an option for lunar missions, this approach is simply impossible for missions which seek to explore the outer Solar System. The substantial distance between Earth and Mars ensures that one way light speed delays of between 4 minutes at closest approach and up to 24 minutes are foreseeable. To this end, robotic manipulation beyond the

simplest operations requires a high degree of closed-loop control in the absence of a human in the loop. The task of drilling without prior knowledge of the physical properties of the target terrain ensures that the sampling system must be capable of autonomously adjusting the rate at which the system progresses in order to prevent faults associated with overzealous advance such as choking, or those aligned with underperformance which may lead to the exceedance of the maximum allowable weight on bit. Accomplishing this level of autonomous control is inherently challenging and the fact that most missions typically seek to explore new locations, utilising new technologies, means there may be a number of 'unknown-unknowns' which may complicate the implementation of complex control algorithms.

Perhaps the single most challenging aspect of designing hardware for planetary drilling missions is the uncertainty in the terrain which is to be targeted. Although a great deal can be established from orbital imagery and other forms of remote sensing, including the estimation of water content [26, 27], the composition of the material to be sampled often remains unknown until close inspection or the commencement of sampling activities. In order to design a tool which is capable of sampling an array of materials, the designer must balance the necessary trade-off of system requirements careful, factoring in worst case scenarios. This task is further complicated by the fact that, while certain materials may share certain physical properties, the approach required to drill each material may be quite different. It is for this reason that the optimisation process of planetary drilling systems is inherently difficult.

An example of such a problem surrounds the need for the sampling system to penetrate material which may be exceptionally hard, such as igneous rock or cryogenically frozen water-bound terrain. While these materials share similar uniaxial compressive strengths, there are few physical similarities beyond this. The approach required to successfully penetrate each of these materials is inherently different due to the water content of the latter material and the type of cuttings which will be produced by each. The importance of the cuttings removal element of the drilling process is of critical importance and cannot be overlooked. To this end, new systems must be capable of removing drilled cuttings from the borehole efficiently in order to facilitate the continued progress of the drill bit through the terrain. While hard materials present a challenge in the breaking of the formation, the low rate of progress and the coarse cuttings typically produced are typically accommodated by auger removal with relative ease. Conversely, the application of a drilling system into terrain which is softer and more easily broken may result in extremely high rates of progress. When combined with the knowledge that soft terrain often exhibits spoil behaviour which tends to

be ‘fluffier’ and finer grained, the burden on the auger may be such that the cuttings throughput rate is higher than that which can be accepted by the auger. In such cases, a phenomenon known as choking may be exhibited, as depicted in Figure 17.

**Figure 17: Example of auger choking caused by excessive input of fluffy, fine grained cuttings. Further spoil clearance is impossible as an impasse has been created by an over-accumulation of cuttings.**

During choking events, the flutes of the auger become filled with cuttings such that pressure exerted on the top, bottom and inside of the flute exceeds that which is being exerted on the borehole wall. The resulting friction prohibits the movement of the cuttings upwards, resulting in a cessation of cuttings ejection from the borehole. Choking is typically indicated through a sudden reduction in the rate of progress seen, while the auger power remains unchanged or increases. Once an auger has choked it is somewhat difficult to clear. Typical strategies include raising the drill bit from within the borehole and rotating it, and the addition of percussion may further aid the clearing process by loosening reconsolidated spoil. The prevention of choking faults may be a more robust strategy, thus any system should be

designed such that rate of progress bounds can be implemented to prevent the over-production of cuttings.

Perhaps the most pertinent of the issues facing the implementation of sampling systems in planetary exploration settings is that of power availability. Robotic landers and rovers typically generate electrical power through one of two means: photovoltaic solar arrays or through the use of a nuclear source such as a Radioisotope Thermal Generator (RTG). Solar arrays benefit from substantial flight heritage and few barriers to implementation. Such systems are also low resource, reducing system mass. On the other hand, as arrays are typically deployed from a stowed position upon landing, the mechanism required to deploy the array (explosive bolts, for example) often presents a possible single-point failure, meaning that the success of the mission may hinge on the successful deployment of the array. In order to maximise the deployable surface area, thus maximising the power available to the spacecraft, solar arrays may be stored in a concertina-like geometry, reducing the volume envelope required during the interplanetary stage of flight. Figure 18 presents the successful deployment of one of the solar arrays of the NASA InSight mission. Note the complex geometry used. Furthermore, the physical laws governing solar intensity are dominated by an inverse square law of distance. This requires solar arrays to be oversized for planetary applications in comparison to terrestrial applications. Arrays may be vulnerable to aeolian effects and anomalies such as dust storms on the Martian surface further increases the risk of arrays failing to produce sufficient power for the mission operations foreseen.

While the design of RTGs ensures a predictable, long lasting source of power which is available during periods of darkness or occultation, the size, mass, and complexity, alongside the cost and human risk factors associated with their implementation, ensures that such systems are primarily reserved for ‘flagship’ missions. Making use of the thermoelectric Seebeck Effect, the heat emitted during the decay of a radioactive source is harnessed to produce power, but there are further risks associated with the operations of a permanent heat source at a planetary surface. Given that certain missions may wish to visit the so-called ‘Special Areas of Interest’ such as the ice-bearing regions of Mars which are considered to be optimal locations in the search for life, the use of RTGs poses a contamination threat should the spacecraft crash land.

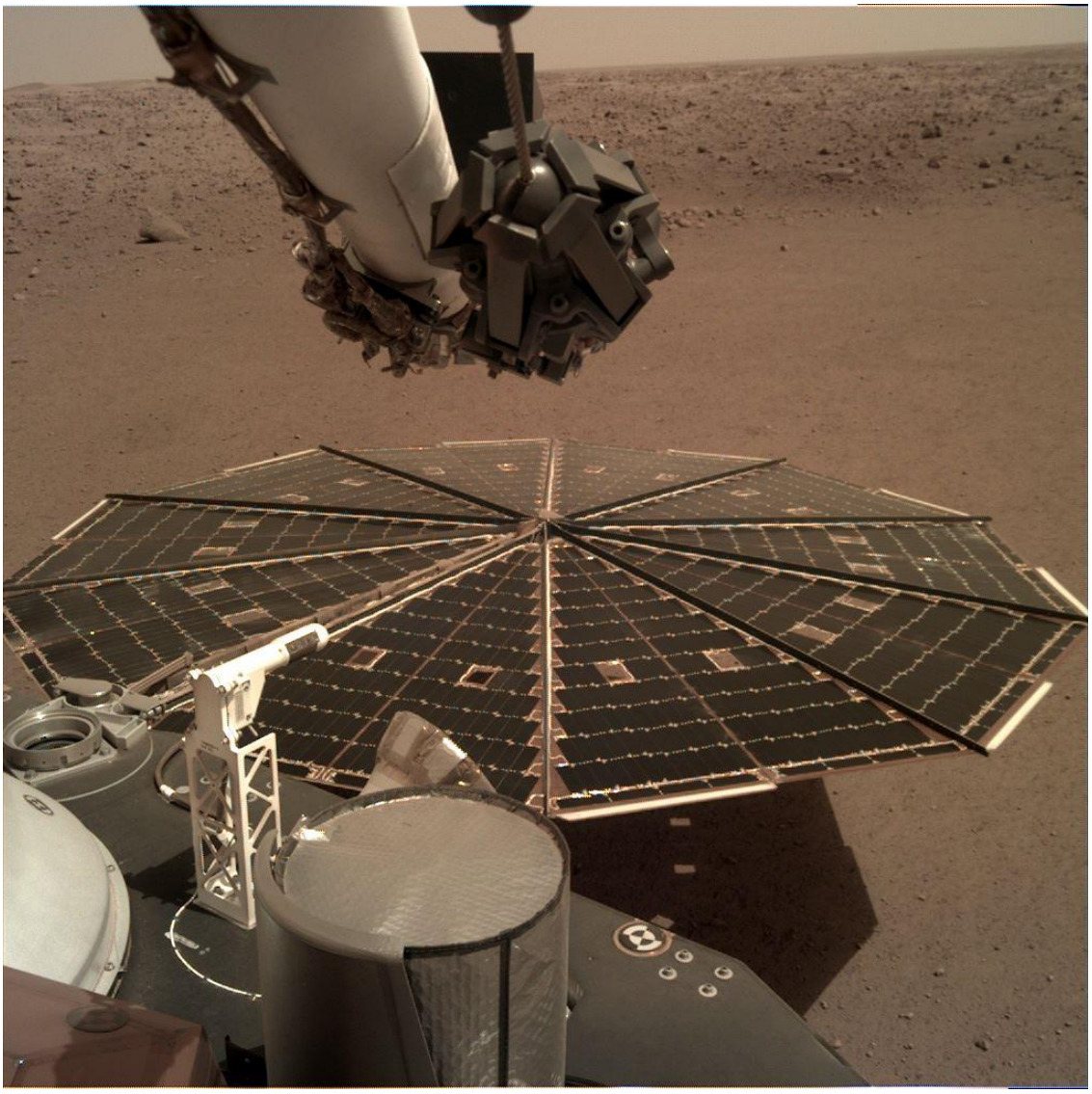

**Figure 18: NASA InSight solar array deployment on Mars. Courtesy: NASA/JPL-Caltech**

# 3.3 Drilling Techniques

## 3.3.1 Rotary Drilling

In order to penetrate the terrain, the mission designer may seek to make use of a particular drilling style, dependent on the class of landed vehicle utilised, in order to accomplish the key mission objectives. Typical planetary drilling systems are often either purely rotary, whereby the action of the overhead force applied to the cutting teeth of the drill bit in combination with the torque used to drive the bit in rotation acts to remove material from the face of the target terrain by shear failure and crushing, schematically depicted in Figure 19 [25].

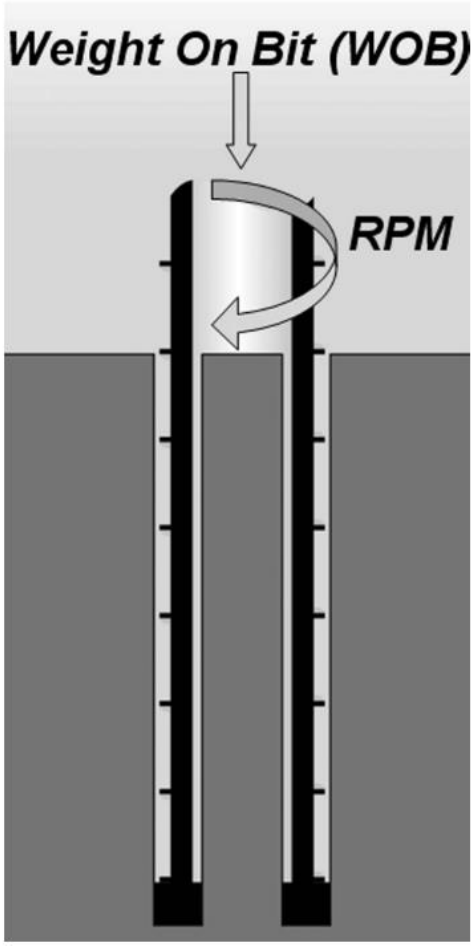


**Figure 19: Schematic of the rotary drilling process whereby the application of Weight on Bit and Torque/RPM act to break the formation and remove spoil** *[25]*.

Figure 20 [28] examines the mechanics of the rotary drilling process in the case where the cutters used are sharp. *Fs* denotes the forward force applied to the cutter as a result of bit rotation, while $F_n$ corresponds to the weight on bit required to keep the sharp edge of the cutter in contact with the rock face.

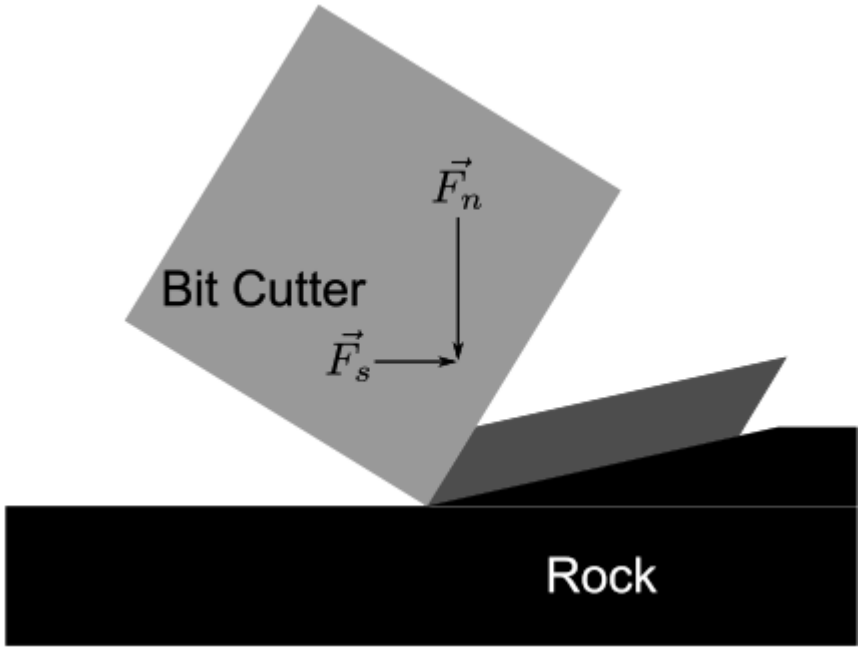


**Figure 20: Mechanics of a rotary drill bit assuming a sharp cutting face. $F_s$ denotes the forward force resulting from the rotation of the drill bit, while $F_n$ denotes the weight on bit required to ensure the bit is engaged with the rock face.**

In order to penetrate the terrain, work is done as the cutting face is moved through a distance, *x*, fracturing the rock which is engaged along this cutting path. Equation 3.1 details the work done in penetrating the terrain using sharp cutting teeth.

In the case where the cutting teeth have partially blunted, the sharp cutting edge features a large, flat surface and a reduced sharp edge. Figure 21 details the mechanics of this case.

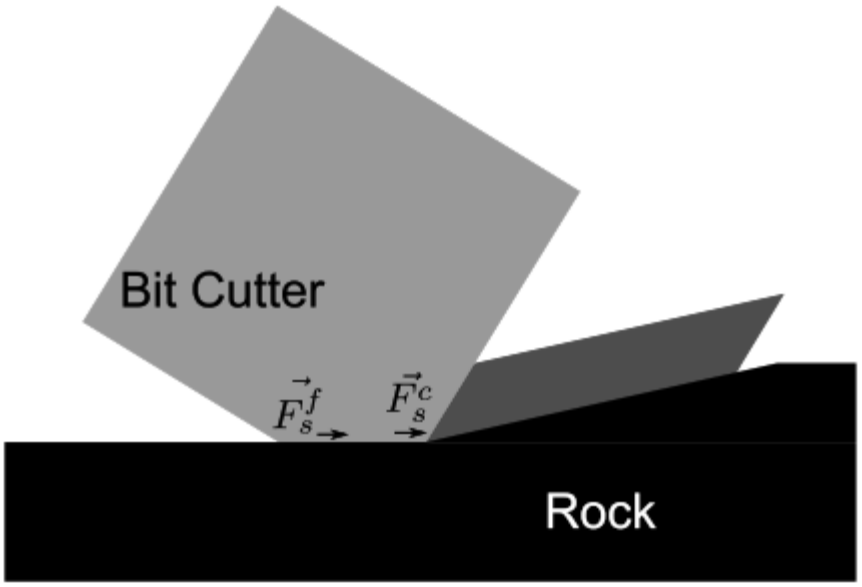


**Figure 21: Mechanics of a rotary drill bit assuming partially blunted cutting face. The forward force, $F_s$, is split and consists of $F_s^c$ at the sharp edge and $F_s^f$ at the surface which has been worn flat.**

The cutting force, $F_s$, is split into two components, $F_s^c$, the force at the cutting edge, and $F_s^f$, the frictional force incurred by the flat face. It is therefore possible to define the intrinsic specific energy, ε, for rotary drilling. The intrinsic specific energy differs from specific energy (SE), discussed later in this chapter, as the former does not include a frictional component, instead capturing only the work done in the breaking of the terrain. This element is introduced in Equation 3.2.

$$E = F_s x \qquad \text{Eqn. 3.1}$$

$$E = x\left(A\varepsilon + F_s^f\right) \qquad \text{Eqn. 3.2}$$

Equations 3.1 and 3.2 are combined as follows:

$$F_s x = x\left(A\varepsilon + F_s^f\right) \qquad \text{Eqn. 3.3}$$

$$(F_s^c + F_s^f)x = x\left(A\varepsilon + F_s^f\right) \qquad \text{Eqn. 3.4}$$

$$\varepsilon = \frac{F_s^c}{A} \qquad \text{Eqn. 3.5}$$

Thus, ε is not completely independent of the drill bit geometry, but it is independent of the properties of the cutting teeth. The particle size generated during the cutting process is a key feature of the intrinsic specific energy and also has an impact on the cuttings removal process required.

The cuttings which are generated are typically removed via the action of an auger (typically machined in to the drill bit wall) and delivered to the surface for disposal or analysis by an instrument suite. The importance of spoil removal is easily overlooked but is in fact an essential part of the drilling process. In situations where spoil is ineffectively removed, there is a tendency for the spoil to accumulate at the bottom of the borehole where the action of the drilling acts to 'regrind' the material, breaking it in to ever smaller particles. In such cases, the build-up of fine-grained powder which are compressed by the drill forms a barrier and impedes further progress. The action of regrinding minimises the energy available for terrain breaking, further slowing the progress of the system.

Typical rotary system make use of cutting teeth which consist of either polycrystalline diamond (PCD) or tungsten carbide (WC) inserts which feature a sharp edge, angled towards the direction of rotation in order to effectively penetrate the terrain. A part reliance upon shear to breach the formation means that rotary bits are particularly prone to blunting, whereby the sharp edges of the bits are worn flat under the action of the drilling process. In order to compensate for the reduced sharpness, the drilling system may be required to increase the weight on bit delivered to the rock face – a strategy which is clearly limited in planetary settings. A gradual blunting of drilling teeth may also be misinterpreted as a drilling fault or a change in the terrain type being drilled leading to misinformation. In order to avoid this, the wear of drilling teeth should be well characterised for a variety of different terrain types before flight.

### 3.3.2 Rotary - Percussive Drilling

In applications where the weight on bit available or the total torque which can be provided is limited, a rotary-percussive drilling system may prove to be the most suitable option. Unlike rotary systems, which rely purely on a shearing-crushing action to penetrate the terrain, rotary-percussive systems make use of a hammering action applied to the drill bit in order to transmit a compressive wave through the material. It is for this reason that percussive drill bits may make use of typically blunt teeth made of tungsten carbide which act in a chiselling manner to fracture rock. The strength of a rock is in its ability to resist tension and compression failure, and rocks are typically more robust to compressive stresses than tensile

stresses. In fact, the tensile strength of a given rock may be as low as 10% of that noted in compression. Typically, most rock cutting techniques rely on the compressive failure of the rock due to the nature of the methods of penetration available, whereby compressive waves act to overstress the terrain target resulting in the formation of fractures and the subsequent breakdown of the terrain material.

Rock failure may be established analytically through an evaluation of the Coulomb-Mohr failure criteria [29]. It is stated that failure occurs in a rock formation when the local shear stress, $\tau$, is in excess of the sum of the cohesive resistance of the material, as defined by Equation 3.6. Shear stress increases with an increasing normal stress on the plane of failure. The criteria is dependent upon the normal stress, $\sigma$, the angle of internal friction, $\theta$, and the rock cohesion, $c$ (the y-intercept of the $\sigma - \tau$ plot).

$$\tau = \sigma \tan\theta + c \qquad \text{Eqn. 3.6}$$

Figure 22 presents an example of the criteria [28].

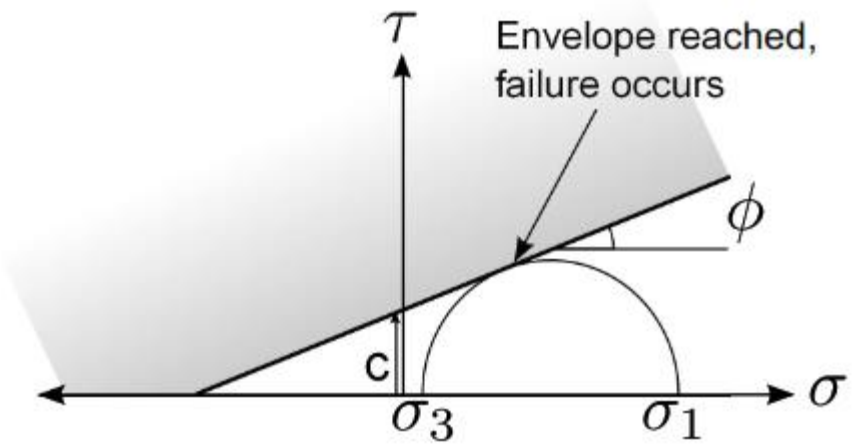


**Figure 22: Example of the Coulomb-Mohr failure criterion used to predict brittle rock failures where the local stresses exceed the line bounded by the overarching equation. Stresses extending into the grey region will result in a failure.**

In the example detailed, $\sigma_1$ and $\sigma_3$ represent the maximum and minimum normal stresses for a given load case, whereby the $\sigma_1$ refers to the compressive strength limit of a given rock sample and the confining stress is $\sigma_3$.s While the Coulomb-Mohr criterion provides a simple means of attributing failure to compressive and tensile failure, it becomes inaccurate when the failure envelope becomes curved, as in often the case for unconsolidated terrain.

The application of percussion to the drilling process has been proven to benefit the rate of penetration of drilling in situation where the target material is particularly hard, allowing the task of drilling to be accomplished more efficiently with less weight on bit required while reducing the total energy required [30].

The use of hammering when penetrating hard material is particularly effective due to the nature of the way in which compressive waves act to cause a fracture of the target material. In order to invoke a failure, the elastic limit of the target must be exceeded. As stated in [28], energy transmitted to the target material may be converted in to either heat (generally considered to be wasteful) and plastic deformation, or may be lost through the elasticity of the target rock and the subsequent transmittance of a seismic wave through the rock target into the surrounding terrain or reflected back through the drill bit. As detailed in Figure 23, the balance of the energy usage during percussive drilling is dependent upon the hardness of the target material. In the case of hard targets, the majority of the energy will be utilised in the heating and plastic deformation of the material with a smaller portion of the energy use attributed to the loss of energy through seismic transmittance. In the case of soft material, the reverse is true, resulting in far greater losses and less plastic deformation.

While the application of percussive hammering when drilling soft target material typically results in an inefficient use of the energy allocated to the generation of percussion, the reduced strength of such material may still result in its failure. While this may result in a wasteful use of drilling power, the application of percussion to hard material targets may result in target depth being achieved up to seven times faster than with the rotary drilling alone [31]. As any extra power used in the generation of percussion may reduce the overall time required to drill, there may be a subsequent reduction in the total energy consumed. This counterintuitive result may be utilised in the development of control systems which monitor the progress of drilling operations, allowing a solution to be developed which ensures percussion is only used in certain circumstances. Implementing such a solution ensures that the parameter most limited, be it available power, energy, weight on bit or the need to reduce the percussive load on the target terrain is prioritised.

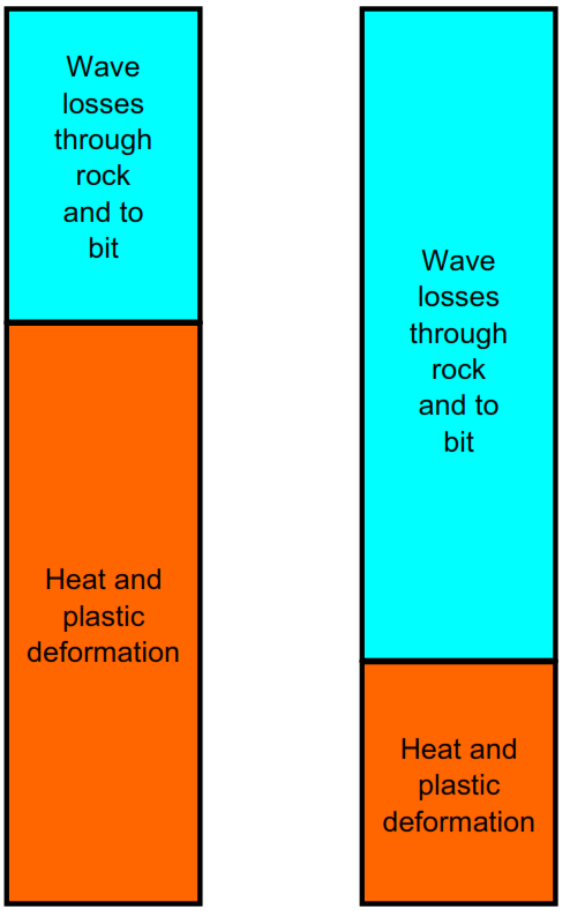


**Figure 23: Energy conversion of compressive wave travelling through hard materials (left) and soft material (right)** *[28]*.

### 3.3.3 Cutting Fluids

Cutting fluids are common in industrial terrestrial drilling systems and fulfil two main roles: cooling of the bit-rock interface during drilling operations which produce excessive heat, and the flushing of cuttings from the borehole. Typically, rotary drilling rigs at a high feed rate/weight on bit produce excessive downhole heat as a by-product of the friction-led shearing of the terrain, thus the application of cutting fluids is most common in such cases. While the use of cutting fluids may have a role within certain extreme environment drilling scenarios, the implementation of both hydraulic and pneumatic fluids presents challenges. In terrestrial applications, pressure losses over deep borehole lengths may reduce the effectiveness of pneumatic borehole clearance (without excessive power consumption from the surface-based compressor) and liquid cutting agents may prove logistically difficult to move to the field location and are often environmentally damaging. Off-world applications are limited by the need to either transport gaseous/liquid phase agents to the mission location, and unwanted phase changes as a result of low atmospheric pressures makes the implementation of such agents inherently challenging. While pneumatic compression of local atmospheres may be possible on-site, those terrestrial bodies which do possess

atmospheres typically offer low pressures and thus requiring increased power levels to generate sufficiently pressurised gas for flushing (Titan, a moon of Saturn, may be the exception to this rule, however). To this end, the use of rotary-percussive systems, whereby the fracturing of the terrain is accomplished through the application of percussion, and spoil is cleared via the use of auger rotation, may prove to be the solution to circumvent the need for cutting fluids.

## 3.4 Drilling Power

The power required to drill using conventional rotary or rotary-percussive techniques can be split in to two areas: the power required to break the target terrain and the power required to remove the drilled cuttings from the bottom of the borehole. While the power required to remove cuttings is somewhat difficult to calculate accurately and tends to increase with depth, Equations 3.6-3.8 [25] examine the power required to break the terrain formation. The total power demanded by a drilling system in accomplishing this task can be subdivided in to a further two elements: the power required in order to physically pulverise the rock (Eqn. 3.7) and the power required to overcome the frictional forces, μ, caused by the contact of the drill bit on the rock target (Eqn. 3.8). It is of note that in this context, R refers to an average tooth radius of the drill bit in question and δ refers to the depth cut per revolution of the drill bit. As is detailed in Equation 3.9, the energy required to penetrate the terrain is directly proportional to the uniaxial compressive strength (UCS) of the rock target. As it may not be possible to predetermine the strength of the terrain to be drilled, it is pertinent that the system be designed to penetrate even the strongest rock formations.

$$\text{Power}_{\text{Total}} = \text{Power}_{\text{Cutting}} + \text{Power}_{\text{Friction}} \qquad \text{(Eqn. 3.7)}$$

$$\text{Power}_{\text{Friction}} = T * \omega \qquad \text{(Eqn. 3.8)}$$
$$= (\mu * WOB * R) * \left[\frac{2\pi}{60} * RPM\right]$$

$$\text{Power}_{\text{cutting}} = \text{Work}_{\text{per revolution}} * \frac{\text{RPM}}{60} \qquad \text{(Eqn. 3.9)}$$

$$= (\text{UCS} * \text{Area} * \delta) * \frac{\text{RPM}}{60}$$

Analysis of these equations shows a correlation between the frontal area of the drill bit and the power required to penetrate the terrain. It is for this reason that, in order to establish the performance of dissimilar drill bit geometries, a useful metric known as specific energy may be used, as detailed in Equation 3.10.

$$Specific\ Energy = \frac{Power}{Rate\ of\ Penetration * Cut\ Area} \quad \text{(Eqn. 3.10)}$$

Specific energy, SE, measured in $MJ/m^3$, also provides a means of comparing the physical properties of different terrain types by keeping variables such as the geometry of the drill bit and the rate of penetration constant.

## 3.5 Spoil Removal Techniques

As has been previously discussed, the challenge of planetary drilling is more complex than the task of breaking the rock target alone. In fact, without the ability to remove the spoil produced by the rock drilling, progress will stall quickly.

Multiple spoil removal strategies exist and the use of any one (or multiple) of these is dependent upon the constraints imposed upon the drill system and the environment in which it shall operate. Perhaps the most commonly utilised spoil removal strategy involves the use of an augering drill bit. In the augering process, dry granular cuttings are conveyed from the bottom of the borehole to the surface by a sliding action over the helical flutes (also known as scrolls) of the auger. The rotation of the auger causes the spoil to be accelerated towards the outside of the spiral by centripetal force where, in the ideal circumstance, the spoil adheres to the borehole surface and is forced vertically upwards by the rotation of the flutes. Figure 24 schematically depicts the key parameters in the design on an auger [32].

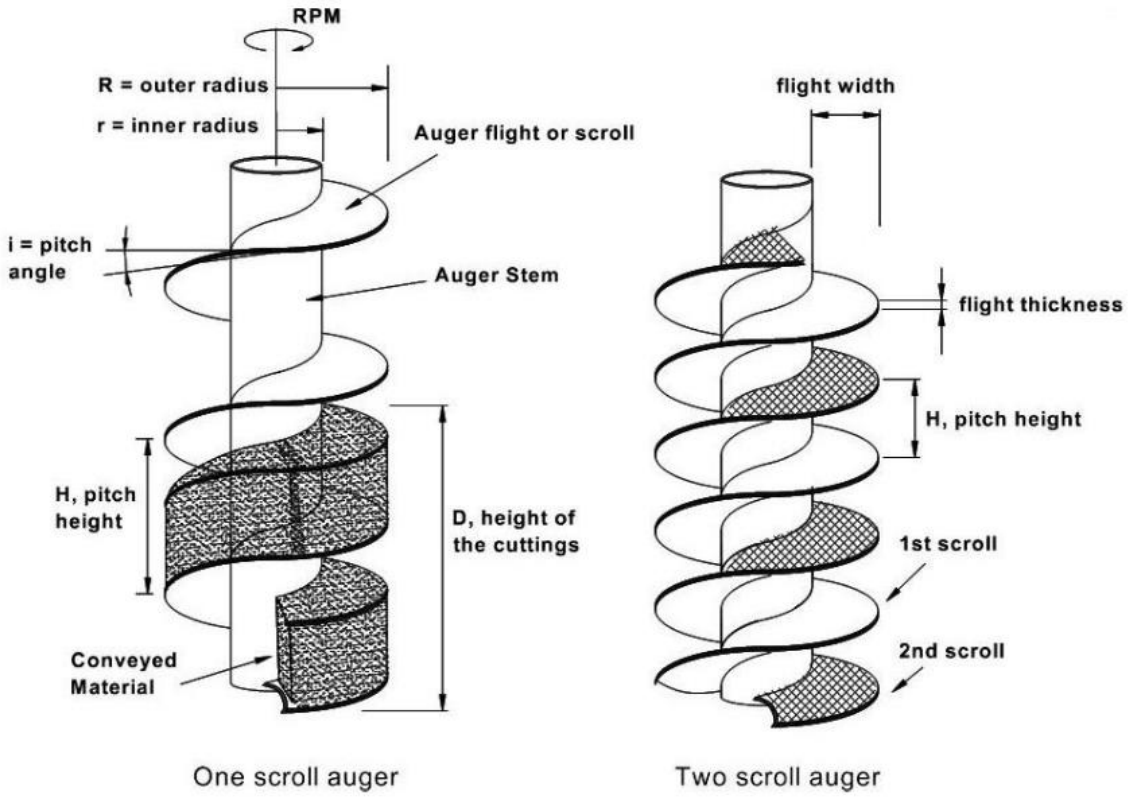


**Figure 24: Schematic of typical one and two scroll augers** *[32]*.

The mechanics of the augering process are somewhat complex and are as detailed in Equation 3.11. The minimum rotational speed, N, (in RPM) required to commence the conveying of material up the auger is dependent upon the gravitational acceleration of the planetary body, g, the diameter of the drill bit used, D, the angle of inclination of the helix, *i*, the coefficient of friction between the particulate spoil and the auger scroll, $\mu_s$, and the coefficient of friction between the spoil and the borehole wall, $\mu_w$.

$$N = \frac{30}{\pi}\sqrt{\frac{2g}{D}\frac{\tan(i)+\mu_s}{\mu_w}} \qquad \text{(Eqn. 3.11)}$$

While the majority of the parameters in the equation are known or can be set by the system designer, it is incredibly difficult to establish the coefficients of friction found during augering due to the unknown nature of the target terrain which may be encountered during planetary drilling scenarios and the fact that there may be a the loss of the oxide layer on the surface scroll (which is unlikely to be replenished) [33]. To this end, the design of the auger geometry requires a trade-off between the angle of inclination of the auger helix and the rotary speed which can be achieved by the mechanics of the complete system. As the design process of drilling systems typically favours the torque available at the drill bit in order to

optimise the rotary drilling capability or provide margin in case of excessive auger friction, gearing may be implemented which reduces the maximum rotational speed which can be achieved. In order to maximise the torque available while minimising the auger starting speed, the designer may wish to use a plot such as that detailed in Figure 25, whereby the auger starting speed can be established for a range of realistic friction coefficients. This ensures that the auger is capable of producing the necessary lifting action while maximising the performance of the drilling system given that planetary drilling system often utilise drill bits which are as narrow as possible, reducing the power required and time to drill to depth. As highlighted in [32], performing drilling operations at non-optimal auger speeds will result in a significant increase in the torque demanded by the drilling system and the non-optimal movement of spoil. Figure 26 details a particular case whereby the auger torque was recorded for drilling operations at a range of auger speeds, ranging from 50 – 200 RPM. While the torque note at 50 RPM approaches 10 Nm, the torque value for auger speeds in the range of 200 RPM appear to be approaching an asymptote at 0.5 Nm, suggesting that this higher speed is the design speed for the auger geometry in question. Hence, operating at a higher speed will reduce the power burden on the system and improve augering effectiveness.

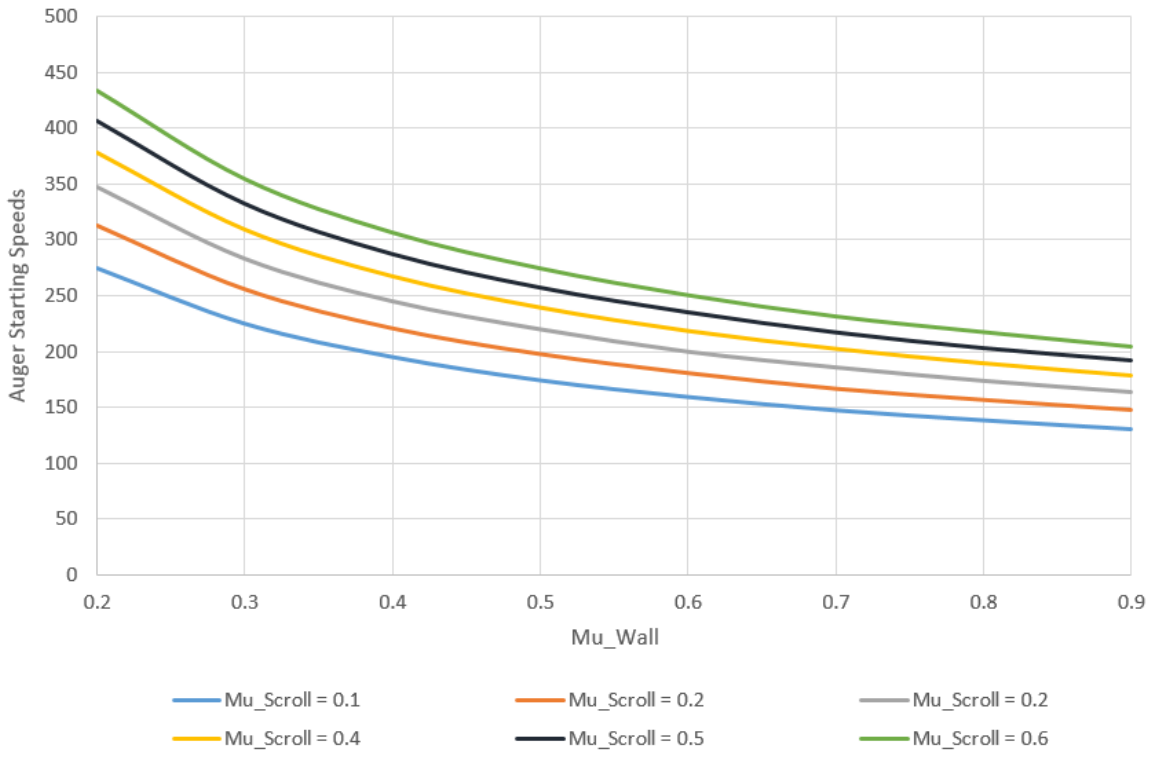


**Figure 25: Plot of auger starting speeds for a range of friction coefficients.**

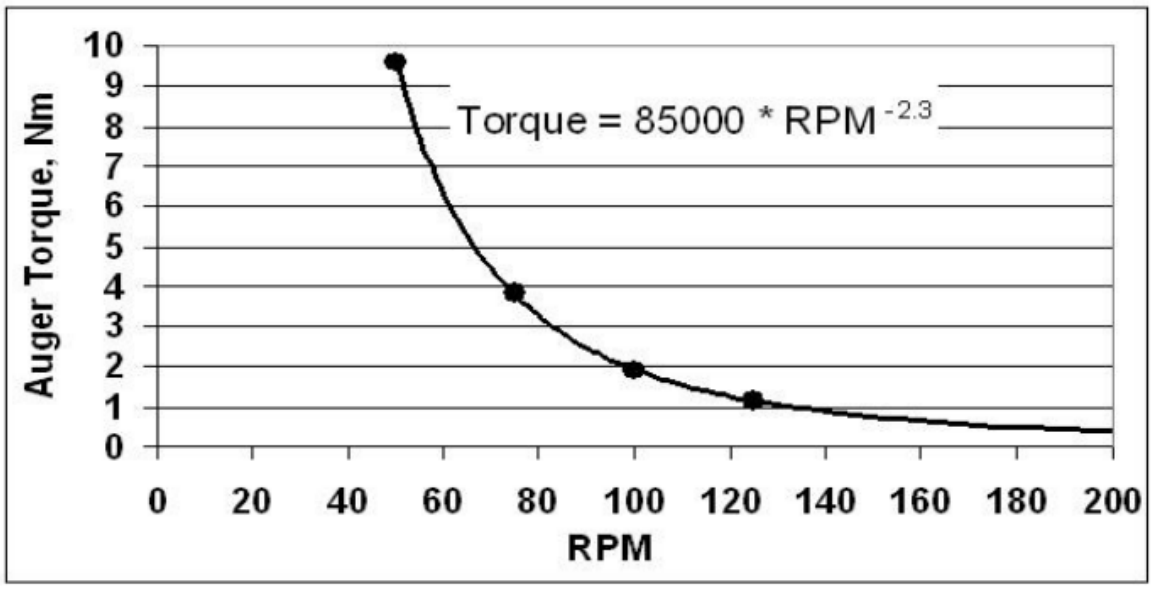


**Figure 26: Augering over a range of rotational speeds. The auger torque demand is shown to significantly decrease as the auger rotational speed increases, suggesting that the design speed of the system is approximately 200 RPM** *[32]***.**

An alternative means of spoil removal comes in the form of gas blasting whereby the release and subsequent expansion of gas at the base of the borehole acts to eject spoil upwards, thus clearing the bit-rock interface of cuttings. The gas in question may be provided by one or more sources. Pressurised gas may be carried by the host spacecraft, generated in-situ by compression of the planetary atmosphere, or other means (discussed in more detail in Section 5.12.6).

The use of pressurised gas as a means of clearing spoil is particularly suitable in a planetary setting due to the near-vacuum conditions which are present in-situ. This ensures that the expansion ratio of the gas is high, optimising the efficiency of spoil flushing. Experiments performed at Mars pressure suggest that for realistic spoil particle sizes and quantities, differential pressures as low as 3300 Pa (at an ambient pressure of 670 Pa) could achieve an acceptable level of spoil clearance. Figure 27 depicts the evacuation of spoil from the simulated borehole during laboratory experimentation. The ejection of the spoil from the simulated borehole is shown to be highly energetic, even at modest differential pressures [34].

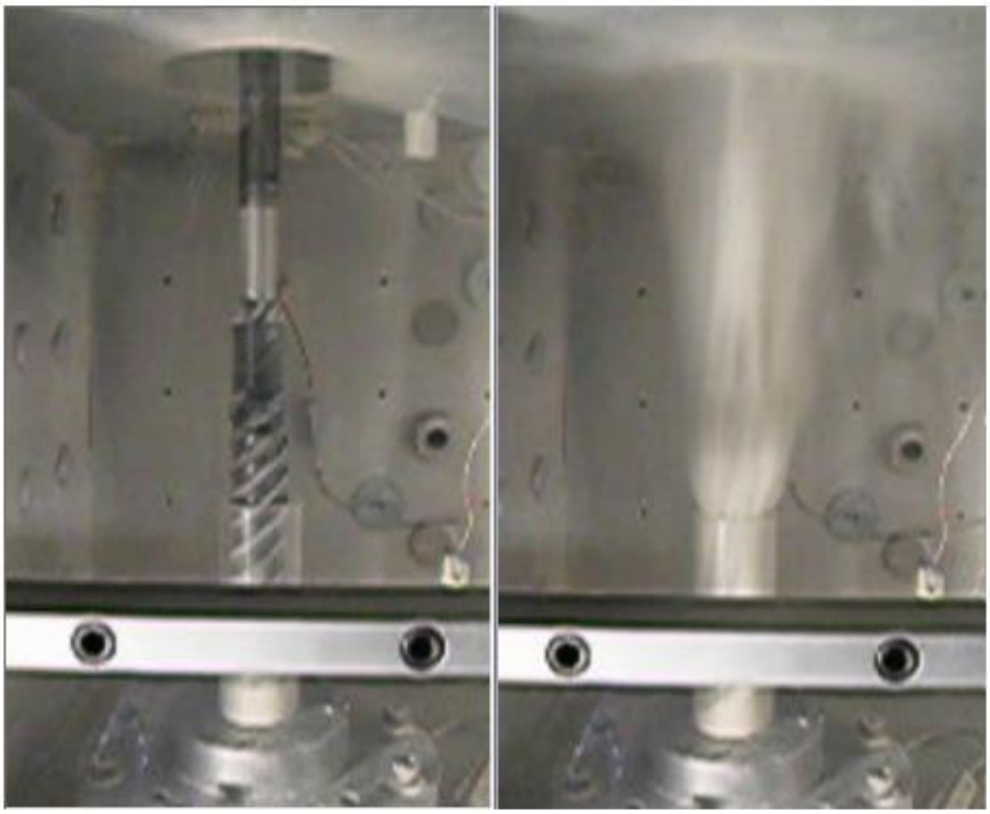

**Figure 27: Evacuation of simulated borehole using a differential pressure of 3300 Pa at an ambient pressure of 670 Pa** *[34]*

# Chapter 4

# Development of the Ultrasonic Planetary Core Drill (UPCD)

## 4.1 Ultrasonic-Percussive Drilling Technique Overview

As discussed in previous chapters, the task of drilling hard formations may be aided by the addition of percussion to conventional rotary drilling. The implementation of a hammering actuator to the planetary drilling system is clearly limited by the need to ensure that such systems are low resource, minimising the power, mass, volume and complexity of the percussive device. It is for this reason that more conventional hammer actuators driven by pneumatics or hydraulics, for example, are excluded from consideration.

The ultrasonic-percussive drilling technique, conceived by engineers at the NASA Jet Propulsion Laboratory (JPL), provides a means of percussion generation while minimising the resource burden on the mission [35]. The fundamental principle of the system involves an energy and momentum exchange between an ultrasonic actuator and a free mass, allowing the free mass to accumulate energy generated by the ultrasonic actuator in order to generate a macro-scale free mass displacement from micro-scale vibrations. Ultrasonic-percussive systems are exceptionally low resource, benefiting from the ability to penetrate terrain with overhead forces as low at 5 - 10 N. In fact, the self-weight of the system is often sufficient to drive the drill forward and ensure the terrain is fully engaged at all times. Furthermore, a total electrical power demand in the range of 10 – 50 W is achievable ensuring compatibility with a broad range of planetary missions.

### 4.1.1 Ultrasonic Actuator

The ultrasonic actuator must be designed in such a way that the energy transfer between the actuator and the free mass is maximised while ensuring that vibrations within the ultrasonic range are maintained. The actuator acts to convert an electrical signal in to a

mechanical (vibrational) output via the use of a piezoelectric (PZT) stack bolted to a resonant horn. Figure 28 depicts a schematic of a typical rock drilling system [36].

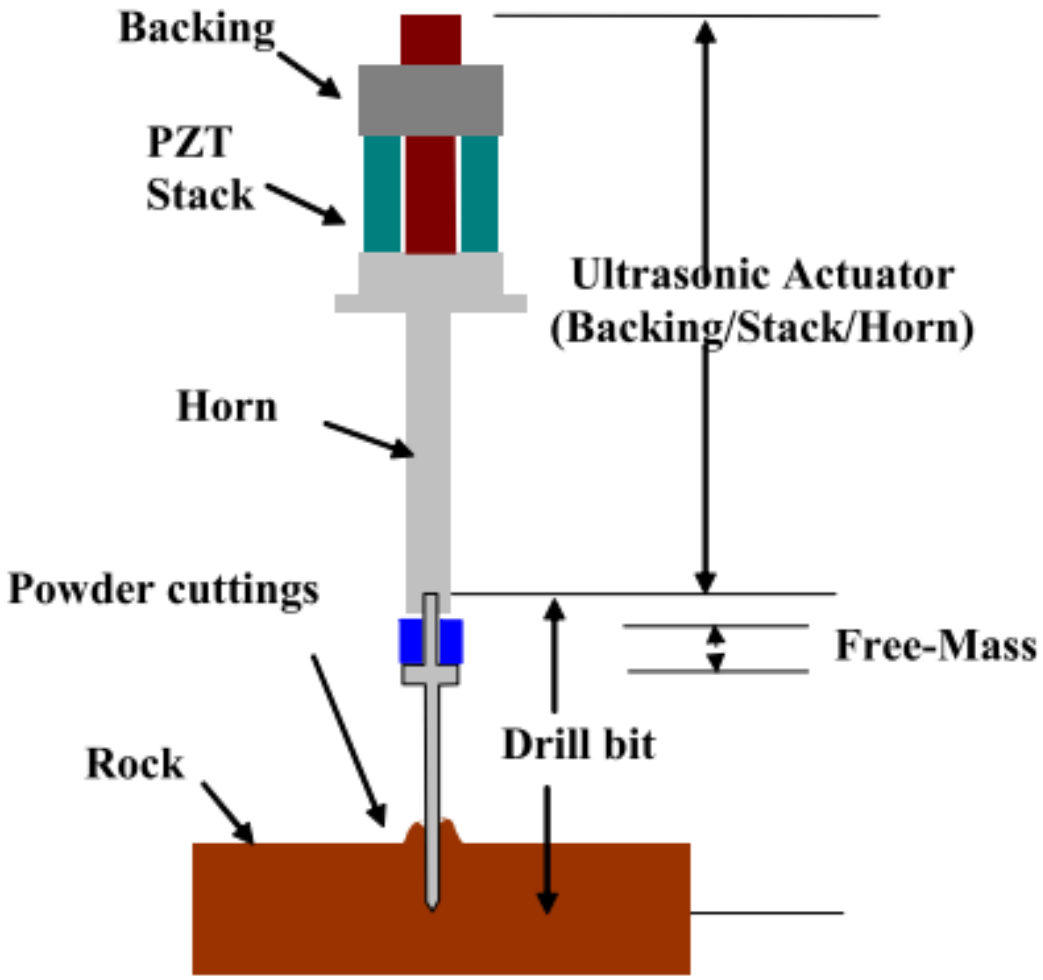


**Figure 28: Ultrasonic-Percussive Drilling Schematic** *[36]*.

As the name suggests, the vibration produced by the ultrasonic stack is typically at or above the ultrasonic threshold of 20 kHz while the output amplitude may be on the order of 1-20 μm. In order to increase the useable amplitude of the vibration, a specifically-tuned ultrasonic horn is bolted to the PZT stack. Figure 29 details multiple geometries of ultrasonic horns which may be implemented in such a system [37].

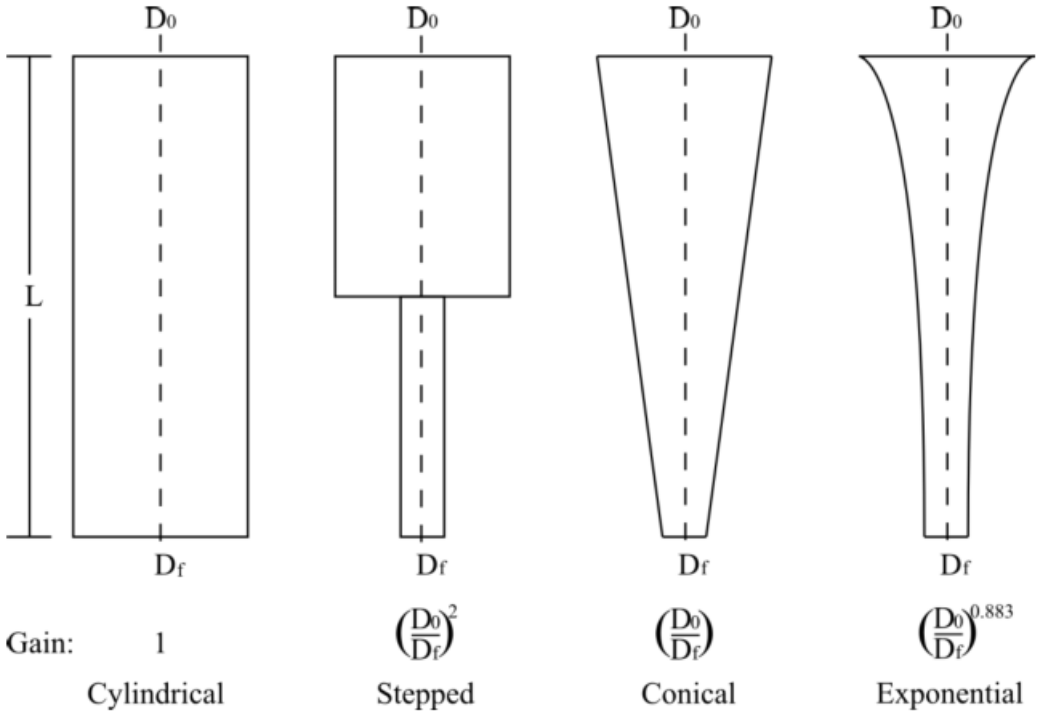


**Figure 29: Typical ultrasonic horn geometries** *[37]*.

The multiplication of the vibrational amplitude generated in the PZT stacks is highlighted in Figure 29. This multiplier, or 'gain', is directly related to the geometry of the horn and allows the amplitude of the vibration generated by the piezoceramic material to be amplified. The amplitude of the useable vibration at the tip of the horn typically increases with a decrease in the cross sectional area. Through this means, a typical piezo stack output vibration of 5 µm may readily be increased by a factor of eight or ten to 50 µm, thus increasing the useable energy at the tip of the horn. The stepped horn is shown to provide the highest gain of those depicted followed by the conical horn and then the exponential horn. While the cylindrical horn has no gain, horns of this type may still find use as a means of ensuring that the wavelength of the vibration is maintained through the device. It is critical that any ultrasonic horn must allow the ultrasonic wave to transfer through the device such that the peak of the wave-front occurs at the tip of the horn. This ensures that the energy delivered to the tip is maximised. Figure 30 depicts the design of a typical ultrasonic actuator with the waveform overlaid. The implementation of a given horn geometry is typically led by system-specific constraints though there may be fatigue life benefits of opting for a horn which has a less extreme transition than the stepped variety. Horns are typically of metal construction, though the robustness required means that typical materials include steel and titanium, with the latter often preferential due to the low acoustical losses it incurs.

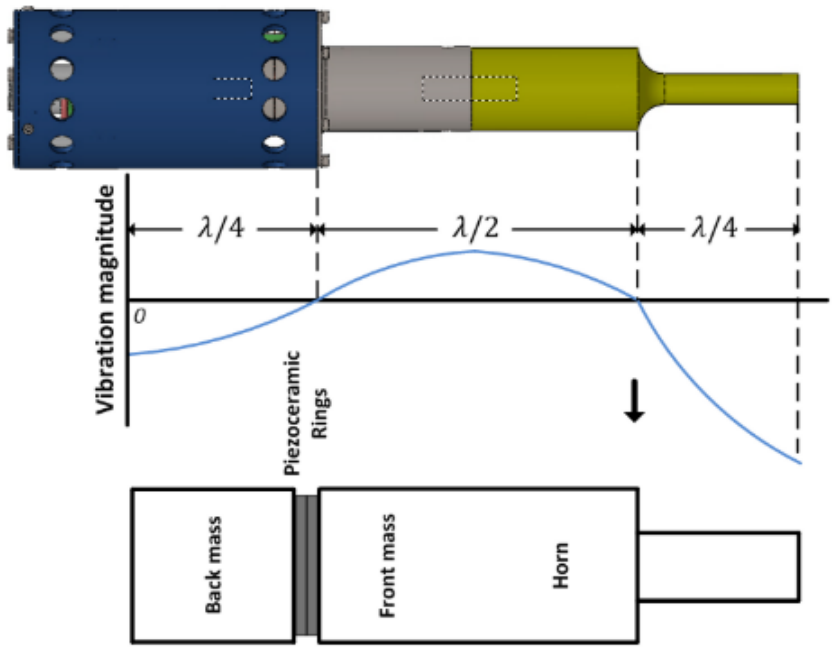


**Figure 30: Full wavelength ultrasonic actuator with waveform overlaid. Note, the tip of the horn is located at the amplitude maxima, ensuring efficient transfer of vibrational energy** *[38]*.

### 4.1.2 Free Mass and Percussive Power

In order to transfer the ultrasonic energy to the terrain, a free mass is added which resonates between the tip of the horn and the drill bit. Through an accumulation of energy, the free mass resonates with a frequency of up to 1000 Hz, though experiments performed at Glasgow suggest that more typical values may be in the range 100-300 Hz [38]. The form of the free mass is variable though there are advantages and disadvantages to each geometry which may be used. Perhaps the most conventional geometry is the stainless steel ball bearing. While the ball bearings are unlikely to be damaged during drilling operations, the point-contact engagement of the ball bearing with the anvil/drill bit means that the high stresses generated upon hammering may damage both the horn tip and the anvil. Figure 31 presents an example of damage inflicted upon these elements of the design.

**Figure 31: Damage to the anvil-bit (L) and the horn tip (R) caused by free mass.**

In order to minimise the damage caused by the free mass on its points of contact, a free mass with an increased surface area may ensure that the stress levels upon contact are reduced. Experimentation with toroidal free masses has shown promise as an alternative, though there are problems associated with the materials used. In certain cases, post-test review of the free masses has revealed evidence of plastic deformation of the masses and even failure due to excessive fretting erosion. While this is likely an attribute of the material choices and may be rectifiable with alternative choices, early failure of the free mass is a limiting factor in the implementation of the ultrasonic-percussive technique.

The energy transferrable by the free mass is dependent upon the geometry of the mass used and the speed at which it travels. Given that typical free masses used within these systems may be in the range of 5-10 g, and experiments which have made use of high speed cameras have noted velocities of approximately 6 m/s, percussive energies in the range of 0.1 - 0.18 J are possible. To this end, percussive powers in the range of 10 – 54 Ware foreseeable, though the efficiency of the energy transfer is uncertain.

## 4.2 UPCD Development Overview

Building upon earlier work performed at the University of Glasgow [39] whereby a prototype ultrasonic-percussive drill was developed and tested at Mt. Teide, Tenerife, Spain, the Ultrasonic Planetary Core Drill (UPCD) project saw the development of a drilling and sampling system with a focus on a Mars Sample Return (MSR) objective. Funded by a European Commission Framework 7 grant, the project saw a consortium of European organisations, led by the University of Glasgow, collaborate to produce a system which was capable of autonomously assembling a drill string consisting of more than three drill bits, before drilling to depth in order to obtain core samples. The core-containing drill bits were then cached in individual silos. The project culminated in a field test at Coal Nunatak (73° S 68° W), Antarctica, during the summer 2016/2017 season, supported by the British Antarctic Survey (BAS).

The University of Glasgow was tasked with delivering a number of work packages including the development of the drill tool, the sample caching carousel and the drill bit exchange clamping mechanism used for constraining bits during assembly and disassembly operations. Aside from hardware development, the concept of operations which governed the approach to the drilling process, and thus heavily influenced the design of the hardware, was developed and a system of autonomous control was implemented.

## 4.3 UPCD Mechanical Architecture

The complete UPCD mechanical architecture consisted of five main elements: the ultrasonic-percussive drill tool, the sample caching carousel, the drill bit exchange clamp, the Z-axis deployer mechanism and the electronics and control module [40]. A table of the key system properties is as shown in Table 2.

| System Mass - kg | System Dimensions (W x B x H) - m | Ave. Max System Power - W |
|---|---|---|
| 25 | 0.35 x 0.4 x 1.25 | 60 |

**Table 2: UPCD system properties overview**

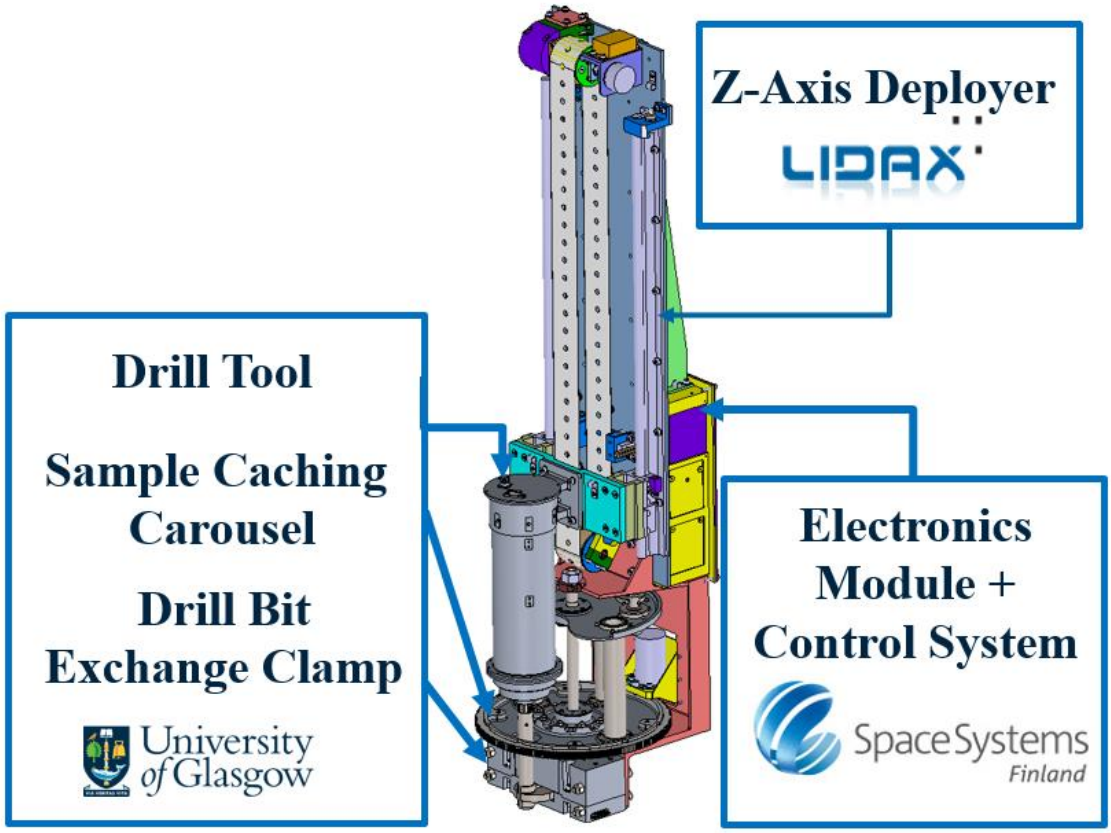


**Figure 32: UPCD Mechanical Architecture. Height of terrain clamp is 75 mm, for scaling reference.**

In order to ensure compatibility with potential future mission scenarios, efforts were made to minimise the envelope of the complete architecture by reducing the volume and mass wherever possible.

## 4.4 Drill Tool Design

The design of the drilling mechanism of the UPCD system involved the encapsulation of an ultrasonic transducer within a set of front and rear springs. The use of springs within the design had multiple benefits: contact with the free mass could be assured even in free-air operation, allowing the drill tool to be percussed without engaging the rock target, and the springs would provide a degree of slack within the system which would ease the process of engaging and disengaging drill bits during the drill string assembly and disassembly phases of drilling operations.

Figure 33 depicts a cutaway model of the drill tool developed for the UPCD project [41]. The ultrasonic transducer used was an off-the-shelf Sonic Systems P500 based upon the Langevin sandwich-type architecture. The transducer is adjoined to a carriage by a flange at the nodal flange allowing the system to slide axially within the drill casing (thus loading against the dual springs) without disrupting the resonant frequency of the stepped ultrasonic horn. The full-wavelength P500 transducer was chosen based upon its heritage use within previous systems [39], though a half-wavelength model, the P100, was also an option. While the P100 offered substantial mass savings over the bulkier P500 with a mass of 414 g compared to almost 840 g, concerns regarding the performance of the smaller system at the time of development meant that the P500 was given precedence. A later comparative analysis of the performance of each system revealed that this concern was more complex than first envisaged. As detailed in Figure 34, the full wavelength device tends to produce higher effective impulses, likely due to the more substantial mass of the system. On the other hand, Figure 35 reveals very little discrepancy between the rates of progress seen when drilling through three rock types. As the single objective of the drilling system is to efficiently penetrate the terrain target, it is the rate of progress which can be achieved for a given system mass which may take precedence. To this end, a marginal reduction in overall drilling performance for a mass saving of 50% may prove to be a worthwhile trade-off in later iterations of the design.

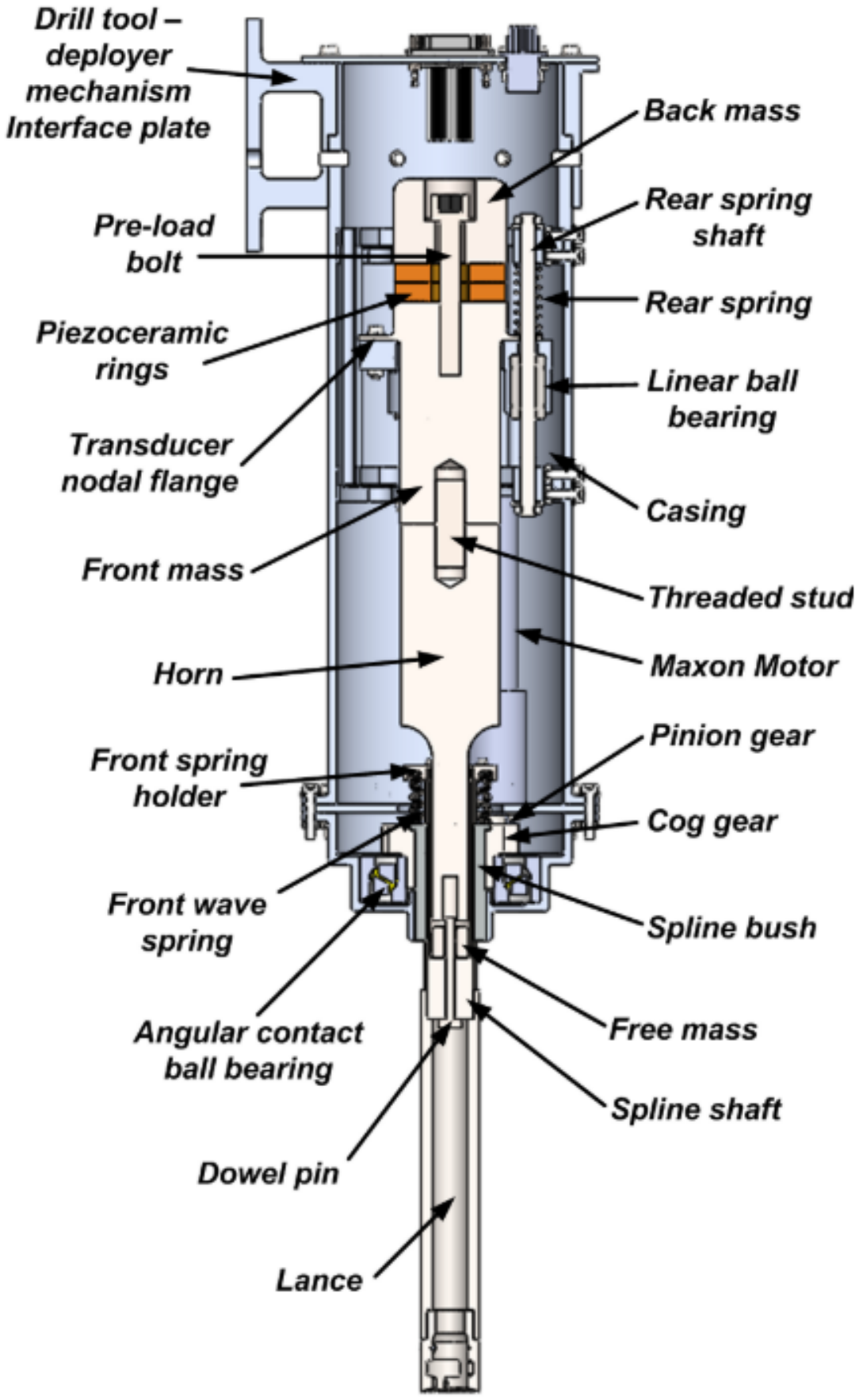


**Figure 33: Full-wavelength UPCD drill tool** *[41]*.

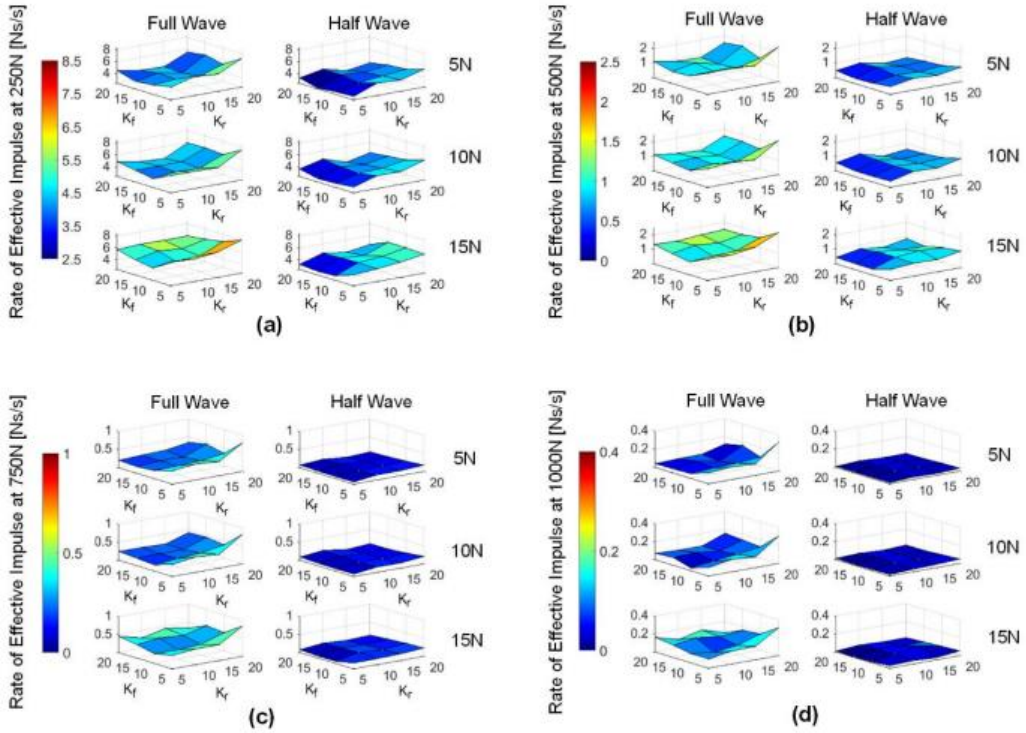


**Figure 34: Experimental results of the effective impulse for the full and half-wave transducers at 5, 10 and 15 N values of weight on bit. Results for forces above 250 N (a), 500 N (b), 750 N (c) and 1 kN (d)** *[41]*.

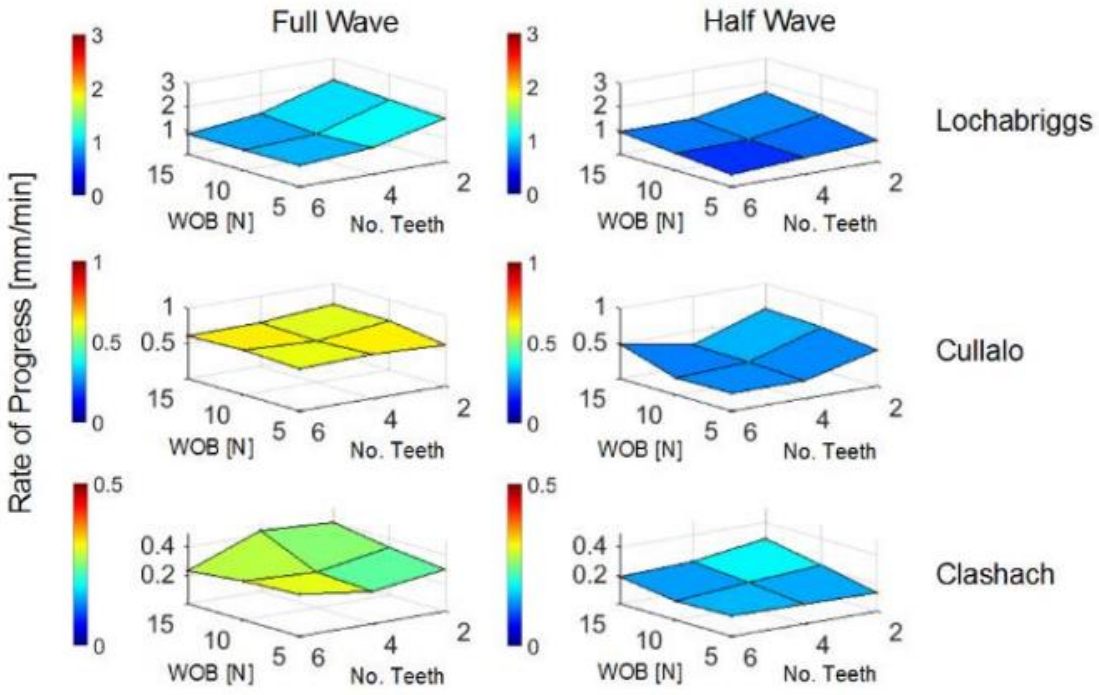


**Figure 35: Experimental Rate of Progress for full and half -wavelength transducers for various teeth and weight on bit levels** *[41]*.

## 4.5 Sample Caching Carousel

The sample caching carousel fulfilled multiple roles in the drilling and sampling process. The carousel was equipped with three silos which were used to store unused drill bits prior to drilling commencement and to take receipt of used, core-containing bits upon cessation of drilling activities. The silos are sealed using ‘cache caps’, which are engaged with the silos through the use of a threaded interface. These caps were stored within locations adjacent to the silos prior to use and provide the silos with a hermetic seal, minimising the loss of volatiles which may be bound within the core sample obtained. Figure 36 portrays the design of the carousel element.

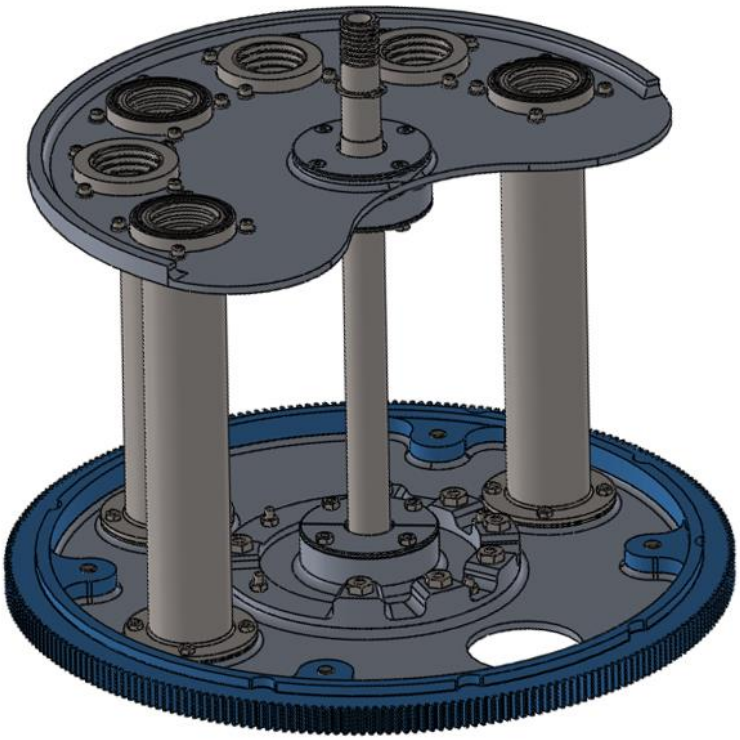

**Figure 36: Sample Caching Carousel Architecture. Diameter of carousel is 240 mm for reference.**

In order to secure the bits in place within the silos prior to use, a hold-down system based upon the bayonet fitting was used. This system provided the basis of the complete Concept of Operations (ConOps) - the process by which the system assembled the drill string, drilled to depth then cached samples. It is of note that the carousel was electrically passive and contained no active clamping/restraining mechanisms unlike those used in other mission architectures. This approach was adopted in order to minimise the mass and complexity of the system and minimises risk within the ConOps procedure. The complete ConOps procedure shall be discussed in greater detail in Section 4.9.

## 4.6 Drill Bit Terrain Clamp

The task of assembling and disassembling the drill string was perhaps the single most complex element of the drilling process due to the vast number of precise steps required to accomplish the task. In order to reduce the complexity of these operations, a ConOps was devised which required the use of only a single clamping mechanism to restrain bits during the connection/disconnection portion, substantially reducing the number of driven mechanisms within the design.

The clamp mechanism was driven by a Maxon brushless DC motor which was geared up to rotate a worm drive, providing the clamps jaws with sufficient torque to overcome the rotation of the drill bit or the axial pull-out of the bits during retraction of the Z-axis system. Figure 37 details the design of the clamping mechanism.

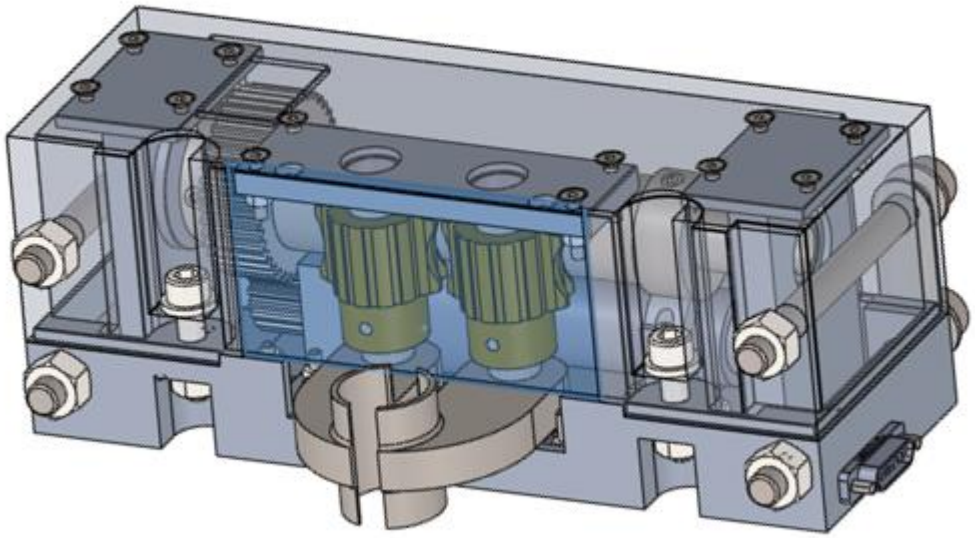

**Figure 37: Drill Bit Exchange Clamp Architecture**

In order to minimise the power required by the system during lengthy assembly and disassembly operations while mitigating against the risk of dropped bits during off-nominal circumstances which would result in a total loss of system power, the clamping mechanism was designed such that clamping would be assured even when the device was in the ‘off’ mode.

## 4.7 Concept of Operations Overview

Although multiple spacecraft have drilled, excavated or abraded the surface of various terrestrial planetary bodies to date, these mechanisms have required only a minimal level of in-situ assembly in order to ready themselves for use. The use of a drill string with a minimum of three individual drill bit elements contributes a great deal of complexity to the drilling process due to the high levels of autonomous control required. In order to increase the reliability of the system, both the assembly routine and the hardware must be robust against the failure mechanisms which are associated with the isolation of planetary exploration and the trials of spaceflight. The development of the UPCD ConOps involved a trade-off between the minimisation of mechanical complexity within the design itself, seeking to reduce the number of clamping mechanism required while ensuring that the procedure could be undertaken in a reliable and repeatable manner. Furthermore, there was a need to ensure that the bit mating system was designed such that it was capable of operating within the harsh conditions that may be expected in a planetary exploration scenario.

## 4.8 Drill String Connections

### 4.8.1 Making and Breaking Drill Strings

Connecting individual drilling elements together to form a drill string is a task most commonly associated with seafloor drilling activities related to energy prospection. The coupling and decoupling of such drill strings, connected by a threaded interface, is accomplished by an abundance of manpower and ruggedized equipment, with the human-in-the-loop approach being a key factor in the process. It is only through the training and intuition of the workforce present that the drill string can be processed in an efficient and safe manner. The operator’s ability to make real-time decisions based on visual or tactile feedback dramatically reduces the potential for lengthy disruptions to the assembly or disassembly process. Human-in-the-loop also allows for the drill string to be less physically constrained, as the operator can easily manipulate the drilling elements in multiple degrees of freedom without difficulty. In the context of planetary drilling, whereby the drilling site in question is typically in exceedance of the range of tele-operation due to light speed delays (with the possible exception of lunar missions), any attempt to bridge this gap with such control would prove to be impossible. Furthermore, as with Earth-based settings, the ancillary hardware required to make and break drill strings, such as clamps and other temporary retraining mechanisms, may be heavy and complex. Clearly, in the absence of an in-situ human operator and with heavily constrained mass and volume budgets, such a

challenge is only amplified. Thus, any system designed for in-situ robotic assembly must be equipped with an autonomous control system fed by a steady supply of data from a sensor suite while ensuring that the design is as mechanically simple as possible in order to reduce risks associated with single point failures.

### 4.8.2 Threaded Connection Operations

Upon analysis of each individual operational element required to make and break a threaded connection, and the subsequent feedback signals which would be required to convert the system to one which is fully autonomous, it is apparent that the task of making and breaking a threaded connection is non-trivial. In order to appreciate the complexity of such an operation, it is essential that the individual steps which compose the complete drill string assembly process are considered. The steps required to make a threaded connection are as follows:

1) Axially and radially constrain female-ended (tapped interface) drilling element.

2) Axially translate male-ended (threaded interface) drilling element until initial contact is made with female-ended element.

3) Ensure that the start of the male and female threads are aligned axially and angularly.

4) Rotate male-ended element in the natural direction of the thread helix while axially translating. Translation rate to be set to match RPM of rotation and thread pitch.

5) Cancel all rotation and translation at maximum thread engagement.

Without prerequisite baseline intuition or ‘feel’ for such operations, the robotic control system must instead rely upon a suite of sensors and actuators to carry out the tasks which are commanded of it.

Step 1, the constraint of the female drill bit, requires that the system be equipped with a means of recognising the angular position of the clamping mechanism and can establish when the criteria for the successful clamping of the drill bit has been met. Typically, it is preferable that the requirement for sensor data is met by at least two independent sources in order to ensure certainty in the success of the operation and redundancy in case of sensor error. In the case of the first step, a typical sensor suite may include encoder data coupled with the use of limit switches to indicate when the motorised clamping operation has reached

the required position. Furthermore, evidence of a surge in motor current, as the clamps fully engage with the drill bit, would provide further confirmation of success.

Steps 2, 3 and 4, the translation of the threaded, male-interfaced bit towards the clamped female-interfaced bit and the subsequent mating of these two bits requires an entirely different set of sensors. It is likely that the axial translation stage, if driven by a belt or ball screw-based system, will be able to make use of encoder feedback alone for positional data. It may also be possible to include a linear potentiometer for redundant position feedback. Furthermore, initial engagement of the two bits is easily identifiable through the inclusion of a force transducer in the axial direction and limit switches for added protection against overrunning. The combination of multiple sensor feedback also acts to ensure the system can compensate for unforeseen degradation in any one of the sensors, such as backlash in motor-gear systems or zero-point floating. Such compensation is particularly important in deep space applications, where the hardware may spend extended periods of time in dormancy during interplanetary cruise. Arduous surface conditions caused by extremes of temperature, radiation exposure and dust ingress also makes sensors suites vulnerable to erroneous readings. Perhaps unsurprisingly, the most risky element of the complete mating operation involves the matching of axial translation with rotation during thread engagement. In order to achieve a successful mating of bits, multiple sensors must work in unison to allow the control system to rapidly respond to off-nominal states.

The nature of the threading operation, in a situation where the female-ended bit is fully constrained, is such that the male-ended bit may be forced into tension by means of a corkscrew-like action through an axial under-advance. Unless the axial translation of the bit is carefully matched, this could result in an overstress of the system resulting in damage to the axial stage or belt-slippage if a pulley-based axial stage is utilised. While tension in the system is clearly undesirable, a net compressive force caused by the over-advance of the axial translation stage may also result in the formation of another unwanted error state. As the compressive force applies axially-directed pressure to the female threads, the resulting rise in friction may induce a periodically increased torque demand. The resulting motion is physically analogous to that of the ‘stick-slip’ condition whereby the threading motion may temporarily stall until the rotary element catches up and reduces the axial load on the bit. In extreme cases where ‘stick’ is particularly high and rotation is sufficiently impeded, an unchecked axial translation may only compound the problem and result in rotary motor stall, necessitating an abort of the operation. It is of note that both an axial over-advance and an under-advance may share a common failure mode in rotary motor

stall, impeding efforts to diagnose the fault and remedy it. Clearly, the action of threading drill bits together through an interplay of translation and rotation is only made possible by real-time data from a large suite of sensors, working to identify fault states as they arise.

Despite the intricate nature of making threaded connections, missions such as the upcoming ExoMars 2020 rover do intend to utilise this method as the primary means of forming drill strings of at least two individual drill bit elements. An example of the ExoMars type male-ended bit interface is as detailed in Figure 38 [42]. While control-based assembly problems may be overcome by the inclusion of a complex sensor package, threaded connection methods have inherent features which may complicate the overall drill system architecture.

**Figure 38: ExoMars type threaded connections. Bit diameter of 20 mm, for reference** *[42]***.**

### 4.8.3 Practical Limitations of Threaded Interfaces

While the process of disconnecting threaded bits may appear to be relatively trivial when compared to the difficulties posed by connecting threaded bits, there are challenges intrinsic to this operation. The primary concern when utilising a threaded system is the inability to rotate the drill string in the counter-clockwise direction without disconnecting one bit interface from another. This is particularly problematic given that the solution to multiple downhole drilling faults requires the application of a reversed drill rotation. Furthermore, upon attaining the required drilling depth, it is foreseeable that the mission may require the disassembly of the drill string and the caching of used drill bits for sample preservation or later reuse. In doing so, the system must remove the drill bits element by element starting with the uppermost bit. In order to ensure that only the uppermost bit is removed, the threaded system requires that both the bit to be removed and the bit immediately attached to it are clamped. This ensures that, when an anti-clockwise rotation is applied, only the connection between the uppermost bit and the bit to which it is directly attached is broken while the connection between the uppermost bit and the drill mandrel itself is maintained. This necessity for multiple clamps only complicates the system and increases the likeliness of single point failures occurring.

While the ease of manufacturing both male and female threaded interfaces allows parts to be manufactured quickly and with a high degree of reproducibility, the physical nature of threads makes them extremely prone to harbouring dusty fines and other particulates which may be present on the planetary surface. As the surface of Mars experiences frequent aeolian activity, wind-borne fines may readily be deposited on all parts of the spacecraft. Figure 39 highlights the distribution of dust particles on the NASA Mars Exploration Rover *Spirit* impeding solar cell efficiency. Although so-called ‘cleaning events’ act to clear surfaces, the complex geometries of the helical thread means that once contaminated by dust the surfaces often remain coated indefinitely. Simple laboratory experimentation suggests that dust on threads can substantially increase the torque demand on the motor as a result of increased friction forces. In the worst case, a failure may occur whereby the threaded connection will be made but cannot be undone. While this problem is certainly common across all mating connection types, it is the high surface area of threaded connections which heightens this effect and is therefore particularly problematic.

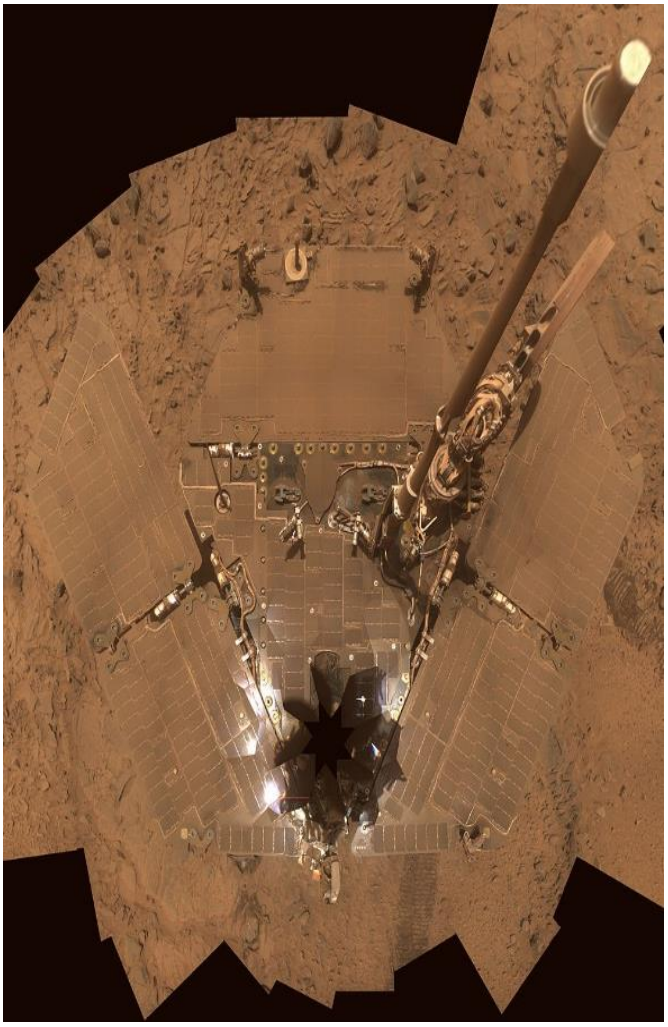

**Figure 39: Mars Exploration Rover, *Spirit* coated in extremely fine dust. Courtesy: NASA/JPL-Caltech/Cornell.**

Drilling systems which are required to penetrate hard terrain often make use of percussive hammering as a means of increasing the rate of penetration of the system without increasing the required weight on bit. In the experience of the authors, the vibration caused by percussion may result in threads shaking loose – a potential risk to the system which is difficult to predict. It is therefore possible to conclude that, while threaded systems can be utilised in a planetary exploration setting, the inclusion of such a system requires an acceptance of certain risks which may drive mission planning and operations.

### 4.8.4 Bayonet Connection Interfaces

Having examined both the benefits and negatives of a threaded mating system, it is clear that, although such systems show a degree of compatibility with planetary missions, they do not represent an ideal solution to the problem of making and breaking drill strings robotically.

The UPCD project aimed to develop a drilling system which was less mechanically and operationally complex than existing designs. During the developmental stages of the design

process, it was established that the key technologies which would add complexity concerned the need to make and break drill strings. As such, a trade-off study focussing on key factors such as the reliability of making/breaking interfaces, the impact each interface type would have on the architecture as a whole (with an emphasis on the need for any in-string clamping that would be required, additional fixed clamping devices, and electrical passivity), the ease of fault mitigation as a result of the use of a particular interface type and the ease of implementing a given interface architecture within the limited material available within individual drill bits, was undertaken. As previously detailed, the most challenging element of the threaded drill string system is the high level of control required to make connections (worsened by dust contamination) and the limitations imposed by the inability to rotate the drillstring counter-clockwise (limiting fault tolerance and the ability to selectively disassemble individual drill bits without the inclusion of a mandrel clamp (with the associated mass and electrical complexity associated). Conversely, threaded interfaces benefit from heritage, thus there exists an understanding of the robotic complexity required to make such connection. Such connections also benefit from an ease of manufacture and implementation within the drill bit geometries.

The bayonet system benefits from a number of key features, as detailed in the next section. Identified risks in the implementation of such a design include the complexity inherent within the need to use advanced machining techniques to manufacture the male and female geometries and the subsequent need for a quality control procedure for all parts to ensure the desired connection post-manufacture. There is little data available within the literature regarding the robotic assembly/disassembly of bayonet interfaces, adding uncertainty to the development. Furthermore, it was foreseen that the bayonet interface would require the addition of a locking feature, potentially in the form of a sprung ball mechanism. The narrow kerf of the UPCD drill bits meant that the inclusion of such a device would be inherently tricky with a delicate installation process required. When considered holistically, the study indicated that the benefits had by undertaking the development of an alternative system, based upon the bayonet system, outweighed the negatives conferred by such an approach.

### 4.8.5 Bayonet Connection Operations

The bayonet approach relies on a connection system based on the use of male studded features and female grooved features. When mated, a connection is formed which allows both the transmission of torque and percussion through the drill bits, with very little attenuation of the percussive energy delivered to the bit-rock interface. Through careful design, it was possible to develop a bayonet connection system which permitted torque

transfer in both drilling directions, aiding the drill string disassembly process and fault tolerance. Furthermore, such a system can be designed with a high degree of dust prevention and tolerance, ensuring robustness. The need to reliably disassemble the drill string necessitates the ability to selectively disassemble only the uppermost drill bit in the drill string without unlocking the lower elements of the string. A rethink of the standard bayonet system ultimately inspired the use of T-shaped female groove alongside the more conventional L-shaped groove. The developed system would rely on the inclusion of the T-shaped groove geometry in both the 'lance' of the drill tool and the 'cache caps' (the lids used to seal the top of each core-containing drill bit prior to caching). The lance component of the drill tool acted as both an anvil, transmitting shock loading from the ultrasonic-percussive hammer within the tool, and also as a connection interface to the drill bits, transmitting torque from the gearbox of the auger motor to the drill string. The implementation of T-shaped grooves in the cache caps allowed the caps to operate effectively as a continuation of the lance itself, easing the caching process. While L-shaped grooves may be axially locked in only one direction, the T-shaped groove allowed the stud to lock in either arm of the groove, thus locking the bits axially while permitting rotation in either the clockwise or anticlockwise direction.

Having established that a combination of multiple female groove geometries was the key to developing a robust drill bit connection system, a trade-off study of the various Concept of Operations was undertaken. Figure 40 [43] details the process by which different groove geometries are utilised to allow only the uppermost drill bit to be disconnected from the drill string. The T-shaped female groove of the lance is shown coupled to the stud of the uppermost drill bit which is to be removed from the string, while the L-shaped female groove connects two lower drill bits. It is of note that the female groove feature of the design presented is internal to the drill bits and lance, reducing the likelihood of dust contamination. The manufacturing of these geometries was accomplished through the use of Electric Discharge Machining and required a rigorous quality control process to ensure that the required tolerances could be met. The quality control process put in place involved the use of a 'benchmark' male-female interface determined experimentally to be an acceptable fit. The torques required to make the connection were established and the axial separation of the benchmark parts evaluated so as to ensure minimal axial rattle between bits. The rectangular stud features were manufactured using a similar technique but featured a sloped upper surface as an additional means of reducing dust build-up.

As discussed in Section 4.8.2, male to female threaded connection interfaces are difficult to make using robotic manipulation. The implementation of an axial compression spring, in line with the lance, aided the process of making the male to female bayonet connection. Furthermore, the compression spring allowed the drill system to axially progress while any over extension was compensated for by the compression of the internal compression spring. As the spring remains compressed until the male bayonet is located within the axial section of the female groove, at which point the decompression of the spring will act to propel the male bayonet into the axial section, this can be exploited as a means of ensuring a successful connection is made which does not require careful control based on encoder feedback. In fact, this method became the standard method of connecting drill bits together in the lab, such is its level of robustness. This simplicity is perhaps one of the main advantages of the bayonet mating system over threaded alternatives.

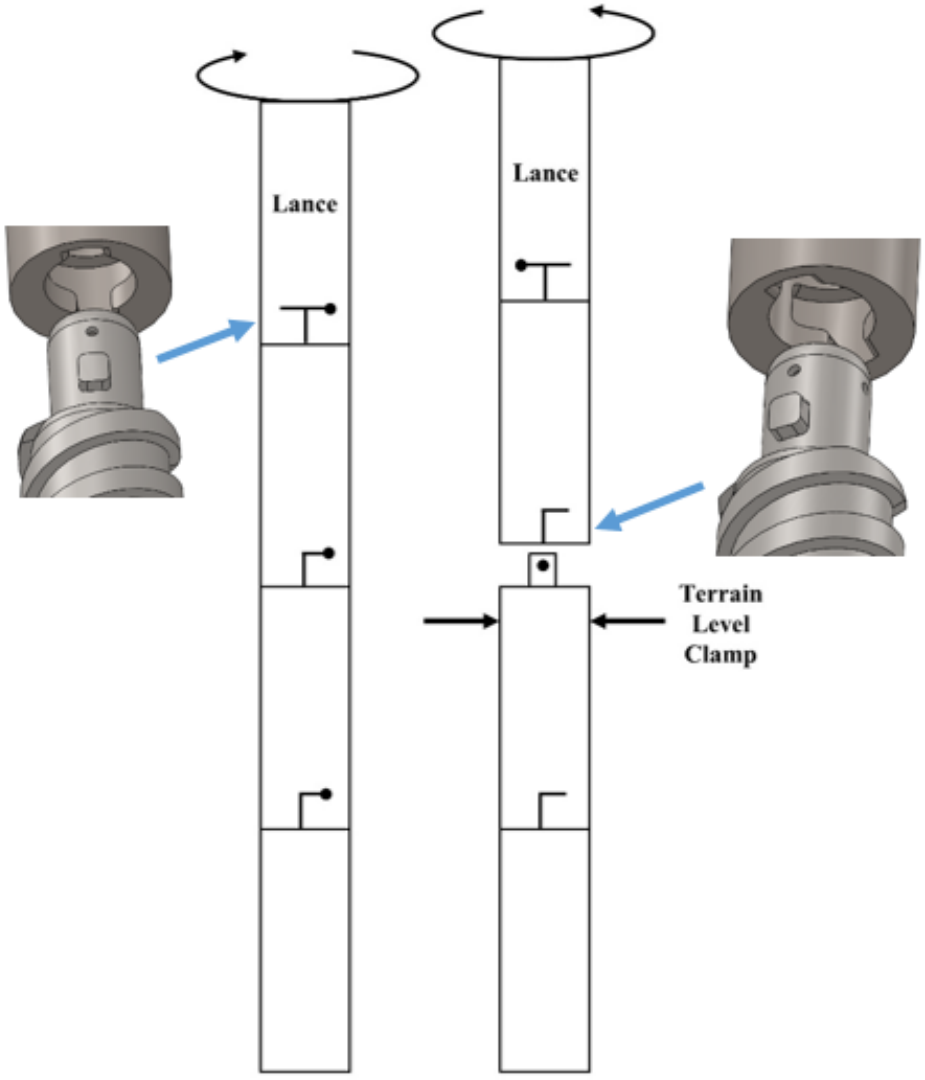


**Figure 40: Drill bit disconnection procedure. Drill string in typical drilling configuration (L) and disconnection event (R)** *[43]*.

## 4.9 Concept of Operations Trade-off Study

The routine by which the drilling system connects and disconnects individual drill bits in order to achieve the required sampling goals is referred to as the Concept of Operations (ConOps). In order to establish the most suitable method of carrying out this task while attempting to minimise both system and operational complexity, a trade-off study was performed [40]. In this study, two competing ConOps were assessed for various criteria, balancing operational complexity with the mass and volume demanded. The selected operational mode, herein referred to as the Continuous Core Method (CCM), relies on the use of a single hollow core cutting bit with multiple hollow bits added as the length of the borehole increases as drilling progresses. Typical drill bit geometries utilised in this method are shown in Figure 41 while the assembly/disassembly routine is shown diagrammatically in Figure 43.

The UPCD architecture is represented by various shapes in the ConOps diagrams. The green shape represents the drill tool itself, the blue rectangle represents the Sample Carousel (which contains the unused drill bits prior to use and also stores used bits and the collected samples in silos. A CAD model of the complete system, labelled with the appropriate colours, is presented in Figure 42.

**Figure 41: CCM drill bits. Two Extension Bits shown (top and centre) and Cutting Bit (lower). Note, male stud interface visible, female grooves within internal bores. Note, the presence of a small detent groove on the drill shank adjacent to the male stud interface. Drill bit length of 100 mm, diameter 20 mm, for reference.**

The terrain is represented by the grey hatched rectangle while the double set of red arrows are to be interpreted as a clamping event as carried out by the terrain clamp. The drill bits are denoted as white rectangles and the cache caps purple crosses. Red arrows denote an actuation of the terrain clamp. The drill tool connects to an unused cutting drill bit, stored in a silo in the carousel, through single axis translation and a rotation manoeuvre to unlock the bit from its passive axial hold-down points. Through a series of axial translations of the drill tool and rotation of the carousel to a location known as the drilling aperture (an aperture in the carousel which allows access to the terrain), the system proceeds to drill to a depth as determined by the length of the individual drill bits. Upon reaching the target depth, the bit

is clamped by the terrain clamp, allowing the lance of the drill tool to disconnect from the cutting bit before axially translating to receive an extension bit. Upon reaching the desired drilled depth through the addition of the required number of drill bits to the string (in the case of Figure 43, three individual drilling bits), it is required that the drill string be disassembled and each core-containing drill bit be cached into a sealed silo. In order to do so, the bit which is to be cached is first sealed at its uppermost end by a cache cap. The cache caps fulfil a dual role in that it seals one end of the drill bit while allowing a hermetic seal to be formed with the silo, preserving the scientific integrity of the captured volatiles. In the case of the three-bit scenario, the carousel must contain three silo positions and three cache cap positions to accomplish the procedure.

As the CCM architecture allows each individual drill bit to store a core sample, the total number of carousel sites required equates to the number of drill bits plus the number of caching lids. While it may be possible to locate the cache caps on the silos before use, requiring each cap to be removed and temporarily stored in a ‘transient’ site during the disassembly process, this would substantially increase the number of operations required, albeit reducing the volume of the carousel. Planetary sampling missions are often limited by particular scientific requirements which insist on a reduction in stratigraphic mixing during sample acquisition and a need to avoid cross contamination between samples [18]. As the CCM consistently maintains a drill bit within the borehole, there is little risk of borehole disruption and the subsequent introduction of surface contaminants.

While the CCM reduces operational complexity through a reliance upon a single cutting bit in order to accomplish its drilling objectives, there exists the possibility that a gradual dulling of the cutting teeth may reduce the efficiency of drilling operations at greater borehole depths. Although uncertainty in tooth wear properties existed during the trade-off study, it was decided that the benefits conferred by the CCM by means of a reduction in the number of operational steps led to its selection for use in the UPCD system.

The second option considered was the Discrete Core Method (DCM). The DCM differs from the CCM in that it does not utilise multiple hollow drill bits connected together to form a continuous, running core. Instead, the DCM relies on multiple, individual cutting bits, sealed at one end, and a series of extension rods. The extension rods act only to lengthen the borehole and are reusable, therefore not sample-bearing. Figure 44 details the DCM procedure. In addition to the diagram shape representations already described, the DCM figure includes black rectangles representing the extension rods. The DCM acquires core samples using the same operational translations and rotations are the previously described CCM, but the core sampling itself is only accomplished by the cutting bits. As the drill string

constructed in the CCM is continuous, with the core sample running the full length of the string, the CCM approach benefits from a reduced number of operational steps relative to the DCM. This reduction in the required number of steps directly translates into a reduction in the time required to complete a drilling run. Furthermore, the reduced number of overall steps (and the subsequent reduction in make/break operations required), directly reduces the mission risk burden. An architecture which allows each individual drill bit to store a core sample means that the total number of carousel sites is limited to only the number of drill bits plus the number of caching lids, ensuring a minimised carousel volume and mass.

Although the use of the CCM ensures a reduction in system complexity, the DCM has hardware-focussed benefits which could not be implemented in the CCM. As the CCM makes use of a single cutting bit to accomplish its drilling objectives, there exists the possibility that a gradual dulling of the cutting teeth may reduce the efficiency of drilling operations at greater borehole depths. While uncertainty in the tooth wear existed during the trade-off study, it was decided that the benefits brought by the CCM meant that it was the method which was selected for integration within the UPCD system.

As both of the ConOps architectures studied allow simultaneous anticlockwise rotation and axial translation due to the tendency of L-shaped female grooves to disconnect under such motion, the replacement of L-shaped grooves with T-shaped grooves throughout would allow complete flexibility in translation and rotation at a cost of operational complexity, requiring an extra clamping stage at each connection stage. Such a modification would come at a cost of operational complexity, however, requiring an extra clamping operation at each connection stage.

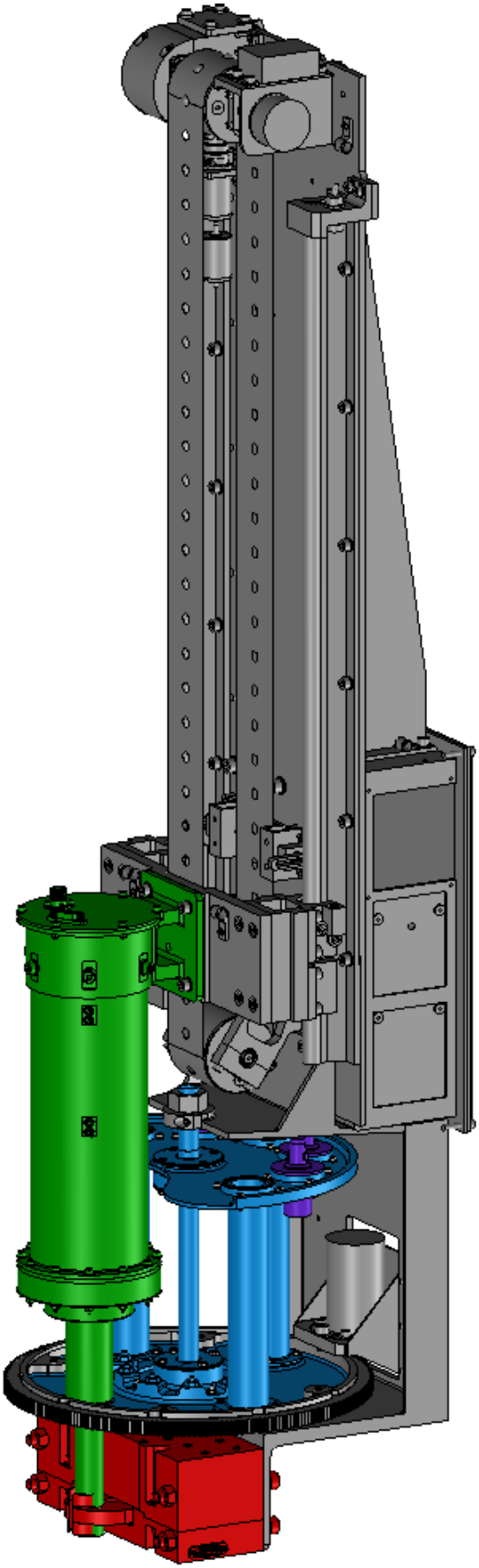

**Figure 42: UPCD assembly colour coded to match ConOps Diagrams**

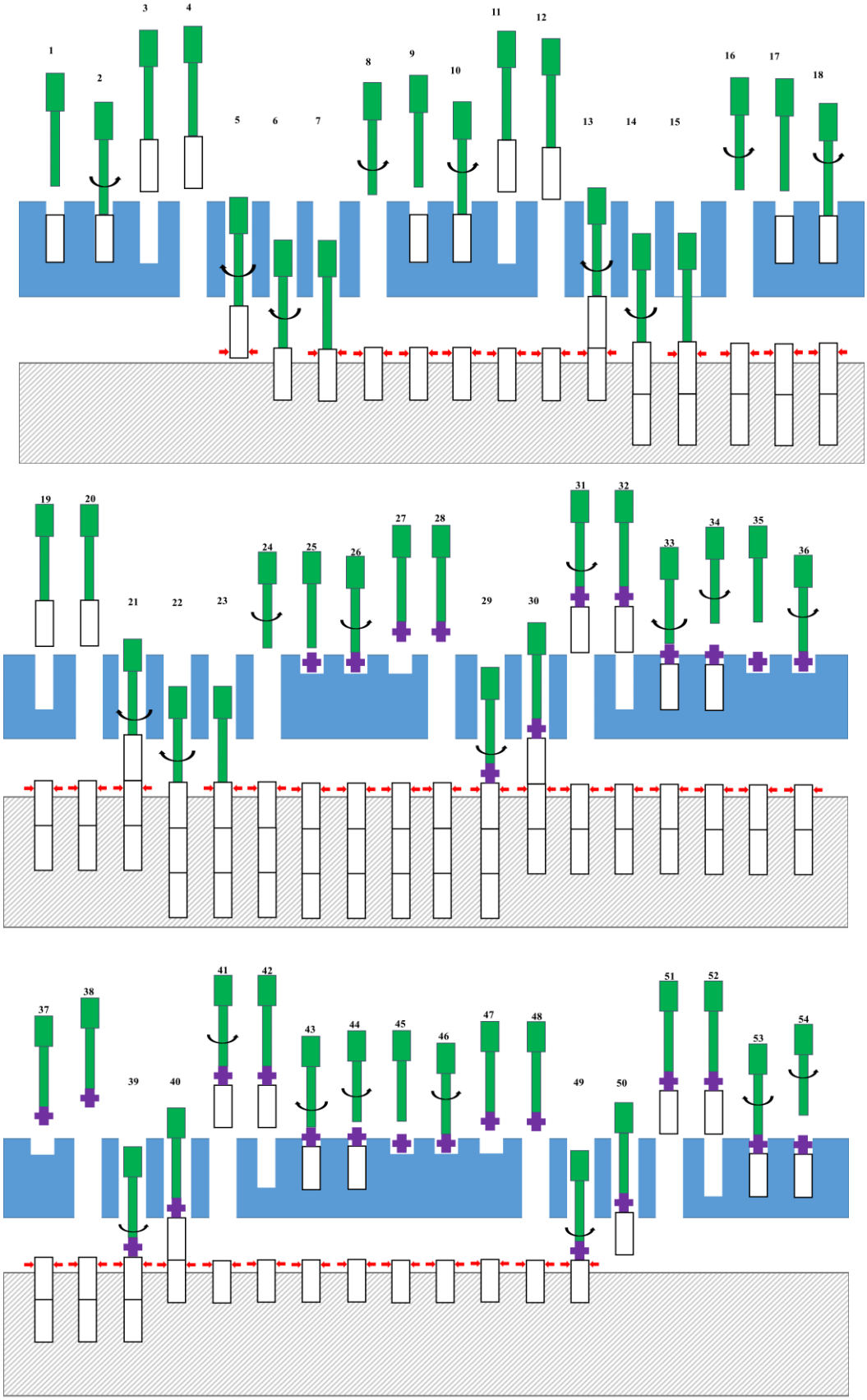


**Figure 43: Continuous Core Method (CCM) ConOps**

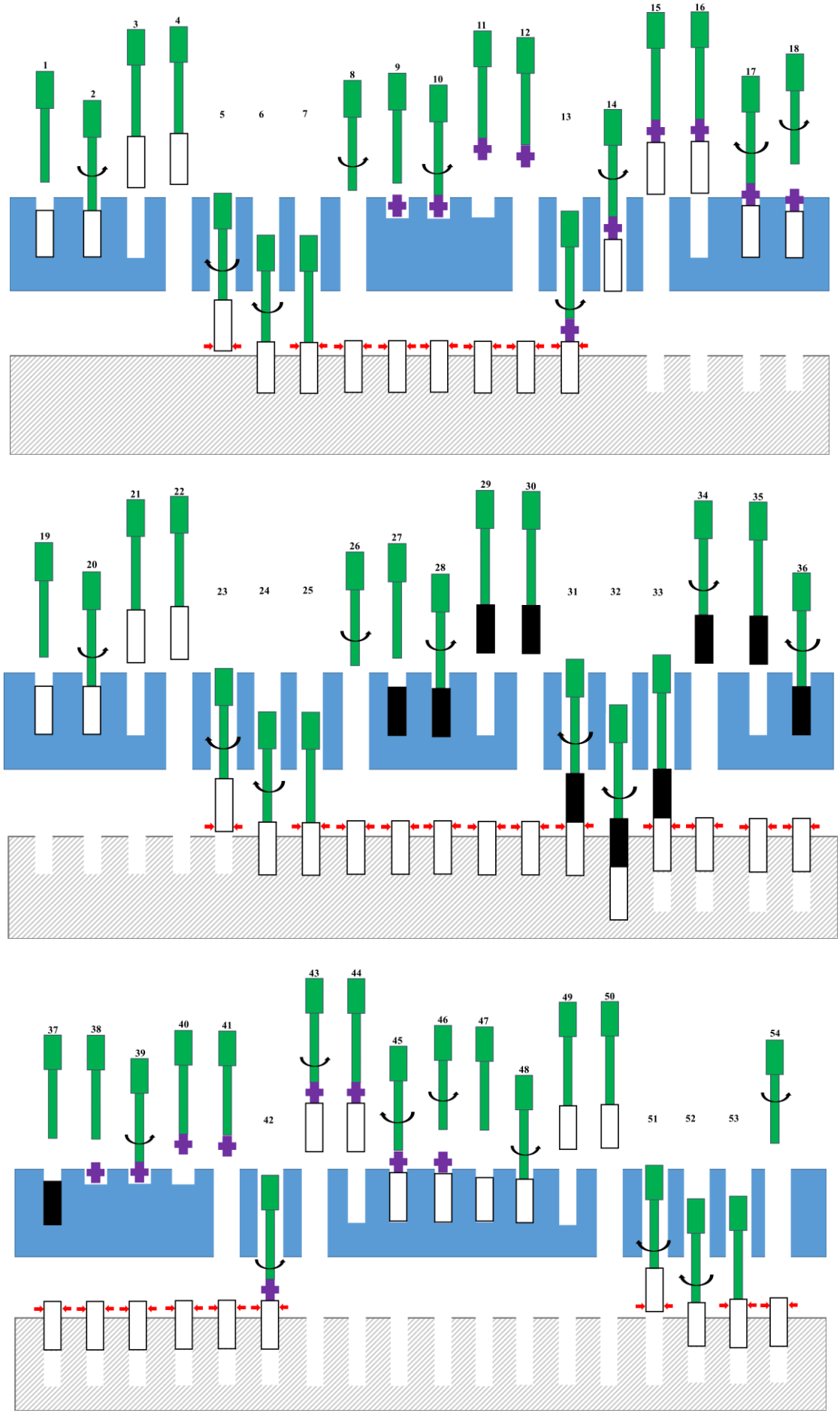
1
2
3
4
5
6
7
8
9
10
11
12
13
14
15
16
17
18
19
20
21
22
23
24
25
26
27
28
29
30
31
32
33
34
35
36
37
38
39
40
41
42
43
44
45
46
47
48
49
50
51
52
53
54

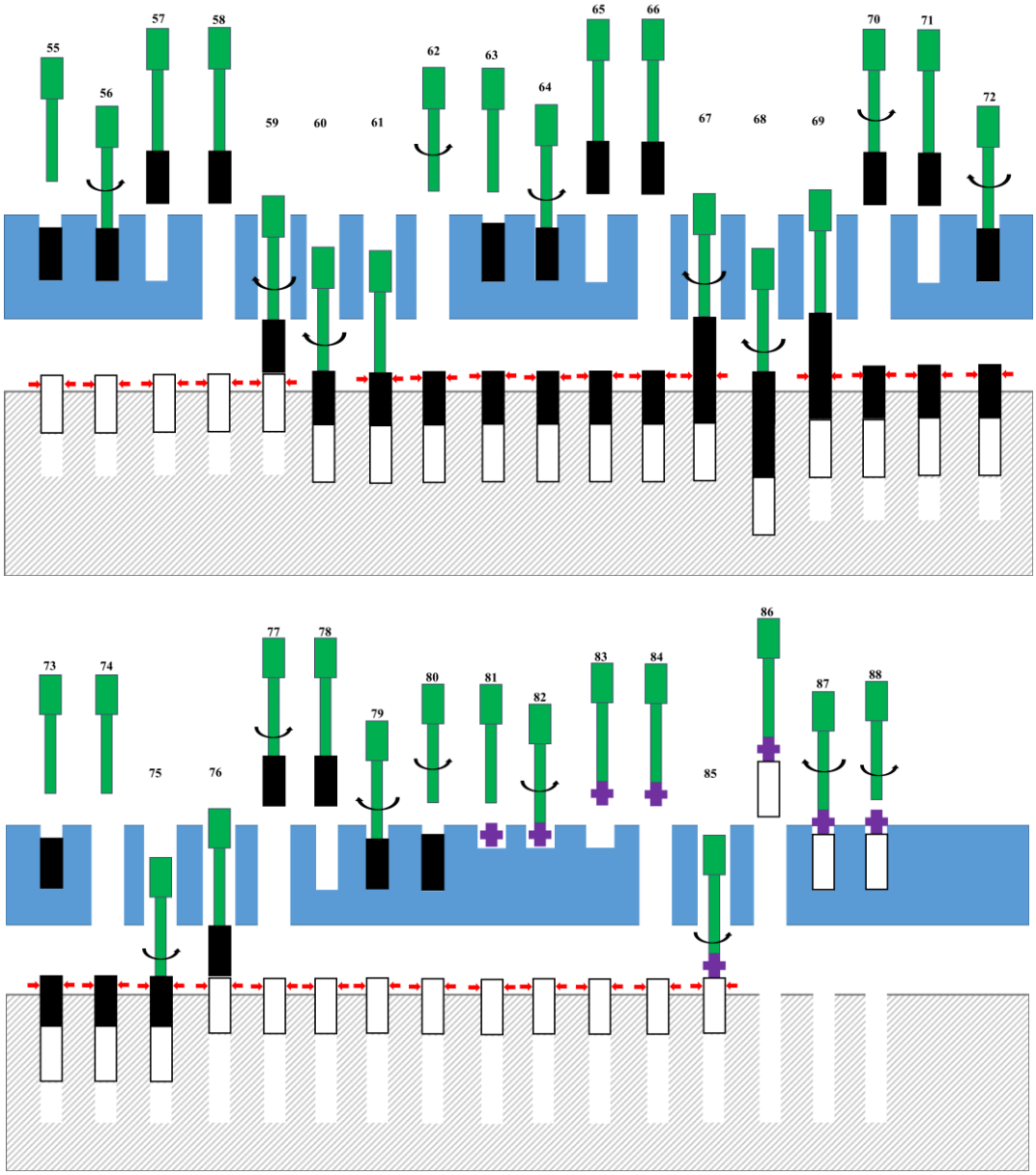


**Figure 44: Discrete Core Method (DCM) ConOps**

## 4.10 Transmission of Percussion

In the context of percussive drilling, whereby the repeated hammering of the drill bit generates a stress wave in the drill bit which causes rock fracture through various mechanisms, there are intrinsic sources of inefficiency which cannot be avoided and are a by-product of the technique. In fact, energy which is lost in the generation of heat and in drill bit rebound far exceeds that which is spent on the breaking of the terrain [28]. Thus, it is essential that an attempt is made to minimise any losses which may occur between interfaces in the multi-bit drill string assembly. Insufficient structural rigidity in the string could lead to rattle and the poor transference of the percussion wave across the bit to bit boundary, limiting the effectiveness of the drill system in penetrating stronger terrain. In order to achieve a high quality mating interface attention was paid to the fit between the male and female parts, aiming to maximise the rigidity of the string while ensuring that the drill bits could be robotically disassembled with ease when required. This was further complicated by the implementation of electric discharge machining (EDM) in the production of the connection interfaces. EDM, or spark erosion, can attain high tolerances, though each application must be assessed on a case by case basis. Close attention to quality control and standardisation was essential in ensuring a high level of repeatability between drill bits and resulted in the production of bits which experienced minimal losses of percussive energy when stacked in a formation of three or more bits.

To ensure that the percussion-induced stress wave is not impeded by the use of the bayonet-style connection as it travels through the drill string, experimentation was required in order to establish if there would be any significant reductions in performance or damage to the studded connector. Experiments were performed using a bayonet-connected lance and drill bit and, for the purpose of comparison, a control piece was also manufactured. The control piece consisted of a lance/drill bit machined as a single component, therefore without any bayonet connection [43]. Figure 45 details the two test items used in experimentation. With the knowledge that contamination would not be problematic in a laboratory set up and to ensure a rapid manufacturing of parts, the bayonet grooves for this series of testing were machined on the exterior of the drill bit using conventional machining techniques. Furthermore, as the testing was to occur on a horizontally mounted rig to shallow depths, it was decided that the test bits would be manufactured without an auger, instead relying on the travel of fine grained cuttings out of the hole through a combination of the action of sonic waves created through percussion, and gravity due to the horizontal mounting of the rig [44].

As the depth of drilling would not exceed a few centimetres, this approach was deemed appropriate and would not compromise the results obtained.

**Figure 45: Percussion transmission test items. Control (L) and Bayonet-connected bit (R). Bit diameter of 22 mm, for reference** *[43]*.

The drill bits were tipped with tungsten carbide teeth which were soldered into place. Though tungsten carbide is extremely hard, care was taken to ensure an even wear on the teeth allowing this variable to be controlled.

### 4.10.1 Test Procedure

In order to carry out performance testing while providing a proving ground for key technologies critical to the development of the UPCD project, a horizontal mechanical rig was constructed. The rig, detailed in Figure 46, allowed a testing variant of the ultrasonic-percussive drill to advance autonomously, utilizing an in-house control algorithm, in to a test sample [45]. The control loop requires a pre-set Reference Power Level, derived from the power electronics of the ultrasonic transducer. The power electronics, an off-the-shelf Sonic Systems P100 control unit, acted to drive the ultrasonic piezoceramic rings at resonance in order to maintain a constant output amplitude or power level, compensating for sonic energy transferred to the drill string and rock formation during percussion.

The control loop advanced and retracted the linear actuator depending on the power feedback it received. A rise in power is typically attributable to the drill encountering

resistance as it penetrates the formation, whilst a reduction in power suggests the drill has penetrated a given section of the formation and is no longer encountering resistance. If the power feedback is lower than a given minimal power value, typically the pre-set minus ten percent, then the control algorithm will detect that the power being supplied to the actuator has fallen. Upon receipt of this control prompt, the linear actuator will be commanded to advance incrementally further in to the formation. Conversely, a rise in power to the upper limit, typically seen when penetrating stronger rock formations, will result in an incremental withdrawal of the drill assembly until the power level is within desired bounds. The use of this variant of closed-loop control ensures that the drill will penetrate through the rock formation in an efficient yet controlled manner, utilizing only a pre-set power level. The Reference Power Levels tested in the experimental campaign were 20, 25 and 30 W to allow for variety in testing.

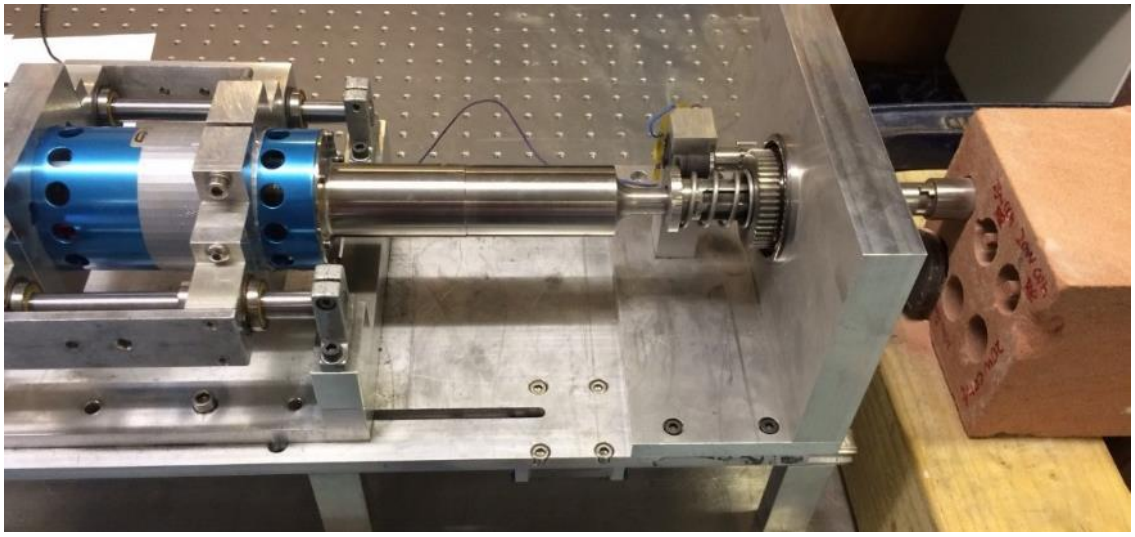

**Figure 46: UPCD Horizontal Test Rig. Bit diameter of 20 mm, for reference.**

Although the drill string tested was not machined with an auger for spoil removal, the test rig is equipped with a gearbox, used to slowly rotate the drill string (~20 RPM), via a spline shaft, to ensure the cutting teeth do not embed in the formation, thus halting penetration.

The routine for testing was as follows:

1) Set internal force preload to be used for all tests (10 N).
2) Set Reference Power Level to be tested (20, 25 or 30 W).
3) Select rock formation to be drilled. Attach securely to rig.
4) Attach drill bit to be tested to the threaded spline shaft interface.
5) Reset data acquisition software and restart control algorithm.

6) Initiate percussion and rotation motor.
7) Ensure nominal action of linear actuator, percussion and rotation.
8) Allow hardware to progress through rock formation for predetermined time.
9) Assess drilling performance: note borehole depth using callipers and drill time.
10) Clean rig and used drill bit. Ensure next drill bit is clean and ready to test.

All data was collected on a laptop and a PicoScope oscilloscope and post-processed on MATLAB, utilizing a low-pass filter to aid signal clarity.

Three sandstones, Locharbriggs, Blaxter and Clashach, were selected for testing as they represent respectively soft, medium and hard variants of the rock type (Table 3). Tests were conducted multiple times, along consistent grain orientations, in order to assess the repeatability of the system. While the simplified horizontal rig-based experiment lacked the ability to test multiple interfaces in series and thus establish the capability of the complete, assembled string in transmitting percussion, setting a suitable pass/fail criteria based upon a percentage loss of 20% per interface ensured that total losses would not exceed approximately 50% over three drill bits.

| Rock Type | Locharbriggs | Blaxter | Clashach |
|---|---|---|---|
| **UCS [MPa]** | 47 | 55 | 132 |
| **Porosity** | 18.2-24.9% | 20.5% | 21.4% |
| **Bulk Density [kg/m$^3$]** | 2173 | 2110 | 2084 |
| **Water Absorption [/wt]** | 5.7% | 6.1% | 6.9% |

**Table 3: Geological Properties of tested sandstone samples (BRE data sheets)**

## 4.10.2 Experimental Results

Results obtained from the experimental campaign are presented in Figure 47 - Figure 53. The graph in the upper-left of each frame, with the signal coloured blue, details the P100 power, the power delivered to the piezoceramic rings of the ultrasonic transducer. In the upper-right of each frame is the time history of the Sample Held Power, coloured red. The Sample Held Power utilizes the P100 power, integrating it over a period of 1 second in order to establish an average for that second. This integrated power then acts as a direct input to the control system, autonomously controlling the progress of the drill system through the rock formation. If this power value is higher or lower than the limits set by the user as a

Reference Power Level the linear actuator will be commanded to advance or retract. The time history extension of the linear actuator is detailed in the bottom of each frame, coloured green.

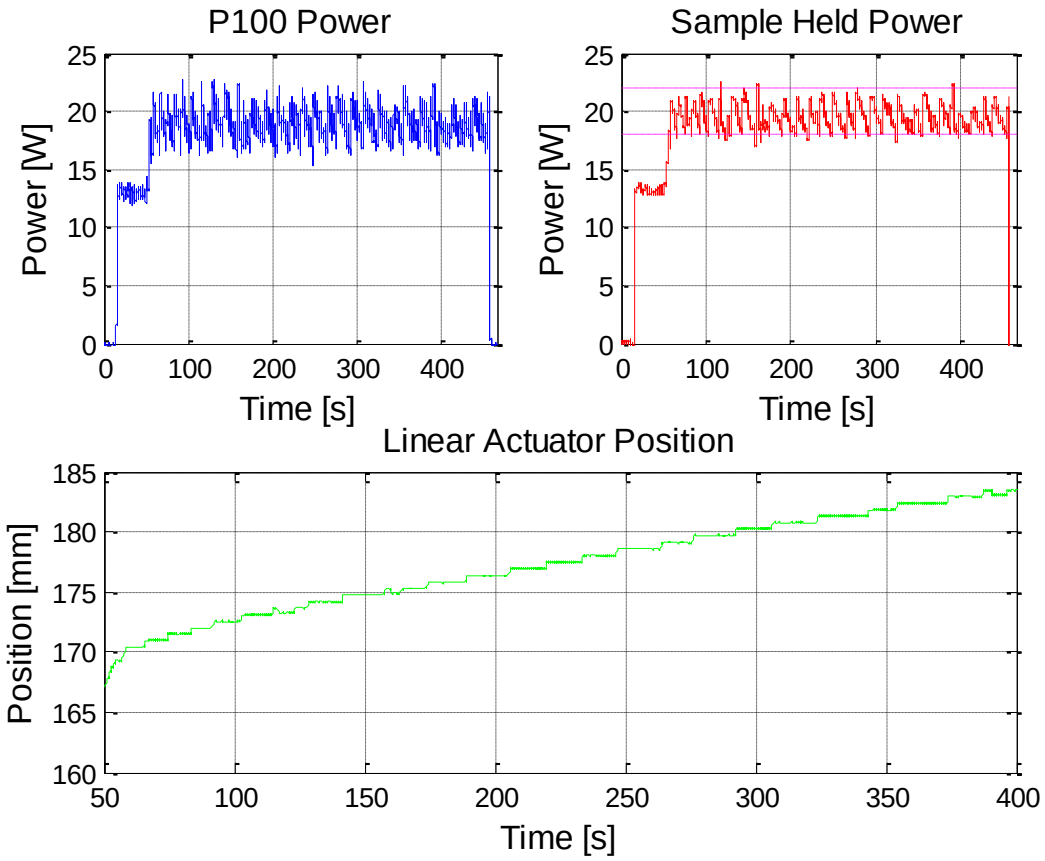


**Figure 47: Locharbriggs sandstone - Bayonet interface drill bit - 20 W**

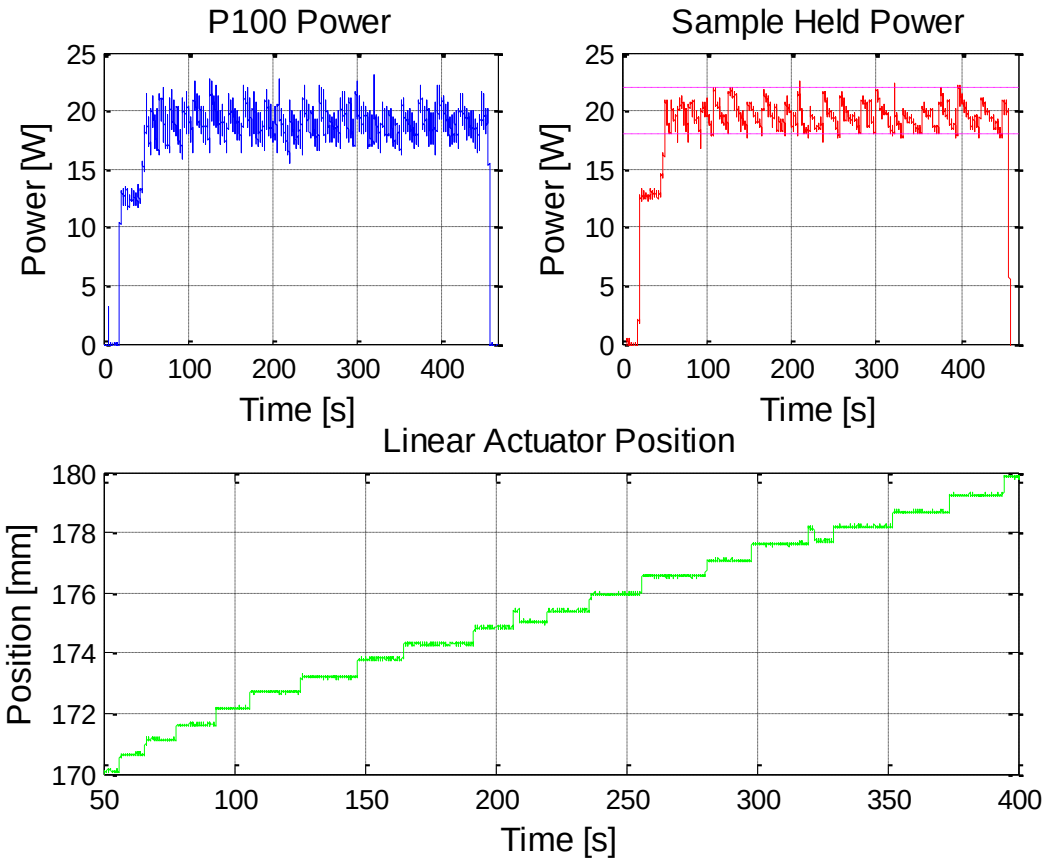


**Figure 48: Locharbriggs sandstone - Control drill bit - 20 W**

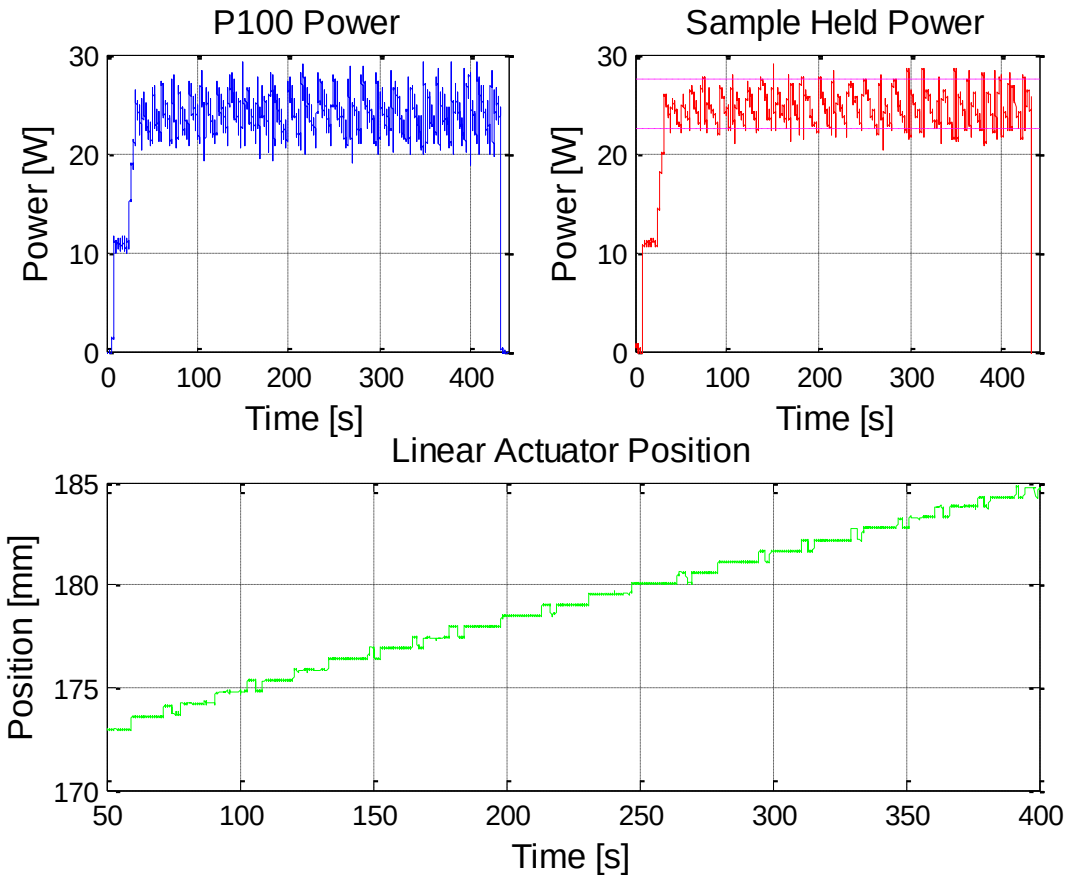


**Figure 49: Locharbriggs sandstone - Bayonet interface drill bit - 25 W**

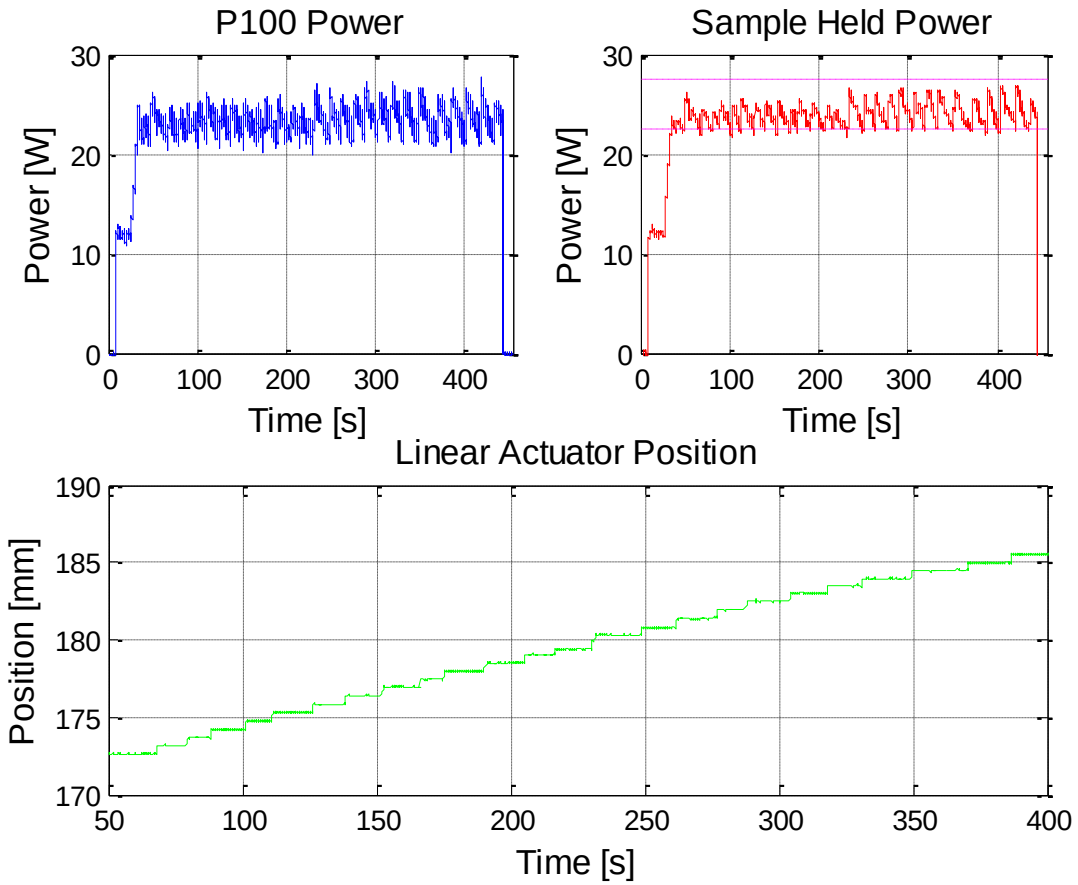


**Figure 50: Locharbriggs sandstone – Control drill bit – 25 W**

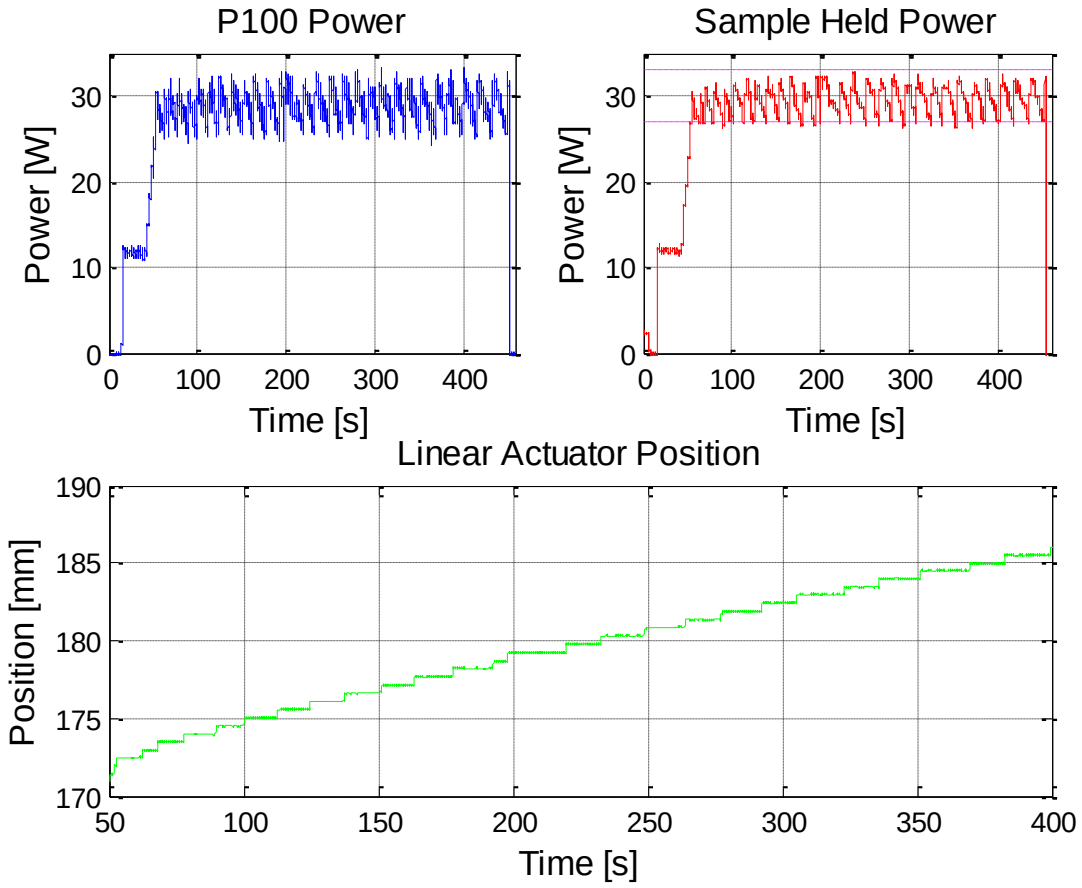


**Figure 51: Locharbriggs sandstone - Bayonet interface drill bit - 30 W**

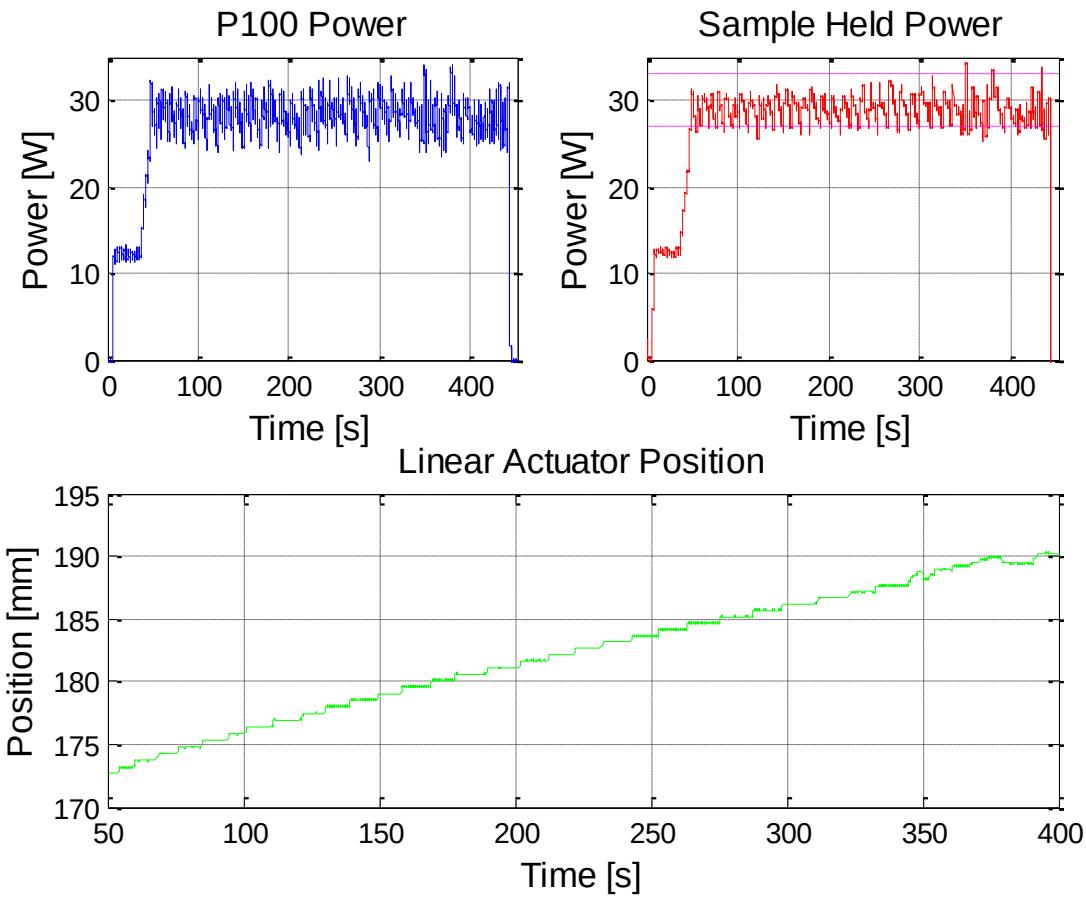


**Figure 52: Locharbriggs sandstone - Control drill bit - 30 W**

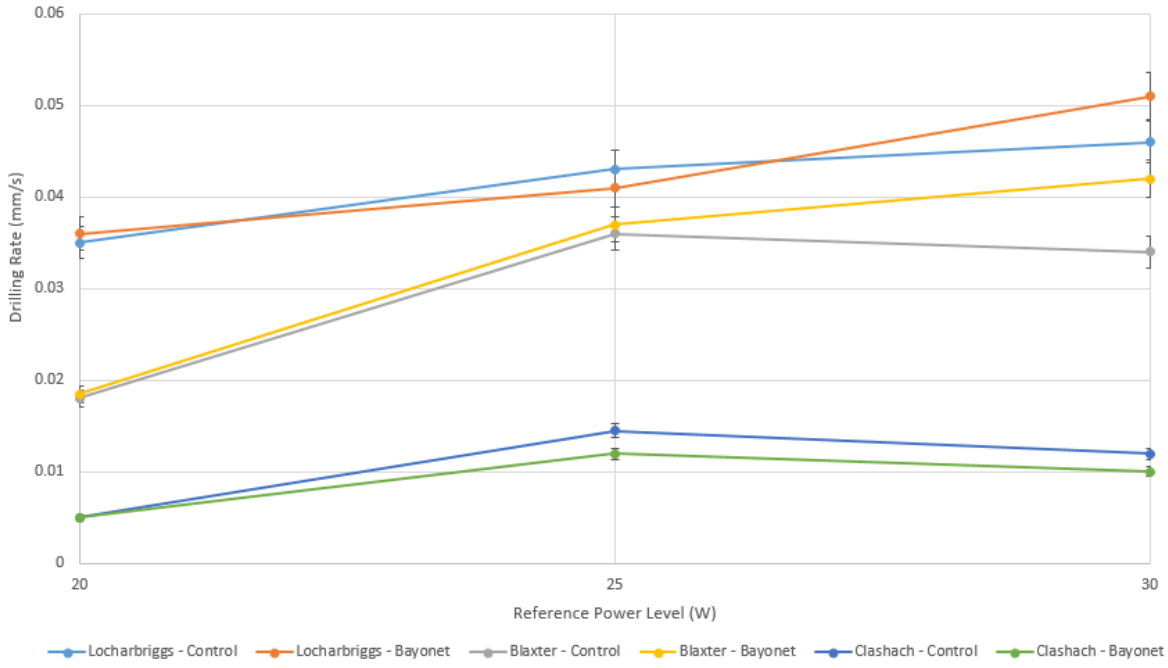


**Figure 53: Comparison of drilling rates through different sandstones using a Control drill bit and a Bayonet interface drill bit at different power levels.**

### 4.10.3 Discussion

Analysis of the results obtained from experimentation allows clear conclusions to be drawn on the use of a bayonet-interfaced drilling bit when utilizing the ultrasonic/sonic percussive drilling technique, combined with rotation, for planetary drilling applications.

Figure 47 and Figure 48 detail data obtained from the testing of the bayonet-interface drill bit and the control bit, respectively, on the relatively weak Locharbriggs sandstone, using a Reference Power Level of 20 W. It is possible to note that the Sample Held Power (SHP) exhibits a similar behaviour in both drill bit tests. The relatively low resistance experienced by the drill when progressing through this medium is easily identifiable by the signal which regularly drops below the minimum power level, thus commanding the linear actuator to advance. Furthermore, the Linear Actuator Position (LAP) graph exhibits frequent steps forward, suggesting that the drill is moving deeper into the formation at regular intervals. The 20 W data exhibits relatively few instances of exceeding the SHP maximum value, suggesting that a steady drilling rate could be achieved without a great demand on power. Figure 49 and Figure 50, results from experimentation using the same Locharbriggs rock sample but at a higher power level of 25 W display a slight reduction in similarity in the SHP signal, with the results from the bayonet-interface drill bit generally consuming marginally more power than the control sample, with an increase in the frequency of the number of power spikes. The LAP data, however, suggests a similar rate of progress through the rock formation. Figure 51 and Figure 52 exhibits further increases in the aggression of the drill as it progressed through the sandstone, observable as an increase in the frequency of the SHP signal. The frequency of power events which have a SHP value lower than the minima value of the Reference Power Level is also increased relative to the 20 and 25 W datasets resulting in an increased rate of progress through the rock formation. Figure 53 provides a comparison of the control and bayonet results for each rock type at all three Reference Power Levels tested. It can be observed that there is very little deviation in the drilling rates of the 20 and 25W experiments of Locharbriggs and Blaxter, with the bayonet-fitted drill bit outperforming the control piece at the 30W power level of both samples. The 25W Clashach test case sees the control piece outperform the bayonet piece, though a close similarity of the drilling rates of the 20 and 25W cases suggest that the 30W case may be erroneous, possibly as a result of inhomogeneity between test sites of a given sandstone block (noted during drilling runs on occasion), as it is unlikely that the bayonet would positively contribute to an increased performance. Post-testing inspection of the drill bits used showed no major deformation or damage to either test drill bit or the ability to connect and disconnect the parts of the bayonet-fitted piece.

### 4.10.4 Conclusions

Testing was conducted in order to establish the effectiveness of drilling when using bayonet-connected drill bits consisting of multiple parts connected together. The key objective of this series of tests was to establish if the use of a multi-piece drill bit mechanically connected through a stud-groove interface would result in the attenuation of the percussive wave transmitted to the rock target.

Results from coring tests in three different specimens of sandstone suggests that the drilling may be readily achieved using either the bayonet or control bits with losses not exceeding the targeted 20%, as seen in Figure 54. The tests provided confirmation that the easily disassembled bayonet-based system used would not limit the percussive performance of the system that could be achieved while confirming that the bayonet interface would withstand the high levels of shock loading delivered. Confidence generated through this series of tests allowed the bayonet-connected interface to be developed further for inclusion into the UPCD campaign model via the development of a novel concept of operations as discussed in 4.9.

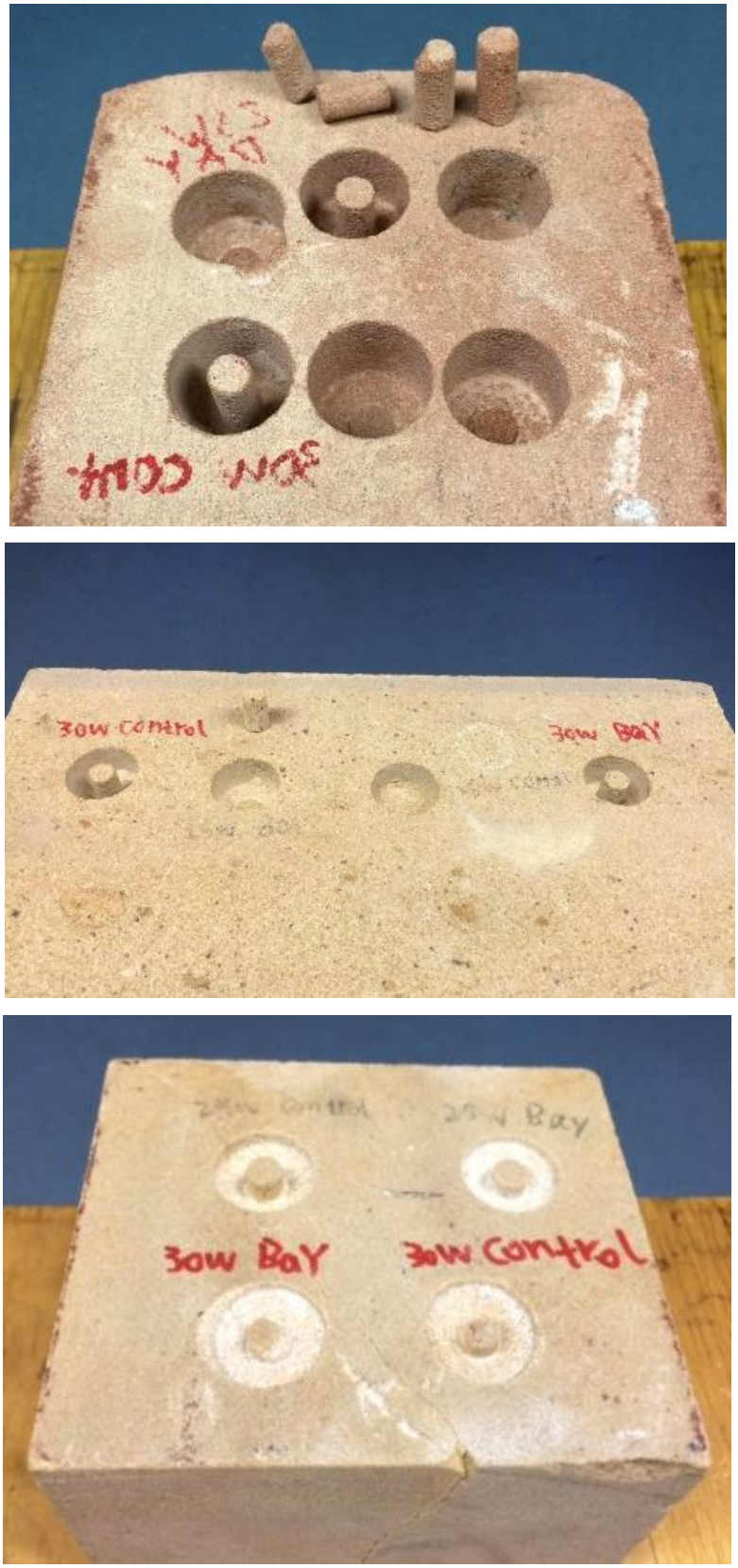


**Figure 54: Locharbriggs (top), Blaxter (middle) and Clashach (bottom) sandstone specimens post-testing.**

# 4.11 Laboratory Dry Drilling Performance

## 4.11.1 Test Setup

In order to evaluate the performance limits of the UPCD system, a series of experimental dry drilling runs were performed in the laboratory. As the core function of these tests was to establish the bounds of the 'campaign model' of the system, an experimental campaign was carried out using the hardware which would eventually be tested in Antarctica. Figure 55 presents a laboratory test featuring a block of Locharbriggs sandstone, a typical medium-hard testing medium. This series of tests concentrated on establishing the capability of the system when attempting to penetrate hard, dry rock, seen as the most challenging aspect of ultrasonic-percussive drilling given the low percussive energy generated in such systems. Predetermined reference power levels were used based upon work previously carried out.

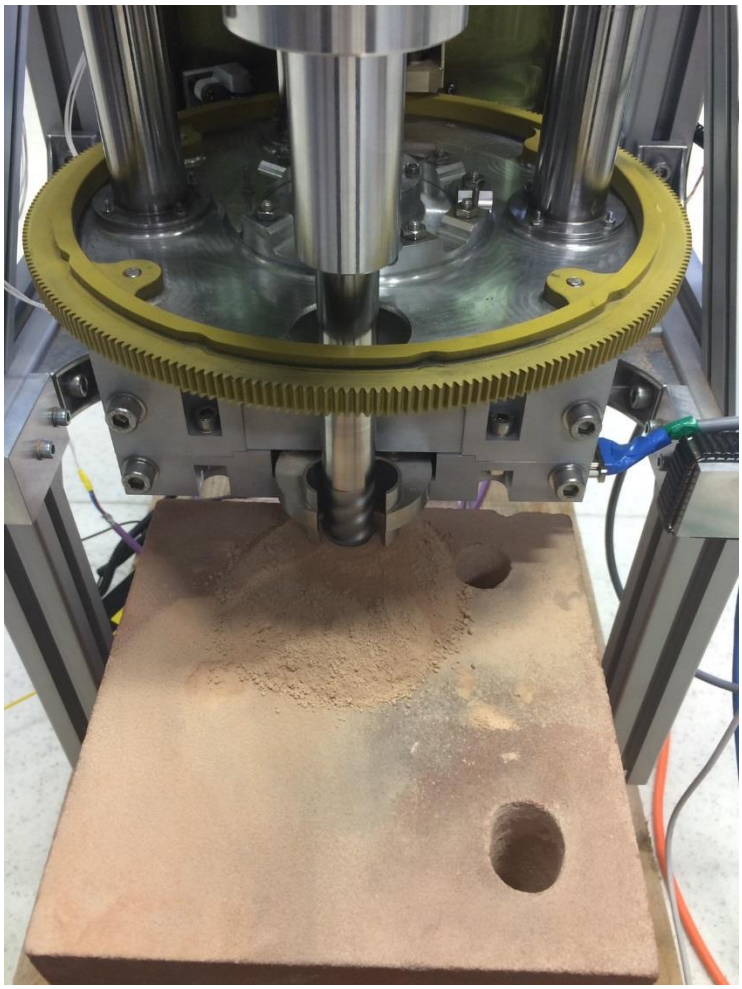

**Figure 55: UPCD drill into dry Locharbriggs sandstone under laboratory conditions. The drill can is shown at the centre of a sizeable spoil heap having almost reached the maximum depth required. Sandstone block measures 200 x 200 mm, for reference.**

### 4.11.2 Experimental Results and Discussion

Figure 56, Figure 57 and Figure 58 present the results of a series of tests which made use of a fully assembled (three-bit) drill string with a diameter of 21 mm and internal core diameter of 10 mm. These tests were conducted in order to evaluate the performance of the drilling system when attempting to penetrate a Locharbriggs sandstone target using 10 W of ultrasonic-percussive power – a reference power level which was proven to offer a reliable generation of percussion. Furthermore, the 10 W test was repeated three times at three different drilling locations in order to establish the effectiveness of the system when attempting to drilling using teeth which has been previously used.

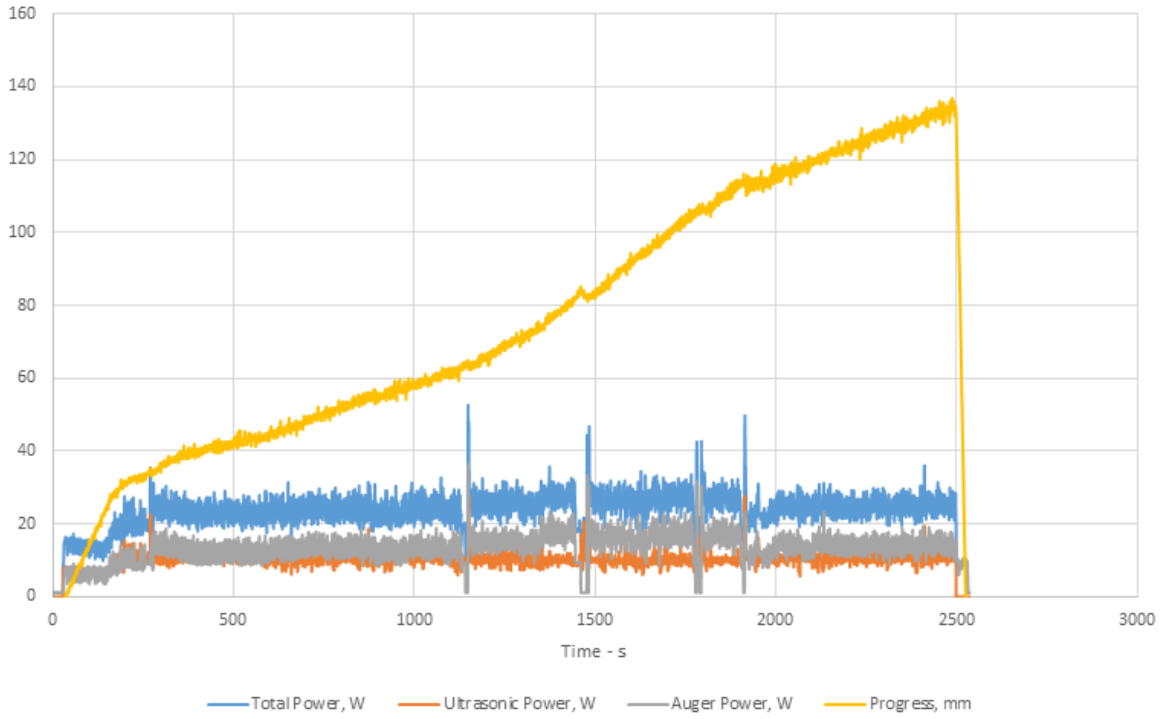


**Figure 56: UPCD drilling run in Locharbriggs sandstone using new teeth and standard UPCD drilling bit. Ultrasonic reference power level set at 10 W.**

Results obtained in Figure 56 indicate that the UPCD system is capable of achieving a rate of progress of 0.045 mm/s when the reference power level is set at 10 W using new drilling teeth. The average total power seen during this run was 23 W, meaning that the system specific energy to reach a depth of approximately 135 mm was 1909 MJ/m3.

A repeat of the 10 W reference power run, making use of once-used teeth, is as seen in Figure 57. The rate of progress is shown to drop to 0.0375 mm/s, in keeping with an increase in the tooth frontal area, while the total average total power was unchanged at 23 W. This

resulted in a slight increase in the system specific energy to 2291 MJ/m$^3$. Maximum depth of 135 mm was reached none the less.

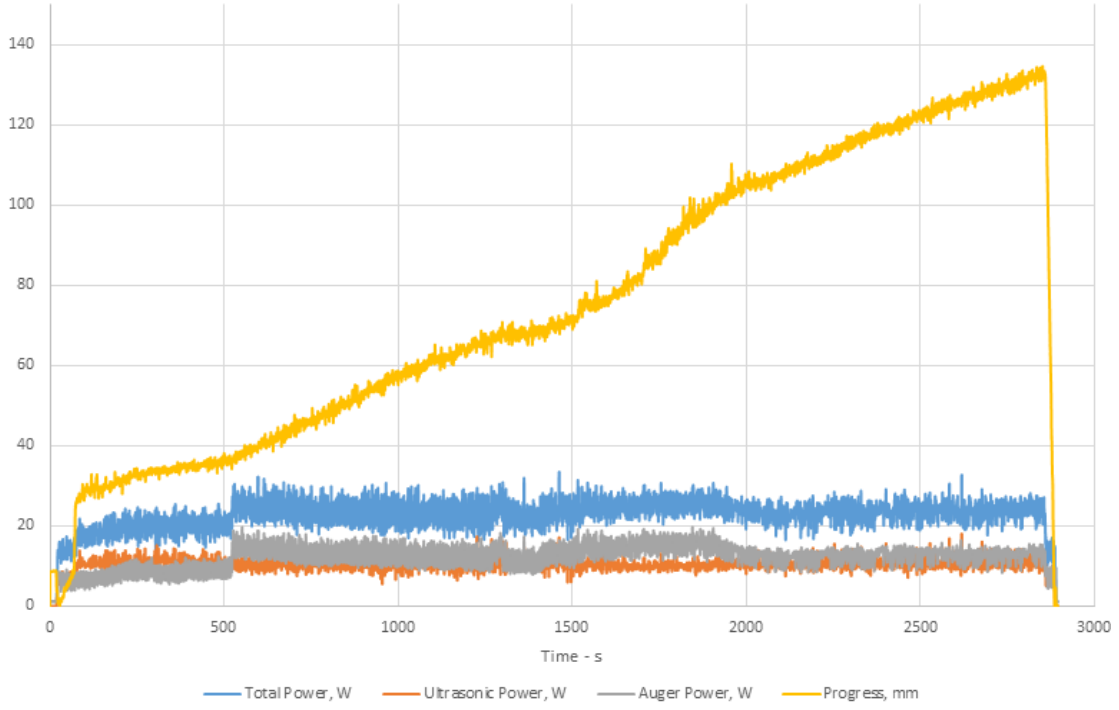


**Figure 57: UPCD drilling run in Locharbriggs sandstone using once-used teeth and standard UPCD drilling bit. Ultrasonic power level set at 10 W.**

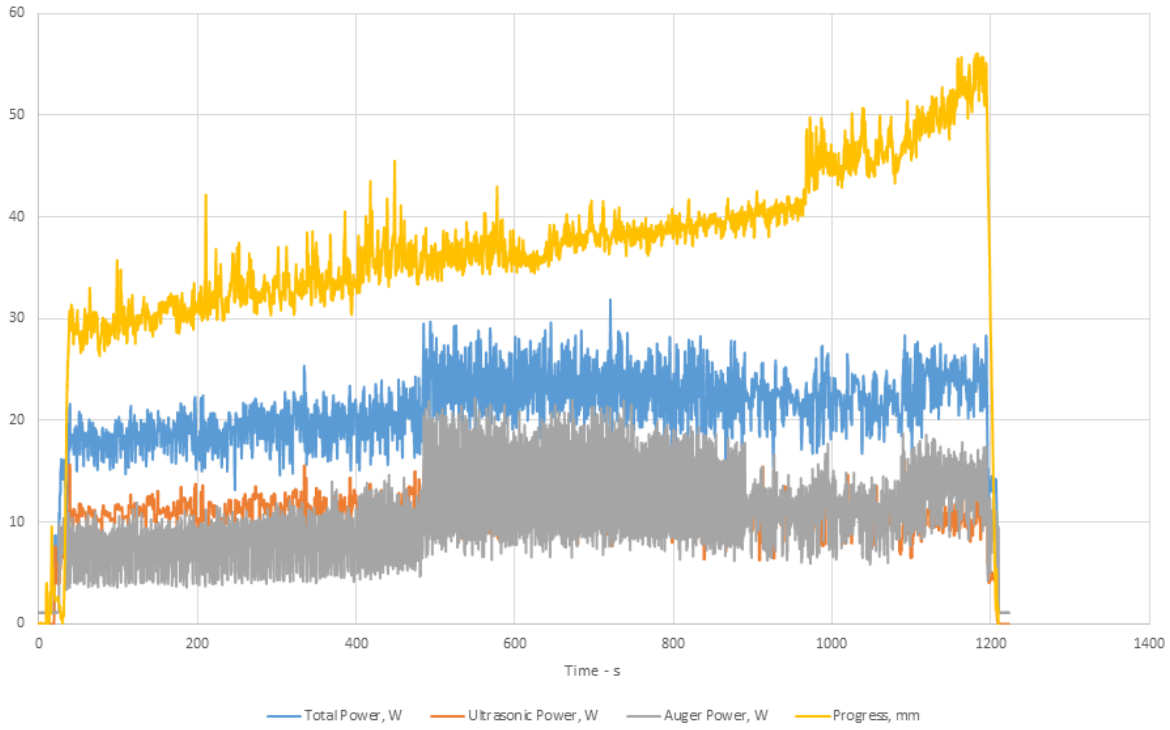


**Figure 58: UPCD drilling run in Locharbriggs sandstone using twice-used teeth and standard UPCD drilling bit. Ultrasonic power level set at 10 W.**

Figure 58 details the result of a third run with the same teeth used throughout. It can be noted that the run fails to achieve the depth attained by the previous two runs, and the rate of progress was substantially reduced to 0.018 mm/s. The average total power throughout the run was also slightly lower than previously noted at 20 W, likely attributable to a reduction in auger power needed at shallower depths. Thus, the specific energy is calculated to be 4150 MJ/m$^3$, more than twice that of the initial run with fresh drilling teeth. A maximum depth of approximately 50 mm suggests that the drilling run failed to progress beyond the acoustic spoil clearance boundary and into a drilling routine that relied upon augering in order to remove spoil. In fact, this behaviour was noted frequently during attempts to drill with well-used teeth and is not well understood. It is of note that spoil regrinding was noted at the depth maxima suggesting that there may be an issue with the spoil removal transition and the effect that this may have on the bottom-seeking autonomous control algorithm when it is forced to advance with less effective cutting teeth.

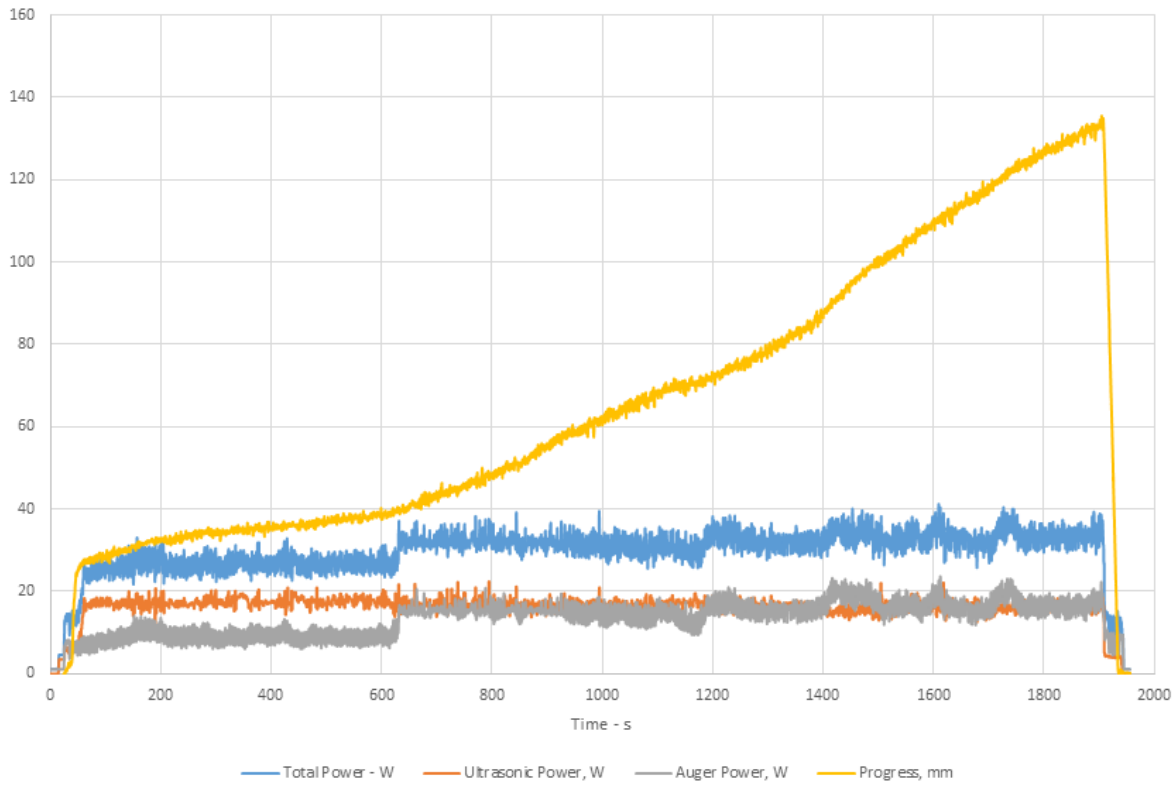


**Figure 59: UPCD drilling run in Locharbriggs sandstone using new teeth and standard UPCD drilling bit. Ultrasonic reference power level set at 16 W.**

In order to further evaluate the effectiveness of the UPCD system at increased power levels, the reference was reset to 16 W – a value considered to be the upper bound of what was deemed acceptable for the system to maintain percussion. An average power of 30.5 W was recorded, with a corresponding rate of progress of 0.06 mm/s. Thus, a specific energy

of 1837 MJ/m$^3$ was calculated. This result suggests that an outlay of approximately 6 W over and above the 10 W reference level generates a 33% increase in the rate of progress. The result is as detailed in Figure 59. An overview of the performance of the system is summarised in tabular form in Table 4.

Figure 60 presents the results of a drilling campaign which more accurately reflects the approach used during the field campaign, making use of the concept of operations developed in order to build a drill string continuously as the depth of the borehole increases. The addition of a second drill bit is noted at approximately 2500 s. As noted in section 4.10, no reduction in the rate of progress, analogous to the attenuation of the percussive wave across the bayonet interface, was found.

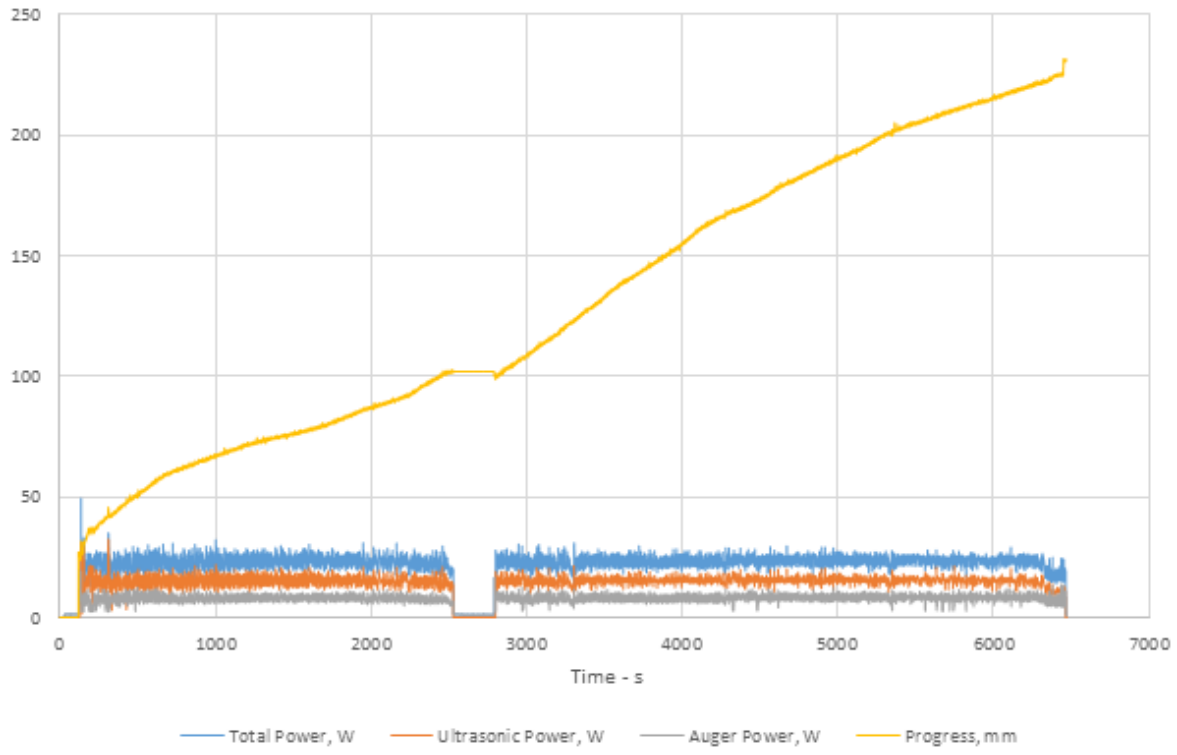


**Figure 60: UPCD drilling run in Locharbriggs sandstone. Drilling is interrupted at approximately 2500 s in order to accommodate the addition of a second drill bit to the string, as per the ConOps.**

| Drilled Material | Ref. Power - W | Total Power - W | Auger Power - W | US Power - W | Depth - mm | RoP - mm/s | SE - MJ/m3 | Teeth Use |
|---|---|---|---|---|---|---|---|---|
| Locharbriggs Sandstone | 10 | 23 | 13 | 10 | 135 | 0.045 | 1909 | New |
| | | 23 | 13 | 10 | 135 | 0.0375 | 2291 | Once |
| | | 20 | 10 | 10 | 50 | 0.018 | 4150 | Twice |
| | 16 | 30.5 | 16 | 14.5 | 135 | 0.06 | 1837 | New |

**Table 4: Overview of UPCD Laboratory results**

## 4.12 Mission Applicability

While the hypothetical mission profile, resource availability and operational scheduling typically form the main constraints which determine the drilling approach used, it is clear that the ultrasonic-percussive drilling approach is a solution which may be particularly applicable in certain scenarios but not others. The system benefits from exceptional energy efficiency, with typical sandstone runs in the range 1800 – 2200 MJ/m$^3$. The generation of percussion is thought to be particularly efficient [38], though the low percussive energy delivered per strike, in the region of 0.1 J for the UPCD system, results in a particularly slow drilling process in the range 0.02 – 0.06 mm/s, and may result in limited success when attempting to penetrate terrain harder than ~50 MPa. Thus, it is likely that ultrasonic-percussive drilling systems are particularly applicable in mission scenarios which are heavily dependent on a high degree of robotic autonomy and constrained by the energy available for drilling. Missions with either a shallow depth requirement or those which are not heavily constrained by time are also favoured due to the conservative rates of progress noted. Furthermore, terrain which is not heavily cemented by cryogenic temperatures or rich in igneous material may be preferable as it is clear that any terrain which is harder than that tested in the laboratory may result in rates of progress which are ineffectual in most mission scenarios. When considered alongside other challenging aspects of the technology, determined through a qualitative assessment, such as the propensity of ultrasonic-percussion to stall when drilling is pursued outside of a narrow set of weight on bit limits, the applicability of the technology may be further reduced. Missions targeting the lower and equatorial latitudes on Mars may benefit from the use of the technology for a number of reasons. Environmental conditions in these regions are likely to preclude the formation of cryogenic ice lenses and inclusions within the near subsurface. Previous missions targeting these regions do not suffer from the same lifetime restrictions which have limited missions to higher latitudes on Mars and this may allow, and perhaps favour, a more conservative approach to drilling progress. Conversely, a lack of seasonal variance in the solar irradiance at these latitudes, and few ‘Special Regions’, allowing nuclear power sources where applicable, may mean that energy availability is not a driving constraint. Thus, the use of a drilling system which utilises the ultrasonic-percussive drilling technique may require a more holistic approach which considers system reliability and other risk-related factors during mission trade-off studies before any firm conclusions can be made.

## 4.13 Antarctic Field Campaign

The developmental stage of the UPCD saw the system tested regularly in the laboratory environment to ensure that the basic functionality of the system was assured, but testing under laboratory conditions is inherently limited by a number of key factors. In the context of planetary drilling, perhaps the most pertinent challenges which a drilling system must overcome include extremes of temperature, tenuous ambient atmospheric pressure and unknown terrain. While it may be possible to replicate various combinations of these factors in a laboratory test campaign, achieving a testing scenario which is sufficiently high-fidelity such as to replicate the planetary environment is incredibly challenging. To this end, testing of planetary drilling systems is often carried out with an incremental approach which exposes the system to individual elements of the planetary environment. While this may prove to be less favourable than a holistic approach, the confidence generated through establishing the robustness of the system against these individual challenges allows the designer to quickly identify the root cause of any failures or underperformance. Furthermore, in some cases, laboratory testing in ambient conditions may represent an over test, thus enhancing confidence levels in the system. This is particularly true when testing the drilling system in water-cemented terrain which may prove to be less challenging at (more realistic) reduced temperatures and atmospheric pressures.

Perhaps the greatest challenge which must be overcome by any planetary drilling system is that of the unknown. Missions seeking to explore planetary bodies typically suffer from a deficit of prerequisite knowledge of the terrain which is likely to be encountered, thus establishing accurate system requirements may prove to be difficult. While partially-realistic planetary terrain can be mocked up in the laboratory through the use of simulants, operator bias is difficult to overcome and the true randomisation of test simulants hard to achieve. It is for this reason that system designers seek to test in conditions which are naturally analogous to the foreseen target location, and the diverse nature of Earth's environments means that planetary analogues exist in a wide number of locations. When setting the UPCD requirements, it was decided that the system would be designed with the goal of extracting core samples from terrain which was consolidated by the presence of frozen water analogous to that which would be encountered in the Polar Regions of Mars or the Moon. Water-consolidated terrain stipulates a different approach to the drilling process and comes with unique challenges which must be overcome (discussed in Section 4.14.2).

In order to establish the capability of the UPCD system in the targeted environment, it was decided that the project would seek to test the completed campaign drill in a suitable Mars polar analogue. While the UPCD system was designed for operation at Mars, and thus not specifically optimised to operate at the analogue site, it was felt that a carefully identified field site could offer a suitable testing environment for the system. Analysis of the various options [46] concluded that a field campaign in the Polar Regions, either in the Arctic or Antarctica, would prove to be a suitable option given the reduced temperatures, polar geology and access to permanently frozen terrain at the near-surface. Testing in such regions offers geological features, such as the presence of frost polygons, which have been identified at polar locations on Mars. Furthermore, while the atmospheric pressure at these sights would always be substantially higher than those which are noted on Mars, it is possible to minimise the significance of this element due to the fact that pressures above the triple point of water (~6 mBar) are routinely recorded at the planet. These relatively high pressure regions on Mars are often coupled with temperatures in or around the freezing point of water, meaning that typical conditions at the planet during more clement seasons may not be dissimilar to those found at Earth's poles. Although these conditions may not necessarily represent the conditions during all stages of Mars' orbit, or at all locations, such conditions are likely the most arduous test of a drilling system which had not been designed to operate effectively in slushy/wet conditions.

While the presence of compatible polar geological features could be assured, the composition of the target terrain was unlikely to match that which would be found on Mars. This was accepted on the basis that the assured volatile content of terrestrial ice-cemented permafrost was of more significance than the strength conferred by the potentially cryogenically frozen Martian equivalent given that the drill had succeeded in drilling hard materials in the laboratory. In fact, the terrestrial saturated terrain was likely to represent an over-test due to the fact that the Mars subsurface is typically less heavily saturated.

The availability of reliable and proven logistics support through the British Antarctic Survey (BAS) meant that, despite the clear discrepancy in distance between both polar options from the UK, the Antarctic option would prove to be the most logistically straightforward. To this end, a field site at Coal Nunatak, Alexander Island, was chosen.

### 4.13.1 Coal Nunatak Field Site

The testing location identified at Coal Nunatak (73°S 68°W) was selected for a number of reasons. Primarily, the fact that the site featured at Nunatak, or protruding mountainous feature, ensured that rocky terrain would be readily exposed and available for shallow

drilling using the UPCD system, designed to drill to a depth of 300 mm. Furthermore, a southerly latitude would enhance the likeliness of temperatures sufficiently below freezing point, ensuring that frozen terrain would be available for drilling even during the Antarctic summer months when the campaign would take place. Finally, the proposed testing location was found to exhibit excellent polar geology similar to that which has been noted at similar latitudes on Mars. Figure 61 reveals the Nunatak where testing took place. The main camp was located at the foot of the Nunatak and the team trekked to the summit daily for field operations. Note the steep gradient and exposed bedrock of the Nunatak. When assessing the fidelity of such a location, frost polygons are an excellent indicator of a robust planetary polar analogue as they have been found at both the Phoenix and Viking landing sites. Figure 62 compares these features both at the field site and on Mars.

**Figure 61: Coal Nunatak field test site. Note, drilling operations were conducted at the summit of the mountainous feature in the background.**

**Figure 62: Frost polygon features at the field site (top). Similar features have been found at both the Phoenix and Viking landing sites on Mars (bottom). Courtesy NASA/JPL/University of Arizona.**

### 4.13.2 Drilling Operations at Coal Nunatak

In order to evaluate the performance of the drilling system, objectives were set which would allow the key elements of the hardware to be tested in multiple terrain types. Missions designated for Polar Regions of the Moon or Mars, or the icy moons of Jupiter or Saturn may encounter terrain replete with bulk ice masses or ice lenses present within the regolith. Is is for this reason that both rocky terrain and ice were selected for testing during the field campaign.

Upon arriving at the field location, it was quickly noted that the ambient temperature, and subsequently that of the near subsurface, were substantially more elevated than had been expected. Historical temperatures in the region suggested that typical values in the region of -10 to -15°C were to be expected, so the team were disheartened to note that air temperatures did not drop below -3°C at any point during the field campaign and were often above 0°C. In fact, heat haze was often noted onsite during mid-afternoon activities. This meant that all drilling operations were conducted in temperatures around that of the melting point of water – a factor which had implications for the drilling process and the fidelity of the site as a planetary analogue.

As discussed in Chapter 3.5, removing drilled cuttings from the borehole in a timely manner is a key element of the drilling process. The UPCD system makes use of conventional augering in order to clear cuttings from the borehole, the cuttings which are to be removed must be completely dry in order for the hole to be efficiently cleared. This proved to be a major limitation due to the environmental conditions found at the site during the test campaign. Figure 63 reveals the extent of the melting found within the subsurface at the testing location. In fact, scouting trenches revealed that the active layer, the layer of seasonally unfrozen terrain) extended to depths in excess of 500 mm, meaning that surface drilling operations would be affected. The moist terrain revealed would prove exceptionally difficult to drill due to its clay-like properties tending to clog the auger as opposed to conveying spoil to the surface. The sticky nature of the terrain also imparted a drag on the auger, increasing the torque levels required to drill and thus inducing motor stall which impacted upon progress. Figure 64 shows the results of an aborted drill run in to the terrain at Coal Nunatak. Upon reaching a depth of 70 mm, further progress was limited due to the aforementioned torque limit. The shallow design of the UPCD system meant that any further drilling attempts in the melt-saturated active layer were abandoned.

In an attempt to reach still-frozen terrain, trenching was attempted in the ice pack in order to expose terrain which would have been protected from seasonal melting. Figure 65 details the attempts made to drill within a trench carved into the ice. While the terrain was less

affected by the effects of seasonal melting, the above ambient air temperature resulted in the production of liquid water during drilling operations. This severely limited the effectiveness of drilling for reasons similar to those previously discussed.

**Figure 63: Extent of the near-surface melting at the Coal Nunatak field site. Active layer proven to exist at depths of up to 500 mm (top) and instability of ice layer caused by unseasonably high local ambient temperatures (bottom).**

**Figure 64: Aborted drill run in sticky terrain. Maximum depth achieved of approximately 70 mm. Drill stalled due to auger torque limit breach preventing further progress.**

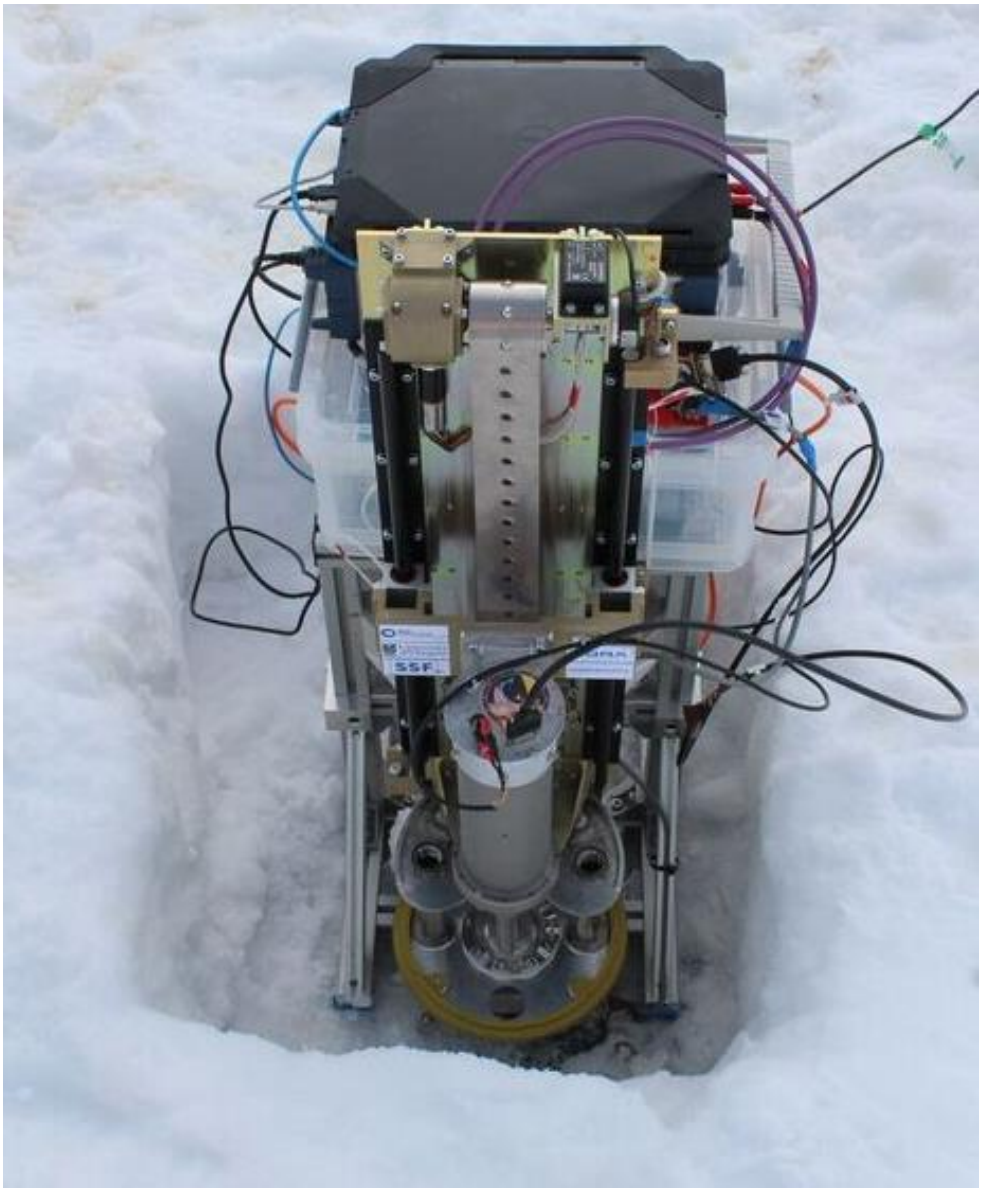

**Figure 65: UPCD operating in trench carved into the ice pack. While the accessed terrain was not as severely affected by seasonal melting, ambient air temperatures above the melting point of water limited the effectiveness of drilling operations.**

While drilling operations into the regolith layer were limited in all cases by the presence of melted water, testing of the system in the ice/snow pack proved more promising. Figure 66 follows the progress of the drilling system into icy terrain. During this sequence of operations, the drilling system successfully managed to assemble a complete drill string and drill to the maximum depth before disassembling the drill string in to individual bit elements and caching them in the sample caching carousel. This was considered to be, perhaps, the greatest achievement of the UPCD campaign and offers enormous potential for future drill system developments.


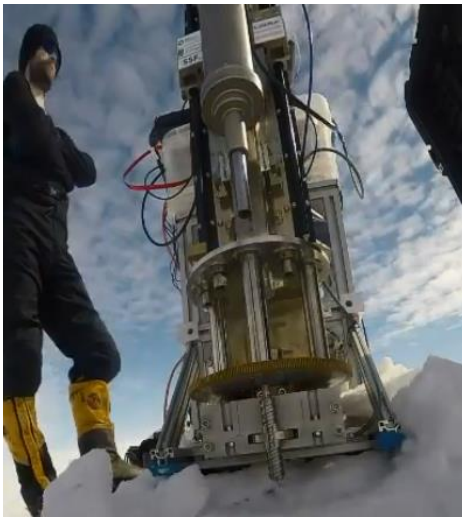



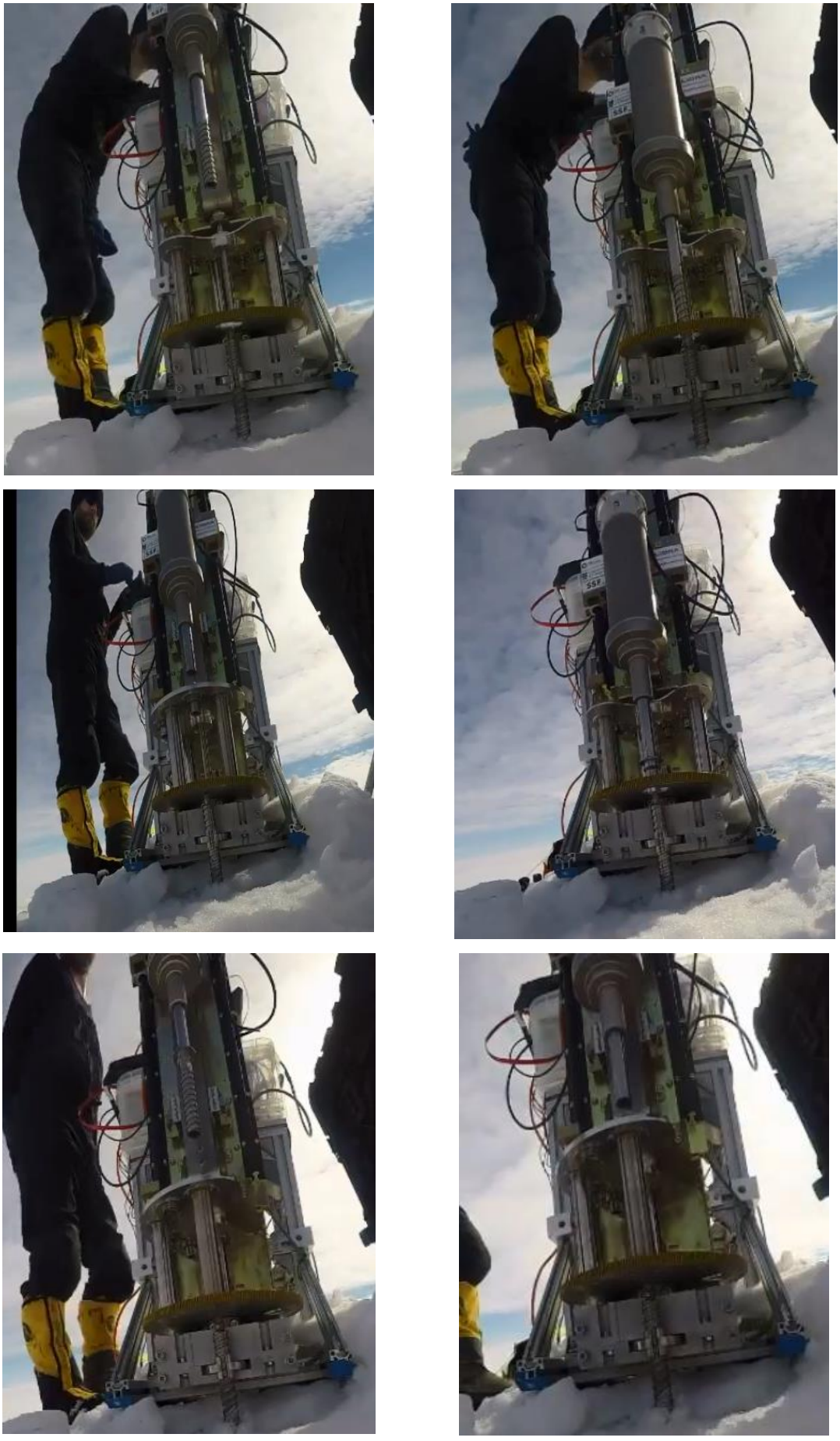

**Figure 66: Assembly and Disassembly of complete drill string in Antarctic ice pack.**

It is of note that the operational procedure detailed in Figure 66 commences with the first drill bit having drilled the terrain, in the process of clamping and disconnecting the drill tool from the clamped bit. Figure 67 highlights the position of the Deployer Module (DM), analogous to that of the position of the drill tool, during the drilling operation. The steps as indicated in the figure are as follows:

1. Collect Bit 2 from Silo 2 of Cache Carousel
2. Connect to Bit 2 to Bit 1
3. Drill to depth with two drill bits
4. Collect Bit 3 from Cache Carousel (failed attempt)
5. Collect Bit 3 from Cache Carousel (failed attempt)
6. Collect Bit 3 from Silo 3 of Cache Carousel
7. Connect Bit 3 to Bit 2
8. Drill to full depth with three drill bits
9. Collect Lid 3 from Cache Carousel
10. Connect Lid 3 to Bit 3
11. Lock Lid/Bit 3 into Silo 3 of Cache Carousel
12. Collect Lid 2
13. Connect Lid 2 to Bit 2
14. Lock Lid/Bit 2 into Silo 2 of Cache Carousel
15. Collect Lid 1
16. Connect Lid 1 to Bit 1
17. Lock Lid/Bit 1 into Silo 1 of Cache Carousel
18. Return to Home Position. Sequence Complete.

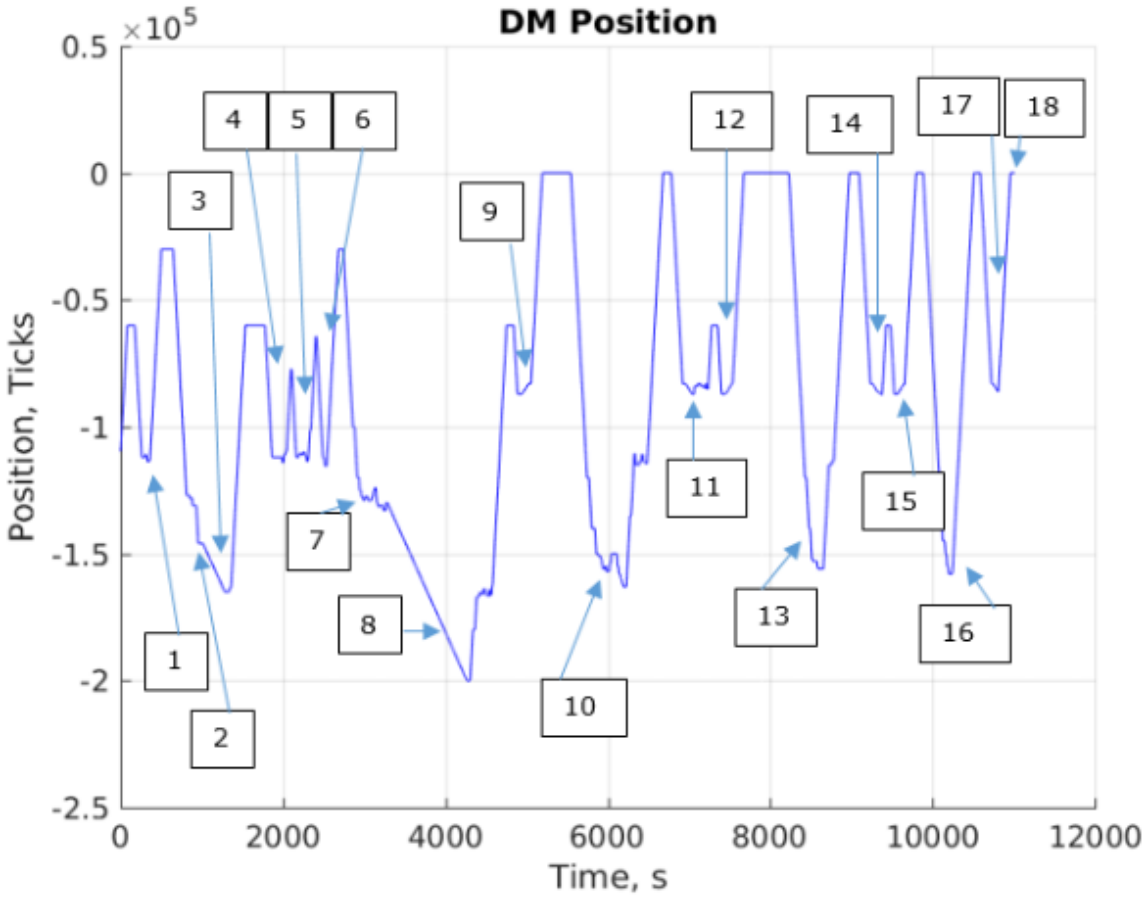


**Figure 67: Position of Drill Tool during drilling operations in ice pack.**

During this complete operation, total power levels were always noted to be below the nominal 100 W limit which is considered to be a typical point of reference for planetary drilling systems. Figure 68 details the total power consumed by the complete system (inclusive of the power consumption during drilling, operation of the carousel and clamping system and the actuation of the belt-driven deployer mechanism). In fact, the average power drawn by the system was approximately 17 W with a peak of 94 W.

The successful execution of a complete drilling cycle into the ice pack generated confidence in the system despite earlier setbacks imposed by the unfortunate conditions at the test site which limited further drilling operations in soil and rocky terrain. While the extended period of drilling operations, in excess of 3 hours, combined with ambient temperatures typically above that of the melting point of water meant that icy core recovery was poor in all operations into the ice pack, small samples of icy core were recovered, as seen in Figure 69.

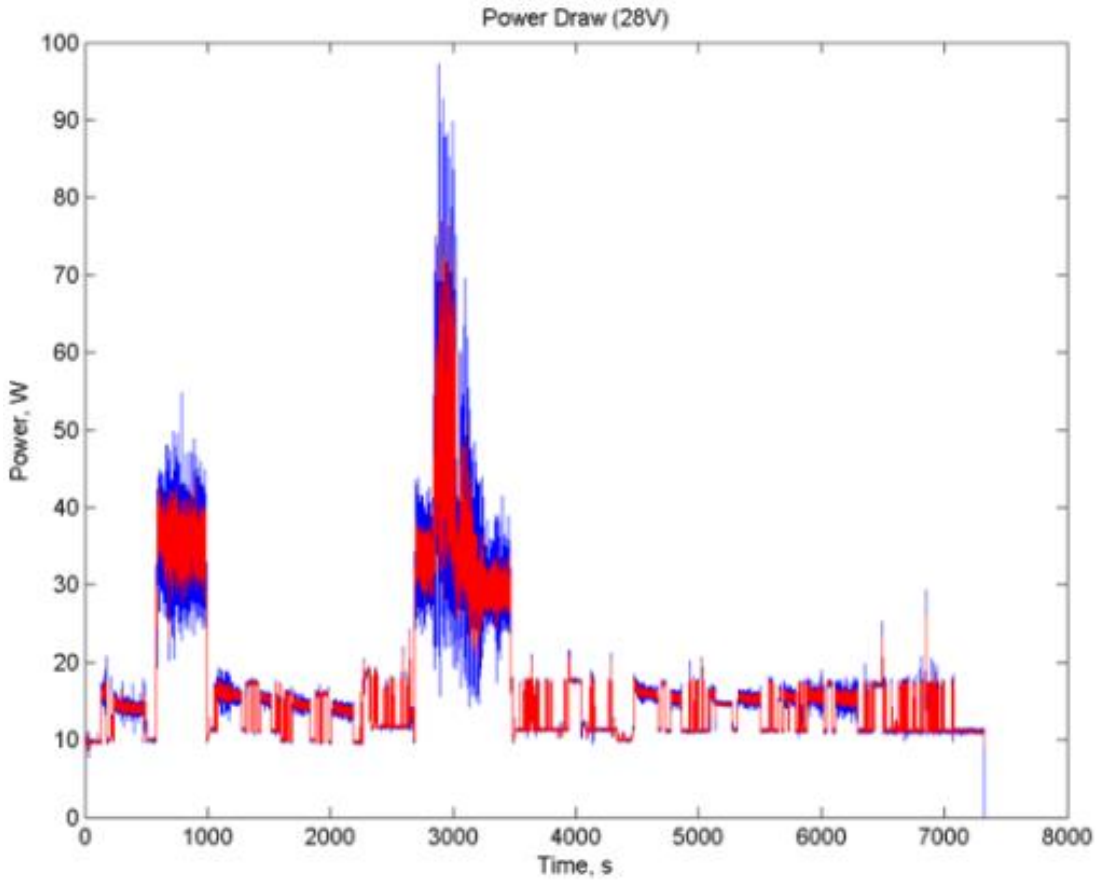


**Figure 68: Total power consumption of the UPCD system during drilling operations into the ice pack.**

**Figure 69: Partially melted ice core recovered from drilling operations. Core diameter ~10 mm, for reference.**

### 4.13.3 Conclusions

The testing of the UPCD system at Coal Nunatak, Antarctica proved to be a challenging yet fruitful campaign which pushed the functional limits of the system in many respects. Unseasonably mild ambient conditions at the field site, resulting in excessive surface water and an extension of the active layer, limited the capability of the drilling system when augering spoil generated by the terrain-breaking process. This in turn limited the depth which could be achieved when drilling the polar regolith. Despite this setback, the drill achieved greater success when operating in the ice pack. The system achieved a complete drill string assembly, drill to depth, and drill string disassembly and caching with little assistance from the operator.

## 4.14 Drill Control

### 4.14.1 Baseline Bang-Bang Algorithm

In order to operate successfully on a planetary surface, systems which are designed for such purposes must feature high levels of autonomous capability in order to progress through unknown terrain and react to changing terrain and spontaneous fault states without human control input. Furthermore, the nature of ultrasonic-percussive drilling is such that if the system is exposed to excessive or insufficient weight on bit levels, the generation of percussion may stall. This is due to a need to ensure that the contact between the horn and the free mass is kept in a 'sweet spot' which is different for every system. Ensuring that the drilling system operates in a region where free percussion is generated while ensuring that the drill progresses through the terrain in an efficient manner is perhaps the most difficult element of ultrasonic-percussive drilling.

In order to accomplish this, a control system was developed that relied upon the power drawn by the ultrasonic transducer as an analogy for the weight on bit of the system. As axial force is applied to the ultrasonic transducer, the auto-resonance system (which, as the name suggests, ensures that the ultrasonic device is kept at a resonant frequency during operation) compensates by delivering more power to the device. These parameters can be considered to be directly proportional to one another. Calibration of the ultrasonic power therefore allows this variable to be used in place of the weight on bit delivered to the drill bit without the need for a force sensor. This ensures both system simplicity and fault tolerance as there is less reliance upon (often fragile) force sensors to determine the weight on bit. The relationship between the ultrasonic power and voltage and the axial force applied is as shown in Figure 70 [45].

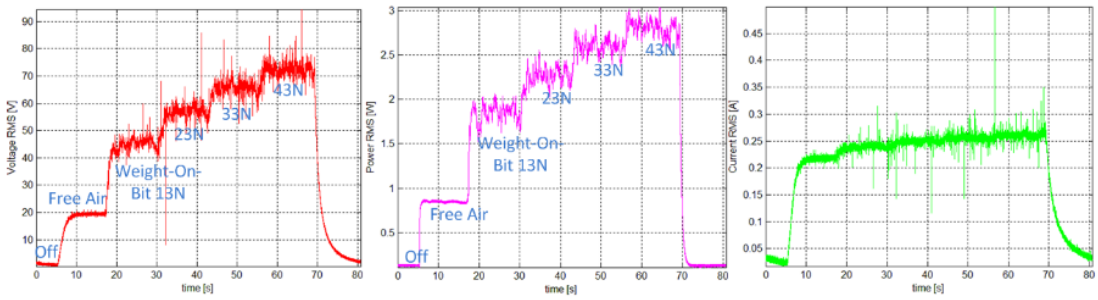


**Figure 70: Measured RMS voltage, power and current of the ultrasonic transducer. Note, the constant current system used to power the device means that the current signal is not usable as a means of controlling the progress of UPCD *[45]*.**

Figure 70 details the experimental data from an attempt to establish the effect of applying force to the ultrasonic transducer. Starting with the device running in free air under its own weight, mass is added incrementally (approximately 10 N per increment). A step change in both the power drawn by the system and the voltage delivered is noted while the current drawn remains approximately level throughout. This is attributable to the fact that the P100 device which supplies power to the ultrasonic transducer operates in a constant-current mode. It is for this reason that the current signal cannot be used as a control signal. As the ultrasonic power increases proportionally to the force applied to the system, and in a very predictable manner, the power can be used as a proxy for weight on bit during drilling.

In order to use power as means of controlling drilling progress, the system must be tested in a variety of terrain types and suitable base power levels determined empirically. Upon establishing a reference power level, upper and lower power levels (typically around 10% of the base figure) are used to trigger the motion of the Z-axis deployer system in a bang-bang control system. Drilling commences and in a well-tuned system, the rate of penetration will be steady such that the deployer mechanism is commanded to step forwards towards the terrain in a fashion that optimises drilling efficiency while avoiding overzealous advance which may stall the drill. In order to ensure that efficient drilling operations are achieved, parameters such as the upper and lower bounds chosen, the frequency which the system evaluates the ultrasonic power and the time step used by the actuator during periods of forward or backward motion must be carefully chosen. The control process used is as detailed in Figure 71 [45].

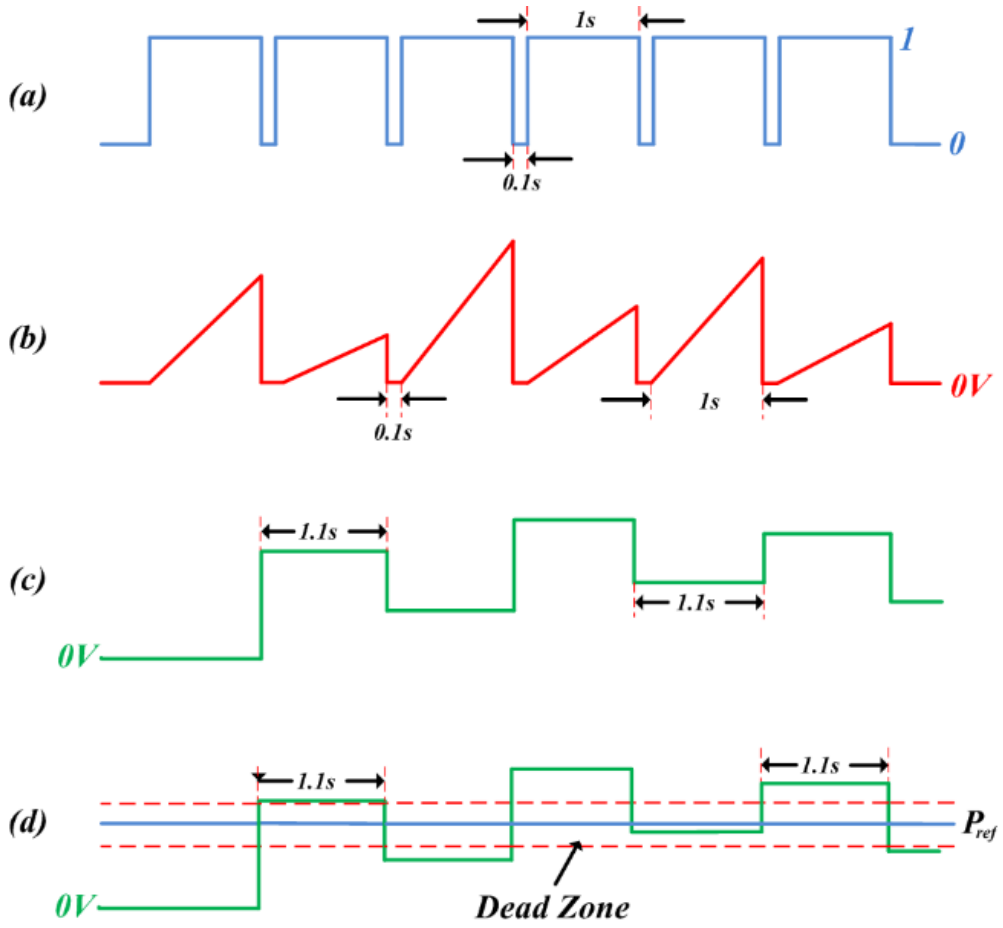


**Figure 71: Control algorithm used in UPCD. (a) Timer output, (b) integrator's output, (c) sample held condition, (d) motion compared with reference level.** *[45]*.

In the algorithm detailed in the Figure 71, the timer, (a), monitors the power suppled to the ultrasonic device for 1 second of on-time which is evaluated and integrated, (b), before the deployer mechanism is actuated during a 0.1 second window. This deployment time of 0.1 seconds has been experimentally proven to ensure a smooth motion of the system. The power levels calculated are then compared to the reference level, (c), and the system adjusts in the next control iteration. Values which are higher than the upper reference level indicate the system is failing to penetrate the terrain at the rate of progress associated with the power setting, while values which are less than the lower reference level suggests that the drill has completely pulverised the terrain and is perhaps over-performing. With respect to the implementation of the control system developed for the UPCD, reference power levels were set through a robust series of tests in many terrain types. This makes the system somewhat exposed to unknown terrains, but this is easily rectifiable. It may be possible to adjust the system such that a starting reference power level is set that tends towards conservative for most terrain types and the reference power level is constantly altered by comparison of the drilling rate of progress with an acceptable value. As the rate of progress ultimately determines drilling stall and auger choke, this is the single most important parameter in the

drilling process. The system as deployed featured decoupled rotation and percussion, but it may be possible to include auger power within the control system such that a rotary stall may be completely avoided.

### 4.14.2 Advanced Thermal Control

In order to maximize the scientific return from planetary missions which seek to explore the planetary subsurface and acquire volatile-bearing samples for in situ analysis or return to Earth, mission scientists, instrument designers and mission planners are often faced with the need to compromise in order to ensure that the acquired samples are of a quality which can fulfil the tier one objectives of the mission. One such compromise is an acceptance of the effects of the utilization of drill systems on the type of samples obtained and the quality of such a sample. While drills prove to be an efficient means of sampling small quantities of material at depth, the physical act of obtaining these samples, and the complex nature of the task means that it is likely that the scientific output will suffer from some level of degradation in the process. For example, although the objectives of a mission may favour the acquisition of terrain core samples over powdered cuttings, the design of a drill and sample handling/processing system is inherently more complex than systems which acquire loose cuttings. Thus, such a system comes with increased costs and associated risks. While it may be possible to work around such compromises, other compromises associated with the drilling process are less avoidable. The work done in breaking terrain formations is directly proportional to the strength of the formation. As the strength of water-bound terrain increases with a decrease in the temperature of the formation and an increase in the level of saturation, saturated permafrost at cryogenic temperatures may exhibit strength which is comparable to that of medium-hard sandstone, [47] and cryogenic water ice may be as strong as structural concrete [48]. An example of this effect is presented in Figure 72.

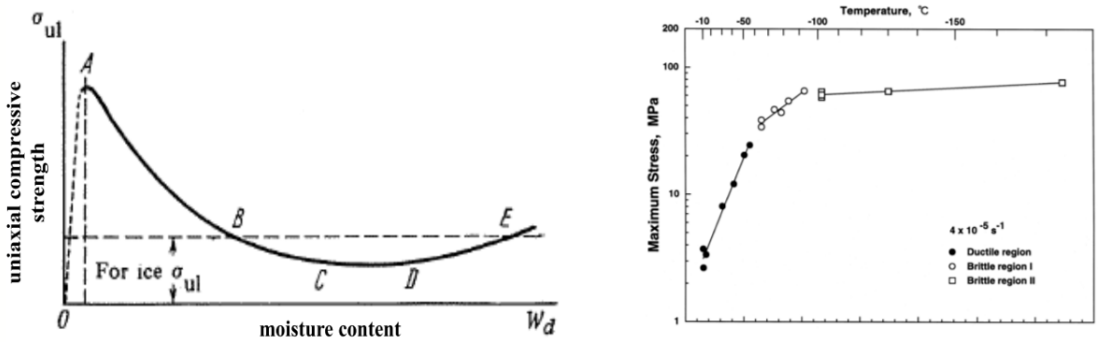


**Figure 72: Figure detailing the relationship between the moisture content within ice-cemented terrain and the strength of the 'composite' mixture created (L) and a plot detailing the effect of reduced temperatures on the strength of pure ice (R)** *[48]*.

This poses an issue when drilling such formations as it is inevitable that heat from the drilling process will be transferred to the drill bit, cuttings and borehole, melting water in the process. In fact, Szwarc [28] established that during core drilling operations, the drill bit, cuttings and core received 11%, 6.6% and 2.5% of the total heat generated, respectively. Clearly, the direct heating of the core and cuttings will result in a degradation of the volatile ratios held within these samples through direct sublimation (assuming suitable atmospheric conditions) or, in the worst case, melting. In planetary applications, the drill bit may act as a heat pipe, wicking heat away from the bit-rock interface to the colder surface. While this offers a means of reducing heat flow to the borehole, the warmed section of drill bit closest to the bottom of the borehole may act to thaw water held within the cuttings which may then refreeze on a colder section of the bit as the cuttings are conveyed upwards by the auger. If the thawed cuttings refreeze on to the auger flights, and subsequently to the borehole wall, the drill will be rendered immobile. In laboratory conditions, where the surface air temperature typically exceeds that of the downhole, the problem is only worsened as the bit temperature increases. These freeze-in events are typically unrecoverable at even shallow depths as detailed in Figure 73 [49]. In this case, the drill depth achieved before freeze-in was on the order of 30 mm and the drill bit was recoverable only through the use of a chisel. This is attributable to the fact that the adhesive strength of ice on stainless steel is approximately 1.65 MPa [50] meaning that the force required to free the bit approached 1200 N. Given the lightweight nature of landed spacecraft and the reduced gravitational acceleration found at candidate locations, it is likely that there would be insufficient axial force available for freeing the trapped drill bit. Furthermore, it is unlikely that the drill system itself would be able to provide the high levels of torque required to shear the bond through rotation alone. Therefore, depending on the scientific objectives of the mission, it may be possible to classify fault modes associated with the permanent seizure of the drill string downhole as single point failures which must be avoided at all costs. As the time scale of a freeze-in fault may be on the order of a few seconds, it is possible to conclude that any mission which aims to deploy a drill system in icebound terrain, which does not wish to impose strict constraints on the scheduling of drilling operations, must have a means of sensing the onset of these faults in real time before taking measures to ensure that drilling activities do not result in a freeze-in. The mechanisms by which thermal control of the drillstring can be achieved shall be discussed in more detail in the next section of this work.

**Figure 73: Freeze-in event at shallow depth. Note, chisel required to free bit from frozen saturated simulant** *[49]***.**

In cases where the drill bit does not succumb to a complete seizure of the drill bit, it is possible that the thaw-refreeze event may still prove critical enough to effect the cessation of drilling due to bit glazing and/or auger blocking.

**Figure 74: Bit glaze and auger blocking event - a result of thawing and refreeze of water present within drilled cuttings.**

Figure 74 details a particularly critical incidence where both of these failure modes occurred simultaneously. While it is possible to avoid a freeze-in event in such a case, it is

likely that the drilling operation must be paused in order to allow the bit to thaw. The bit must then be cleaned and re-cooled before it can be utilized for future drilling attempts.

### 4.14.3 Sensing Refreeze Faults

In order to develop a control system which is capable of sensing the onset of the fault modes attributable to the melting and refreezing of volatiles contained within cuttings and taking action to prevent seizure of the bit, it is critical that the 'markers' of such events are identified. While the onset of a freeze-in event may be marked by a sudden increase in the auger power demanded (as the auger begins to stick downhole, as seen in Figure 75 from 400 s onwards), auger torque increases may be attributable to other fault states. Work by Zacny [51, 30] suggests that the surest method of sensing the onset of such faults is through a combined approach of monitoring both the physical state and the temperature of the fresh cuttings at the bit-rock interface. The need for sensing the physical state of the cuttings is necessitated by the presence of salts and minerals, such as perchlorates, which are found ubiquitously on Mars and act to depress the melting point of the eutectically depressed briny solutions it forms [52]. The resulting solution will have a melting point which is a few degrees lower than pure water, though there exists the possibility for super-eutectic ice lenses to form with concentrations of perchlorate far in excess of the average distribution and subsequently, a far greater depression of the melting point. It is this uncertainty which ensures that temperature data is insufficient as the sole means of detecting the presence of water downhole. In order to sense the physical state of the icy cuttings directly, an electrode system can be integrated in to the cutting face of the drill bit, protruding to a depth such that they are recessed with respect to the cutting teeth to avoid damage, but directly in the path of accumulating cuttings. The electrode circuit measures the resistance between two opposing electrodes and it is this change in the resistance value which can be used to sense a change in the physical state of the ice trapped in the cuttings. An example of a typical drill bit architecture, instrumented to sense downhole conditions, is as detailed in Figure 76. Icy cuttings which are completely frozen will inhibit the flow of ions between the electrodes, resulting in a resistance reading which is extremely high, analogous to that of an open circuit. However, the conduction properties of water in its liquid phase acts to close the circuit allowing ions to flow between the electrodes and in turn reducing the measured resistance. Thus, the presence of dissolved salts will act to aid the detection of liquid water due to an increase in the concentration of ions within the solution. Furthermore, it may be possible to utilize the drill bit as a scientific probe in itself by measuring the resistance of the terrain at increasing temperatures during drill operations. This, in turn, may

allude to the concentration of dissolved salts in the regolith - useful data in the context of ISRU or astrobiology.

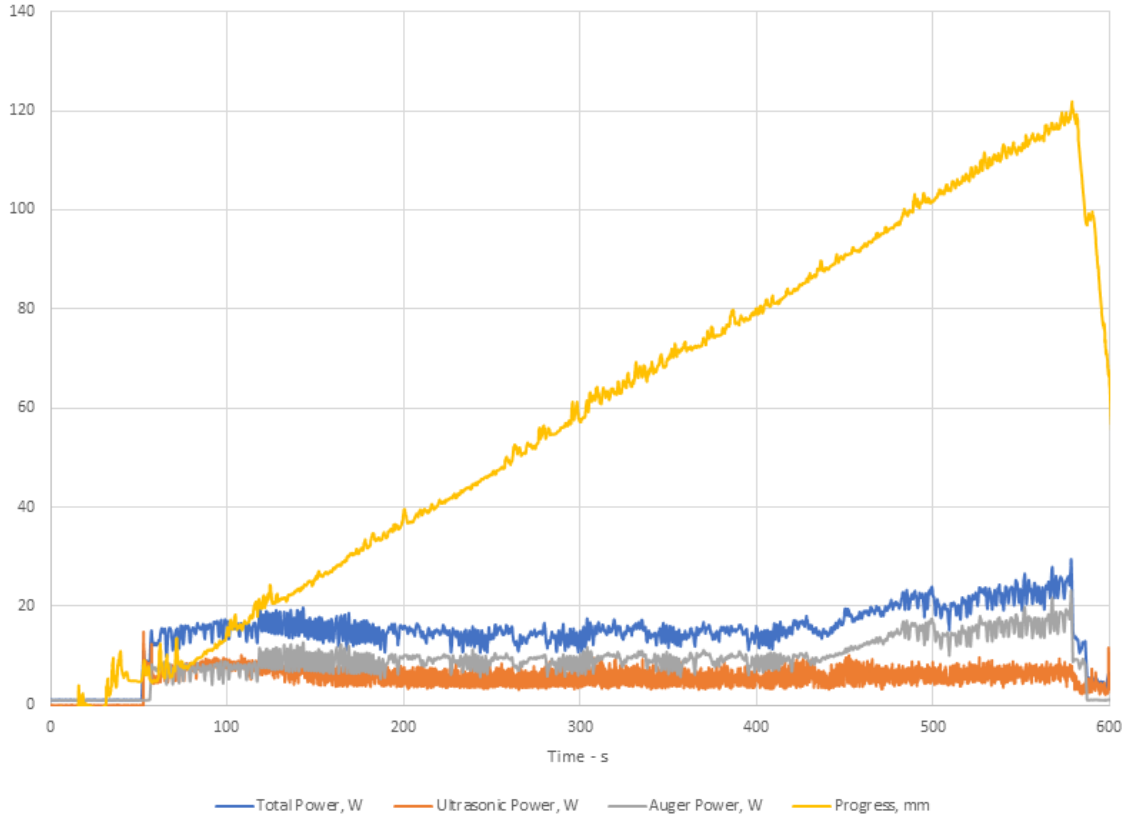


**Figure 75: UPCD drilling run in 10% saturated regolith. Note, steady increase in the auger motor level from 400 s. Drill bit seizure occurred at 580 s.**

**Figure 76: Drill bit instrumented with thermocouples (brown sensors) and electrodes (yellow sensors) for use in the thermal control system. Bit diameter of 20 mm, for reference.**

This combination of thermal and resistance data from embedded downhole sensors utilizes this raw data, and through a series of logical operations, commands the drill to reduce its rate of progress in order to minimize the thermal load imparted on the formation, or retreat from the cutting frontier entirely to allow both the terrain formation and the drill to cool off. Such a system acts as the first defensive line against the onset of bit freeze-in and can be coupled with data from the auger motor in worst cases.

The thermal control system can operate in multiple modes, whereby the logic based on the resistance parameter can act based on an absolute value or a change in the value sensed over time. Basing the system off of an absolute value, whereby the control system triggers a command upon receiving a signal that the resistance has decreased past a certain threshold limit, is most robust when foreknowledge of the thermal behaviour of the volatile is available. While such an approach may prove tricky to implement in in the context of planetary exploration whereby knowledge of the terrain is not certain before drilling commences, this approach benefits from relatively uninterrupted drilling until a certain level is attained. Basing the control system upon a sudden change in the resistance level is more robust against uncertain terrain physical properties, but there may be a tendency for such a system to be overly cautious in its drilling approach, compromising drilling effectiveness.

### 4.14.4 Experimental Setup

In order to evaluate the preliminary performance of the instrumented drill bit architecture for use within the Ultrasonic Planetary Core Drill, a series of tests were planned which would utilize the instrumented hardware, Figure 77, in combination with the UPCD control system, previously tested in the laboratory and in the field. The hardware was tested in a chest freezer within the laboratory, with the contents of the freezer chilled to -25ºC, at ambient pressure. The bulk of the drill system was kept outside of the freezer until testing was to commence, but the instrumented drill bit was always chilled to freezer temperature before testing began. Although such a system would result in a large thermal soak to the drill bit due to the temperature differential, the short duration of testing meant that heating of the drill bit from external sources was minimized.

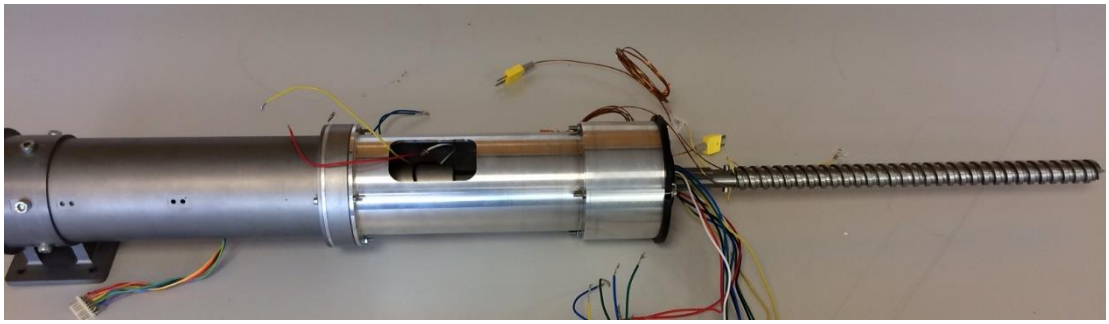

**Figure 77: Instrumented UPCD hardware. Thermal control hardware includes the addition of downhole thermocouples and electrodes, and a slip ring assembly to transfer these signals from the rotating bit.**

Simulated permafrost samples were developed using an in-house simulant which has previously been characterised and frozen with 10% and 20% water by weight, respectively. The latter mix represents the fully saturated case. These samples were compressed to 2 g/cc density and frozen overnight, with an embedded thermocouple to ensure the samples were completely frozen upon testing. Furthermore, small samples of each mix were made and tested using impregnated thermocouples and electrodes in order to characterize the thermal behaviour of the samples. These results, presented in Figure 78, plot the resistance of the mix against temperature allowing a baseline value to be selected for the thermal control system to act upon. It is of note that the 10% water/weight sample features multiple trends, with a transition zone between –9 and -1 ºC. Knowledge of the expected resistance ranges proved extremely useful when designing the circuitry to complement the electrode, allowing sensing accuracy to be improved within certain resistance bands, thus improving the robustness of the control system.

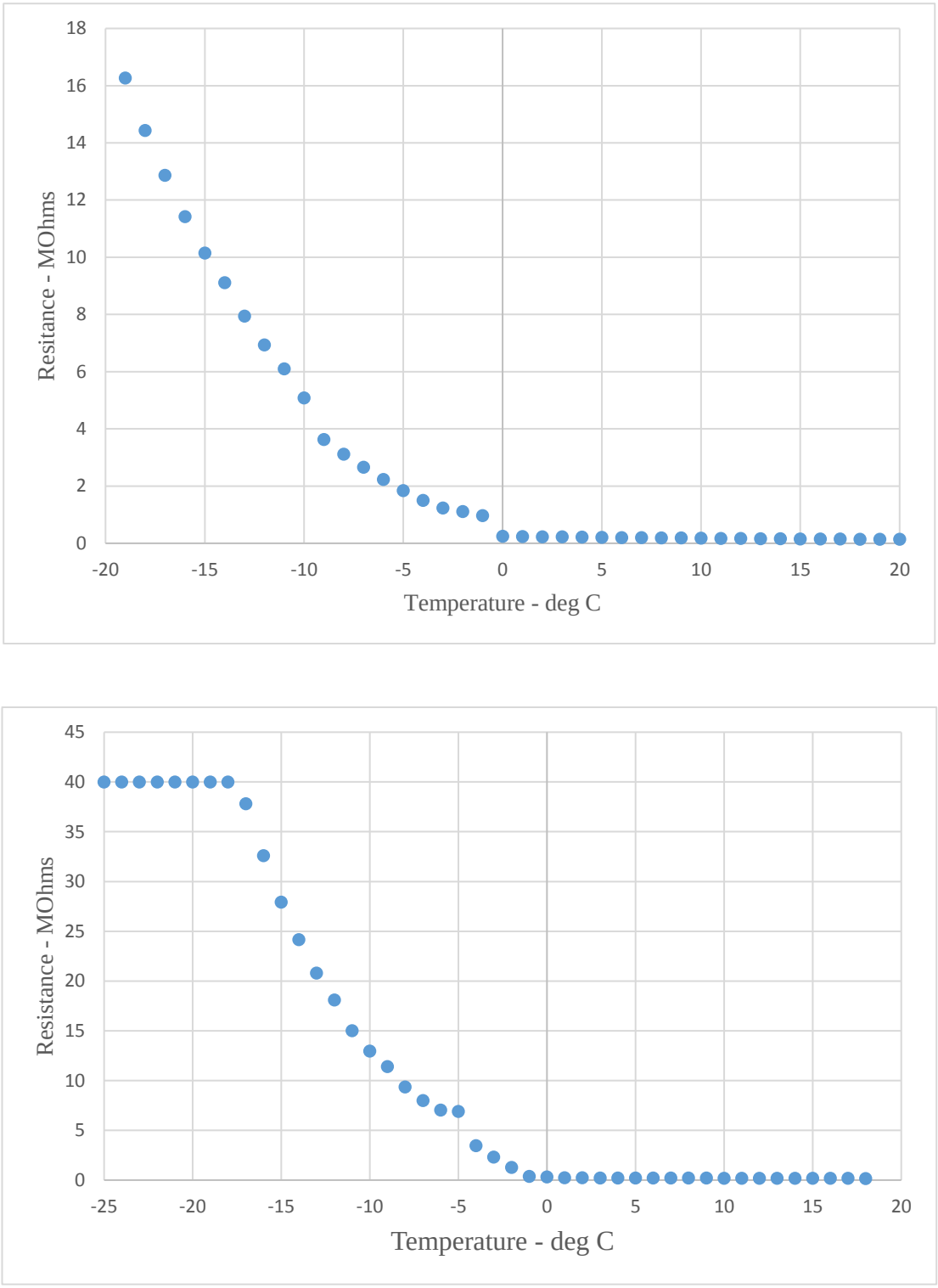


**Figure 78: Temperature – resistance plots for 10% water/weight (top) and 20% water/weight (bottom) simulated permafrost mixes.**

### 4.14.5 Experimental Results

In preparation for the 10% water/weight test, it was noted that the presence of a transition period between 4 MOhm (-9ºC) and 1 MOhm (-1ºC) would allow a baseline pre-set trigger value to be included within the control system allowing the drill system to progress until this threshold was reached then retreat. Upon testing, the drill system progressed efficiently through the sample without triggering the activation of the thermal control system. This was, perhaps, attributable to the low strength of the mix only weakly bound by the low percentage of water present. Figure 80 (top) details a typical run in the 10% water/weight mix, clearly showing that there is little deviation in the resistance measured over the course of the run. The progress of the drill is never impeded and total drilling power averages 40 W. The test setup allowed multiple runs in the same sample with a high degree of repeatability noted throughout. This provided reassurance that even under laboratory conditions, weaker permafrost samples do not heat up sufficiently to engage the thermal control algorithm. Furthermore, the tests allowed the collection of multiple, still-frozen permafrost cores, as shown in Figure 79, providing further evidence to support this conclusion.


**Figure 79: Frozen 10% water/weight permafrost core obtained during experimentation.**

While the less saturated simulated permafrost mix proved to be of little challenge to the drill system, the harder, fully saturated mix proved more reliable in its tendency to engage the thermal control algorithm. The thermal control algorithm was programmed such that, upon the drill sensing a limit threshold resistance, the drill retreated from the bit-rock interface for a fixed period of time before it re-engaged the terrain. This behaviour is noted in Figure 80 (bottom).

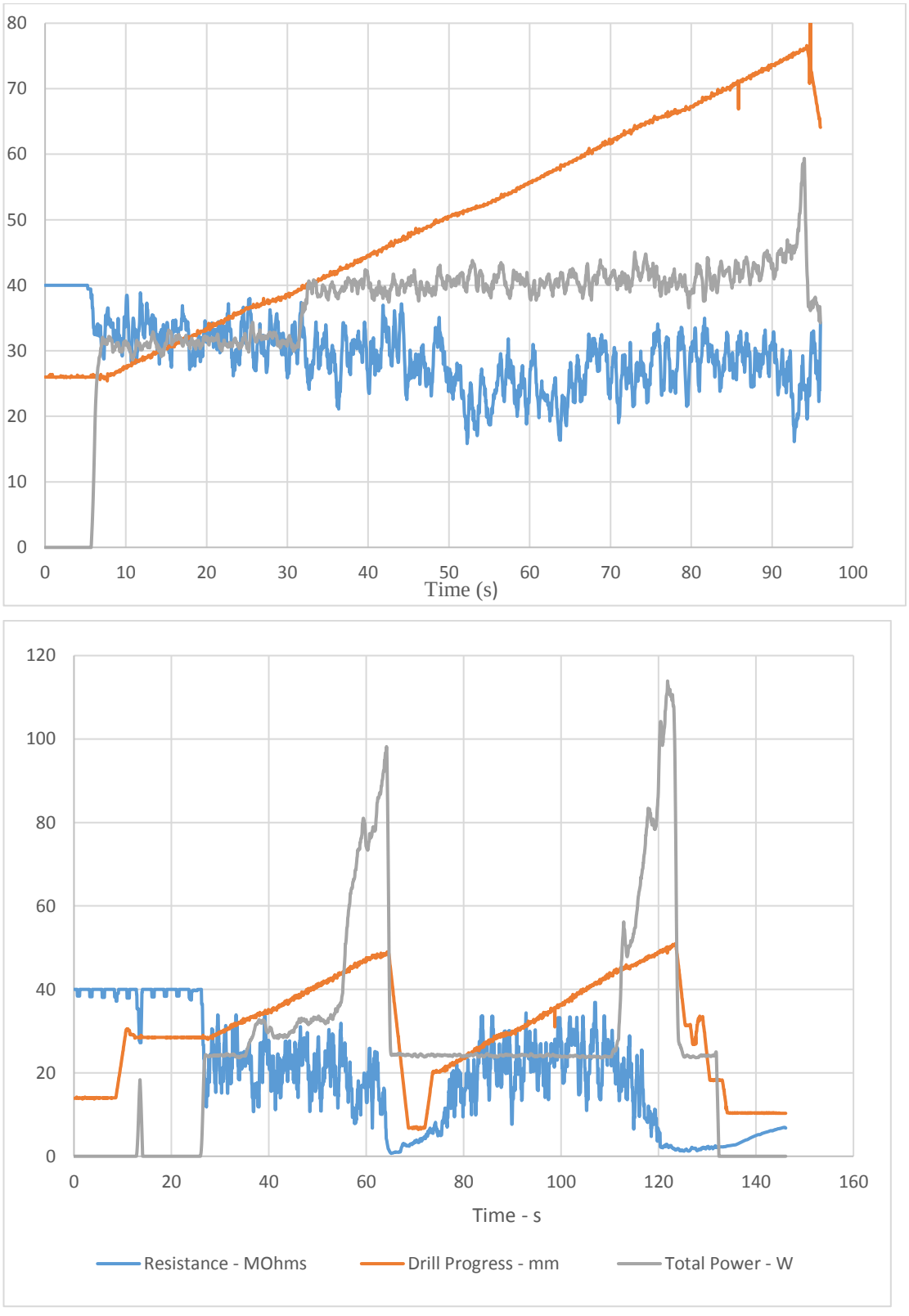


**Figure 80: Experimental results from test run in 10% water/weight sample (top) and fully saturated (20% water/weight) sample (bottom). Note, in the case of the 10% water/weight test, progress is unimpeded due to the low strength of the mixture, thus very little heat was delivered to the cuttings and resistance readings are always high. Results for the fully saturated samples show clear periods of drill retreat upon surpassing a lower threshold resistance.**

Following a period of drilling between T=25 and T=55 s, a gradual increase in total drilling power resulted in a gradual decrease in the resistance reading from the electrodes. As drilling power increases rapidly between T=55 and T=65 s, a sharp reduction in resistance was noted suggesting that the sudden input of power had resulted in an increase in the rate of ice melting within the cuttings. As the resistance fell below the pre-set minimum threshold, the drill suddenly retracted and idled for a portion of time in an attempt to cool the terrain and the bit itself. As the bit advanced forward, power consumption was minimal until the bit-rock interface was re-engaged at T=110 s. Total drilling power then proceeded to ramp up, mirroring the behaviour of the previous rapid increase, resulting in another drop in resistance and the subsequent withdrawal of the bit.

A further example of the thermal control algorithm in operation is detailed in Figure 81 whereby the control system was programmed to retreat when the thermocouple sensors detected a temperature in excess of an upper bound. In the example shown, the drill retreats when a temperature of 0 °C is reached. Between T=50 and T=100 s the drill progressed into the target terrain resulting in an initial cooling of the drill bit followed by a warming behaviour as work was expended in formation breaking. This process repeated as the drill made progress through the target terrain, retreating only when the upper temperature bound was exceeded. It is of note that there is a trend towards a general increase in bit temperature over time. Future control logic will alleviate this through increased periods of dwell, whereby the drill is disengaged from the target and powered down to reduce the thermal load at the drill tip.

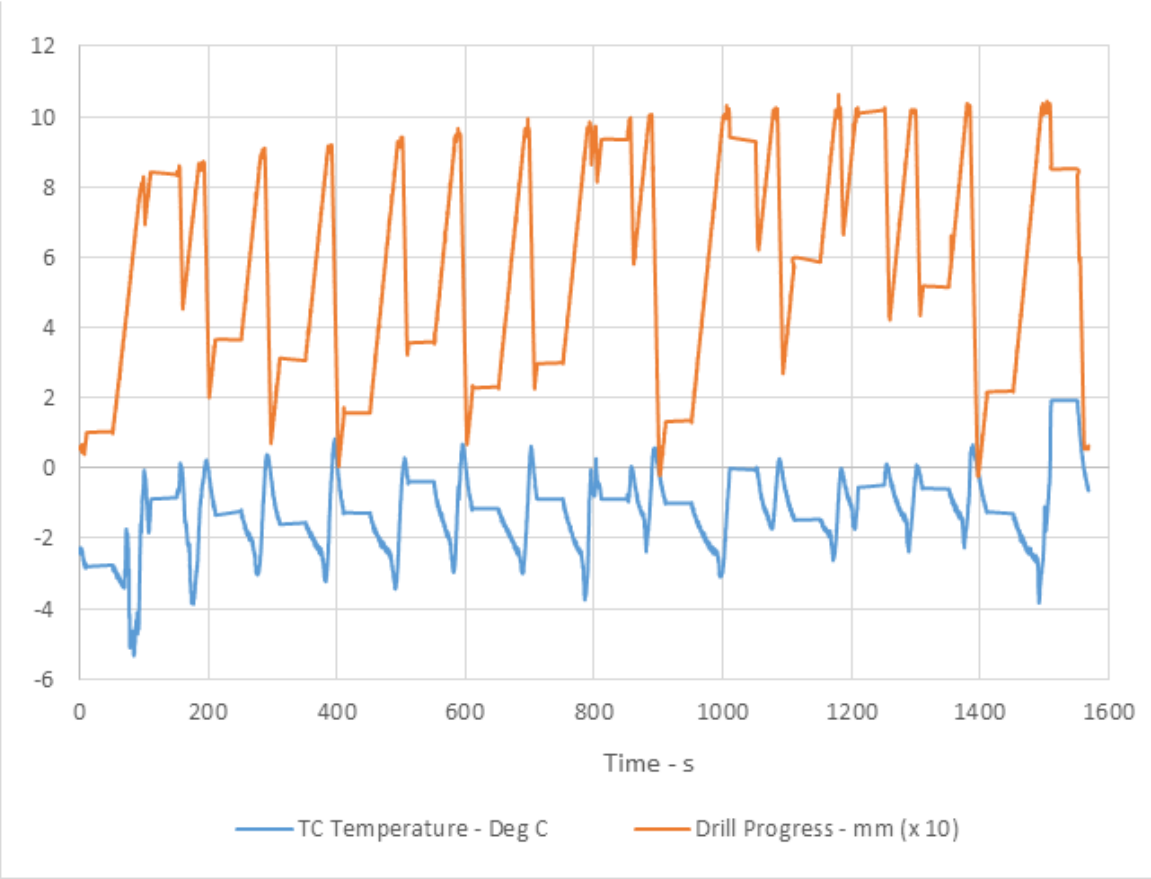


**Figure 81: Results from an experimental test run in fully saturated simulant. The behaviour of the drill is that of an advance as drilling progresses followed by the retreat upon a surpassed upper temperature bound of zero degrees Celsius. The frequency of this behaviour suggests that the drill has been granted insufficient time to cool between retreats. This is confirmed by a general upwards trend in the temperature recorded by the thermocouple embedded within the bit.**

### 4.14.6 Conclusions

Testing of the Ultrasonic Planetary Core Drill in various ice-bound terrains, both in the laboratory and at the field site on the Antarctic Peninsula, has revealed that there is a need for the development of an expansion in the capability of the control system in order to prevent potentially mission-ending drill seizures caused by the thawing and refreezing of volatiles held within the drilled cuttings. Through the implementation of a sensor suite at the cutting face of the drill bit, data pertaining to the thermal and physical state of the volatiles can be attained allowing the development of control logic which can provide the drill system with a safeguard against freeze-in events. The use of a dual thermocouple pair rapidly monitored downhole temperature at rates which exceeded those expected. This permitted frequent sampling of the downhole thermal conditions, useful for both fault prevention and for bonus scientific return. The small diameter of the thermocouples used meant that care was required when affixing the sensors to the drill bit to ensure that damage to the sensors

was minimised. More work is required to improve the location of these sensors in order to maximise scientific return while reducing the potential for damage. The electrode pair used were simpler in nature and required very little supporting electronics to obtain accurate readings. The simplified nature of these sensors meant that physical damage was all but impossible, enhancing the robustness of the system. The electrode pair may also function well as a means of providing additional science through the ability of the suite to sense water/salt concentrations. Thus, the simplified nature of the electrode pairing combined with the abilities in fault prevention and additional scientific data acquisition means that the inclusion of such a system should be prioritised. Laboratory testing has proven that the preliminary development of the sensor suite functions well by preventing bit freeze-in, and further refinement of the technique will only improve its capability within planetary drilling architectures.

## 4.15 Chapter Conclusions

The UPCD project resulted in the successful development of a planetary drilling system, based upon the ultrasonic-percussive drilling technique, with a sample return mission from the polar regions of Mars at the forefront of requirements setting. A solution was developed which was based upon a carefully constructed Concept of Operations, making use of a system of drill bit connections and disconnections using a bayonet-like interface. This system was proven to reliably construct a drill string of up to three individual bits and capable of drilling to the required depth in terrain as hard as Locharbriggs sandstone (~50 MPa) before breaking the string and caching the core-containing used bits into a sample caching carousel. A system of autonomous control was developed which allowed drilling to proceed without human input and this control system was expanded to operate within volatile-rich terrain where a risk of refreeze faults exists. The drill was tested extensively in both the laboratory and at a field site in Antarctica. The knowledge harnessed during the development of the system combined with lessons learned from the field provided a solid baseline for the development of the Subglacial Bedrock Sampler system, a collaboration with the British Antarctic Survey.

# Chapter 5

# Development of the Subglacial Bedrock Sampler

## 5.1 Subglacial Exploration

The acquisition of subglacial bedrock samples from the Polar Regions has been a long standing aim for researchers in the field of glacial geology and paleoclimatology [53, 54, 55]. As almost all of continental Antarctica, and perhaps 80% of the surface of Greenland is covered by ice, the extent of geological science in these regions has mostly been limited to the exploration of isolated nunataks and airborne geophysical survey. Direct sampling of bedrock is necessary to enable cosmogenic surface exposure dating of the ice sheet bed; if sites are carefully chosen then they have the potential to record the length of time for which the bedrock has remained covered by ice. Put another way, bedrock samples can yield information on the last time that the ice sheet had retreated sufficiently to expose the bed at that site. By obtaining samples from multiple sites, data on the last exposure of the bedrock can be used to deduce the evolution of the ice sheet, with emphasis on the thickness and extent of the ice sheet over time [53, 56].

The past configuration of the ice sheet is of particular importance as there is widespread evidence that during previous geological warm intervals, such as the last interglacial, sea level was significantly higher [57]. Moreover, the last time that the Earth experienced current $CO_2$ concentrations (>400 ppm) the entire West Antarctic Ice Sheet (WAIS) and significant parts of the East Antarctic Ice Sheet may have been unsustainable, resulting in global sea level increases of between 6 and 20 metres in excess of current levels. Despite clear evidence of higher sea level, the source of the melted ice is not well-constrained and as yet there is no ‘smoking gun’ for the area of Greenland and/or Antarctica from which the sea level rise may have originated.

Understanding the relationship between these atmospheric ($CO_2$) and glaciological (ice volume) trends can help reduce the uncertainty in predicted future sea level rises. This was

deemed to be of critical importance by the recent Intergovernmental Panel on Climate Change (IPCC) fifth assessment [58]. These considerations, both geological and glaciological, led the International Partnerships in Ice Core Sciences (IPICS) drillers' meeting to identify "sampling bedrock at the bottom of the hole" to be one of the key challenges in their Ice Core Drilling Technical Challenges White Paper [59].

Furthermore, the development of lightweight wireline drilling technologies may prove to be an essential step in the path towards freely accessing terrestrial Antarctic or Martian subglacial lakes [60].

## 5.2 Challenges Facing Subglacial Bedrock Sampling

### 5.2.1 Logistical Challenges

Obtaining subglacial bedrock samples from Polar Regions is difficult due to the numerous technical and cost challenges associated with deep drilling activities, exacerbated by the extreme conditions present at the drilling locations. Furthermore, the need to constrain deep field operations to the polar summer months ensures that light aircraft are typically utilised for the rapid transportation of equipment and personnel. As light aircraft operating in these regions typically operate at the edge of their performance envelopes, it is essential that the development of any new deep drilling system must be approached with a holistic view of the problem, placing the supporting logistics effort as one of the major constraints on the solution that is to be developed.

As an example, the de Havilland Canada Twin Otter aircraft, which forms the backbone in the logistics effort of most organisations operating in the Polar Regions, has a maximum operational capability limited to the transportation of four scientific personnel and up to one tonne of cargo at any one time. Furthermore, the internal cargo volume of this aircraft may limit the use of lengthy or bulky hardware. Clearly, in order to ensure that any deep drilling system is compatible with the majority of field locations which are of interest, any new architecture must be compatible with transportation by aircraft of this size and payload capacity [61]. As the exact number of light aircraft logistics flights able to support any single drilling campaign may be limited due to aircraft availability and the demand placed on them by crowded scientific scheduling, an optimal system would ensure that all drilling and support hardware and personnel could be transported to the field location on one flight.

In order to reduce the resources required at deep field sites, it is essential that any new drill development must be relatively power efficient as only small scale electrical generators,

capable of a few kilowatts of power, may be made available. As these generators typically utilise petroleum-based fuel, an efficient system will reduce the volume of fuel which is required, extending the operational time available for a given available fuel volume. Moreover, while it is common for many drill systems to operate 'wet', making use of cutting fluids and anti-freeze, these fluids also have to be transported to the field site and the use of large quantities of heavy, potentially polluting fluids has implications for the preservation of drilling sites. Organisations such as BAS tend to operate 'leave no trace' policies, in keeping with the Protocol on Environmental Protection to the Antarctic Treaty 1991. Thus, any system which can operate 'dry', without the need for these fluids, is highly favourable.

## 5.3 Technical Challenges

The development of subglacial bedrock sampling technologies faces technical challenges similar to those encountered when designing planetary drilling hardware. Predominantly, uncertainty surrounding the target terrain to be sampled means that the system must be capable of extracting material from a host of potential terrain types. As described in [62], the subglacial environment may consist of sequential layers of debris-rich basal ice, an un-frozen layer, till, debris beneath the unfrozen layer and bedrock, or some combination of these layers. Figure 82 details the potential makeup of the subglacial zone. A high degree of robustness is therefore required in order to ensure that the developed system is capable of breaching multiple layers of material before extraction of a bedrock sample can be achieved.

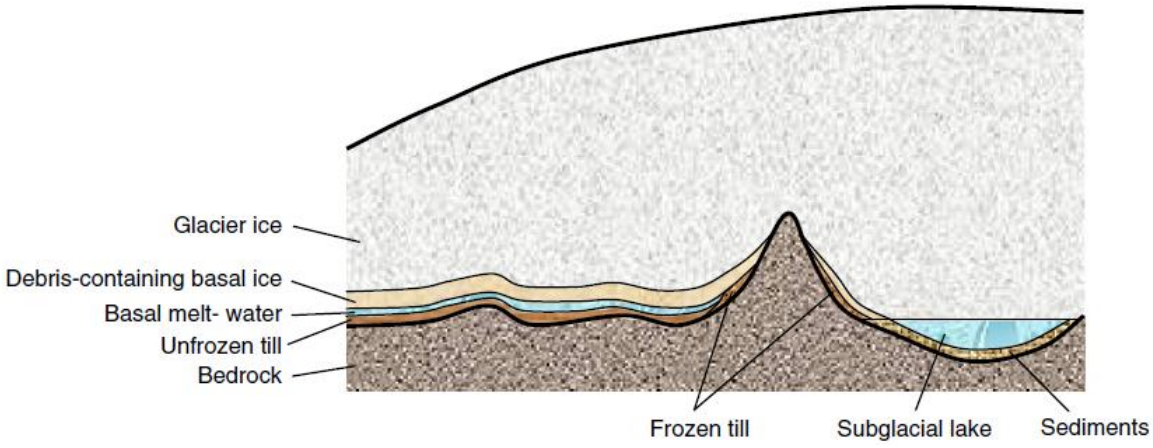


**Figure 82: Schematic of subglacial layering** *[62]*.

It has been suggested that the topography and geology of subglacial Antarctica remains less understood than the surface of Mars [63], and any uncertainty surrounding the depths at which bedrock layers may be found introduces limitations on the technology which can be

employed when bedrock sampling is to be achieved. While previous BAS ice-core drilling operations in coastal areas such as Berkner Island [64], James Ross Island and the Fletcher Promontory [65] have reached bedrock at 948 m, 363 m and 654 m respectively, it is widely acknowledged that the continental ice sheet may extend to depths of up to 4897 m in the Astrolabe Basin [66]. While glacial drill systems are typically designed with a targeted maximum depth limit, a flexible drilling system which is capable of sampling at both intermediate and deeper depths with only minor modification may prove to be favourable. Approaches utilising a wireline system, whereby the drilling system is attached to an umbilical spool, may allow even the most extreme depths to be targeted. Wireline systems also benefit from reductions in logistical and operational complexity as bulky drill pipes are superfluous, though there are technical constraints which govern their implementation.

While glacial drill systems are typically designed with a targeted maximum depth limit, a flexible drilling system which is capable of sampling at both intermediate and deeper depths with only minor modification may prove to be favourable. Approaches utilising a wireline system, whereby the drilling system is attached to an umbilical spool, may allow even the most extreme depths to be targeted. Wireline systems also benefit from reductions in logistical and operational complexity as bulky drill pipes are superfluous, though there are technical constraints which govern their implementation [62]. Clearly, the multitude of rock types which may be found beneath the ice will not respond equally to the drilling process and as such, any new system would seek to mitigate the risks associated with this uncertainty by designing for the worst case scenario. While harder rocks, typically of the igneous or metamorphic variety, may be the most difficult to penetrate, softer rocks which are more easily drilled may increase the failure rate in drilling operations through the onset of drill choking or other associated error states. Thus, a holistic approach must be adopted during the design process to ensure that any and all terrain types which may be encountered can be drilled reliably.

Clearly, the development of a lightweight subglacial bedrock sampling solution capable of rapid and low resource drilling is highly desirable. While systems capable of bedrock sampling do exist, deployment of these systems in the field may be logistically intensive and the use of such systems may prove to be excessive for shallower targeted depths [67, 68]. To this end, it was decided that an existing wireline drill architecture, the BAS Rapid Access Isotope Drill (RAID) would be utilised to provide access to the bedrock and act as a host for the bedrock sampling hardware.

## 5.4 BAS Rapid Access Isotope Drill (RAID) Redevelopment

The RAID system is part of the electromechanical wireline family of drills and is designed to capture ice cutting from depths up to 600 m. The RAID offers a new approach to the problem of ice drilling as it attempts to reduce operational complexity whilst increasing drilling speed at the expense of high resolution core sampling. Inspired by many electromechanical ice drills but mainly developed from the BAS medium-depth ice corer [69] the RAID is able to acquire multi-metre 'pecks' of loose, icy cuttings from the icepack utilising an anti-torque device which reacts drilling torque from the rotating cuttings barrel. The cuttings rotate around and climb the ice auger until the peck depth is reached. At this point the complete RAID system is winched to the surface where the stored icy cuttings are emptied for future isotopic laboratory analysis. Though the RAID is highly capable of reaching its maximum depth in as little as seven days of operation, the device is unable to sample subglacial bedrock as the terrain-facing end of the drill is entirely optimised for ice samples (Figure 83) owing to its low torque capability and ice-optimised design. The system benefits from a lightweight design, with the supporting two-part mast for ease of transportation by light aircraft, as highlighted in Figure 84, providing an excellent baseline for the new development. Furthermore, as the drill is designed to penetrate the ice sheet in an efficient manner, relying on a single, off the shelf Maxon brushless DC motor, the total power requirement of the system is less than 1 kW, with commercially available electronics used both downhole and at the surface level.

**Figure 83: RAID Cutting Face. Outer diameter of 80 mm, for reference.**

**Figure 84: The Rapid Access Isotope Drill (RAID) in service. Note, the minimal support equipment required for drilling operations ensures minimal logistical complexity.**

Having succeeded in operating at multiple Antarctic field sites over the course of a number of seasons in service with BAS, a degree of confidence in the RAID system has been developed which provides strong foundations upon which the drill can be modified, reducing the need for a costly new development from the ground up [70].

## 5.5 Subglacial Bedrock Sampler Design Methodology

### 5.5.1 Analogies to Planetary Exploration and Design Implications

The task of obtaining subglacial bedrock samples from the Polar Regions shares substantial commonality with many of the challenges associated with the subsurface exploration of the terrestrial planets within the solar system. Robotic landers and rovers which seek to extract samples from Mars, for example, are presented with multiple complications which must be overcome if a reliable solution is to be designed. Uncertainty surrounding the geological composition of the target locations means that the developed solution must be well equipped to deal with multiple potential drillable terrains or off-nominal operational modes.

Primarily, however, the physical constraints of spaceflight ensures that landed vehicles are typically of a lightweight construction, and as Earth has the highest gravitational acceleration of any terrestrial planet, the weight available to react drilling operations is likely to be severely limited. In the context of subglacial bedrock sampling using electromechanical systems, the available downhole weight on bit and torque must be reacted by the self-weight of the drill and the anti-torque stage. These mechanisms typically consist of a series of skates or blade which, once actuated in the ice, provide a means of torque reaction. As there is a reliance upon the frictional force between the device and the icy, low friction interface at the borehole wall, it is foreseeable that there may be limitations on the torque levels which may be reacted by such a system.

Planetary drilling systems also face challenges relating to the significant distance between Earth and the planetary body to be explored. Real time control of the system may be impeded due to communications delays which may be on the order of several tens of minutes, depending on the alignment of the planets. As the onset of critical fault states may arise within a matter of seconds, this demands that the robotic drilling system must be able to operate entirely autonomously, capable of adjusting progress and power settings by process of the interpretation of inbuilt sensor feedback and on-board logical analysis. While

downhole subglacial sampling is unlikely to experience such delays, it is possible that the sampling system implemented may wish to take advantage of autonomous control of the drilling process in order to reduce the burden on the operator over lengthy drilling cycles in inclement environmental conditions, and to reflect the inability to observe drill behaviour at the base of a deep hole. Autonomous control may also allow the drill system to react quickly to fault modes, such as bit freeze-in or auger choke which are difficult to predict, have onset times as little as a few seconds, and may be sources of single-point failures in a system.

Finally, planetary drilling hardware may be limited by the power which can be delivered by the host platform, which typically utilise photovoltaic arrays or radioisotope thermoelectric generators in conjunction with a suitable battery pack. A system which is capable of obtaining core samples using only modest power levels is therefore highly suitable for lightweight subglacial sampling. As the power which is available at the field site is limited to that which can be supplied by small petrol generators, a drilling system which can utilise one of these generators as its main power source allows for easy integration into the existing drilling ground support infrastructure.

## 5.6 Rock Cutting Methods

Any lightweight, electromechanical-wireline drilling system which seeks to obtain bedrock core samples from beneath glaciers is inherently limited by the axial ‘weight on bit’ force and torque that the system can apply to the target terrain. This is simply a by-product of the mechanical limitations of the anti-torque stage upon which the system is dependent, and the physical mass of the drill assembly. To this end, it is in the interest of the designer to minimise the reliance of the system on both axial force and drilling torque.

Drilling systems may utilise pure rotary drilling, whereby a combination of the overhead weight on the drill and the application of rotation acts to crush and fracture the rock through compression and shear. As noted in Equations 3.7 – 3.10 (Section 3.3.2), the total power demanded by the drilling process is shared by multiple elements and, given that it may not be possible to predetermine the composition of the target terrain, it is pertinent that any drilling system be designed for the worst case (strongest) rock species that may be encountered.

In the case of rotary drilling systems, it is essential that any such system is capable of delivering a sufficient weight on bit to the rock face in order to fracture the rock, complemented by the ability to deliver torque levels which are capable of overcoming the frictional forces incurred by this overhead force at rotational velocities which are sufficiently high enough to convey cutting from the bottom of the borehole through an augering action.

Rotary drill systems which are designed to operate using reduced drilling forces and torques may still require overhead forces on the order of 3-5 kN, with corresponding torque draws of up to 50 Nm, with power draw in the region of 3 kW when drilling igneous and metamorphic formations [71]. While such systems may be classified as 'low-resource' when compared to industrial-scale drilling rigs, it is unlikely that an electromechanical system on the scale of the BAS RAID system would be capable of supplying force, torque and power levels at these levels.

It has been suggested that percussive drilling, whereby the process of penetrating the bedrock target is assisted by the application of a repeated hammering load to the rock face, may prove to be a viable alternative to conventional rotary drilling in a low resource setting [72, 73]. To date, there have been no attempts made to incorporate a percussive actuator into a bedrock sampling drill of any form. While the reasons for this are not explored in the literature, it is assumed that industrial-scale bedrock sampling rigs do not require a percussive action to obtain bedrock cores due to the availability of high forces and torques at the cutting head. In the case of lightweight electromechanical cable-suspended drilling, it is foreseeable that the constraints imposed by the need to house the percussive actuator within the narrow housing bore of the drill has restricted the application of a hammering system. In fact, the implementation of percussive drilling techniques are increasingly common in systems which have been designed for the robotic sampling of the subsurface of planetary bodies. Percussive actuators for use in planetary drilling systems typically utilise one of the following technologies:

1) Spring-cam actuated hammer mechanism
2) Voice coil actuated hammer mechanism
3) Ultrasonic-percussive hammer mechanism

The spring-cam actuated hammer has been utilised in various sample extraction systems designed for operation on the Moon and Mars [74, 30, 75]. The working principle of these mechanisms involves the rotation of a spring-loaded follower-hammer around a static cam profile. The cam profile is typically inclined, with the slope geometry carefully designed in order to improve wear resistance and prevent unwanted vibration. Figure 85 details the motion of the spring-cam system. As the follower-hammer is rotated around the cam profile (position 1 to position 2), the spring compresses as the follower climbs the slope. As the follower-hammer bearing approaches the top of the slope, the position of maximum vertical travel is reached, and any further rotation results in the follower bearing moving over the

sharp edge of the vertical limit. At this point, the stored elastic energy in the spring is converted to kinetic energy, propelling the hammer assembly downwards until a collision with the anvil occurs. The anvil is mechanically coupled to the drill bit, allowing a stress wave to transfer through the drill bit and into the target terrain, resulting in a fracturing of the terrain which may extend to depths which are significantly in excess of the initial indentation [76].

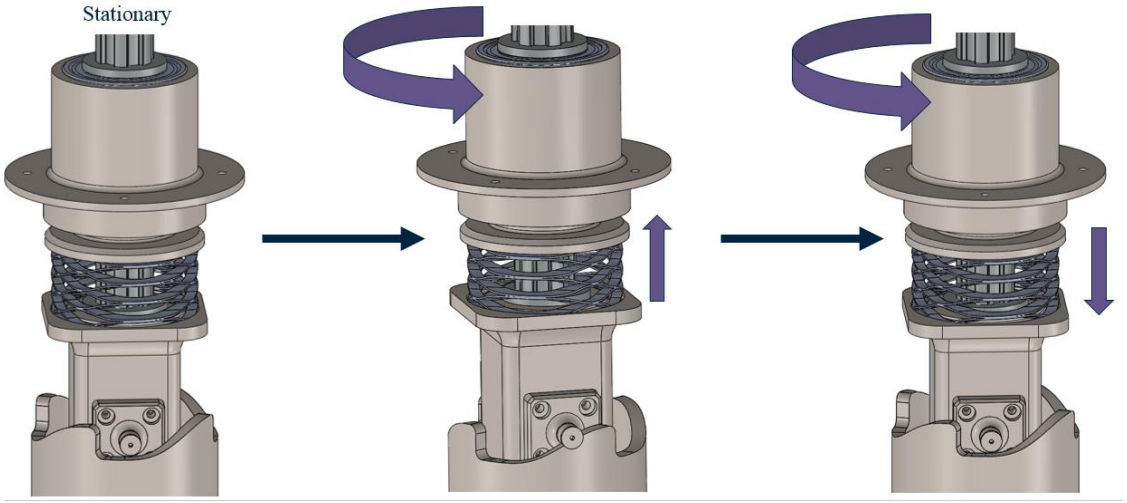


**Figure 85: Typical motion of the spring-cam actuated mechanism. The middle panel shows the spring being compressed as the follower-hammer rises up the inclined cam slope, and in the right hand panel, percussive energy is transmitted as the hammer drops over the lip of the cam.**

Spring-cam systems benefit from being adaptable to almost any system, with the single constraint being the torque which can be delivered by the motor and the size of motor which can be accommodated within the volume available. Percussive energies in the range 0.5 – 5 J per blow are typical, with total percussive power on the order of 15 – 100 W. Perhaps the most prominent drawback of this system involves the need for careful design in order to ensure that the cam profile does not wear down after frequent cycling.

Percussive systems may also utilise a voice coil mechanism to generate a hammering action. Upon providing electrical power to the voice coil device, an electromagnet retracts the hammer, compressing a spring in the process. When the device is powered off, the spring is released, allowing the hammer to impact the anvil on the down stroke. While the principle of the device is similar to that of the spring-cam device, voice coils have a reduced number of moving parts, improving the mechanical reliability of the system. Power efficiency is generally extremely high in such a device due to the ability to recover rebound energy from the percussive collision [77]. However, while such a device is mechanically simple by design,

the control electronics involved in implementing a voice coil for use in percussive hammering may be complex.

As discussed in Section 4.1, the ultrasonic-percussive technique is a low-resource means of generating percussion within planetary drilling systems though there are challenges which must be overcome in order to implement the technique within such a device. The high voltage electronics which drive the ultrasonic actuator are inherently complex and somewhat bulky by design. Furthermore, the relationship between the power consumed by the ultrasonic device and the weight on bit applied to the device means that control of these systems must be particularly delicate in order to prevent a percussive stall due to excessive forces on the bit. Mechanically scaling such systems is also inherently difficult due to the resonant nature of the ultrasonic transducer meaning that the frequency of vibration is often compromised with changes in the mass of the system. Finally, the percussive energy which can be transmitted by the drill bit may be limited by the restrictive free mass which may be implemented within ultrasonic-percussive systems.

## 5.7 Spoil Removal Techniques

As detailed in Section 3.5, the process of rock drilling is divisible into two main areas: breaking the terrain and the removal of spoil, or drilled cuttings, from the bottom of the borehole. While the importance of terrain breaking is clear, the removal of cuttings is often overlooked yet it plays an essential role in the drilling process.

Spoil removal may be accomplished by multiple means depending on the application. Techniques which commonly feature include pneumatic clearing through the use of compressed gas, the use of a drilling fluid, or dry clearing using a mechanical auger.

In the context of glacial drilling activities, drilling fluids are commonly utilised as a means of preventing borehole collapse and serve a dual purpose by aiding in the removal of cuttings from the borehole. As drilling fluids may be chemically polluting to the environment if left in place, these fluids are typically removed following a cessation of drilling activities.

Pneumatic clearing, whereby pressurised gas is delivered to the bottom of the borehole from a pressure vessel, is an effective means of clearing spoil with efficiencies of up to 100%, depending on the differential gas pressure. Inexpensive gases such as compressed air may be utilised for this purpose.

Augering is the process of the vertical conveyance of cuttings using a drill bit which has fluted, helical features along its length, utilising centrifugal forces and friction to convey the cutting from the borehole. The process is heavily dependent on both the rotational speed of the drill bit and its diameter and is best suited to transporting dry fines

Given the lightweight, low resource and environmentally sensitive nature of the development, it was decided that drilling fluids would be excluded as a means of spoil removal, and the complexity of installing a pneumatic system within the borehole diameter constraints meant that augering was prioritised as the sole means of spoil removal. Furthermore, the use of augering in rock drilling is well understood and relatively straightforward to implement within the bounds of the system.

## 5.8 Subglacial Bedrock Sampler Design

### 5.8.1 Subglacial Bedrock Sampler Architecture

The subglacial bedrock sampler prototype was designed in a modular manner such that multiple, individual elements could be brought together to form a functional assembly, but each section could be removed and maintained with ease. This was deemed essential in order to allow the performance of the rig to be assessed while ensuring minimal assembly and disassembly complexity. The footprint of the prototype was also designed to be in keeping with the RAID borehole diameter constraint so as to ensure that the kinematics of the percussive actuator were of the correct order of magnitude as any future field-ready models. The system consists of a percussive actuator assembly, a multi-motor auger gearbox assembly and a slip ring assembly. These shall be discussed in more details in later sections.

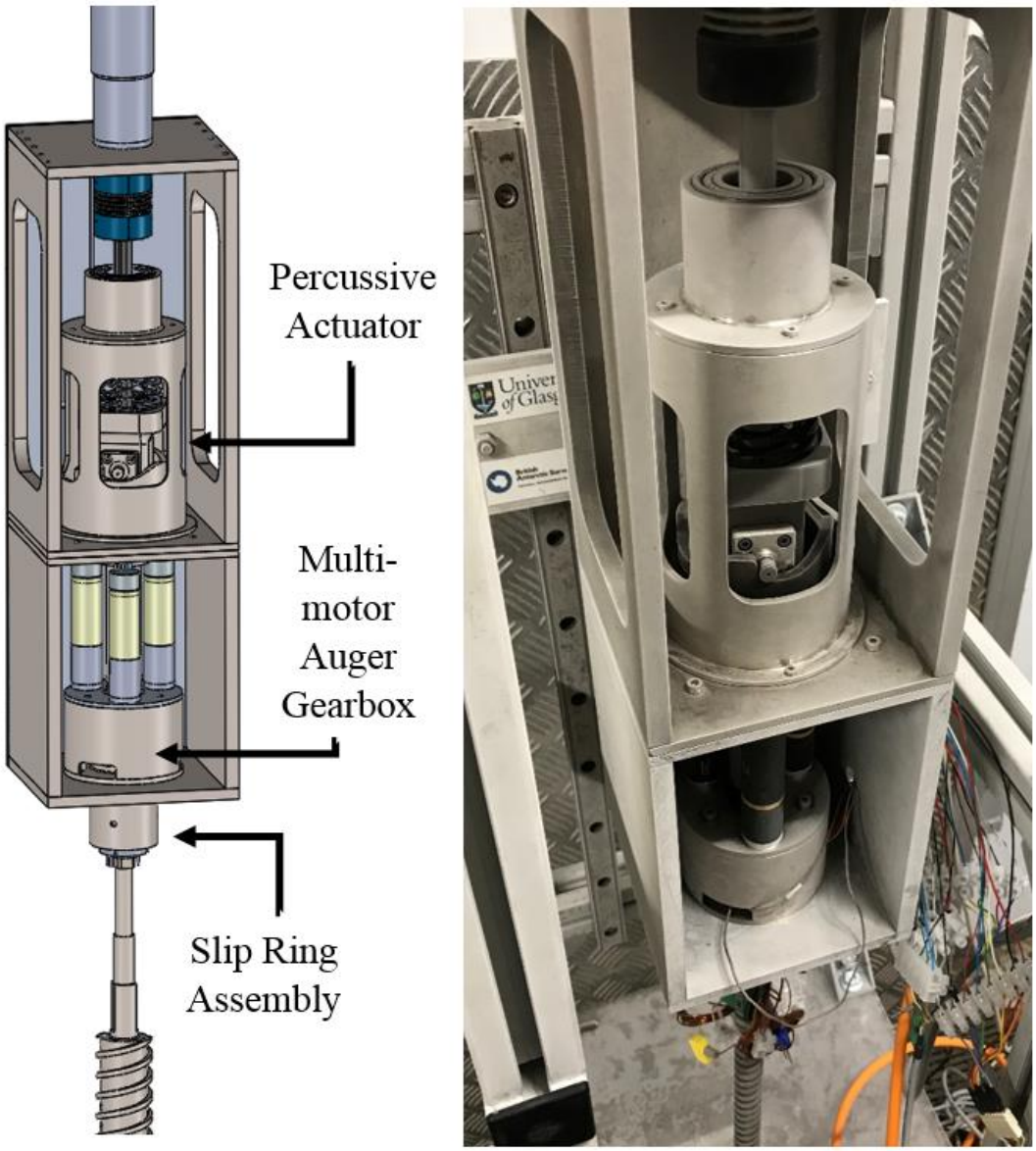


**Figure 86: Subglacial Bedrock Sampler prototype assembly CAD (L) and following a series of successful tests in the BAS Cold Chamber Facility designed to replicate Antarctic field conditions (R). Auger gearbox diameter of 80 mm, for reference.**

## 5.9 Percussive Mechanism Design

As discussed in Section 5.6, multiple options exist for the generation of a hammering action for the fracturing of rock in subglacial bedrock sampling. Upon undertaking a trade-off study whereby each option was compared with a set of requirements, a device based on the ultrasonic-percussive actuation method was discounted due to uncertainty surrounding the capability of such a system when required to penetrate igneous or metamorphic terrain. Field testing of such systems by the University of Glasgow has established that, while the ultrasonic-percussive drilling technique is highly capable of penetrating sedimentary stacks

with extremely low power consumption, the low percussive energy which can be delivered by the system reduces it effectiveness in harder terrain types [78]. Furthermore, despite the promising efficiencies conferred by the use of a voice coil, complexities associated with the electronic design of such a system and control issues associated with the technique meant that it was excluded from further consideration in the development, meaning that the spring-cam percussive system would be prioritised.

The spring-cam system features two central elements: the barrel cam and the follower-hammer. The barrel cam consists of a hollow cylinder of hard metal with a cam profile milled into the wall. The design of the cam geometry is perhaps the single most important element of the percussive mechanism as without due care the cam geometry may be worn away by the friction generated by the repeated movement of the follower-hammer over the cam profile. As it was foreseen that that the cam-hammer system would generate percussive frequencies up to 20 Hz, the cam could be classified as the "high speed" variety [79] and thus particularly susceptible to wear. Figure 87 [8] details an example of an un-optimised cam geometry which has suffered excessive wear. The source notes that this wear occurred within two hours of operation with a frequency of 88 Hz and a cam made of 17-4 stainless steel hardened to H900 condition.

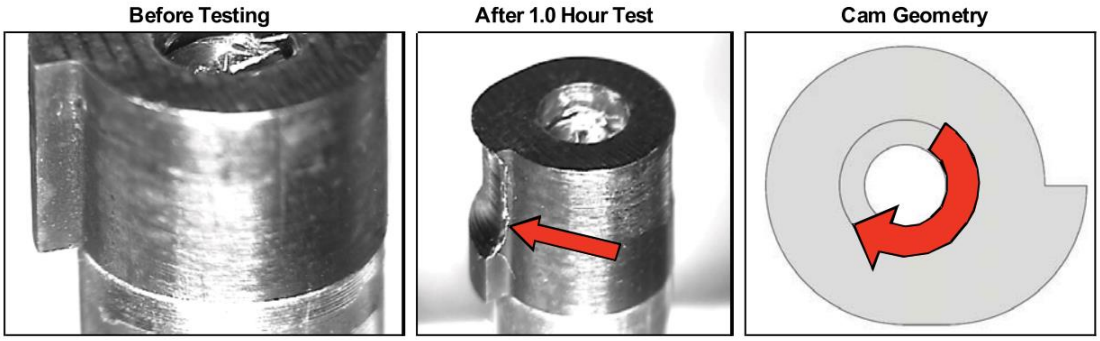


**Figure 87: Example of barrel cam wear. Wear shown occurred after one hour of operation at 88 Hz** *[8]*.

Clearly, the levels of wear displayed in the noted example are unacceptable, and any system which wishes to utilise a spring-cam mechanism should seek to optimise the cam geometry to mitigate against premature failures. To this end, the use of a cycloidal cam geometry was explored whereby the cam acceleration profile is based upon the application of a full-period sinusoid. Cam design requires particular attention to the acceleration profile which is generated by the geometry to be used, and 'jerk', analogous to the rate of change of acceleration. In order to reduce wear and excessive vibrations, an ideal cam geometry

would result in acceleration and jerk profiles which are continuous, or, at worst, feature discontinuities which are finite in nature.

Equations 5.1, 5.2 and 5.3 detail the respective acceleration, $a$, velocity, $v$ and displacement, $s$ profiles of the cycloidal geometry, where $h$ denotes the maximum follower vertical rise, $\beta$ denotes the total angle of the segment and $\theta$ is the cam angle.

$$a = 2\pi \frac{h}{\beta^2} sin\left(2\pi \frac{\theta}{\beta}\right) \qquad \text{Eqn. 5.1}$$

$$v = \frac{h}{\beta}\left[1 - cos\left(2\pi \frac{\theta}{\beta}\right)\right] \qquad \text{Eqn. 5.2}$$

$$s = h\left[\frac{\theta}{\beta} - \frac{1}{2\pi} sin\left(2\pi \frac{\theta}{\beta}\right)\right] \qquad \text{Eqn. 5.3}$$

Analysis of the jerk, acceleration, velocity and displacement characteristics of the cycloidal geometry suggested that it is well suited for use as a high-speed barrel cam, allowing it to be baselined for use. The designs of the specific barrel cam geometries to be used were bounded by several key constraints, as follows:

1. The torque required to rotate the follower-hammer around the cam geometry must be deliverable by an off-the-shelf electromagnetic motor which has heritage gained from previous operations within the harsh conditions of downhole polar operations.

2. The motor in question must be suitable for accommodation axially when concentrically mounted within an 80 mm bore, in-keeping with the existing RAID borehole size.

3. The power demanded by the follower-hammer motor should not exceed 500 W, or approximately half of the total power which would be supplied from a surface-mounted electrical generator.

4. The percussive system is required to generate percussive energies in the region of 1-5 J per blow, and a percussive power of up to 90 W to account for uncertainty in the

maximum compressive strength of the terrain to be penetrated, targeting drilling rates between 0.1 – 0.5 mm/s, depending on target material to be drilled, allowing drilling activities to be completed within a realistic timeframe for subglacial/planetary drilling operations.

5. The design of the barrel cam geometry should be capable of surviving up to 250,000 revolutions of the hammer without significant degradation of the cam to account for prolonged drilling campaigns, based upon the need to withstand drilling to depths of 500 mm using levels of percussive power and targeting drilling rates as stated in key constraint 4.

Noting that the most prominent driver in the process of designing the percussive actuator was the availability of motors compatible with the strict diameter and power constraints imposed by the need to adhere to the existing RAID borehole diameter and downhole power delivery architecture, it was decided that the most prudent design path would first seek to identify the most capable motor and gearbox combination. Given that BAS have a long history of using the Maxon electronically commutated (EC) range of brushless DC motors for Antarctic drilling solutions, it was decided that this series of motors would be baselined for use in the P-RAID system. Furthermore, the development would benefit from an existing relationship between BAS and Maxon which could take advantage of a number of small modifications to the standard motors which Maxon have developed for BAS. Modifications such as the repackaging of the standard, bulky terminal cap of the EC45 and EC60 allows these motors to be accommodated within the restricted borehole constraint, significantly increasing the motor options available. Identification of the motor and gearbox options available for use in the percussive actuator permits an upper bound to be set on the deliverable torque available for rotating the follower-hammer around the cam profile. While a physical upper bound on the maximum percussive rate, or ‘beats-per-minute’ (BPM), of the percussive actuator may be determined by the RPM of the gearbox output shaft, the maximum BPM which is achievable is further limited by the mechanics of the system. In order to optimise the delivery of percussion to the drill bit and avoid a hard collision of the follower-hammer on to the ramped section of the cycloidal cam geometry, the natural frequency of the spring-mass system and the quarter-periodicity must be established.

Equation 5.4 details the quarter-periodicity ($T_{1/4}$) of a simple spring-mass system:

$$T_{1/4} = \frac{\pi}{2\sqrt{\frac{k}{m}}} \qquad \text{Eqn. 5.4}$$

The quarter-periodicity of the system is indicative of the time taken for the system to complete a percussive down stroke, the period between the follower-hammer rolling over the edge of the inclined section of the cam geometry and the tip of the hammer engaging the anvil. As such, this calculation allows an upper limit on the RPM of the percussive actuator motor to be set such that the hammer-follower will not rotate past the flat, 'idle' portion of the cam before a collision has resulted, ensuring that percussion is transmitted to the drill bit as required. Furthermore, awareness of the quarter periodicity allows the motor speed to be set such that a hard contact of the follower bearing and the cam profile can be avoided, preventing damage to the fragile follower bearings or excessive wear of the cam.

Having constrained both the maximum torque deliverable by the motor and the percussive rate which can be achieved, cam geometries can be designed which adhere to the percussive energy and power requirements which have been previously established. Utilising a series of kinematic equations of cycloidal motion [75], multiple cam geometries were designed which fulfilled the performance requirements of the percussive actuator. The design of the cycloidal barrel cams to be considered for implementation consisted of multiple geometries which were characterised by the number of drops and the height of each drop.

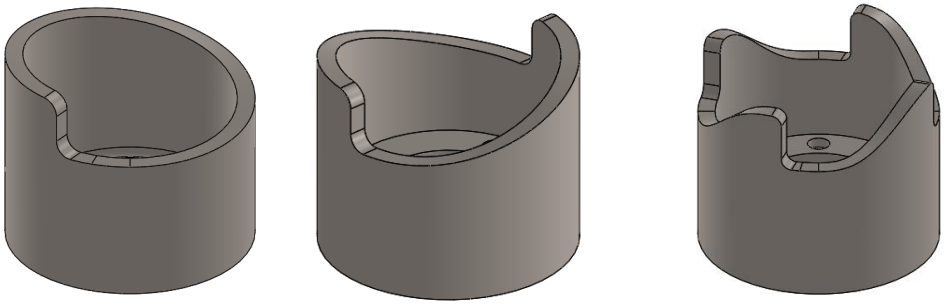

**Figure 88: Cycloidal barrel cam geometries. 1-Drop, 2-Drop and 4-Drop (L-R).**

Each geometry was designed in order to optimise either the percussive energy or power for a given motor and gearbox selection. A reduced number of drops ensured that the maximum torque required to rotate the follower-hammer over a fixed height was minimised,

but in the case of the single drop profile, the force is delivered in an unbalanced manner which may result in the stalling of the percussive actuator. Such a system is perhaps most useful for delivering less frequent but more energetic hammer blows to the terrain as the total deliverable percussive power is primarily limited by the rotary speed of the motor. Conversely, multi-drop cam profiles generally require higher torque levels to overcome ramps of a fixed height, but the addition of multiple drops allows for some flexibility when setting the percussive power.

When developing the percussive actuator, a number of wave springs, chosen over coil springs in order to ensure a true axial force, were down selected based primarily on whether they could be accommodated within the diameter constraint of the system. Furthermore, the particular maximum working range and stiffness of those selected would enable the largest possible range of percussive energies, accommodating multiple potential cam geometries. The torque required to rotate the follower-hammer around the different cam geometries was then calculated for certain cam vertical displacements, allowing a range of possible options to be established.

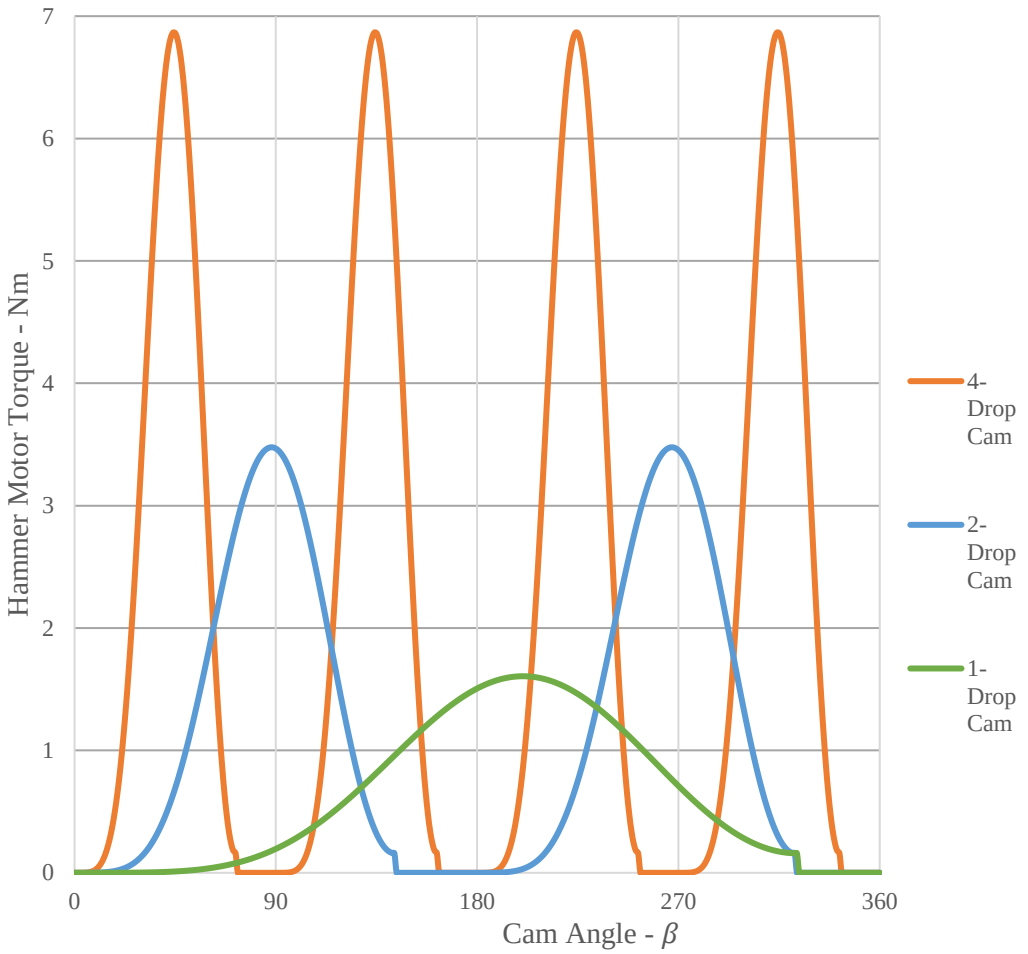


**Figure 89: Hammer motor torque requirements for single, double and quad drop cycloidal barrel cams with a vertical displacement of 17 mm.**

Figure 89 [80] details the torque required for rotation around single, double and quad drop cam geometries for a vertical cam displacement of 17 mm, while Figure 90 allows for a comparison of the required torque for the four drop profile with the geometry of the cam

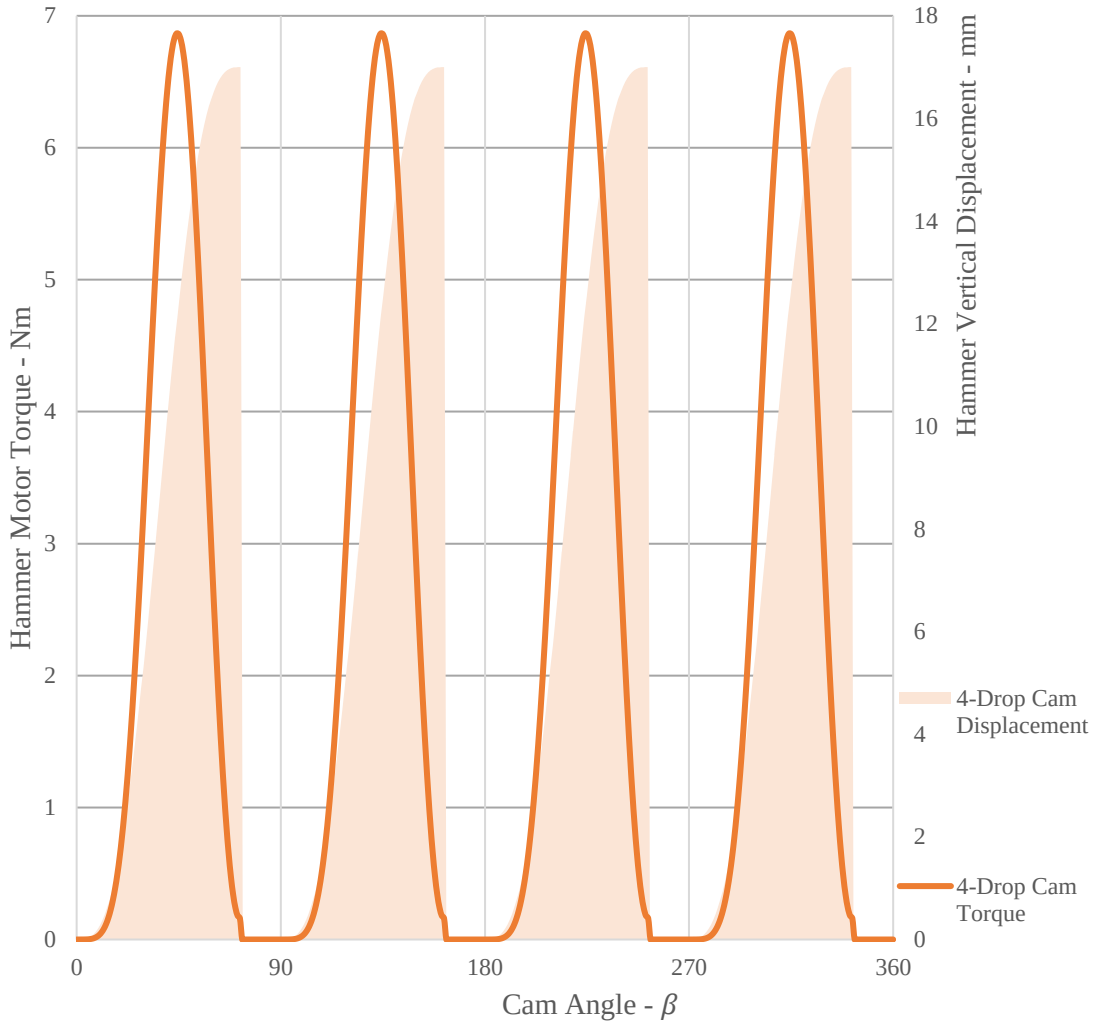


**Figure 90: Hammer motor torque requirement for 4-Drop cam compared to cam geometry.**

Establishing the maximum torque requirement for a given cam geometry allows the cam to be optimised for the selected motor and gearbox combination, ensuring that the maximum percussive power can be achieved. An ideal geometry selection would see the cam geometry torque requirement closely match the torque deliverable by the system via the motor and gearbox combination as geometries which require significantly less torque than is deliverable by the motor/gearbox combination may be deemed overly reduced, thus incapable of maximising the percussive power output.

## 5.10 Multi-Motor Auger Gearbox

While the subglacial bedrock sampling system makes use of a hammering action as the primary means of penetrating the target formation, decoupled rotation of the coring drill bit is essential in order to index the cutting bit and to remove spoil from the bit-rock interface. Indexing of the drill bit ensures that the hammer blows which are transmitted to the terrain

do not repeatedly impact upon the same location, ensuring that the complete circumference of the drill bit kerf is impacted. This in turn allows the drill to progress efficiently through the terrain without imprinting the cutting teeth. As previously described in Section 3.5, in order to minimise logistical complexity, the P-RAID system should operate independently of cutting fluids, relying solely on the use of augering (screw conveying) for removal of spoil from downhole. As detailed in Equation 3.11 (Section 3.5), the minimum rotational speed required to convey material through the helical auger is dependent on factors such as the inclination angle, the diameter of the auger and the coefficients of friction between the conveyed spoil and the surface of the auger scrolls and the borehole wall. Given that the material to be drilled is likely to be unknown, the need to design an auger which is capable of moving a wide variety of spoil types was critical.

Increasing the diameter of the drill bit as a means of reducing the auger starting RPM alone should be avoided because of the impact that this has on the kerf area which increases with the square of the bit radius, thus significantly increasing the area which must be drilled. Fortunately, when setting the requirements for the system it was decided that there was a scientific need for a larger rock core than in previous systems. While this acted to reduce the burden on the design of the auger geometry, closer attention to the task of terrain breaking was required.

As the development progressed it became clear that the diameter constraint imposed on the system, due to the need to ensure compatibility with the existing RAID borehole diameter, would prove troublesome with regard to accommodating an auger motor/gearbox combination capable of delivering sufficient torque levels. To this end, a solution was devised which would make use of multiple motors/gearbox combinations driving a single, central spur gear mounted to the drill bit. This solution also offered advantages including redundancy in the case of single motor failure, although careful control was required in order to prevent excessive back driving of each additional motor as the torque demand increases.

# 5.11 Laboratory Drilling Performance

## 5.11.1 Experimental Setup

Making use of a modular test rig which was designed in order to facilitate multi-parameter experimental campaigns (Figure 91), a series of experimental campaigns were conducted in order to evaluate the performance of the drilling system. In order to prevent bit walk during initial contact between the cutting bit and the rock target, an acrylic plate with a laser-cut aperture was installed immediately above the rock target to be drilled. This proved sufficient in preventing any undesirable lateral motion of the drill bit during the crucial first stages of rock engagement. Rock targets consisting of Portland limestone and Locharbriggs sandstone were selected and samples were procured measuring 200 x 200 x 300 mm (L x W x D). The use of multiple rock types ensured that different elements of the drill system were tested due to the unique properties of each target material.

Limestone is typically used in performance testing due to the minimal quartz content present within the material. As quartz acts to blunt the WC cutting teeth used, an absence of the mineral within the rock sample ensures repeatability between drilling runs. Naturally soft and weak, with a low UCS of approximately 25 MPa, limestone does not tend to present the hammering/penetration element of the drilling system with a challenge when breaking the material, though progress may be counterintuitively reduced regardless. This is attributable to the nature of the cuttings produced by the process of breaking limestone. The chalky, flour-like cuttings produced have a high bulking factor, thus have a tendency to overload the cuttings removal system, reducing the effectiveness of the removal process, and in turn reducing the ability of the drill to progress. In systems which utilise cuttings removal via an auger, this phenomena is known as choking and shall be discussed in more detail in the sections to follow.

The use of sandstone in the experimental campaign allows for the drill to be tested in a harder and stronger material. As noted in section 4.10, Table 3, the strength of typical sandstones may be in excess of 130 MPa, though more typical strengths are in the region 40 – 50 MPa. This strength ensures that sandstone targets prove challenging to the rock breaking element of low resource systems designed for planetary sampling applications. As previously discussed, the quartz content of sandstone acts to blunt cutting teeth over time, thus experimental testing using sandstone targets will generate a ‘worst case’ scenario for bit longevity, allowing the limits of the cutting teeth to be established. The granular nature of sandstone cuttings and the associated low bulking factor means that sandstone cuttings are unlikely to choke the cutting removal system. This ensured that the effectiveness of the

terrain-breaking element of the system could be evaluated independently of the cuttings removal, allowing the system to be optimised for penetrating multiple terrain types.

**Figure 91: Subglacial Bedrock Sampler laboratory test rig. Note, an acrylic plate with a laser cut aperture is included in order to stabilise the drill bit during initial bit-rock contact.**

### 5.11.2 Experimental Results and Discussion

Table 5 details the experimental campaign which was undertaken in order to evaluate the performance of the drilling system across multiple parameters. In order to better understand the complete capability of the system, a number of different core drilling bit geometries were tested. Ranging in size from 21 – 35 mm diameter, the drill bits tested allowed the performance of the system to be characterised for multiple sampling requirements. Two different cam geometries were also examined: a 2-drop, 17 mm high geometry capable of delivering 3.34 J of percussive energy per impact and a 4-drop, 11 mm high geometry designed to deliver 1.4 J of percussive energy. Furthermore, the rotational velocity of the cam-hammer system was varied from 500 – 3500 RPM in order to examine the role played by the percussive power on the overall performance of the system. In addition to these tests, the weight on bit used to engage the terrain was altered.

Values relating to electrical power were obtained directly from voltage and current data collected by the power supply used to run the percussive and auger motors using Ohms law, while the hammer mechanical power was established using by multiplying the torque and rotational speed of the hammer motor. The progress of the linear actuator is as acquired by the system, converted to a useable metric through the use of a provided conversion factor.

| Rock Type | Drill Bit | Cam Geometry | Hammer Motor Speed - RPM | Upper WoB - N | Lower WoB - N |
|---|---|---|---|---|---|
| Portland Limestone | Small | Rotary Only | 0 | 20 | 10 |
| | | 2-Drop | 500 | 12 | 8 |
| | | | 1500 | | |
| | | | 2500 | | |
| | | 4-Drop | 500 | | |
| | | | 1500 | | |
| | | | 2500 | | |
| | | | 3500 | | |
| | | | 1500 | 17 | 13 |
| | | | 2500 | | |
| | Medium | | 500 | 12 | 8 |
| | | | 1500 | | |
| | | | 2500 | | |
| Locharbriggs Sandstone | Small | Rotary Only | 0 | 40 | 30 |
| | | 2-Drop | 500 | 12 | 8 |
| | | | 1500 | 30 | 10 |
| | | 4-Drop | 500 | 12 | 8 |
| | | | 1500 | | |
| | | | 2500 | | |
| | Medium | | 500 | | |
| | | | 1500 | | |

**Table 5: PRAID experimental campaign overview**

### 5.11.2.1 Portland Limestone

In order to establish the effectiveness of the percussive element of the system, it was determined that the progress through the target terrain using rotary-only drilling would establish a baseline for comparison. Figure 92 presents the results of a rotation-only drill run through Portland limestone using the small bit geometry (21 mm OD, 10 mm ID). An average power consumption by the auger motors of 163 W resulted in a rate of progress of approximately 0.20 mm/s, generating a specific energy of 3450 MJ/m$^3$. This was accomplished with modest weight on bit values of 20/10 N, upper/lower bounds. A steady rate of progress is noted with very little variability with time despite auger power peaking at approximately 450 s and falling over the rest of the run. A sharp spike in power is noted at 650 s, close to the conclusion of the run.

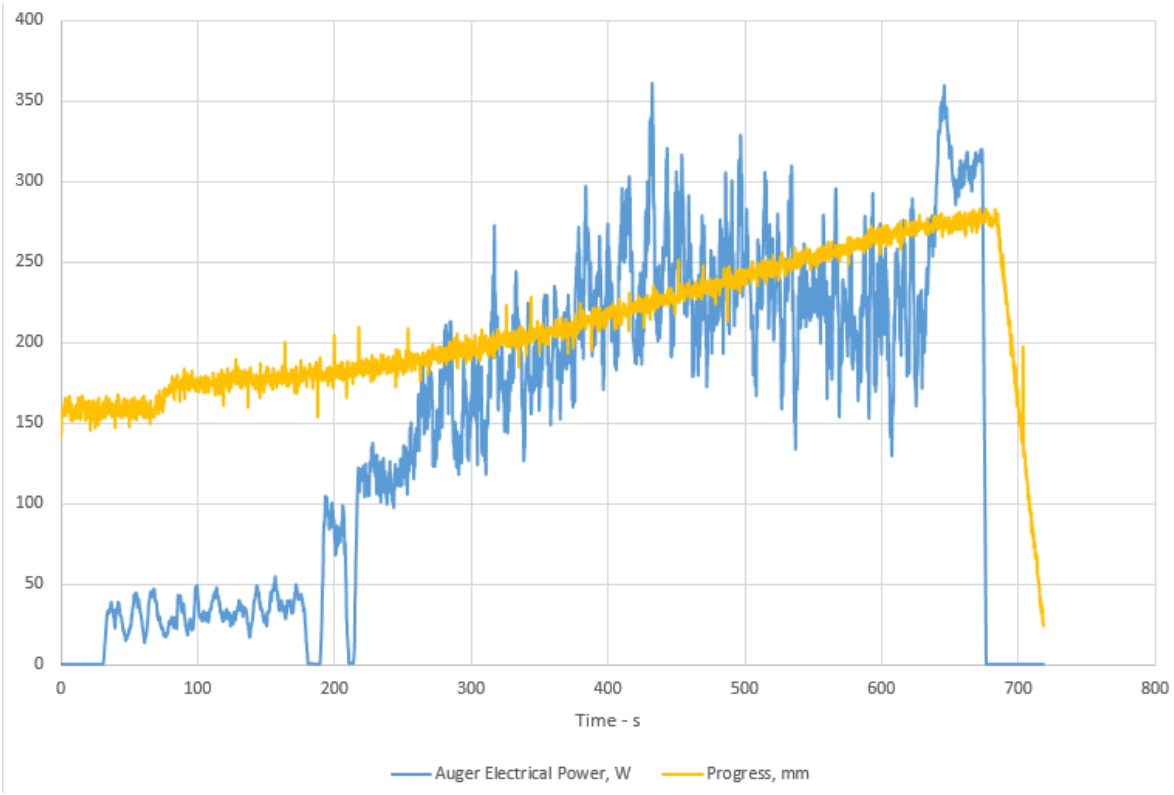


**Figure 92: Portland limestone experimental run using small drill bit and rotation-only drilling. 20/10 N WoB.**

Having established the capability of the system when attempting to progress with the use of rotary drilling alone, percussion was introduced. Figure 93 details the use of a 2-drop, 17 mm high cam profile with a hammer motor rotation of 500 RPM, generating a net percussive power of approximately 5 W. Pre-set weight on bit bounds of 12/8 N generated a rate of progress of 0.1 mm/s from drilling commencement until approximately 150 s using rotary drilling alone. At this point, the hammer motor was engaged and a sudden increase in the

rate of progress to 0.47 mm/s was observed. An average total power of 233 W was demanded by the combination of augering and hammering, with 16 W typically attributable to the driving of the hammer motor. Thus, the system operated with a mechanical efficiency of 31.3% at this hammer power level. Auger power was noted to rise upon the introduction of the hammer motor at 150 s, averaging 217 W, accompanied by an audible indication of pre-choke behaviour in the form of auger rubbing. This behaviour was indicative of a rate of progress on the upper limit of acceptable as the auger struggled to throughput drilled cuttings at the rate which they were produced. However, the increase in auger power appeared to stabilise over time and the drill proceeded to reach the maximum possible depth attainable, recording a specific energy of 1825 MJ/m$^3$.

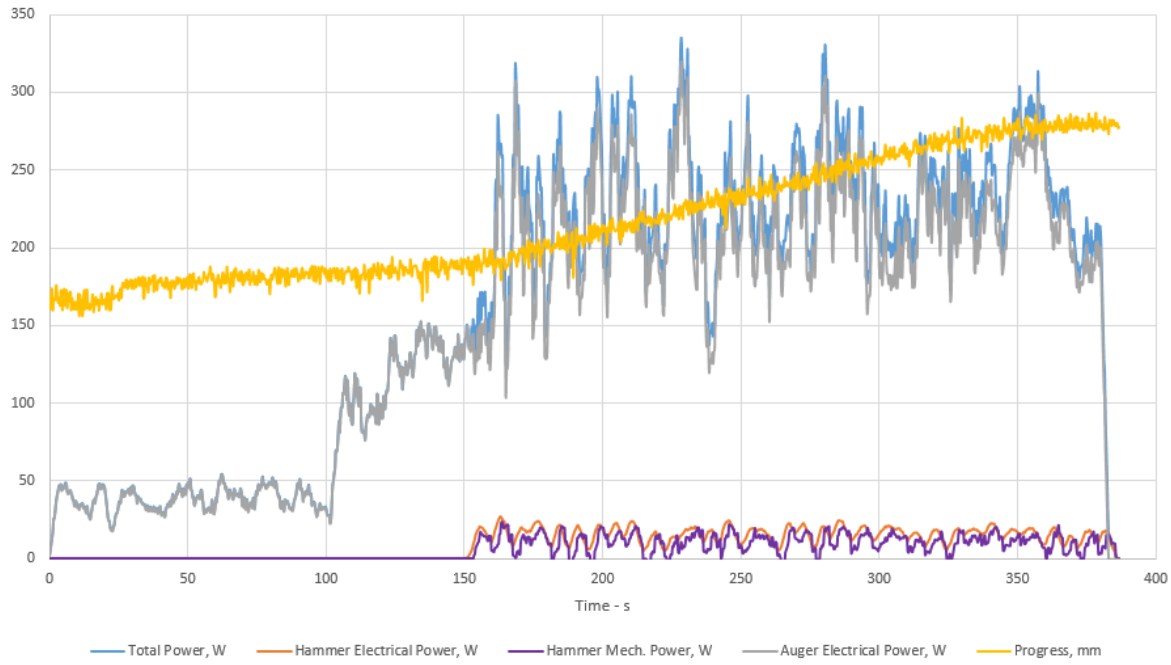


**Figure 93: Portland limestone experimental run using small drill bit, 2-drop cam and 500 RPM hammer velocity. 12/8 N WoB.**

The data presented in Figure 94 corresponds to the first run conducted using a 4-drop cam geometry with a reduced drop height of 11 mm. An average power consumption of 164 W, with 22 W of percussive motor power used to generate 4 W of net percussive power, thus 142 W of average auger motor power was noted. An increase in auger power was noted during the run alongside audible signs of pre-choking behaviour, though a more modest rate of progress of 0.13 mm/s suggests that the accumulation of spoil downhole may have had an adverse effect on the rate of progress noted through re-grinding behaviour. A specific energy of 4713 MJ/m$^3$ was therefore calculated.

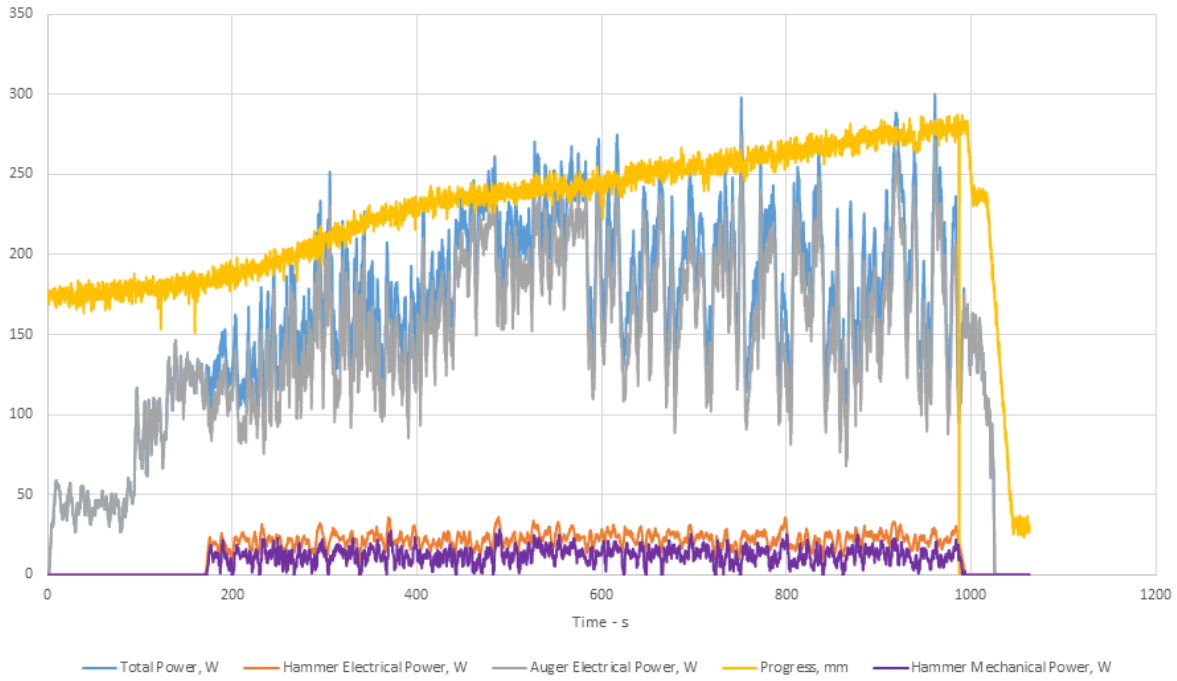


**Figure 94: Portland limestone experimental run using small drill bit, 4-drop cam and 500 RPM hammer velocity. 12/8 N WoB.**

In order to evaluate the capability of the drilling system across a broad range of parameters, the use of a drill bit with an increased outer diameter of 35 mm and inner diameter of 25 mm was incorporated within the test campaign. Figure 95 presents the performance of this drill bit when using the 4-drop cam geometry and 500 RPM of percussive motor speed. A total average power consumption of 142 W was used to generate a net percussive power of 4 W from a percussive motor power of 12 W (33.3% efficiency) and 130 W attributable to the auger motor. This resulted in a rate of progress of 0.11 mm/s, and a corresponding specific energy of 2741 MJ/m$^3$. It is also of note that the enlarged internal diameter of this medium bit geometry tends to produce intact core samples with enhanced reliability – a consideration which is of importance to certain mission scenarios. General progress through the run was exceptionally smooth with very little variance.

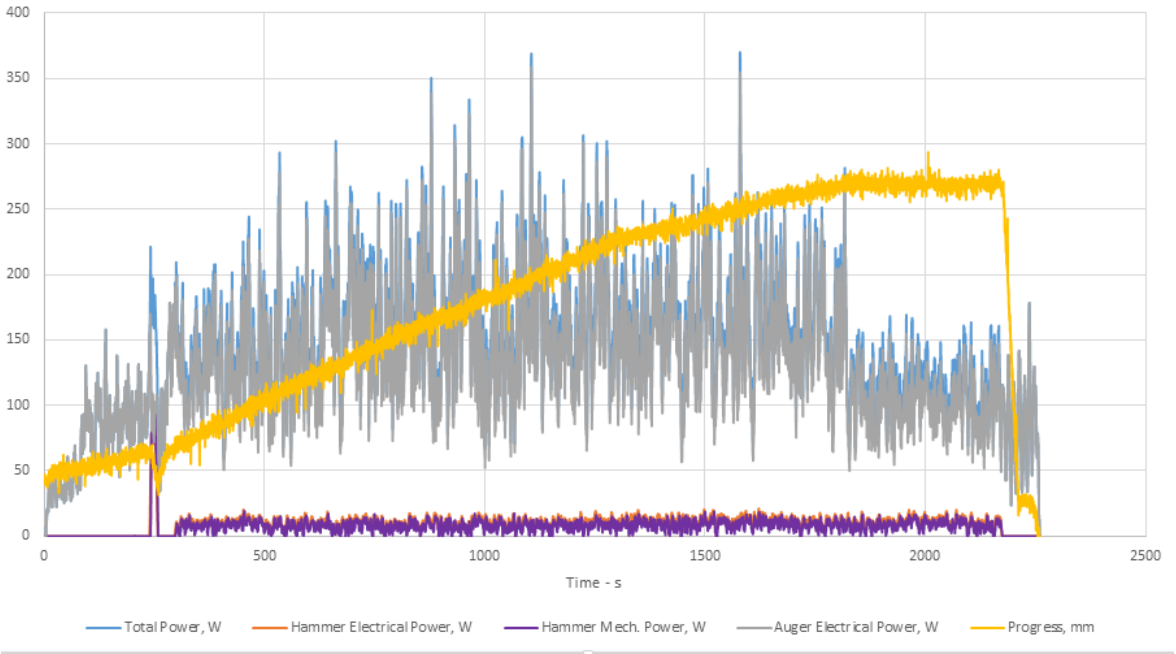


**Figure 95: Portland limestone experimental run using medium drill bit, 4-drop cam and 500 RPM hammer velocity. 12/8 N WoB.**

Results suggest that Portland limestone is drillable with both the small and medium bit geometries, with rates of progress in the range 0.19 – 0.49 mm/s for the former and 0.11 – 0.14 for the latter geometry. The material is readily drilled using rotary drilling alone, achieving a rate of 0.20 mm/s with the small bit geometry, a rate which was noted to surpass certain low percussive energy runs using the same drill bit. This may be attributable to the possibility of better contact being made with the terrain than that achieved when making use of a percussive drilling regime, or that a fine balance between low percussive energy and auger choke was encountered which limited progress. High percussive energy runs using the 2-drop cam geometry resulted in exceptionally high rates of progress, though these runs encountered pre-choking conditions frequently. A case may be made for the application of higher percussive rates when drilling limestone as this appears to have a positive effect on the auger power draw. While this is not immediately understood, it is thought that the hammering action may act to fluidise the spoil being conveyed by the auger, reducing the contribution of auger power to the total power draw. Specific energy analysis suggests that the medium bit geometry is more efficient than the small bit geometry, and the use of the higher energy, 2-drop cam is approximately 2.25 times more efficient than the lower energy, 4-drop cam.

### 5.11.2.2 Locharbriggs Sandstone

Testing progressed to the use of Locharbriggs sandstone, a strong and harder material than most limestones with a reduced bulking factor. Furthermore, the quartz content of sandstone acts to blunt the tungsten carbide teeth used, allowing the teeth performance to be evaluated. It is for this reason that sandstone was used in order to test the percussive capability of the system.

Figure 96 details the results obtained during a rotary-only drilling attempt in sandstone. While the drill bit geometry used in the system was designed with chisel-like teeth, suitable for fracturing rock through a percussive overpressure at the tooth-rock interface, previous attempts at using rotation alone with the small bit geometry proved to be relatively successful, as seen in Figure 92. Similar attempts to penetrate sandstone were proven to be much less successful, achieving a rate of progress of only 0.01 mm/s using a maximum weight on bit combination of 40/30 N. Over the course of the experiment, the weight on bit bounds were increased from an initial combination of 20/10 to 30/20 (at approximately 125 s) when it was established that little progress was being made. This was further increased to 40/30 at approximately 175 s. An average auger power of 87 W was recorded throughout the run, corresponding to a specific energy in excess of 32500 MJ/m$^3$. It can be concluded, therefore, that rotary-only drilling at reduced weight on bit values, using the standard bit geometry, is an ineffective means of penetrating sandstone.

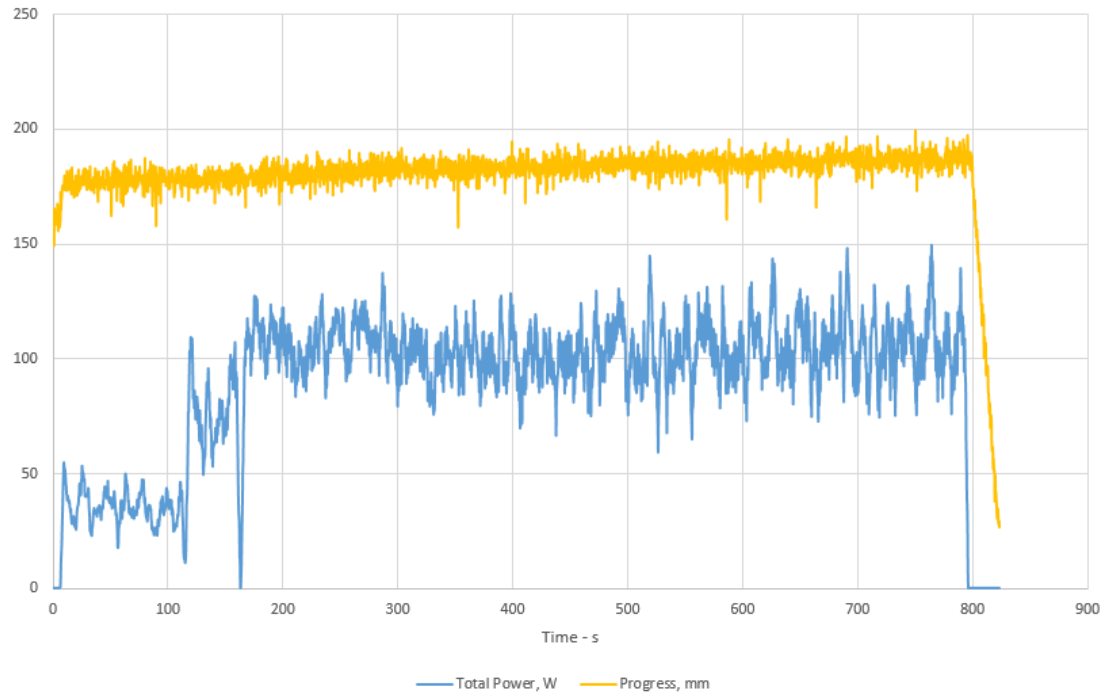


**Figure 96: Locharbriggs sandstone experimental run using small drill bit and rotation-only drilling. 40/30 N WoB.**

Figure 97 presents the results obtained during a run using the small drill bit and the 2-drop, 17 mm high cam geometry with a percussive hammer speed of 500 RPM, generating a net percussive power of 5 W. The drill was shown to progress though the terrain effectively, averaging only 103 W of total power throughout the run, with 14 W attributable to the generation of percussion (35.7% efficient). No notable auger throughput events were noted, resulting in a low auger power contribution of 89 W. A rate of progress of 0.14 mm/s and a corresponding specific energy of 2748 MJ/m$^3$ may be calculated.

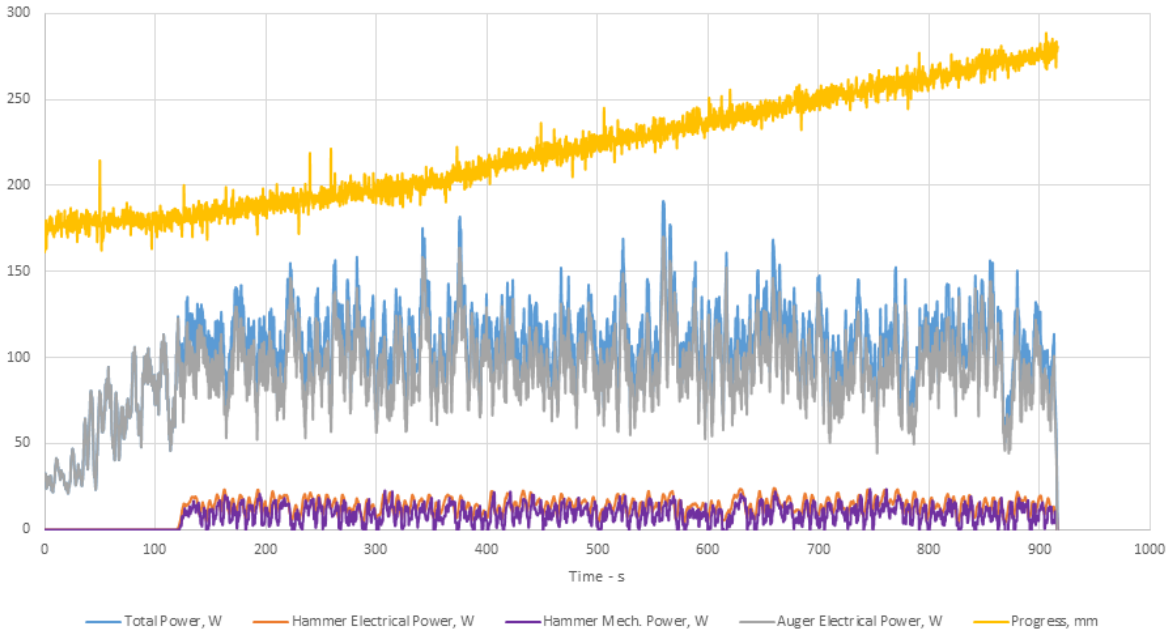


**Figure 97: Locharbriggs sandstone experimental run using small drill bit, 2-drop cam and 500 RPM hammer velocity. 12/8 WoB.**

Figure 98 details the findings of a 4-drop cam, small bit geometry run which made use of 500 RPM of percussive motor speed. Generating a net percussive power of 5 W, the system consumed an average of 138 W comprising of 24 W of percussion motor power and 114 W of auger rotation. This resulted in a percussive efficiency of 20.8% and a rate of progress of 0.08 mm/s. A corresponding specific energy of 6444 MJ/m$^3$ is therefore calculated.

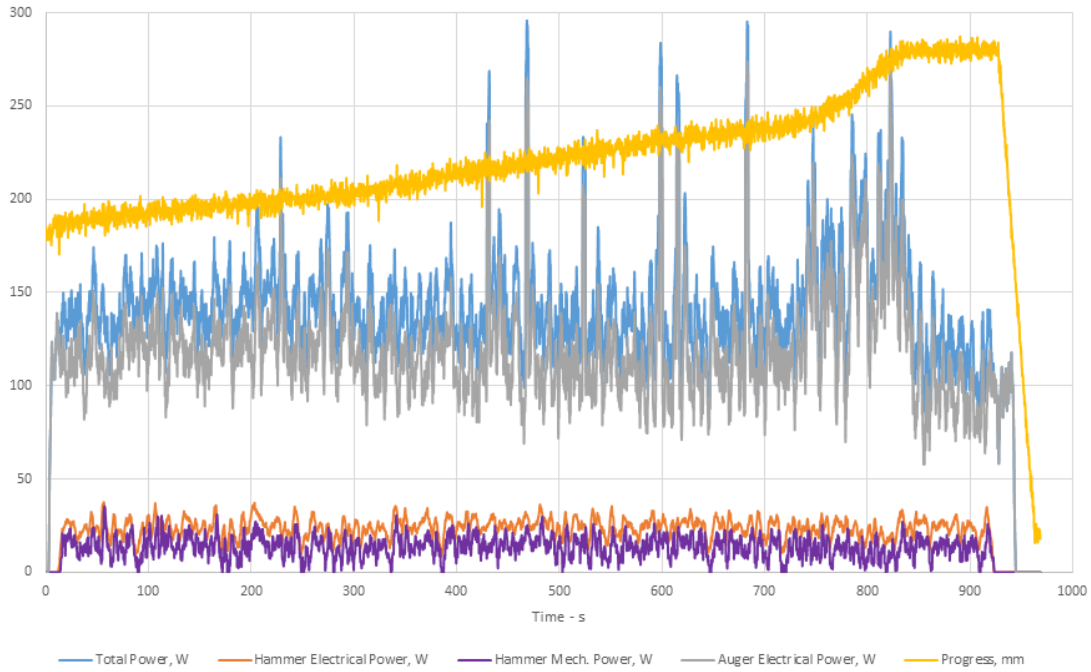


**Figure 98: Locharbriggs sandstone experimental run using small drill bit, 4-drop cam and 500 RPM hammer velocity. 12/8 WoB.**

The introduction of the medium drill bit allowed for a direct comparison between the geometries when operating in sandstone. Figure 99 details the result of such a run with a hammer motor speed of 500 RPM (5 W net percussive power). The average total power consumed in this run was 136 W with 26 W used in the generation of percussion (19.2% efficiency) and 110 W in auger rotation. This resulted in a rate of progress of 0.04 mm/s and a specific energy of 7219 MJ/m$^3$. The run generated a strong core with little evidence of fracture.

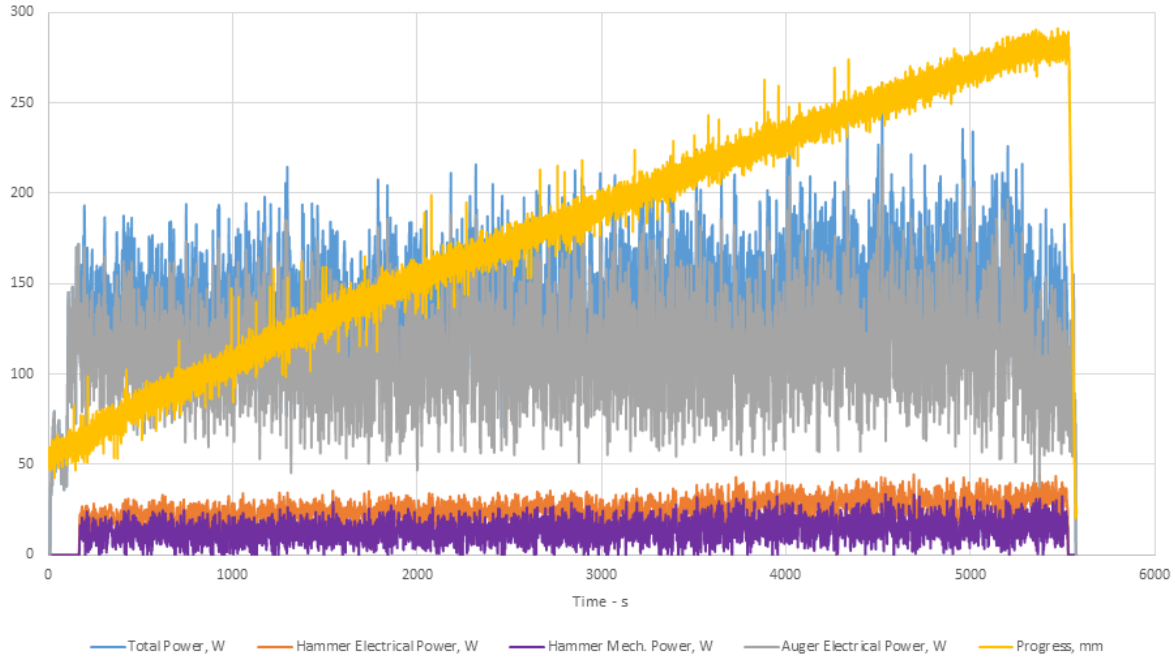


**Figure 99: Locharbriggs sandstone experimental run using medium drill bit, 4-drop cam and 500 RPM hammer velocity. 12/8 WoB.**

An increase in the hammer motor speed to 1500 RPM is depicted in Figure 100, resulting in a modest increase in the rate of progress to 0.05 mm/s. The average total power remained effectively unchanged at 132 W, with 36 W directly attributable to the generation of percussion. An auger motor power consumption of 96 W shows a reduction in power over the previous run, corresponding to a specific energy decrease to 5605 MJ/m$^3$. Multiple cores were produced, though an increase in the number of fractures was noted over the previous run.

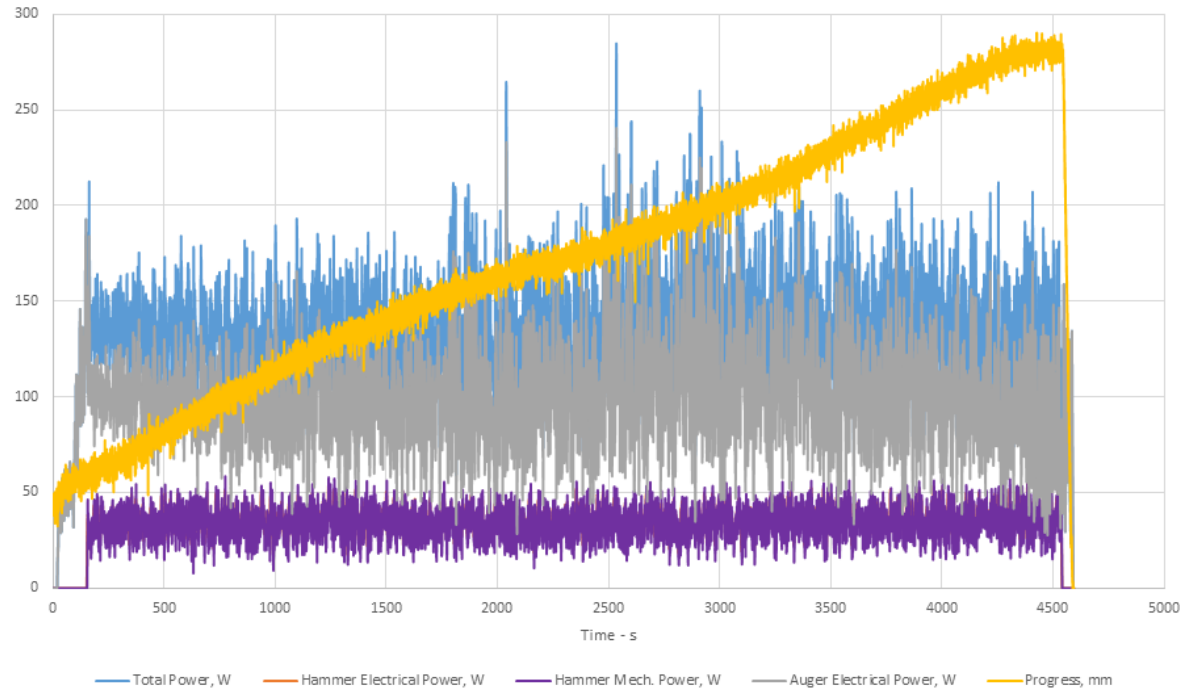


**Figure 100: Locharbriggs sandstone experimental run using medium drill bit, 4-drop cam and 1500 RPM hammer velocity. 12/8 WoB.**

Sandstone was found to be readily drillable by the system. Unlike the drilling of limestone, which produces powdery, highly bulking cuttings, sandstone cuttings are typically much grainier and thus unlikely to choke the auger. This acts to reduce the power demanded by the auger motors and the overall number of throughput-related faults encountered. Rotary-only drilling was found to be functionally ineffective when drilling sandstone, with a rate of 0.01 mm/s achieved at a weight on bit range of 40/30 N. The material responded well to the use of the higher energy, 2-drop cam geometry which generated drilling rates in the range of 0.14 – 0.2 mm/s for the small bit geometry. When using the lower energy, 4-drop cam, the small bit recorded rates on the order 0.05 – 0.08 mm/s, and 0.04 – 0.05 mm/s when using the medium bit. Specific energy analysis suggests that the medium bit may be more efficient than the small bit, perhaps attributable to an enhanced performance of the larger diameter bit at the rotary speeds used, and the use of the 2-drop cam is approximately 2.5 times more efficient than the 4-drop cam profile in most cases.

Table 6 details an overview of the results obtained. Figures for all tests completed during this campaign can be found in the appendix section.

| Rock Type | Drill Bit | Cam Geometry | Hammer Motor Speed - RPM | Upper WoB - N | Lower WoB - N | Ave. RoP - mm/s | Ave. Total Power - W | Ave. Hammer Power - W | Ave. Auger Power - W | SE - MJ/m3 |
|---|---|---|---|---|---|---|---|---|---|---|
| Portland Limestone | Small | Rotary Only | 0 | 20 | 10 | 0.2 | 163 | N/A | 163 | 3450 |
| | | 2-Drop | 500 | 12 | 8 | 0.47 | 233 | 16 | 217 | 1825 |
| | | | 1500 | | | 0.49 | 210 | 58 | 152 | 1601 |
| | | | 2500 | | | 0.45 | 191 | 90 | 101 | 1586 |
| | | 4-Drop | 500 | | | 0.13 | 164 | 22 | 142 | 4713 |
| | | | 1500 | | | 0.21 | 210 | 45 | 165 | 3736 |
| | | | 2500 | | | 0.19 | 171 | 75 | 96 | 3362 |
| | | | 3500 | | | 0.43 | 236 | 110 | 126 | 2050 |
| | | | 1500 | 17 | 13 | 0.2 | 176 | 38 | 138 | 3287 |
| | | | 2500 | | | 0.2 | 165 | 83 | 82 | 3082 |
| | Medium | | 500 | 12 | 8 | 0.11 | 142 | 12 | 130 | 2741 |
| | | | 1500 | | | 0.14 | 151 | 37 | 114 | 2290 |
| | | | 2500 | | | 0.14 | 199 | 82 | 117 | 3018 |
| Locharbriggs Sandstone | Small | Rotary Only | 0 | 40 | 30 | 0.01 | 87 | N/A | 87 | 32500 |
| | | 2-Drop | 500 | 12 | 8 | 0.14 | 103 | 14 | 89 | 2748 |
| | | | 1500 | 30 | 10 | 0.2 | 186 | 51 | 135 | 3474 |
| | | 4-Drop | 500 | 12 | 8 | 0.08 | 138 | 24 | 114 | 6444 |
| | | | 1500 | | | 0.05 | 125 | 39 | 86 | 9339 |
| | | | 2500 | | | 0.07 | 153 | 71 | 82 | 8165 |
| | Medium | | 500 | | | 0.04 | 136 | 26 | 110 | 7219 |
| | | | 1500 | | | 0.05 | 132 | 36 | 96 | 5605 |

**Table 6: Results overview of drilling campaign**

### 5.11.3 Core Quality

Missions which feature a sample drilling component may be subdivided into two categories: those which seek to capture core samples and those which wish to sample drilled cuttings. While a high degree of core integrity is not always a critical requirement, it may be preferable in situations such as Mars sample return, whereby broken or fragmented cores may impede the capture of the sample.

Over the course of experimentation, trends were identified between the percussive power/energy of a given drilling run and the quality of the core. Figure 101 presents a sandstone core captured with only a single fracture at the lower end (deepest point in the drilling cycle). It was found that the brittle nature of the harder sandstone medium meant that core fracturing was frequently present, as noted in Figure 103. Analysis of the results suggests that core fracture in sandstone is generally more likely when a high percussive power is used, with a particular emphasis on the effect of high percussive motor speed. While high percussive energies do tend to increase the likeliness for multiple fractures, this has been shown to not play as crucial a role as the high vibration environment caused by high rotary speeds.

**Figure 101: Locharbriggs sandstone captured during a laboratory experimental campaign using the medium drill bit geometry. Note, only a single fracture was present within the core sample. Core diameter of 25 mm, for reference.**

Despite a reduction in strength, limestone is generally less brittle than sandstone and thus more likely to produce complete cores samples. A similar rule may be applied to core integrity. Figure 102 portrays a classic result of a limestone run – a complete core sample with a high degree of structural integrity retained. In both rock types, the small bit does not tend to generate core samples, while the medium bit geometry almost always generates a core.

**Figure 102: Limestone core captured during a laboratory experimental campaign using the medium drill bit geometry. An absence of fractures noted.**

**Figure 103: Core samples obtained from experimental drilling campaign. Note, all cores were obtained using the medium drill bit geometry. Cores obtained from medium including Locharbriggs sandstone (red, top left), Portland limestone (white, lower right), and microgabbro (grey, top-centre). All core diameters 25 mm for reference.**

A system for core quality classification was developed in order to quantitatively evaluate the obtained core samples post-drilling. The length of core achieved relative to the length of the borehole and the number of breaks in the core were ranked from one to five, with the latter denoting a longer core ratio obtained and a higher degree of intactness, respectively. Table 7 details findings from the laboratory campaign. In the case of subglacial bedrock sampling, core length is prioritised over intactness. This is a result of the chemical processing which is foreseen for any cores captured, thus an intact core is not deemed to be essential if the lithography of the sample can be assured.

| Rock Type | Drill Bit | Cam Geometry | Hammer Motor Speed - RPM | Upper WoB - N | Lower WoB - N | Core Length | Core Intactness |
|---|---|---|---|---|---|---|---|
| Portland Limestone | Small | Rotary Only | 0 | 20 | 10 | 0 | 0 |
| | | 2-Drop | 500 | 12 | 8 | 0 | 0 |
| | | | 1500 | | | 0 | 0 |
| | | | 2500 | | | 0 | 0 |
| | | 4-Drop | 500 | | | 0 | 0 |
| | | | 1500 | | | 0 | 0 |
| | | | 2500 | | | 0 | 0 |
| | | | 3500 | | | 0 | 0 |
| | | | 1500 | 17 | 13 | 0 | 0 |
| | | | 2500 | | | 0 | 0 |
| | Medium | | 500 | 12 | 8 | 4 | 5 |
| | | | 1500 | | | 4 | 3 |
| | | | 2500 | | | 3 | 2 |
| Locharbriggs Sandstone | Small | Rotary Only | 0 | 40 | 30 | 0 | 0 |
| | | 2-Drop | 500 | 12 | 8 | 0 | 0 |
| | | | 1500 | 30 | 10 | 0 | 0 |
| | | 4-Drop | 2500 | 12 | 8 | 0 | 0 |
| | | | 1500 | | | 0 | 0 |
| | | | 2500 | | | 0 | 0 |
| | Medium | | 500 | | | 3 | 3 |
| | | | 1500 | | | 3 | 2 |

**Table 7: Quantitative assessment of core length and intactness**

## 5.11.4 System Capability and Robustness Discussion

Upon completion of the test campaign, the physical condition of the system was evaluated in order to establish both areas of strength and weakness following the extensive period of testing.

The system appears to be capable of achieving the rates of progression required of it, allowing coring operations to be accomplished in realistic timeframes for both subglacial bedrock extraction and planetary drilling scenarios as previously detailed.

It is clear that the percussive mechanism is particularly capable. Despite completing over 250,000 revolutions, the cam profiles tested displayed no physical degradation. While this result is exceptionally promising, there exists the possibility that the system was over engineered. While the manufacture of the system made use of somewhat costly exotic steel alloys in the manufacture of the cycloidal barrel cam, the decision to do so was based upon the planetary drilling design methodology that requires all elements of the design to operate without the need for replacement for a period as determined by the probable operational lifetime plus substantial margin. While the application of the system to terrestrial subglacial bedrock sampling means that there is scope for the replacement of the cam profile if required, operations within the Polar Regions precludes the ease of replacement of parts, and failures may have costly repercussion. Thus, it is felt that the robustness of the cycloidal barrel cam is to be viewed positively, with the excess expense over and above that of an untested, cheaper alloy justified.

The importance of the inclusion of a hard stop, located between the cam profile and the bottom face of the hammer, was noted. When operating in free air, or during drilling operations where the weight on bit limits have been poorly set such that the drill bit has

extended periods disengaged from the terrain, there is a tendency for the cam follower bearings (which allow the hammer to follow the profile of the cam during rotation) to make a hard impact with the cam. The fragile nature of the cam follower bearings means that there is a tendency for these bearings to rapidly degrade. Degradation of the bearing results in a transition from smooth rolling over the profile to sliding, with a corresponding increase in the torque demanded by the percussive motor. While this increase (in the region of 25%) is undesirable, the effect of this increased torque demand is easily accommodated by the hammer motor and has little impact on the overall power draw for the device. As previously noted, the increased friction does not appear to wear the cam geometry. The installation of a hard stop prevents such impacts from occurring and is easily integrated within the architecture of the system.

Analysis of the power draw of the auger motors suggests that the torque generated during the drilling process often approaches or exceeds the nominal continuous operational limits of a single motor, thus vindicating the use of a triple motor gearbox. While the triple motor setup appears to function as required, further improvements could be made through the integration of the setup within the autonomous control system to ensure that no single motor is overexposed to excessive torque levels.

### 5.11.5 Drill Performance Discussion

Over the course of the experimental campaign, two cam geometries were tested. The 2-drop, 17 mm high geometry generated a percussive energy of 3.34 J per strike of the hammer, while the 4-drop, 11 mm high profile generated 58% less percussive energy at 1.4 J per strike. Although the inner and outer diameters of the cycloidal barrel cam body was maintained across both geometries, the increased power required by the system in overcoming the additional height of the 2-drop cam was largely offset by a reduction in the number of drops present. Thus, it was possible to reduce the gradient of the cycloidal profile. This attempt at minimising the power required to rotate the cam-follower over the cam profile was largely reflected in the data via the capturing of the hammer efficiency ratio. Results from the campaign suggest that for drilling runs at speeds of 500 – 2500 RPM, the efficiency of the 2-drop cam averages 28.8%, while the 4-drop cam profile 29.7%. Thus, it is possible to conclude that the cam profiles are approximately equal in the ability to convert hammer motor rotation to a percussive action.

In the case of Portland limestone, the results obtained by the 2-drop cam were particularly interesting. When operating the hammer motor at speeds of 500 – 1500 RPM, rates of

progress for the small drill bit in the range 0.45 – 0.49 mm/s were recorded. At a hammer motor speed of 500 RPM, the system operates at a rate of 0.094 mm/J of net percussion, while an increase to 1500 RPM sees a reduction in efficiency to 0.035 mm/J. A further increase in the hammer motor speed to 2500 RPM shows a further reduction in efficiency to 0.020 mm/J of net percussion. Comparing these results to that of the 4-drop cam geometry allows for a more clear evaluation to be made. In the latter case, testing in the range of 500 – 2500 RPM generated rates of progress in the range 0.11 – 0.21 mm/s, with the 500 RPM run operating at a rate of 0.028 mm/J of percussive energy, the 1500 RPM run at a rate of 0.018 mm/J and the 2500 RPM run at a rate of 0.010 mm/J.

Results from 2-drop Locharbriggs sandstone tests at 500 and 1500 RPM detail rates of progress of 0.14 and 0.20 mm/s respectively. Efficiency rates of 0.035 mm/J and 0.014 mm/J of net percussion are therefore calculated. Analysis of the 4-drop sandstone data of runs ranging from 500 – 2500 RPM shows rates of progress in the range of 0.05 – 0.10 mm/s. With regard to the 500 RPM run, an efficiency rate of 0.025 mm/J of percussive energy is noted. At 1500 RPM, this rate is substantially reduced to 0.004, and an increase in hammer motor speed to 2500 RPM has no further effect on the efficiency rate.

These findings allow multiple conclusions to be drawn. Primarily, it may be concluded that the effect of implementing percussive energy levels which are greatly in excess of the overpressure threshold required to fracture the terrain may result in a disproportionately high rate of progression over an equivalent percussive power delivered at lower percussive energy levels, and that any increase in the percussive power through an increase in the rate of hammer strikes has little effect over and above this baseline power. In the case of the relatively soft and weak limestone samples, this effect may be particularly pronounced. In the 500 RPM test case, a comparison of efficiency rates between the 2-drop and 4-drop cam profiles suggest the former is approximately 3.5 times that of the latter. This relationship is noted for all percussive motor speeds, though the principal of diminishing returns is a factor as the efficiency rate when penetrating limestone using the 2-drop profile at 2500 RPM is reduced to only twice that at of the equivalent 4-drop test. Furthermore, while the rate of progress is, in some cases, shown to increase with an increase in the percussive rate (particularly in low strength terrain at low percussive energies), these gains are marginal in comparison to those which are achieved through altering the percussive energy. Thus, it is clear that precedence should be given to ensuring that the profile of the cam geometry used in any system can generate hammer-driven fracturing which is substantially in excess of the

minimum pressure required to penetrate the terrain, at the expense of the rate at which this hammering is delivered. This conclusion also benefits the stability of the system as high percussive rates are synonymous with excessive vibration within the system. This vibration often results in a misinterpretation of the weight on bit feedback (with obvious ramifications for the control system), and may also result in the poor formation of a pilot hole necessary for effective drilling.

While it is clear that the role of the percussive energy is of a greater importance than the rate of percussion when efficiently penetrating terrain, the value of an increased percussive rate requires a more holistic approach to the analysis of the results of the test campaign. In the case of the 2-drop cam profile tests in limestone, the average total power was shown to reduce as the hammer motor speed was increased from 500 – 2500 RPM. While an increase in hammer speed results in a subsequent increase in hammer power, the percentage contribution of the auger power to the total power reduced at a greater rate. At the lowest percussive rate, the auger contributed 93% of the total power, decreasing to 53% at the highest percussive rate. This was accompanied by an overall reduction in the total power from 233 W to 191 W. This trend is noted frequently through the data and suggests that hammer frequency is directly related to the power required to rotate the auger. It is postulated that drill bit vibration induced through percussive striking may act to energise the spoil present on the auger flights at any given point, reducing the friction between the spoil and the auger and in turn lowering the power consumed by the system. In the case of the 4-drop profile in limestone, a reduction in the specific energy of the system is noted from 1852 – 1586 $MJ/m^3$ as the hammer speed is increased from 500 – 2500 RPM.

Over the course of the test campaign, both a ‘small’ bit geometry and ‘medium’ bit geometry were tested. With regard to the testing of each geometry in limestone, like for like comparisons using identical percussive energy levels suggest that the medium bit geometry performs, on average, 47% better when testing with the 4-drop cam geometry compared to the small bit. Similar testing with sandstone revealed the medium bit to be more effective gain, but with an improvement of 23% over the small bit. This is likely a factor of the added mass of the medium bit and the increased diameter proving more effective at lifting spoil at a given speed of rotation.

The quality of the core samples collected was found to vary significantly over the course of testing. Use of the small drill bit geometry ubiquitously resulted in a lack of core produced,

suggesting that a core diameter of 10 mm is simply too fragile to sustain the highly vibratory percussive environment generated by the system. Generally, limestone was shown to produce a greater length of core relative to the length of the borehole and the core collected was typically more intact with few breaks than sandstone. In both terrain cases, higher percussive powers typically result in a degradation of core length and quality, with a particular emphasis placed on the negative affect of percussive rate in particular.

## 5.12 TVAC Testing Campaign

The development of the Subglacial Bedrock Sampler prototype saw the design of the system geared towards the low-resource extraction of samples from terrestrial Polar Regions, but a planetary drilling approach was adopted throughout the development process in order to ensure that the new system would be compatible with the British Antarctic Survey's existing logistical operations. It is for this reason that the prototype developed may also serve as a baseline technology for planetary drilling tests in simulated planetary environments.

### 5.12.1 Mars Environmental Testing

In order to accurately replicate the environmental conditions of extraterrestrial drilling operations as closely as possible, the key factors likely to affect the drilling process must first be identified. Perhaps the most significant difference when drilling in off-world settings (either on the moon or other outer solar system targets such as Mars) is that of both the ambient temperatures at the surface and within the terrain. A reduction in the temperature of the ambient environment primarily affects the functioning of electronics within the drill system including the operation of electro-mechanical motors. It may be assumed that flight hardware would be designed with heaters integrated within the design in order to pre-warm motors and any other vulnerable mechanisms and electronics, thus the need to test the system at reduced ambient temperatures may be negated due to there being little benefit for the complexity cost involved in cooling vacuum environments. The need to cool the target terrain to be drilled is generally more critical if high fidelity testing is to be ensured, but there are caveats. While the strength of dry, rocky terrain in cryogenic conditions increases, these increase may be considered marginal when compared to the change in the physical properties of water-cemented regolith or ice (as discussed in Section 4.14.2). To this end, if the target terrain to be tested consists of dry, rocky terrain, it may be easier to replicate cryogenic testing by replacing the rock type with a harder variant instead of cooling the terrain unnecessarily. It is therefore possible to conclude that the most challenging planetary terrain to investigate is that which simulates the water-rich Polar Regions found on Mars and, to a

lesser extent, the Moon. Figure 104 [81] details the typical regolith temperatures, at a depth of 5 cm, over one sol within multiple excavated trenches at the Phoenix landing site in the Mars Northern Regions. The lowest recorded temperature, found within the Vestri trench, approached 180 K which suggests that the ice-cemented terrain may be extremely strong in these regions.

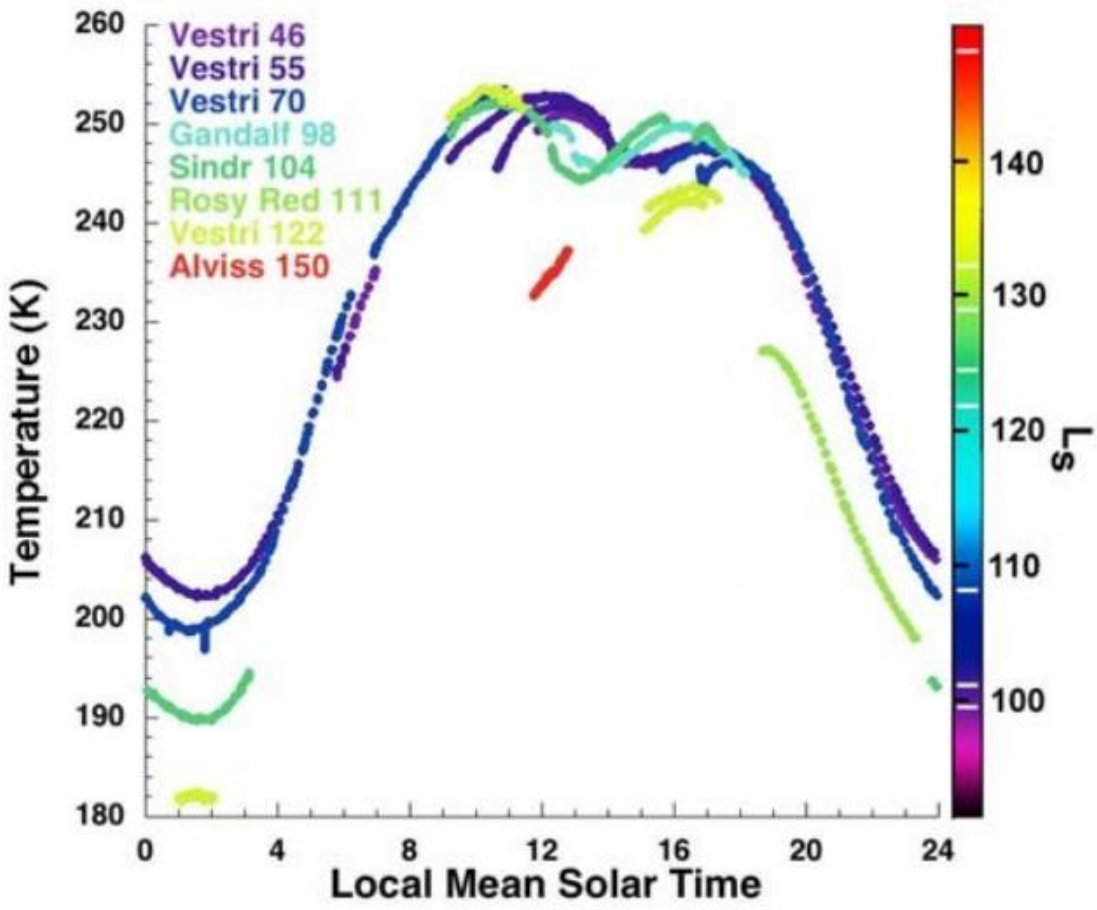


**Figure 104: Regolith temperatures profile over the course of one Martian day at Phoenix landing site. Results from a number of excavated trenches accessed by the Thermal and Electrical Conductivity Probe (TECP) instrument attached to the robotic arm of the lander. Note, the depth of trenches did not exceed five centimetres** *[81]***.**

While cryogenic temperatures may hinder drilling progress, there are features associated with the ambient pressure on Mars which may have an effect on the drilling process. Mars has a tenuous carbon dioxide atmosphere in the range 300 – 1200 Pa, but it is the unique combination of the typical ambient temperature and pressure range which may be possible that may have an effect on drilling operations. In Figure 105, a phase diagram for water with the possible atmospheric conditions for Mars overlaid, given the range of temperature and atmospheric pressure which may be found on Mars, water may exist in all three physical states with a number of possible positive or negative impacts on the drilling process. As

discussed in Section 4.14.3, the presence of liquid water in drilled cuttings, a product of residual heat from formation breaking melting ice trapped within the terrain, may result in a multitude of fault states which may have potentially mission-ending consequences. This is further compounded by the ubiquity of perchlorate salts on the planet. Studies suggest that the widespread presence of small quantities of these salts (0.5% by weight) could lead to a reduction in the melting point of ice by a few degrees Celsius [82]. More concentrated solutions of magnesium perchlorate and water are capable of depressing the melting point such that eutectic temperatures of 206 K may be possible, though such concentrations are unlikely on Mars [83]. Furthermore, it has been suggested that liquid brines may exist on the surface. These brines may translate between the overburden layer and the ice table beneath [84].

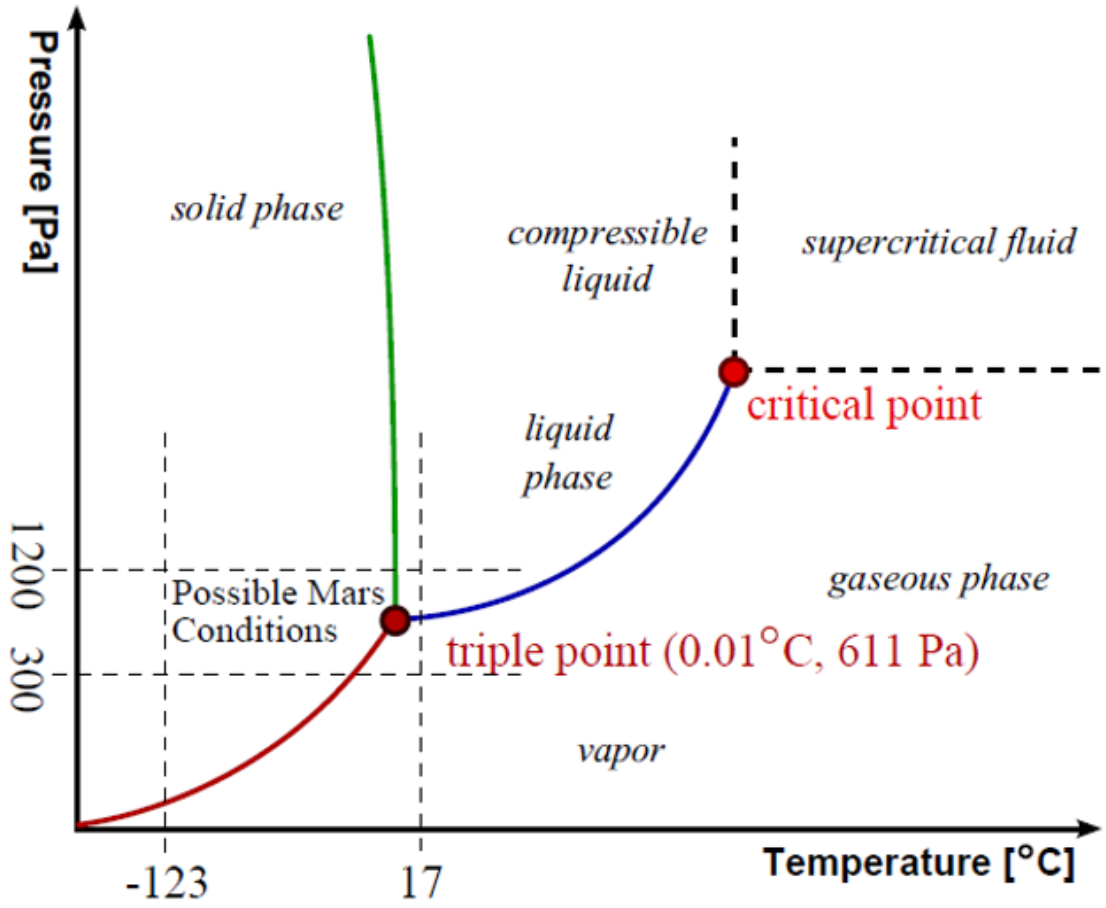


**Figure 105: Phase diagram for $H_2O$ with Mars ambient pressure and temperature ranges noted (based upon recorded maxima and minima from in-situ sensing)** *[28]*.

While drilling in certain temperature-pressure regimes may lead to water phase changes from solid-liquid, under certain conditions a solid-vapour phase change (sublimation) is also possible. In such cases, ice present within the drilled cuttings could be directly sublimated to vapour, completely bypassing the liquid stage. If sufficient heat is supplied to the cuttings

then it may be possible for these cuttings to become completely desiccated by this process, in effect freeze-dried. While glazing and bit freeze-in faults may thus be avoided, such a situation could have direct implications for mission architectures which seek to perform analysis of the spoil. This is problematic to such a degree that the requirement for the minimisation of volatiles loss is a leading design driver of the forthcoming ProSPA drilling system for the proposed Lunar 27 mission [85].

### 5.12.2 FH Aachen Test Campaign

It is clear that performing drilling operations in simulated planetary conditions may expose drilling systems to conditions which simply cannot be replicated at ambient conditions in the laboratory. To this end, it was decided that the subglacial bedrock sampler prototype would be tested at the FH Aachen TVAC facility, Aachen, Germany, in order to better characterise the system under Mars-like conditions. The facility available for testing, Figure 106, was particularly useful due to its vertical orientation and large diameter ensuring that the drilling system was seamlessly integrated with the chamber.

**Figure 106: Aachen TVAC Facility with subglacial bedrock sampler prototype in the foreground during preparations. Rig height of 1.8 m for reference.**

Perhaps most importantly, the cleanliness criteria of the chamber is low, thus the use of highly outgassing components and dusty regolith simulants is acceptable – the latter of which is clearly of great importance when drilling activities are to occur. Upon installation of the drilling system, it was found that a chamber pressure of 1 mBar could be consistently maintained allowing the solid-vapour transition phase to be studied

### 5.12.3 Experimental Setup

The experimental rig was fundamentally unchanged from previous performance tests conducted under ambient conditions in the laboratory or in the BAS Cold Chamber Facility. It was decided that, given the low vacuum levels in which tests would be conducted, there was no need for vacuum-rated motors given that extensive testing of the off-the-shelf Maxon

BLDC motors used had been conducted by the manufacturer in similar conditions with positive results [86].

As the primary goal of the experimental campaign was to test the performance of the drilling system in ice-cemented regolith simulant at cryogenic temperatures, it was essential that a method of containing these samples during testing was developed. It was decided that, in order to minimise the complexity of the experimental process, a passive system of cooling the test samples would be utilised which would negate the need for a complex active cooling system. The use of a passive cooling system, whereby the samples are precooled outside of the test chamber before the drilling rig is integrated within the chamber, relies upon a combination of the thermal inertia of the mass of simulant used and short testing times in order to ensure that the samples are at cryogenic temperatures during drilling operations. The cooling system assembly consisted of a set of concentric nested tubes which had been fabricated so as to ensure a leak-proof seal with a central spigot part, as shown in Figure 107. It was found that simulant temperatures of approximately 100 K could be achieved through this means but this was shown to slowly rise before the experiment could commence. To this end, temperatures at the start of the drilling tests were often in the region of 150 K or higher, following a preparation time in the region of 15 minutes of integration with the chamber and pumping down. When integrated and pumped down to the required pressure, the rate of heating was notably reduced – likely a result of the removal of convective heating. Thus, any delays which arose once the chamber had been pumped down were less disruptive to testing than those which arose outside of the chamber. When combined with typical drilling runs not exceeding 30 minutes, the effects of passive heating of the sample were minimised. As the main goal of the tests were to evaluate the performance of the system cryogenically frozen terrain, passive heating was deemed acceptable if the heating occurred in a standardised way, affecting all samples produced and tested. This was achieved through the development and refinement of the process, ensuring a high degree of repeatability. It is of note that the drill bit was also often precooled using $LN_2$, however this was a variable that was studied over the course of the experimental campaign thus was not a consistent element of the testing procedure.

**Figure 107: Passive cooling system used for pre-cooling saturated regolith simulants to cryogenic temperatures. Regolith simulants are compacted within the volume of the inner tube before liquid nitrogen is carefully transferred into the void between the inner and outer tubes, cooling the saturated simulant to the desired starting temperature. Drill bit diameter of 20 mm. for reference.**

In order to capture images and video during the vacuum tests, it was decided that a vacuum-rated imaging system would be installed with a view of the top of the borehole, allowing the progress of the drill to be captured and the accumulation of spoil at the surface. This imagine system proved to be extremely useful for monitoring drilling progress as the chamber was without viewing ports. In order to integrate the imager with the drilling rig, the imager was mounted directly to the rig frame. While this allowed a clear field of view, the quality of the video which was produced suffered as a result of the vibration environment generated by percussive drilling. Future tests would seek to isolate the imager from the rig

in order to mitigate against these issues. Figure 108 details the locations of the imager on the right side of the drilling rig.

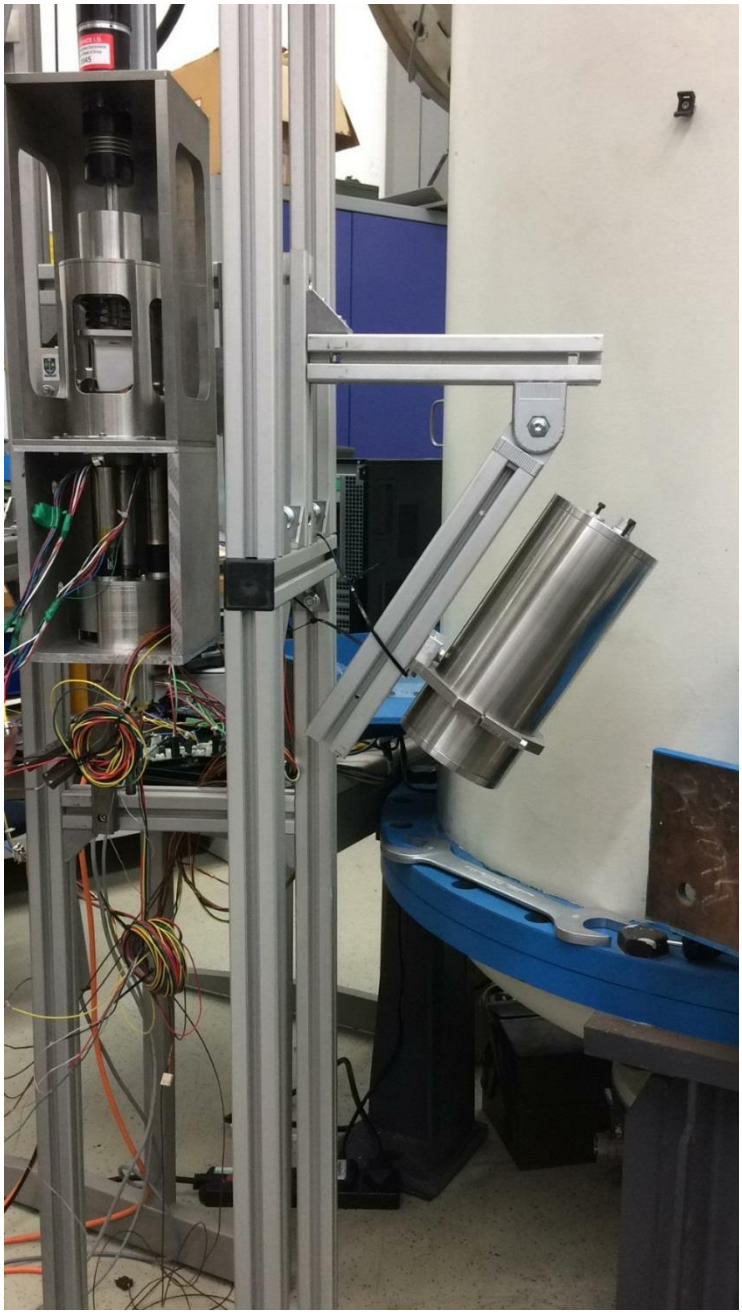

**Figure 108: Test rig prior to chamber insertion. A vacuum-rated imaging system was attached to the rig. This allowed real-time monitoring of drilling progress while the system was in the TVAC chamber.**

### 5.12.4 Experimental Procedure

In order to ensure consistency during experimentation, a rigorous approach to the preparatory procedure was taken. This procedure is as follows:

1) Measure correct ratios of dry regolith simulant and water by weight.

2) Slowly add water to dry regolith while mixing thoroughly so as to ensure an even distribution within mixture.

3) Add small quantities of water-saturated regolith simulant to the inner void of the cooling system, compacting to desired 2 g/cm$^3$ at predetermined height intervals.

4) Connect passive cooling system to base of rig to ensure rapid turnaround upon cessation of cooling procedure, minimising excessive heat flow to the sample.

4) Carefully pour $LN_2$ into orifice between inner and outer tubes in order to cool the metal assembly and saturated regolith mixture to desired cryogenic temperature. Temperature established via use of embedded T-type thermocouple in preliminary runs but excluded in later runs due to drill bit impinging.

5) Raise rig using overhead crane and carefully lower the rig into the chamber. Make all electrical connections, activate imaging system and close chamber, as shown in Figure 109. Proceed with drilling operations only upon reaching desired chamber pressure of 1 mBar.

6) Upon reaching the desired depth in regolith simulant (approximately 250 mm), retract drill and return chamber to ambient atmospheric pressure. Reset experiment for next run.

**Figure 109: Drilling system fully integrated into TVAC chamber and awaiting pump down.**

### 5.12.5 Experimental Results and Discussion

In order to establish the capability of the system in cryogenic terrain at Mars ambient pressures, various drilling scenarios were examined with a multitude of interesting results obtained.

Figure 110 presents the results from a drilling run in fully saturated regolith simulant, making use of a 2-drop cam of height 17 mm. Drilling was conducted without the use of manual control in order to establish if the human operator could track the progress of the drilling system using drilling data alone and without the use of visual cues. This was performed by mimicking the behaviour of the control system – advancing the drill when the drill dropped below a lower force threshold and retracting the system when an upper force threshold was reached. While a human operator is incapable of reacting as quickly as the automated system, a rate of progress of approximately 0.15 mm/s was achieved through cryogenically frozen terrain using approximately 382 W of average total power to accomplish this, comprising of 346 W of auger power and 36 W of power used in the generation of percussion. This translates to a specific energy of 9514 MJ/m$^3$. Auger power consumption is generally much higher than in the laboratory, likely attributable to the vacuum environment in which the drill was operating. As the motors used were of the off-

the-shelf variety, they were not rated for vacuum use. A sudden drop in auger power is noted at the 700 s mark. This is particularly interesting and correlates to an increase in the rate of progress. Analysis of the imagery obtained during the run suggests that, at this point, a transition from spoil clearance via augering to clearance through sublimation-induced gas blasting was noted.

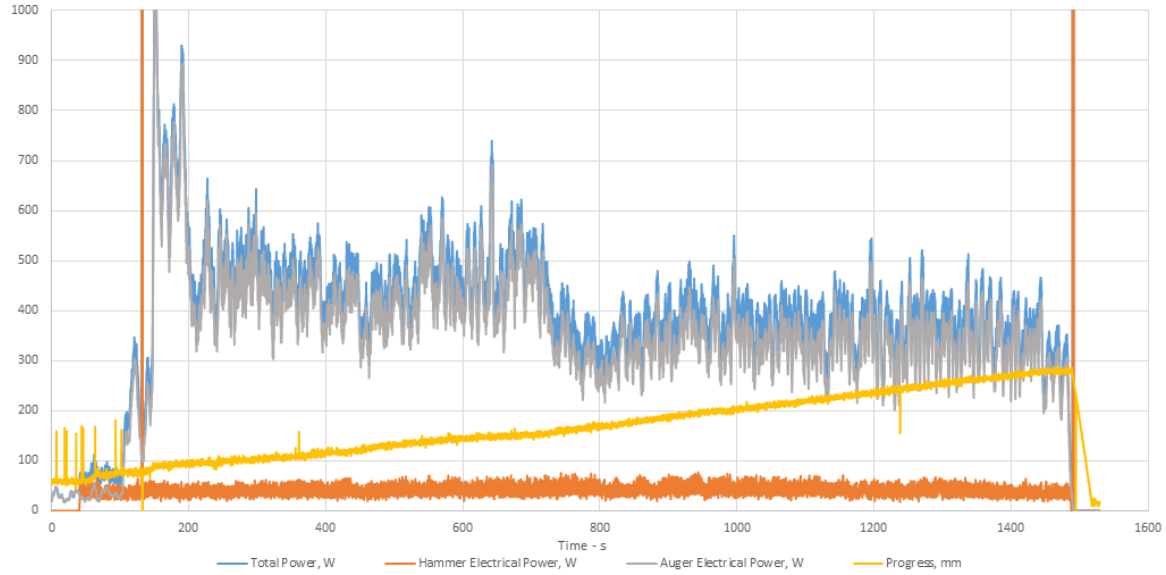


**Figure 110: Drilling run in fully saturated cryogenic BP simulant. 2-drop cam profile, 17 mm height. Small bit geometry. Percussive motor speed set to 2000 RPM. Manual control (no autonomy). Note, a reduction in auger power at 1200 s correlates with an increase in the RoP and is indicative of a transition from spoil clearance via augering to gas blasting from sublimation of ice trapped within the simulant.**

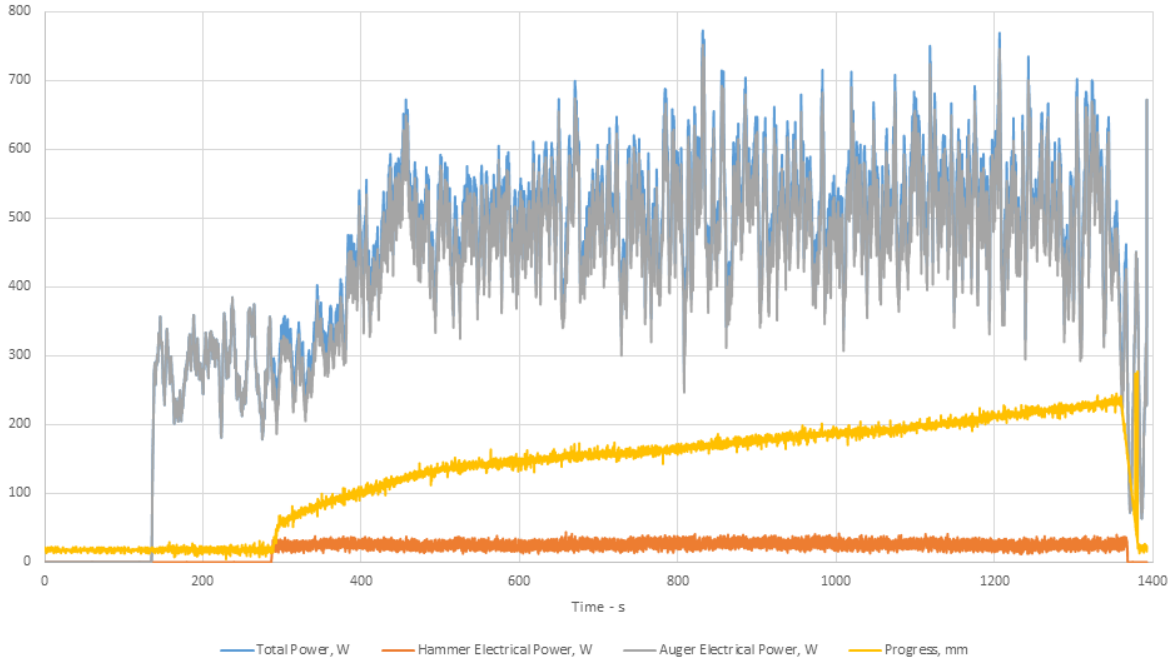


**Figure 111: Drilling run in fully saturated freezer temperature BP simulant. 4-drop cam profile, 11 mm height. Autonomous control. Note, sublimation-induced gas blasting throughout the run thus generally low auger power.**

In order to further explore this phenomena in more detail, another run was conducted in freezer temperature (~250 K) fully saturated permafrost (Figure 111). This drilling run did not make use of a pre-cooled drill bit in order to increase terrain heating (promoting sublimation) in order to inject excessive energy into the less heavily ice-cemented terrain. The resulting sublimation gas blasting was noted to be more consistent than that of the previous run, though the differences in the strength of the cryogenic terrain and the freezer temperature terrain make a direct progress comparison difficult. Figure 112 presents the resulting spoil patterns produced from the initial run in cryogenic terrain. The spoil which was produced by the use of augering was noted to be much darker in tone, still containing water. This spoil also tended to be of a larger grain size as the water present tends to generate inter-particle bonding and clumping. The spoil removed by gas blasting tended to be extremely small grained and lighter in tone due to the effects of desiccation. The process of gas blasting also tended to eject the spoil over considerable distances. Figure 113 details the distribution of desiccated cuttings around the base of the sample tubes.

The total average power consumed during the drill process was noted to be 422 W, consisting of 24 W required in order to generate percussion (for a net percussive power of approximately 12 W), while the auger contribution averaged 397 W. A rate of progress of 0.16 mm/s resulted in a specific energy of 9853 $MJ/M^3$.

**Figure 112: Spoil pattern produced due to a transition from auger-dominated spoil removal to sublimation induced gas blasting. The darker spoil (centrally located) is indicative of the former and was noted to be of a larger grain size than the lighter, desiccated spoil (around the perimeter of the spoil pile) which was produced by gas blasting. Drill bit diameter of 20 mm, for reference.**

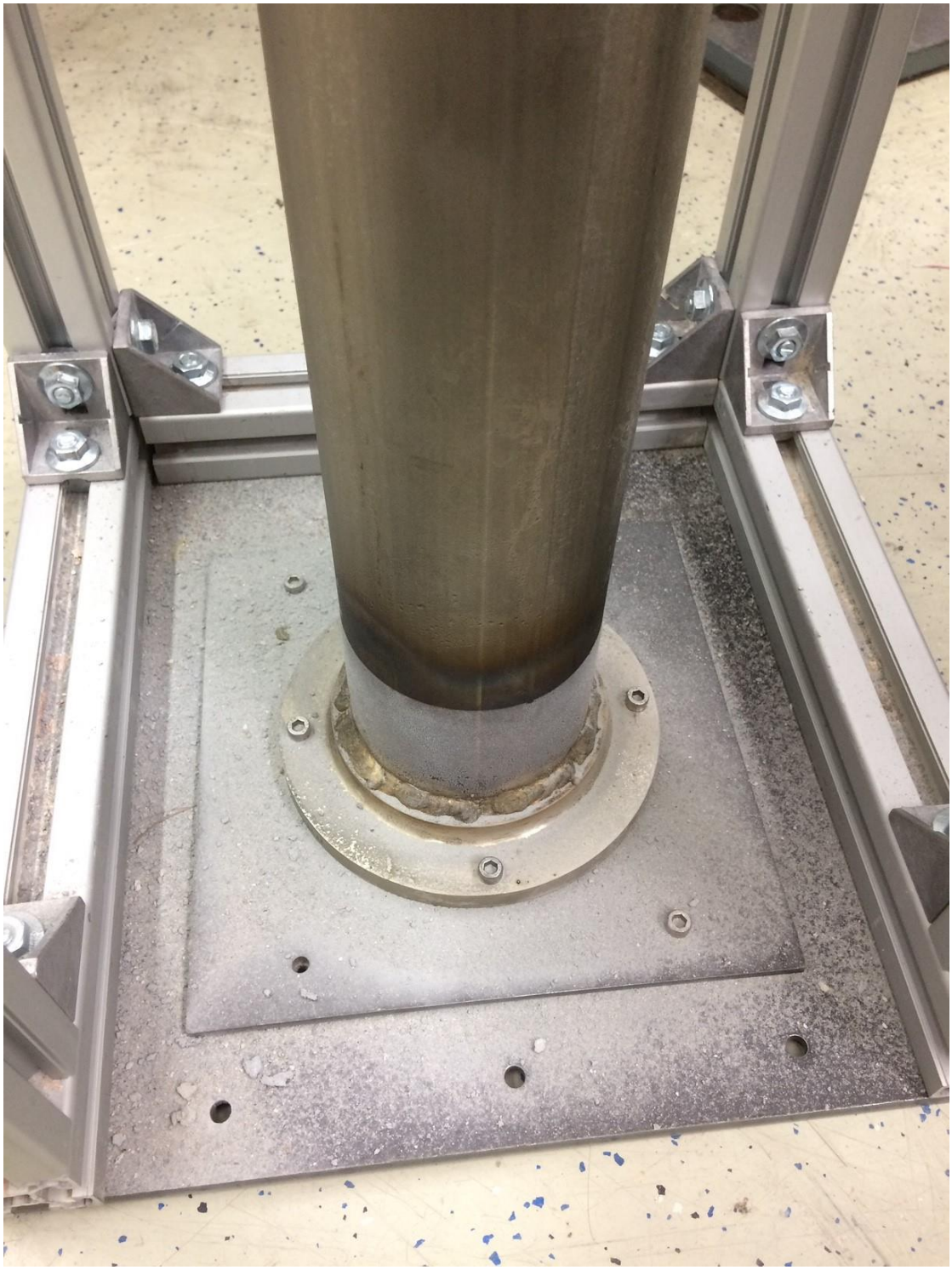

**Figure 113: Spoil ejected by gas blasting distributed at the base of the test rig - a substantial distance from the borehole.**

In order to characterise the performance of the system when drilling cryogenic terrain in an environment with an atmospheric pressure above that of the triple point of water, an experimental run was carried out whereby cryogenically frozen saturated simulant was drilled outside of the TVAC chamber. While this experiment allowed triple point effects to be negated, convective warming at the increased atmospheric pressure levels meant that conditions were not completely analogous to those experiments conducted in-chamber.

Figure 114 details the results from this run. Results show similar rates of progression as to that which was seen in chamber tests at reduced ambient pressure, though the behaviour noted throughout was somewhat different. Perhaps the most significant difference noted was that the system exhibited a behaviour which saw it frequently step forward and backwards without fully engaging the terrain. This periodically reduced the power draw across all of the actuators but did not appear to affect progress.

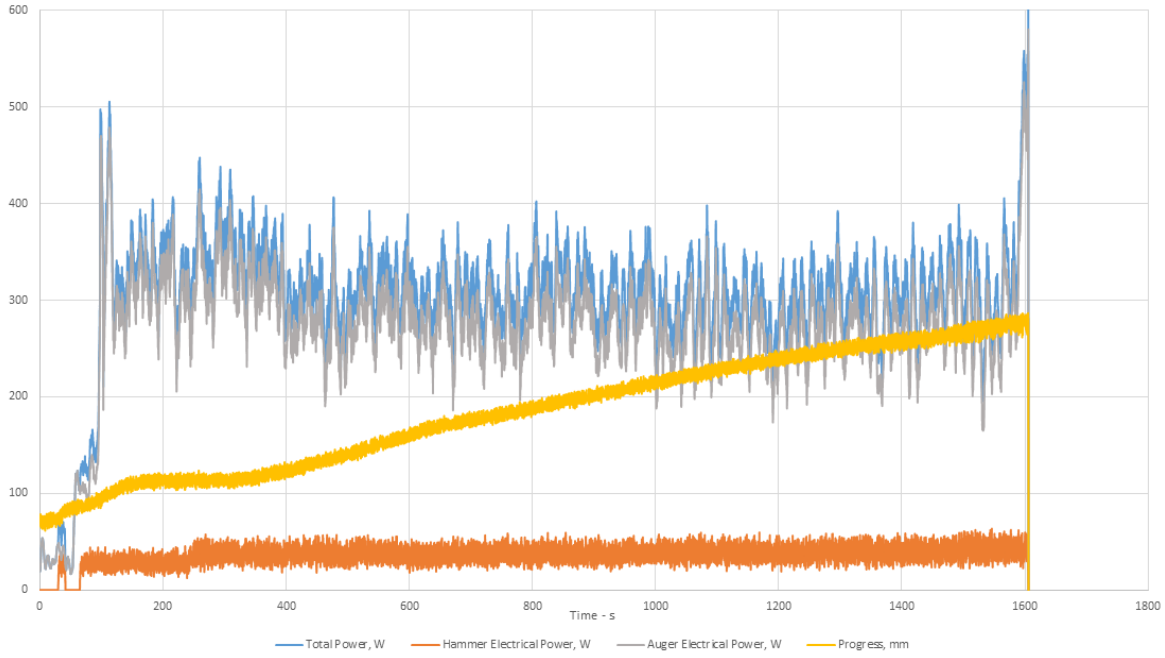


**Figure 114: Drilling run in fully saturated cryogenic BP simulant. 2-Drop cam profile, 17 mm height. Autonomous control. Run conducted at ambient pressure outside of chamber. High degree of melting and generation of mud noted.**

As drilling continued, it was noted that the excessive heat generated during the process of breaking the terrain rapidly melted water bound within the cuttings generating mud and reduced the capability of the auger when attempting to clear the spoil. Figure 115 highlights the creation of this muddy spoil and its tendency to completely clog the auger. It is postulated that the drilling process quickly transitioned from terrain fracture to terrain melting, thus accounting for the unusual control behaviour noted. Interestingly, it was noted that the high degree of integrity upon the conclusion of the run suggesting that heat dissipation throughout the sample was not complete. Figure 116 details the intact nature of the borehole upon the retraction of the drill suggesting that, while melting is found within the borehole, the most notable melting is limited to the spoil directly in contact with the cutting face of the drill bit.

**Figure 115: Production of muddy spoil during the drilling process at ambient pressure conditions. The slushy, muddy spoil was noted to completely clog the auger suggesting that the drilling process had transitioned to a form of melt-led penetration.**

**Figure 116: Borehole comparison following cryogenic drilling runs at ambient atmospheric pressure (top) and in-vacuum at pressures of ~1 mBar (bottom). Note, while the structure of the borehole remained intact during the atmospheric pressure drill run, melting did affect the borehole wall to a high degree. In the vacuum chamber run the borehole structure remained intact and largely frozen as indicated by the frost layer present.**

### 5.12.6 Discussion

Over the course of the TVAC test campaign, the drilling system was tested in a number of different scenarios in order to characterise the capability of the system when operating both at reduced atmospheric pressures and in cryogenically frozen terrain. Overall, the drill performed favourably and was capable of making reasonable progress in all scenarios, though not with complete reliability.

While progress was typically modest through all cryogenically frozen terrain, this was to be expected based upon the strength of the simulant likely approaching 100 MPa [48]. The rates of progress noted were shown to significantly increase upon transitioning from spoil removal via augering to removal by sublimation gas blasting, correlating with a reduction in auger torque. This proved that there may be an advantage to pursuing drilling regimes which produce sufficient excess heat so as to promote sublimation or water-bound volatiles within the cuttings, though this may provide damaging to drilling objectives which seek to analyse the cutting produced. In fact, an appreciation of the processes which drive sublimation when drilling may allow the operator to develop strategies to minimise such losses where required.

Furthermore, it was proven that the system can be controlled both manually and autonomously through such terrain, though manual control typically suffers from reduced rates of progress. Perhaps one of the more interesting phenomena noted was the tendency of the drill to develop freeze-in faults during runs where the ambient pressure was less than that of the triple point of water. In such cases, it would be expected that the generation of liquid water would be impossible, but such faults were noted with surprising frequency, occurring 4 times (approximately one third of all runs). The chamber typically allowed for an achievable air pressure of between 1-3 mBar. While this is less than the approximately 6 mBar triple point, it is foreseeable that local increases in the temperatures downhole, coupled with the formation of vapour from sublimation and the ‘capping’ of the top of the borehole by the accumulation of spoil may allow liquid water formation within the cuttings by a locally increased pressure. While the experimental campaign exposed the possibility of such faults occurring, the exact parameters required for the occurrence of these faults was not fully identified, thus further work in this area is required. These findings may prove pertinent when considered within the framework of future hardware development and testing campaigns for lunar exploration. While the prevalence of ‘low-vac’ vacuum chambers means that such facilities may be considered for the purpose of testing lunar hardware, conducting experimental campaigns in these conditions may be viewed as an over test in scenarios which involve penetrating volatile-bound terrain. In the context of icy moon exploration, the design of heat probes, envisaged as a key solution to deep subsurface

penetration, will rely on the characterisation of borehole closure in order to promote melting in place of the more power intensive sublimation of ice. Thus, a balance must be struck between power reduction and the prevention of freeze in faults.

Drilling runs at ambient atmospheric pressures proved that the drilling process may result in substantial melting within the spoil generated which may lead to the formation of mud-like material. This has clear implications for drilling scenarios on Mars where the local atmospheric conditions on the planet fluctuates around the triple point. Careful scheduling may prove essential in such cases in order to prevent unwanted melting of water bound within the terrain. Lessons were learned in the design of a TVAC experimental campaign, whereby unknown challenges and small failures can have a compounding effect on the number of experimental runs which can be achieved in a given timeframe. Future tests will seek to build in more time at the facility with the expectation that the experimental run rate may be as low as one test per day.

## 5.13 Chapter Conclusions

Presented with an opportunity to develop a novel subglacial bedrock sampling system which was to be compatible with the logistical constraints imposed upon the end user, the British Antarctic Survey, a solution is proposed adopts a planetary drilling methodology in order to reduce the resource footprint of the new system. Theoretically required to sample at depths of up to 600 beneath the West Antarctic Ice Sheet, the development harnessed breakthroughs made during the developmental phase of the UPCD system, proposing a breadboard system which was capable of achieving rates of progress in keeping with the timescales available during operational scenarios constrained by borehole refreeze. Furthermore, the proposed system was proven to operate with power and weight on bit levels which were well within predetermined bounds.

A trade-off study was initiated which resulted in the selection of a rotary-percussive drilling system based around a spring-cam actuated hammering mechanism, and a prototype system was developed and tested in the laboratory, a cold chamber facility and within a thermal-vacuum chamber in order establish the capability of the system in both terrestrial polar and planetary applications. Testing with the laboratory and cold chamber focussed on multi-parameter studies focussed on the evaluation of the system when penetrating terrain targets including limestone and sandstone in order to examine the performance both the ability of the system to fracture and progress through both hard and strong abrasive terrain which would effectively test the capability of the percussive actuator, and through soft, weak material which tended to exceed the throughput capability of the spoil removal system. The system generally performed favourably across both mediums tested, with lessons learned which shall inform future iterations of the drill development.

Testing at the FH Aachen thermal-vacuum facility attempted to evaluate the capability of the system when penetrating water-laden regolith at atmospheric pressures emulating those which are present on Mars. The system prove capable of penetrating both cryogenic and freezer temperature permafrost simulant at ambient and Mars atmospheric pressures, and cases of volatile sublimation were recorded. Poor performance of the off-the-shelf auger motors was noted and instances of liquid water formation at air pressure levels which contravene this physical state (alluding to localised increases in atmospheric pressure downhole) were found and shall prove to be worthwhile lessons going forward.

# Chapter 6

# Percussive Rapid Access Isotope Drill (P-RAID)

## 6.1 Modification of the Subglacial Bedrock Sampler

Assured by the capability of the subglacial bedrock sampler following a series of trials in a multitude of terrain types and environments, it was decided that the system would be re-developed for full deployment in Antarctica. While the fundamentals of the existing prototype design would be retained, modifications to the form factor were required in order to accommodate the system within the borehole diameter as set by the RAID system. Perhaps the most challenging of all the modifications that were required was the need to ensure that the key elements of the existing design would fit within the strict 81 mm diameter constraint of the new design. In order to accomplish this, the aspect ratio of these components were modified such that the diameter of these key components was reduced. In order to do so, it was required that the components be lengthened axially, though the constraint in this direction was deemed to be loose. Furthermore, the new drill design would not be rig mounted and thus required to react all the torque generated at the bit-rock interface to prevent self-rotation of the complete drill assembly or damage to the linear actuator unit which deploys the drill bit once the complete system is at the bottom of the ice borehole. Furthermore, the electronics and control module was required to be accommodated within the drill itself in order to avoid loses and further complicate the umbilical connection of the RAID drill with the surface. Figure 117 details a CAD cutaway of the internals of the P-RAID sonde, highlighting the key areas of the development including the percussive assembly, torque motors used to drive the rotation of the drill bit and coring bit replete with a passive core breaking and catching solution. The sonde is the main element of the complete P-RAID architecture and translates axially within the outer casing of the assembly making use of a dual set of ball transfer unit (BTU) assemblies. These BTU assemblies, as detailed in Figure 118, allow the smooth running of the system as the drill progresses through the terrain while also providing a means of reacting drilling torques.

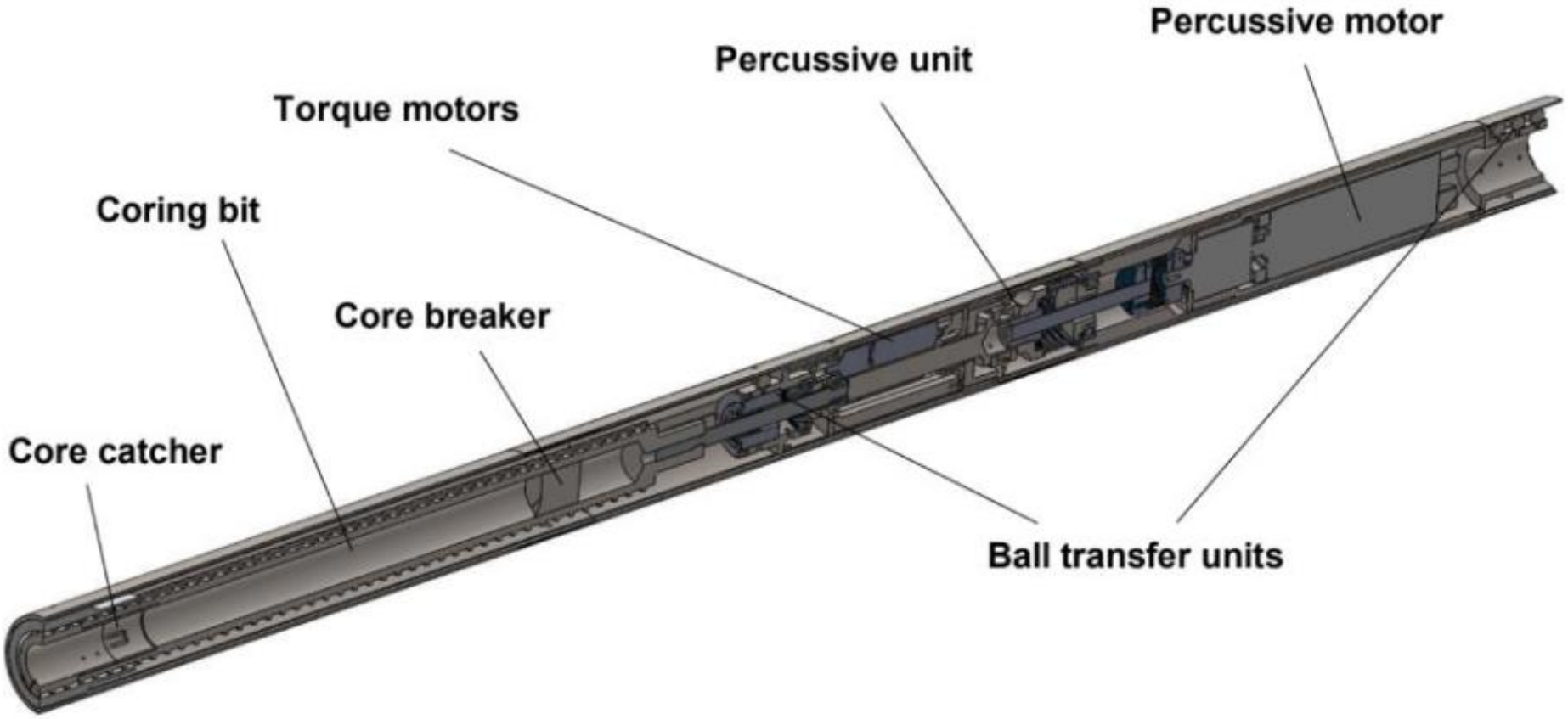


**Figure 117: P-RAID Design Cutaway. Length of assembly detailed is 3 m, outer diameter of 80 mm.**

**Figure 118: Ball Transfer Units (BTU) roller assembly. Note, the roller assembly forms part of a gearbox assembly for driving the drill bit using the splined spur gear at the top of the assembly.**

The sonde with the drill bit connected is shown adjacent to the outer casing in Figure 119, while Figure 120 presents a schematic of the P-RAID system in both the 'bit stowed' and 'bit fully deployed' configuration. In order to progress through the terrain, an off-the-shelf linear actuator is used to advance the complete sonde component of the drill assembly towards the terrain. Upon reaching the desired depth within the bedrock, drilling is halted and the complete drill assembly is winched to the surface for sample extraction.

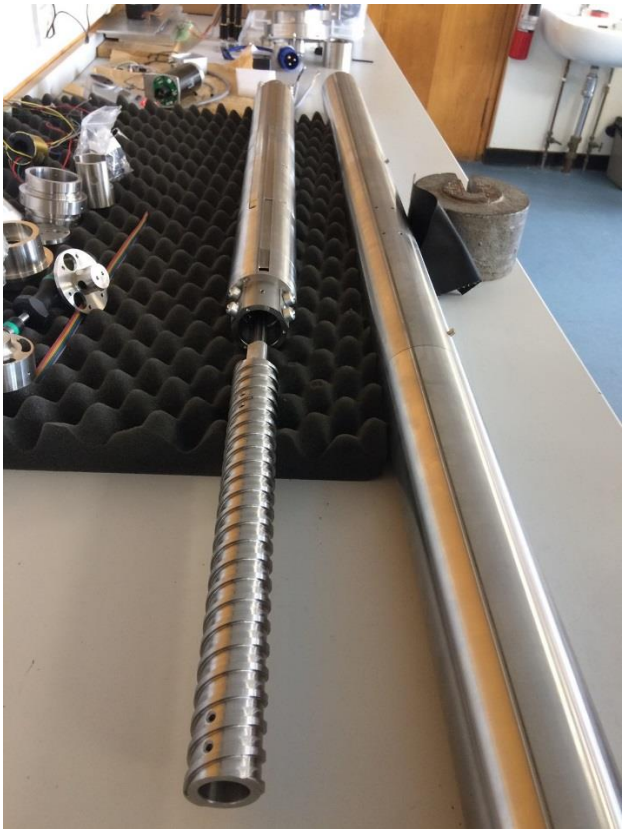

**Figure 119: Sonde with drill bit shown adjacent to the outer casing assembly.**

**Figure 120: P-RAID system with drill bit stowed (L) and deployed (R) from within the outer casing of the assembly. Length of assembly 4 m, outer diameter of 80 mm.**

By taking advantage of the fact that the axial (height) constraint imposed upon the development of P-RAID was loose, the resulting drill development was successfully integrated within the diameter constraint of 81 mm with the drill length expanded to approximately 5 m.

The formation of rock cores by percussive drilling is a delicate task due to the high vibration environment which is generated downhole by the hammering action. However, the task of detaching these rock cores from the base of the borehole and retaining them within the drill bit for later analysis is particularly challenging. In order to accomplish this, a two-part solution was devised which made use of a core breaking wedge and a core catching device. The core breaking wedge was located at the top of the drill bit and acted to provide a lateral force on the uppermost part of the rock core. In turn, the lateral force acts to generate a stress at the base of the core, snapping it free of the terrain. In order to prevent the core from simply remaining within the borehole during the retraction of the drill upon the cessation of drilling operations, a core catching device was fitted at the lowermost point of the drill bit, as detailed in Figure 99. This device consisted of a tubular section of stainless steel with three flexural ‘fingers’ milled from the walls. These fingers were then deformed inwards so as to grip the rock core as it passed within the internal aperture of the device.

**Figure 121: Core catching device installation. Diameter of catcher 20 mm, length 25 mm.**

Perhaps one of the most challenging elements of the design was ensuring that the core catcher devices were decoupled from the rotation of the drill bit. This was deemed essential as any rotary coupling of these parts would induce substantial torque loads on the drill bit and likely damage the integrity of the core sample contained within. While the use of generous slide fits between the internal cavity of the drill bit and the core catching device helped in this matter, experimentation found that this alone was insufficient for decoupling the parts. It was noted that upon drilling, the dusty spoil generated in the breaking of the formation would transfer from the internal cavity of the core catcher via the horseshoe milled sections in the walls of the device and accumulate between the device and the internal bore of the drill bit. This tended to clog this volume and in turn coupled the drill bit to the device. At this point, the torque required to rotate the bit rose substantially and generally stalled the drilling system. In order to solve this problem, it was decided that a solution would be found in preventing the dusty spoil from transiting through the milled section. To this end, a barrier was added to the device in the way of a coating of Kapton tape around the circumference of the bit. Kapton was selected due to its low friction qualities and the fact that it could be easily replaced between runs without any adhesive remnants being left on the core catcher part. While this was proven to be a reliable solution to the problem, wear of the Kapton layer was noted after multiple drilling runs. While this is not an issue for the drilling application in question, a more permanent solution may involve the use of a low friction plastic sleeve (or similar) fastened to the core catcher, or a rework of the design of the part such that there is no through access from the internal bore of the part to the external seating bore. The combination of the core breaker and catcher device proved successful in capturing core samples as noted in Figure 122.

In order to ensure that the internal breaking and catching components of the system were retained within the bore of the drill bit bore, a feature known as the ‘crown’ was added to the design. This part had a dual role within the design, tasked with both retaining the internal features and core sample and also acting as an extension of the drill bit. In order to ensure that the drilling crown would not prevent the smooth transit of spoil over the length of the bit, it was essential that the auger scroll of the crown acted as a continuation of the scroll of the drill bit. Ensuring the alignment of the parts upon connection was therefore a manufacturing priority. Any mismatch in the alignment between the two parts would result in the disruption of the spoil removal process, thus a tolerance of one degree was imposed upon assembly. It was found that this could be achieved with careful manufacturing. Figure 123 details the design of the crown and drill bit. As the tungsten carbide drilling teeth are bonded to the crown and not the drill bit, the task of changing used teeth during laboratory

experimentation, for example, is easily accommodated by the use of multiple crowns. In the context of field trials, this reduces the dependence upon the oxy-acetylene torches used to solder the teeth in place. As these torches may be considered hazardous cargo, this is of no doubt a logistical benefit to field operations.

**Figure 122: Limestone borehole following a successful drill run (top). The core generated during drilling was captured within the drill bit (bottom).**

**Figure 123: Toothed drill crown next to the drill bit. Crown interfaces with the drill bit as a continuation of the auger scroll in order to allow a seamless transit of spoil. Bit diameter of 40 mm, length of bit 450 mm.**

## 6.2 Skytrain Ice Rise Campaign – January 2019

Having reached a state of readiness through the completion of a laboratory drilling campaign, an opportunity arose to perform a series of initial shakedown tests of the P-RAID system in Antarctica with the British Antarctic Survey. By taking advantage of a pre-existing drilling campaign which was set to reach bedrock at a depth of approximately 640 m beneath the glacier at the Skytrain Ice Rise (79.4°S, 78.3°W), the need to make use of the RAID drill, which was undergoing essential maintenance and thus was not planned to operate in the field, was negated. Furthermore, the financial and logistical costs associated with the deployment of the relatively immature P-RAID technology was minimal and thus the result of a cost/benefit analysis of the opportunity suggested that this opportunity may be worthwhile.

As the ice drill used to access the bedrock on this occasion was planned to be the Medium-depth Ice Core Drill and not the RAID system which the P-RAID had been designed to complement, alterations to the foreseen deployment protocol were required. Perhaps the most pertinent issue that was required to be addressed was the difference in borehole diameters between the drill types. The Ice Core Drill which was to be deployed generated a borehole diameter of approximately 120 mm, thus substantially wider than the ~80 mm diameter RAID borehole. While this increased borehole diameter meant that the drill would be less restricted upon deployment, a diameter expansion part would be required in order to accurately align the drill system with the borehole in question. Fortunately, this piece was easily manufactured using Delrin in order to minimise friction and the risk of freeze-in. Drilling operations would be further complicated by the fact that the ice core drilling system used was dependent upon the use of drilling fluids in order to prevent the icy borehole from refreezing at depths below approximately 400 m. As part of the environmental protection protocols which must be adhered to when operating in Antarctica, the stack of drilling fluid which would be generated in the drilling process was required to be removed following the completion of core extraction. As the P-RAID system was designed to operate in a dry borehole and therefore was not designed to be watertight, the removal of the drilling fluid was deemed to be essential in order for the system to operate as required. While the bulk of the fluid could be removed (based upon past experiences on previous drilling campaigns), it was thought that the final 0.5 m at the base of the hole would prove to be more difficult due to the design of the bailing hardware used. As the rock coring drill bit measured approximately 400 mm, there was a concern that the presence of even a relatively small volume of drilling fluid may affect drilling through the attenuation of percussion or increased frictional drag on the drill bit. This was a risk that was accepted in order to proceed with the opportunity which was presented. Figure 124 presents the P-RAID drilling system as

mounted to the winch system at the field site. This was an important first step in ensuring that the system was compatible with the anti-torque upper stage of the drill and the winch hardware. Note, the drill system is in the 'bit deployed' configuration. Upon initial deployment in the hole the bit would be stored within the outer casing. The Delrin alignment ring can also be seen.

**Figure 124: P-RAID system during fit checks at Skytrain Ice Rise. Note, the drill bit is fully deployed. Total assembled length of 5 m.**

While the integration and fit checks with the rig infrastructure were accomplished successfully, issues arose upon the commencement of drill system functional tests. Having previously assembled elements of the drilling system at Rothera base, Antarctica, only a few days prior to field deployment (to ensure that all the systems checked out following a month of transit from the UK), it was expected that a repeat of these checks at the field location would be a formality. In fact, upon testing the drill bit rotation motors, unusual behaviour was noted. When attempting to raise the rotary speed of the motors to that which would be used during rock drilling, it was noted that a fault had developed which prevented all three of the motors tested from reaching the necessary speed. This fault was entirely unexpected and is as yet not fully understood. While the Antarctic environment is cold and dry, the temperature limit of operation were not exceeded during these tests at any time. Furthermore, no further progress was made upon substantially raising the temperature of the motors using heaters. While the dry environment could foreseeably degrade the greases which are used within the motor and gearbox, identical motors were proven to operate for extended durations in a low vacuum environment during testing at Aachen, so it is unlikely that this was the root cause of the problem. It is postulated that the gearbox assembly may have witnessed a shock load at some point during transit to the field site, but this can only be identified through investigative dissection of the motors.

While the underperformance of the drill gearbox was a major cause for concern at the field site, the campaign was hindered further by electromechanical failures of the winch system. While the campaign was successful in its attempt to reach bedrock, the winch system used to lower and raise the drill developed an intermittent failure soon afterwards. As previously alluded, removal of all drilling fluids from the borehole was imperative for reasons of environmental sensitivity and also to allow the P-RAID system to access the bedrock. Unfortunately, efforts to bail the drilling fluid from the hole were abandoned at a depth of 450 m, leaving over 150 m of fluid remaining within the borehole. Disappointingly, this prevented the P-RAID system from being deployed on this occasion. The test campaign was not without some success though given that the drill was shown to integrate well with the winching system used and a potential problem affecting future field campaign (in the failure of the auger motors) was identified. This problem shall be rectified before future deployments.

## 6.3 Chapter Conclusions

Confidence generated during the development and testing of the subglacial bedrock sampler allowed the translation of that device in to a field deployable model. Careful repackaging of the prototype system allowed compatibility with the ice borehole generated by the RAID, ensuring future compatibility with field campaigns featuring the heritage system. An emphasis was placed on the task of core breaking and catching given that this was deemed to be an area with which reliability was not always assured and a solution was developed which conferred promising results during initial laboratory testing. This solution required the implementation of 'drilling crowns', an extension of the front end of the drill bit which could be easily removed, re-toothed and refitted as needed. The crown also axially constrained the core catcher mechanism upon installation and allowed for the captured core samples to be removed with ease when required. The P-RAID project took advantage of an opportunity to perform initial testing of the system at Skytrain Ice Rise, Antarctica during the summer season 2018-19, though this was not without problems. While various modifications to the design were required in order to ensure that the system was compatible with the increased diameter ice borehole created by the primary ice coring system used, the campaign faced numerous challenges from the outset. Perhaps that most detrimental to the drilling objectives set was the development of an intermittent failure of the primary generator used to drive the winch. This prevented the clearance of cutting fluid from the ice borehole, thus preventing dry access to the bedrock which was essential for the operation of P-RAID. Furthermore, the unexpected and abrupt failure of the motor units used to drive the rotary gearbox of the drill prevented the system from operating at an optimal rotary speed, limiting the effectiveness of any deployment had the situation allowed. Notwithstanding, the campaign provided the team with a deep insight in to challenges associated with subglacial drilling beneath Antarctica. Fit and integration checks were also successfully carried out and a number of 'unknown-unknowns' were learned which would not have been identified in the laboratory environment.

# Chapter 7

# Conclusions and Future Work

## 7.1 Summary of Drilling System Applications

Two different rotary-percussive drilling systems have been developed and tested in both the laboratory and in the field in analogous conditions. While both systems offer promising performance characteristics for the resource required, it is clear that each system has an application niche where the design of the system is most suited.

As detailed in Section 4.12, the ultrasonic-percussive drilling system is exceptionally well adapted to applications which are limited by the power, energy and weight on bit available. Furthermore, the mass of the drilling system is exceptionally lean, and the low impulse generated by the percussive mechanism corresponds to a low recoil force, minimising reaction forces required. While modest percussive energies are suitable for applications where the target terrain is not heavily consolidated or stronger than 50 MPa, applications of the system are limited to areas without igneous/metamorphic or cryogenically frozen ice-cemented terrain. Furthermore, the propensity of the system to exhibit stalling of the percussive actuator means that particular care should be taken when applying the drilling architecture to remote drilling scenarios which rely upon high levels of autonomy. Thus, such systems are perhaps most suited to dry lunar applications or, if the stalling exhibited by the device can be minimised, equatorial regions on Mars which are devoid of icy terrain.

Drilling systems making use of a spring-cam mechanism offer more flexibility than ultrasonically-driven systems for a variety of reasons. The percussive energy and power available for terrain penetration are factors of the design of the cam profile and the motor used to actuate the mechanism, thus a system which is suited to multiple terrain types can be designed. The percussive mechanism is shown to exhibit a high degree of reliability, with negligible wear or fatigue noted following extensive test campaigns. While the percussive rate is typically lower than ultrasonic systems, testing has shown that harder terrain is more effectively penetrated with high energy, low power applications, though the vibration environment generated on the auger from an increase hammering rate may reduce the power

required to convey drilled cuttings. The generation of cam-driven percussion is typically less efficient that the ultrasonic-percussive technique, but an increased rate of progress demonstrated by these systems may result in more efficient drilling operations despite higher power consumption. While a system can be designed which is capable of penetrating soft, medium and hard terrain, fixed cam geometries (in planetary applications) means that high percussive energies may result in excessive rates of progress when drilling soft terrain, resulting in an excessive auger throughput and subsequent failures related to choking. Such issues may be mitigated through the use of a holistic control algorithm, ensuring that the cam geometry can be optimised for harder terrain if uncertainty exists with regard the composition of the material to be penetrated.

## 7.2 Chapter Overview

**Chapter 2**

The exploration of the Solar System has achieved many paradigm-shifting findings, but the majority of these have been through remote sensing instrument packages mounted upon robotic orbiters and fly-by missions. Technological advancements have enabled the implementation of surface missions in the form of landers and rover, alongside landed human missions to the Moon, to further explore in-situ. Efforts by the Apollo astronauts in sampling lunar regolith with handheld drilling hardware is detailed alongside the Rock Abrasion Tool (RAT) mounted upon the Mars Exploration Rovers, *Spirit* and *Opportunity*. An overview of the achievements of the ambitious Phoenix mission to the northern regions of Mars are provided, highlighting prevalence of ice in the near subsurface. An overview of the Mars Science Laboratory drilling system is provided, highlighting the capability of the voice coil driven percussive actuator and the issues encountered and overcome throughout the duration of the mission. A brief overview of SD2, a rotary drilling system mounted to the ill-fated Philae lander element of the ESA Rosetta mission, is provided, with the development linked to that of the ExoMars 2020 multi-metre class rotary drilling system. The NASA ‘Mars 2020’ mission, featuring a core drilling system designed to extract near-subsurface samples is evaluated alongside European/Russian plans to sample volatile-laden terrain from the Permanently Shadowed Regions of the lunar South Pole-Aitken Basin.

An overview of the technologies designed to sample at the ice-bedrock interface within Earth’s Polar Regions is provided, identifying the driving constraints of existing hardware.

**Chapter 3**

A deep analysis of the theoretical aspects governing the planetary drilling process, including the challenges faced by robotic missions performing complex robotic manipulations related to light speed delays, uncertain terrain (and related 'unknown unknowns'), standard faults which may be encountered during drilling, and issues relating to the low resource nature of robotic spaceflight. An introduction to both rotary and rotary percussive drilling is made with the challenging aspects of both exposed. In particular, rotary drilling was shown to suffer from a dependency upon gravity to provide the necessary weight on bit required to drill. It is this dependency which makes the use of rotary drilling alone more suited to penetrating soft terrain in a planetary setting. Furthermore, the misinterpretation of teeth blunting during the drilling process and subsequent misidentification of the fault state as another fault type may act to hinder the autonomous control of the system. The rotary-percussive technique does not rely upon weight on bit alone to penetrate the terrain. Instead, such systems make use of a hammering action in order to overstress the terrain through the transmission of a compressive wave through chisel-like drilling teeth. Percussive drilling techniques were shown to better suit the penetration of hard materials due to the elastic properties of soft terrain. The power levels required to penetrate terrain were explored, and a useful metric known as the system specific energy was introduced in order to establish the performance of dissimilar drilling systems through the removal of a dependence upon drill bit geometry from the analysis. Finally, spoil removal techniques including dry augering of cuttings and gas blasting were explored. Augering was shown to be an effective means of removing dry cuttings in most cases, but suffers from a dependency upon foreknowledge of the frictional coefficients of the terrain in order to optimise the system. The importance of identifying the optimal auger speed for a given terrain was emphasised as a means of reducing the power consumption of the spoil removal process. Gas blasting was detailed as an alternative to classic augering and may be enabled by residual pressurised ullage gas carried upon landed spacecraft, through compression of planetary atmospheres (on Mars or Titan, for example).

**Chapter 4**

The successful development of the UPCD, a drilling system based upon the ultrasonic-percussive drilling technique, is detailed. Challenges overcome in the development of each element of the hardware are detailed. The development of a robust solution to the challenge of autonomous assembling drill string, making use of a novel concept of operations

combined with a mating interface similar to that of the bayonet fitting, is described, and the successful deployment of this concept in the Antarctic icepack detailed. Results obtained from a series of laboratory tests in order to mitigate against an uncertainty relating to percussive attenuation across the novel bayonet-like interface are provided. The UPCD system was shown to operate effectively in the laboratory setting, achieving rates of progress on the order of up to 0.06 mm/s using a total average power of 30.5 W. This corresponds to a specific energy of 1837 $MJ/m^3$ in Locharbriggs sandstone. It is noted that, while the efficiency of the system makes it desirable in certain mission scenarios, the low percussive energy of the system means that it may be less desirable when attempting to penetrate harder terrain, as concluded in Chapter 5. An overview of the successful implementation of an autonomous control system governing drilling progress is provided, and an advanced control system which makes use of a set of sensors at the drill bit tip in order to evaluate the thermal state of drilled cuttings is described. Results of the successful testing of this thermal control system are also detailed.

**Chapter 5**

The technical challenges facing the development and deployment of a subglacial bedrock sampler are laid out. The limitations imposed by operation in the remote Polar Regions are described and the influence upon the design process is described. The design methodology undertaken is explored with an overview provided of the trade-off studies performed when evaluating the architectures most suited to the task of extracting deep bedrock samples. It was concluded that a rotary-percussive drilling system would be used, making use of the spring-cam percussive actuator. The design of an optimised percussive actuator is carefully detailed, with steps taken to minimise the power consumed by the system while maximising the percussive capability deliverable. A novel solution to the problem of delivering sufficient drilling torque within a tightly constrained borehole diameter is proposed via the multi-motor gearbox. Finally, the results obtained during a robust multi-parameter experimental campaign are detailed. The drilling system was shown to operate optimally when fitted with a high percussive energy cam geometry, with the data suggesting that percussive power generated with an emphasis on the energy delivered per strike was most effective when penetrating both limestone and sandstone samples. Conclusions were drawn on the production of pristine core samples through the use of drilling routines which minimise vibration and radial disruption downhole. Finally, the drill was tested at the FH Aachen thermal-vacuum facility in order to emulate Mars atmospheric conditions. The primary objective of this test campaign was to evaluate the use of the system as a pure planetary drill.

This was deemed to be appropriate given the planetary heritage of the design implemented. While the drilling system suffered from excessive auger power as a result of auger motors not designed for use in a vacuum environment, the system was shown to be capable of penetrating cryogenically frozen, water saturated regolith with modest percussive power levels. In penetrating the terrain, excessive heating at the bit-terrain interface resulted in the direct sublimation of bound water ice. The result vapour stream act to blast spoil clear of the borehole. In doing so, the auger power demand was reduced as the gas blasting minimised the workload. While this has clear benefits to the overall system power consumption, care must be taken to minimise such events if the drilled cuttings are to be sampled. Sublimation leaves the spoil desiccated as the water within the spoil is converted to vapour, thus this may interfere with the scientific output. Perhaps the most interesting findings were noted when drilling at atmospheric pressures marginally lower than the triple point pressure of water. While drilling in such an environment should prevent the formation of liquid water, incidences of liquid formation downhole and the subsequent encountering of refreeze faults proved to be a worrisome result. It is thought that this may be a result of a local increase in the borehole pressure caused by the presence of gas vapour, thus drilling at or around these pressure levels should be approached with caution. This result further emphasises the importance of the implementation of a thermal control system, as detailed in Chapter 4.

**Chapter 6**

The design of an industrialised version of the subglacial bedrock sampler, the Percussive Rapid Access Isotope Drill (P-RAID) is detailed. The constraints placed upon the development as a result of a need to design to a pre-existing borehole diameter are noted and steps were taken to reduce the impact of this on the development. The design of the system is described with key areas, such as the BTU roller assembly, introduced. Breakthroughs in the implementation of a reliable core catching mechanism are discussed. The lessons learned from an initial shakedown campaign at Skytrain Ice Rise, Antarctica, are highlighted with the key issues encountered during this campaign detailed.

## 7.3 Future Work

In the completion of this Ph.D. thesis, three individual drilling systems were conceived, developed and tested in the laboratory and at field sites in Antarctica. While the development of these systems has resulted in a step forward in the existing state of the art in planetary drilling and subglacial bedrock sampling technologies, work remains in order to utilise the key elements of these technologies for deployment at the respective target locations.

While the autonomous control systems developed for controlling the advance of both ultrasonic-percussive and spring-cam driven rotary-percussive systems are promising, further emphasis must be placed upon increasing the robustness and fault tolerance of these systems. The ability to integrate the control of the auger motors into the overall control logic is perhaps the most pertinent step forward. While the inclusion of a triple motor gearbox ensures that no one motor should be forced to operate at the upper bound of acceptable continuous operations, an autonomous means of controlling this would prove beneficial. Testing both in the field and the laboratory indicated the need for thermal control in order to mitigate against the heating of the terrain, and subsequent melting of volatiles within. While a solution to this problem has been developed for core drilling applications, developments are needed to make this architecture more robust to a variety of terrain types and to the failure of the delicate thermal sensors used. An extended, multi-parameter lifecycle test of the ultrasonic-percussive drilling technique would also further establish the bounds and capability of this system.

As noted in Chapter 6, the P-RAID system, while highly promising as a technology offering, faced a number of teething issues during its first field trials. Further maturation of the technology will only bolster the offering and its usability by the scientific community. A clearer of the failure of the auger motors will assist in the decision making process going forward, ensuring that the problem does not recur.

It is clear that the developments made and lessons learned with regard to autonomous control for extreme environment drilling may have immediate applications in terrestrial, industrial-scale drilling operations. As energy prospecting seeks to place drilling assets in more extreme environments less suited to human in the loop operations, fault tolerant control, with latency on the order of 1 second or less, may have immediate applications. Thus, it is clear that further developments in the field should be made, perhaps with the direct involvement of industrial partners in order to catalyse this interesting and worthwhile area.

## 7.4 Publications

### 7.4.1 Book Sections

- Firstbrook, D. G. , Harkness, P., Li, X., **Timoney, R**. and Worrall, K. (2018). Ultrasonically-assisted penetration of granular and cemented materials. In: Badescu, V. and Zacny, K. (eds.) *Outer Solar System: Prospective Energy and Material Resources.* Springer International Publishing, pp. 261-268. ISBN 9783319738444 (doi:10.1007/978-3-319-73845-1).

- **Timoney, R**., Worrall, K., Harkness, P., Rix, J., and Mulvaney, R. (2019). Extraterrestrial Drilling. In: Bar-Cohen, Y. and Zacny, K. (eds.) Advances in Terrestrial and Extraterrestrial Drilling: Ground, Ice, and Underwater. CRC Press/Taylor & Francis Group LLC. (In-Print)

### 7.4.2 Articles

- Li, X., Harkness, P., Worrall, K., **Timoney, R.** and Lucas, M. (2017). A parametric study for the design of an optimized ultrasonic-percussive planetary drill tool. IEEE Transactions on Ultrasonics, Ferroelectrics, and Frequency Control, 64(3), pp. 577-589.(doi:10.1109/TUFFC.2016.2633319) (PMID:27913339).

- Firstbrook, D., Worrall, K., **Timoney, R**., Suñol, F., Gao, Y. and Harkness, P. (2017). An experimental study of ultrasonic vibration and the penetration of granular material. Proceedings of the Royal Society of London Series A: Mathematical, Physical and Engineering Sciences, 473(2198), 20160673. (doi:10.1098/rspa.2016.0673).

- **Timoney, R**., Worrall, K., Firstbrook, D., Harkness, P., Rix, J. et al. (2018). The Development of a Low Resource Subglacial Bedrock Sampler Inspired by Planetary Drilling Technologies: The Percussive Rapid Access Isotope Drill (P-RAID) **(Accepted by Cold Regions Science and Technology).**

- **Timoney, R**., Worrall, K., Li, X., Firstbrook, D., and Harkness, P. (2019). Development of a Robust Mating System for Use in the Autonomous Assembly of Planetary Drill Strings **(Accepted by ASCE Aerospace).**

Note:

Articles on the following topics are currently in-writing and are to be submitted for publication in 2019.

- Ultrasonic Planetary Core Drill (UPCD) Overview
- Drilling Performance of the Percussive Rapid Access Isotope Drill (P-RAID)

### 7.4.3 Conference or Workshop Proceedings

- **Timoney, R**., Harkness, P., Worrall, K., Li, X., Bolhovitins, A. and Lucas, M. (2015). European Ultrasonic Planetary Core Drill. In: 12th International Planetary Probe Workshop, Cologne, Germany, 15-19 June 2015.

- Firstbrook, D. G., Doherty, P., **Timoney, R.**, Harkness, P. and Suñol, F. (2015). Preparations for Variable-Gravity Regolith Penetration with an Ultrasonically-Active Probe. In: 12th International Planetary Probe Workshop, Cologne, Germany, 15-19 June 2015.

- **Timoney, R.,** Harkness, P., Worrall, K., Li, X., Bolhovitins, A., Cheney, A., and Lucas, M. (2015). The Development of the European Ultrasonic Planetary Core Drill (UPCD). In: AIAA Space 2015 Conference, Pasadena, CA, USA, 31 Aug - 2 Sept 2015, ISBN 9781624103346

- Li, X., Worrall, K., Harkness, P., **Timoney, R**., Bolhovitins, A. and Lucas, M. (2015). A Motion Control System Design for an Ultrasonic Planetary Core Drill (UPCD) Unit. In: AIAA Space 2015 Conference, Pasadena, CA, USA, 31 Aug - 2 Sept 2015, ISBN 9781624103346

- **Timoney, R.**, Li, X., Worrall, K., Firstbrook, D. G., Harkness, P. and Lucas, M. (2017). Push-and-Twist Drillstring Assemblies. In: ASCE Earth and Space Conference, Orlando, FL, USA, 11-15 Apr 2016, ISBN 9780784479971

- Firstbrook, D., Worrall, K., Doherty, P., **Timoney, R**., Harkness, P. and Suñol, F. (2017). Ultrasonic Penetration of Granular Materials in Varying Gravity. In: ASCE Earth and Space Conference, Orlando, FL, USA, 11-15 Apr 2016, ISBN 9780784479971

- **Timoney, R.,** Worrall, K., Li, X., Firstbrook, D. G., Harkness, P. and Lucas, M. (2016). Preliminary Testing of the European Ultrasonic Planetary Core Drill (UPCD) in Simulated Permafrost Terrain. 13th International Planetary Probe Workshop, Maryland, USA, 13-17 Jun 2016.

- Worrall, K., **Timoney, R**., Harkness, P., Li, X. and Lucas, M. (2017). Ultrasonic Planetary Core Drill: Overview and Results from Field Trial. 14th Symposium on Advanced Space Technologies in Robotics and Automation, Leiden, Netherlands, 20-22 Jun 2017.

- **Timoney, R**., Worrall, L., Firstbrook, D. and Harkness, P. (2018). Development of a Heuristic Thermal Control System for the Ultrasonic Planetary Core Drill. In: ASCE Earth and Space 2018, Cleveland, OH, USA. 10-12$^{th}$ April 2018.

- **Timoney, R**., Worrall, K., Firstbrook, D., Harkness, P. and Rix, J. (2018). Mars Sample Return to Subglacial Polar Science on Earth. 15th International Planetary Probes Workshop, Boulder, Colorado, USA. 11-15th Jun 2018.

- **Timoney, R**., Worrall, K., Firstbrook, D., Harkness, P. and Rix, J. (2018). P-RAID: Deep Subglacial Bedrock Sampling. AGU Fall Meeting 2018. Washington DC, USA. December 2018.

- **Timoney, R.,** Worrall, K., Harkness, P., Rix, J., R. Mulvaney., and Bentley, M. (2019). Subglacial Drilling Technologies for Future Deep Mars Exploration. 9th International Conference on Mars, Pasadena, CA, USA. July 2019.

### 7.4.4 Press Publications

- Planets and Poles – The Geographer. June 2019

- Antarctic Drilling – The National. January 2019. https://www.thenational.scot/news/17334375.scots-team-to-use-mars-drill-on-antarctic-ice-to-probe-earths-climate/

- Antarctic Drilling – New Atlas. January 2019. https://newatlas.com/mars-drill-antarctica/57869/

# Appendix

## Subglacial Bedrock Sampler Test Campaign

## Portland Limestone Figures

**Test: Portland limestone experimental run using small drill bit, 2-drop cam and 1500 RPM hammer velocity. 12/8 N WoB.**

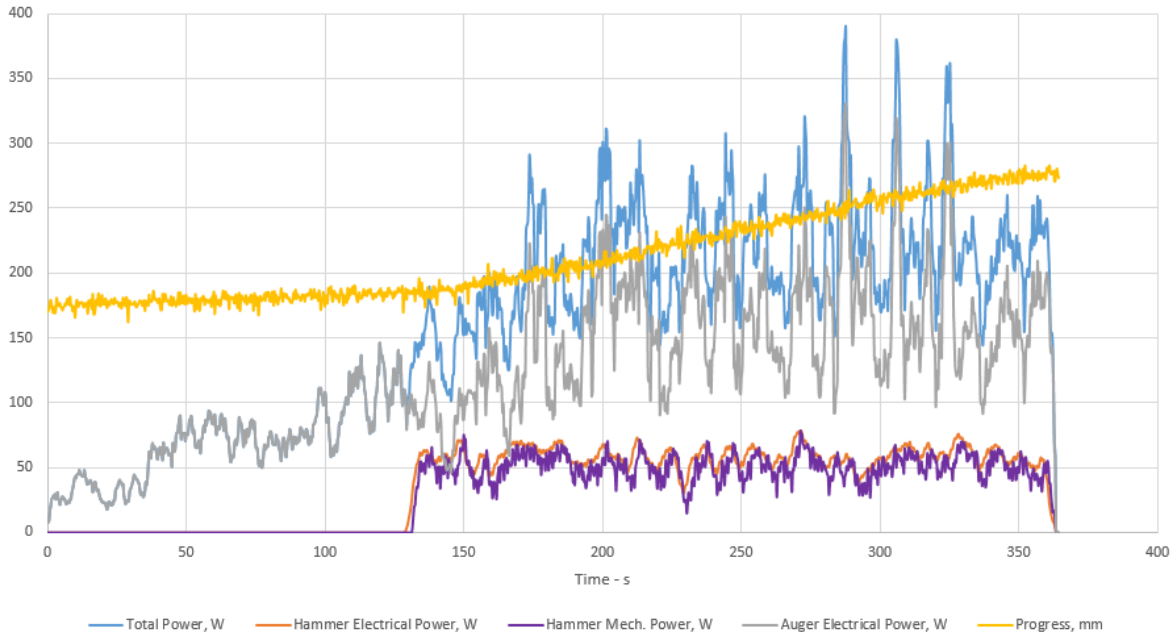

**Test: Portland limestone experimental run using small drill bit, 2-drop cam and 2500 RPM hammer velocity. 12/8 N WoB.**

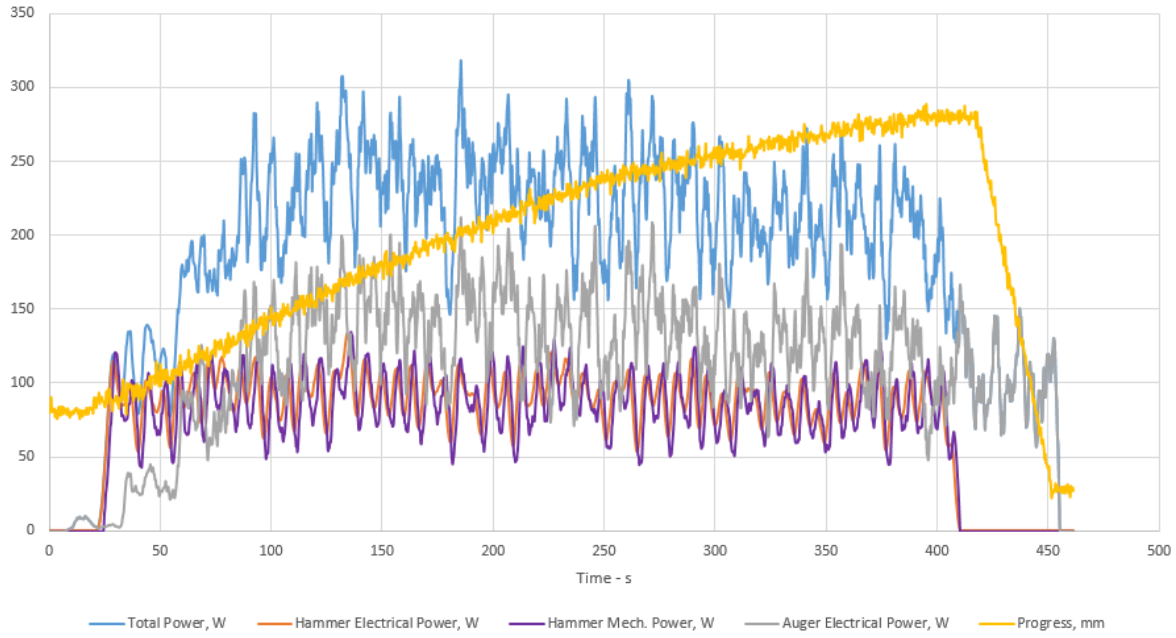


**Test: Portland limestone experimental run using small drill bit, 4-drop cam and 1500 RPM hammer velocity. 12/8 N WoB.**

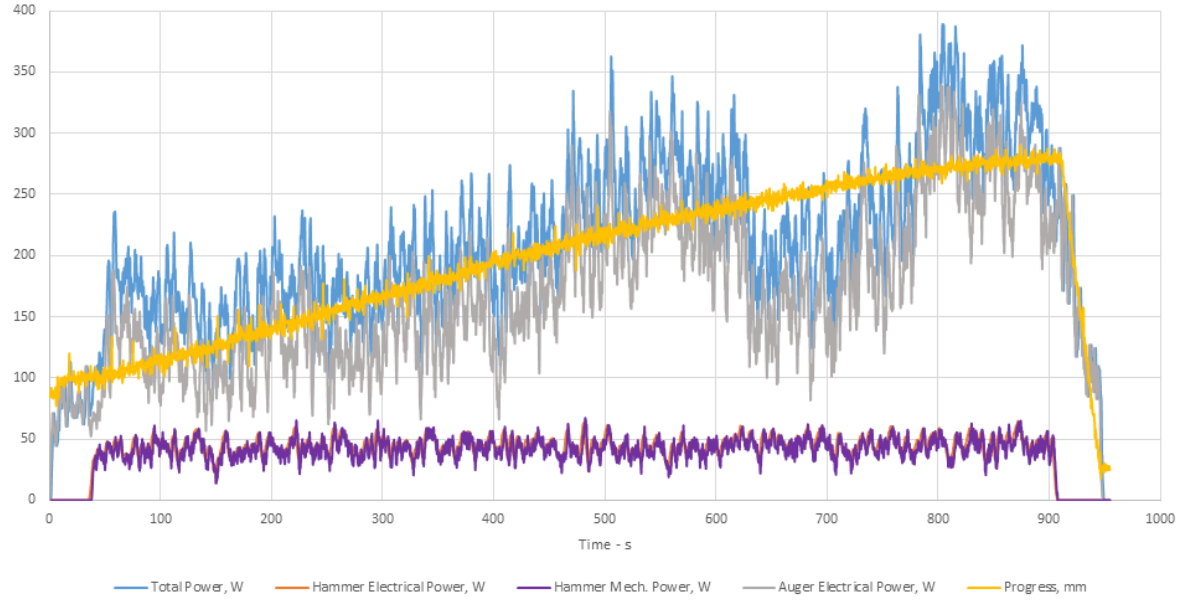

**Test: Portland limestone experimental run using small drill bit, 4-drop cam and 2500 RPM hammer velocity. 12/8 N WoB.**

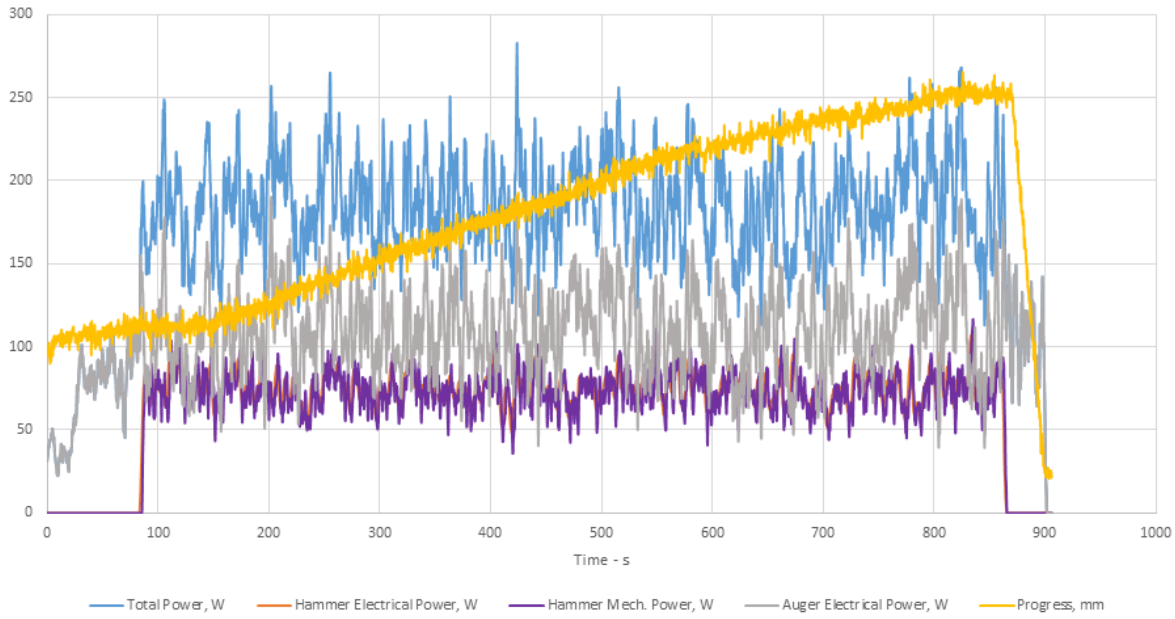


**Test: Portland limestone experimental run using small drill bit, 4-drop cam and 3500 RPM hammer velocity. 12/8 N WoB.**

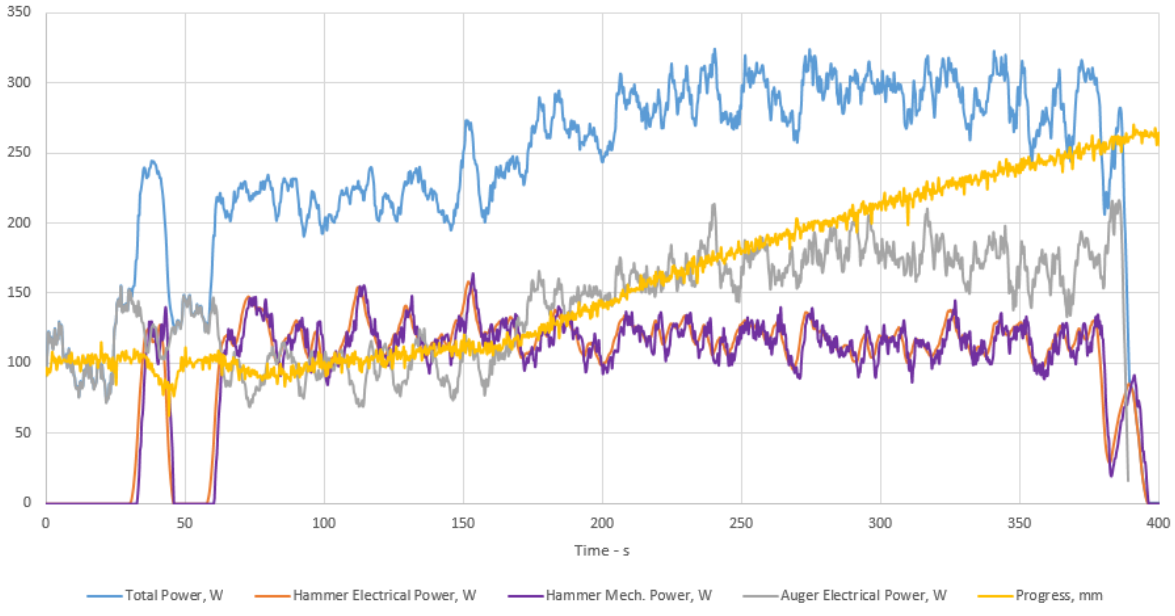

**Test: Portland limestone experimental run using medium drill bit, 4-drop cam and 1500 RPM hammer velocity. 12/8 N WoB.**

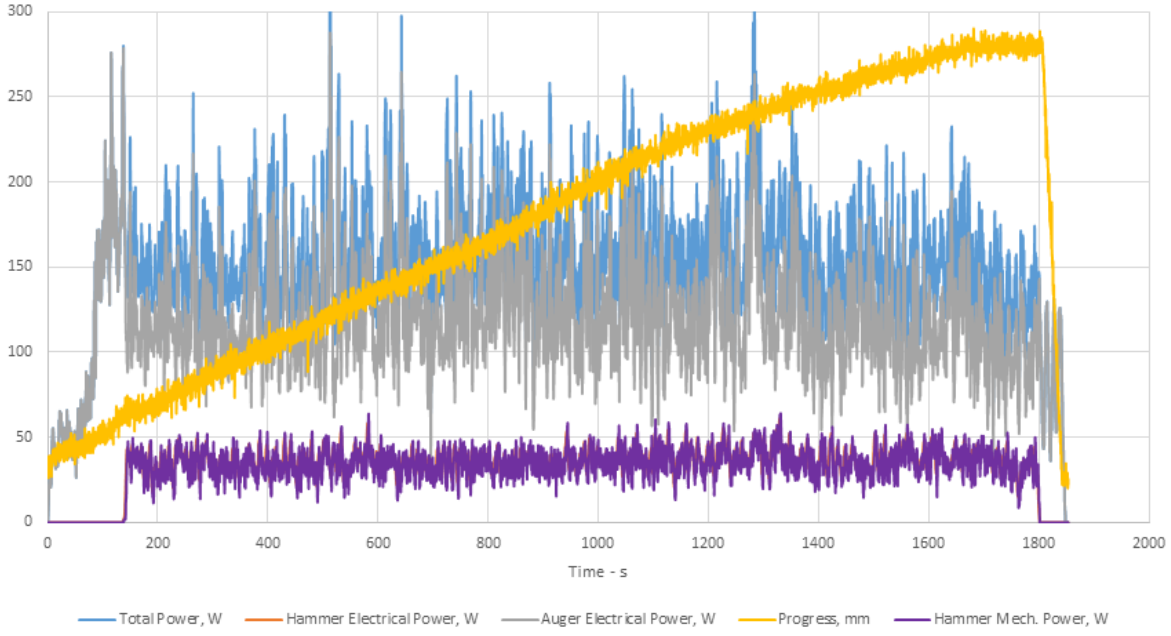


**Test: Portland limestone experimental run using medium drill bit, 4-drop cam and 2500 RPM hammer velocity. 12/8 N WoB.**

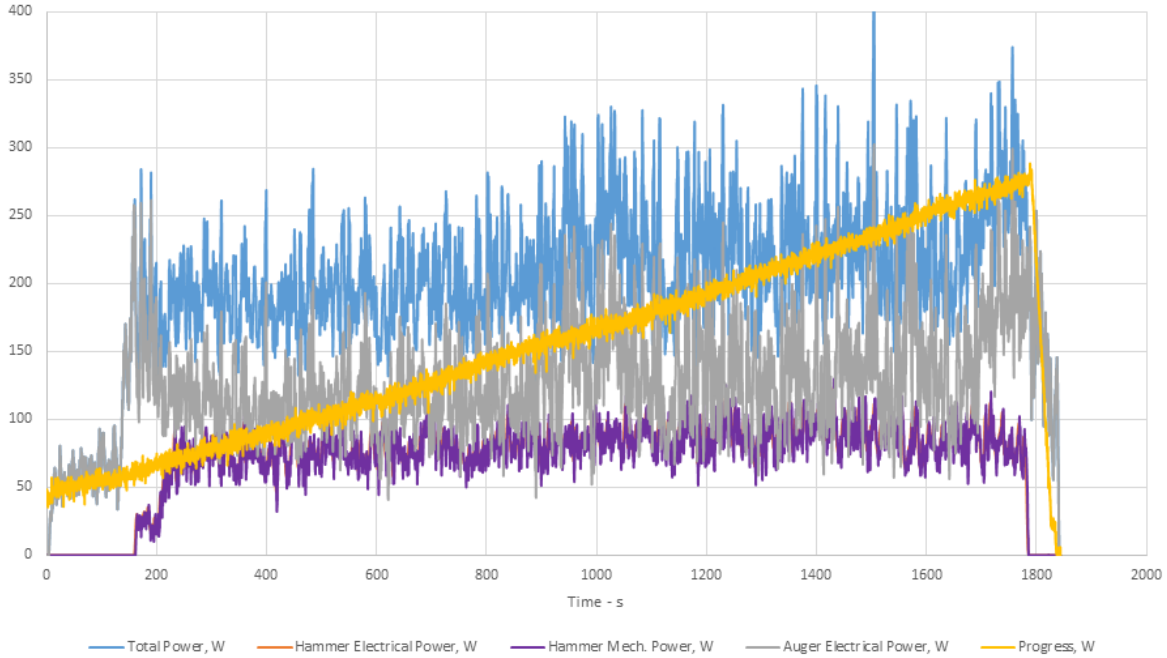

**Test: Portland limestone experimental run using small drill bit, 4-drop cam and 1500 RPM hammer velocity. 17/13 N WoB.**

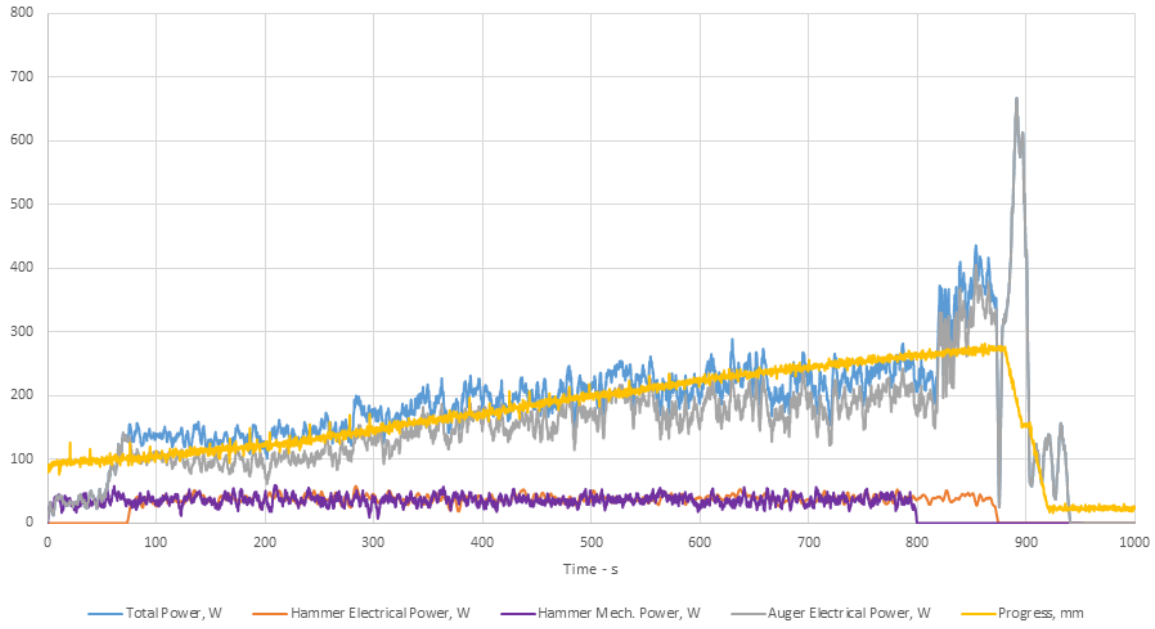


**Portland limestone experimental run using small drill bit, 4-drop cam and 2500 RPM hammer velocity. 17/13 N WoB.**

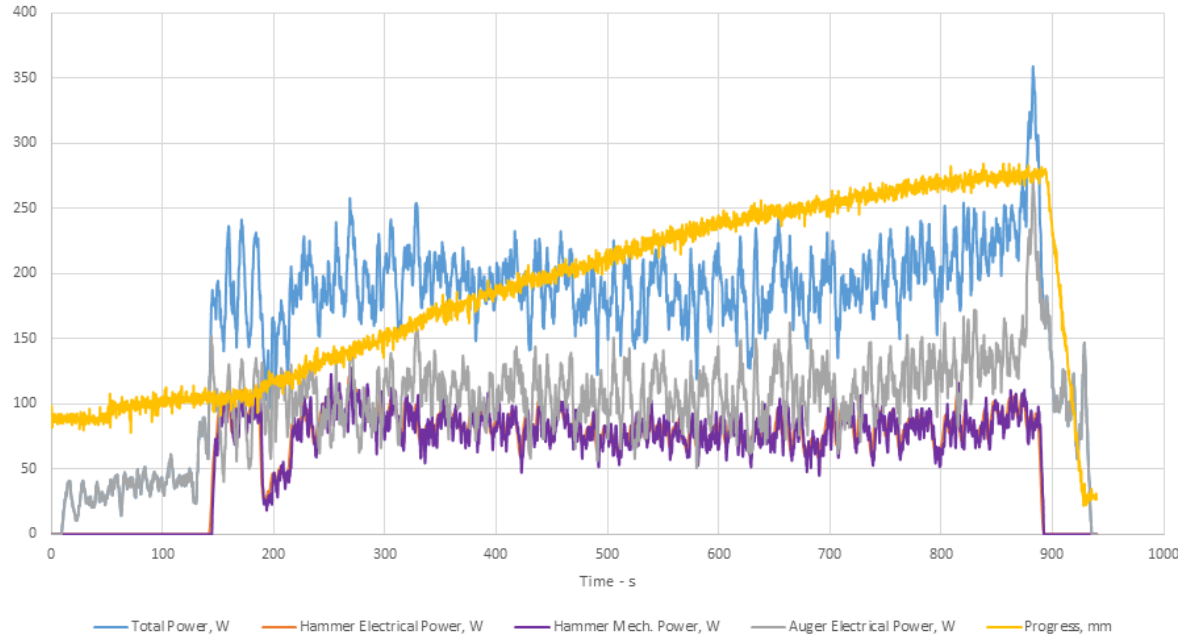

# Locharbriggs Sandstone Figures

**Test: Locharbriggs sandstone experimental run using small drill bit, 2-drop cam and 1500 RPM hammer velocity. 30/10 WoB.**

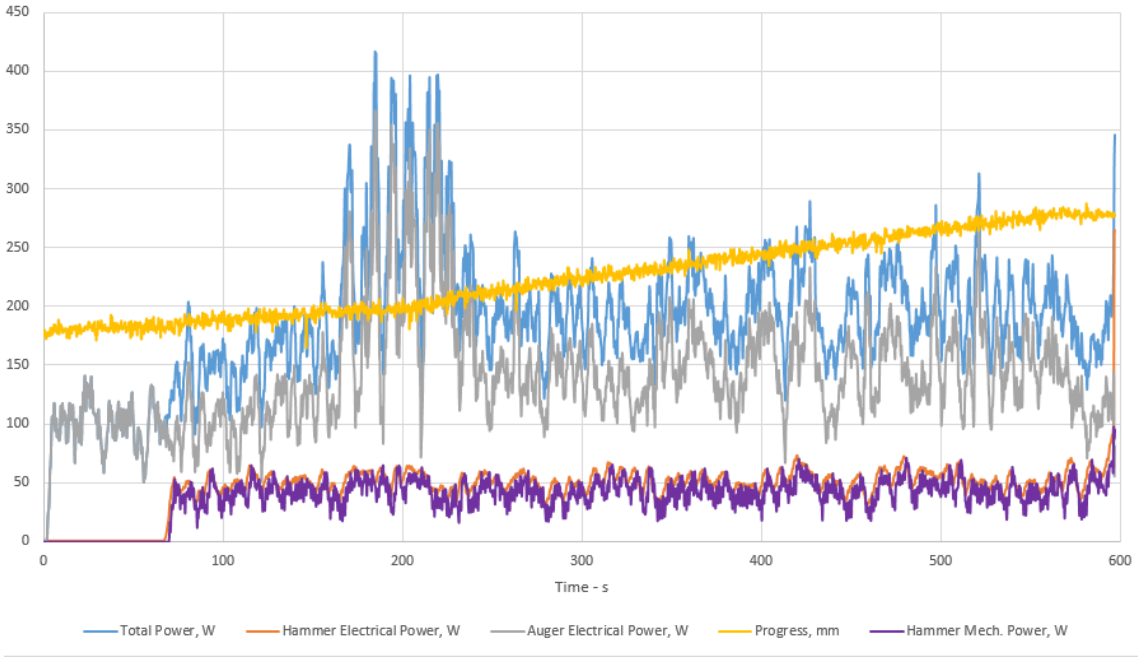


**Test: Locharbriggs sandstone experimental run using small drill bit, 4-drop cam and 1500 RPM hammer velocity. 12/8 WoB.**

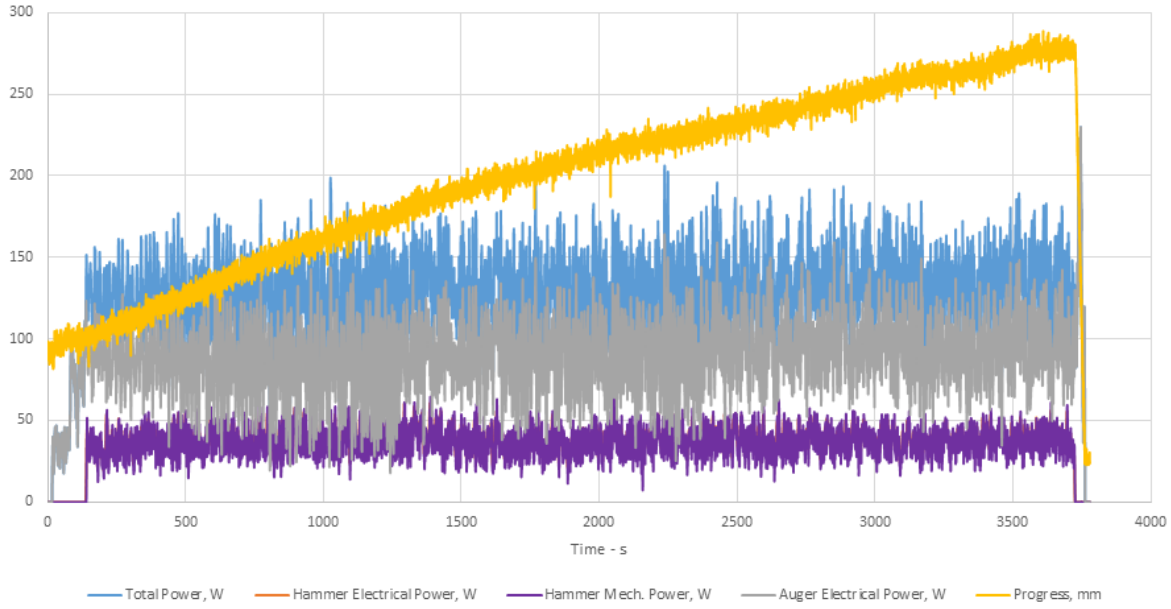

**Test: Locharbriggs sandstone experimental run using small drill bit, 4-drop cam and 2500 RPM hammer velocity. 12/8 WoB.**

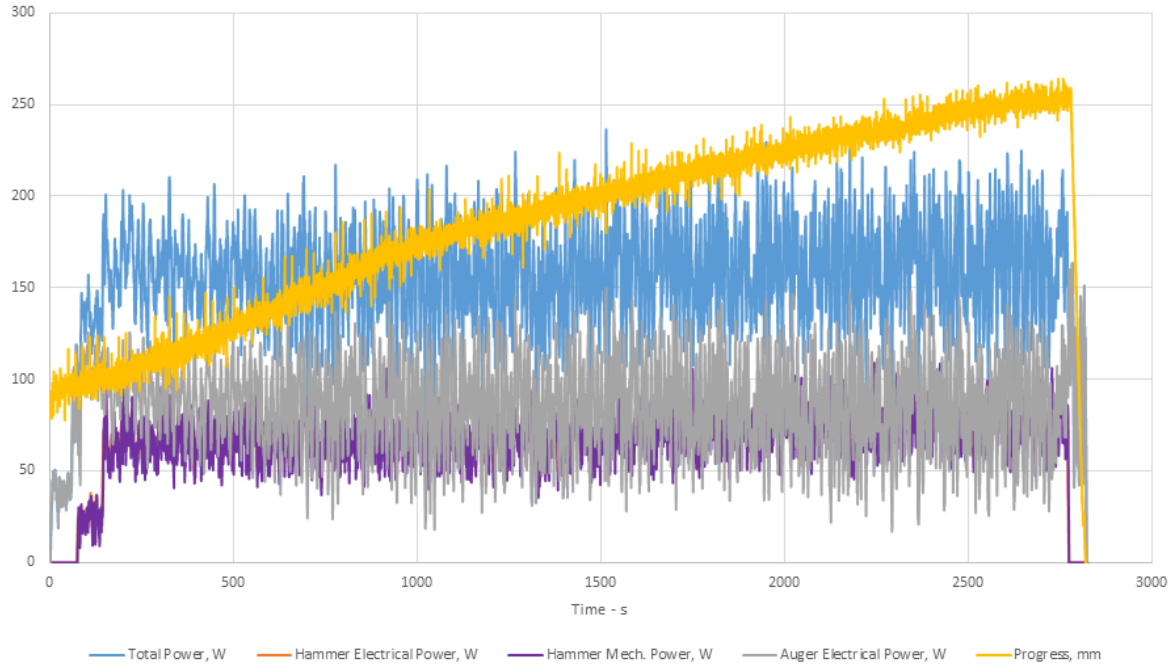


**Test: Locharbriggs sandstone experimental run using medium drill bit, 4-drop cam and 1500 RPM hammer velocity. 12/8 WoB.**

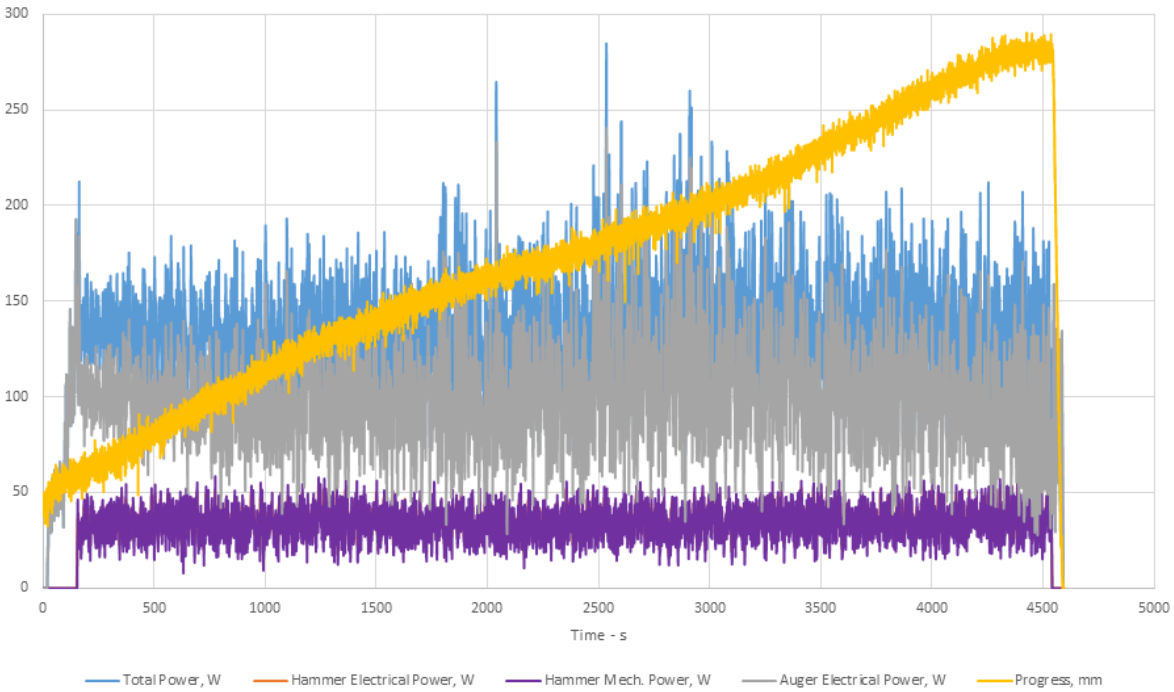

# Chapter 8

# Bibliography


[1] U.S. Geological Survey, “Circum-Arctic Resource Appraisal: Estimates of Undiscovered Oil and Gas North of the Arctic Circle,” USGS, 2008.

[2] G. J. Moridis, T. S. Collett, M. Pooladi-Darvish, S. Hancock and C. Santamarina et al, “Challenges, Uncertainties and Issues Faceing Gas Production from Gas Hydrate Deposits,” Lawrence Berkeley National Laboratory , 2011.

[3] M. Watt, R. Rafati and H. Hamidi, “The Applicatoin of Robotic Drilling Systems in Extreme Environments,” in *IADC/SPE Asia Pacific Drilling Technology Conference*, Singapore, 2016.

[4] R. Beckwith, “Drilling in Extreme Environments: Space Drilling and the Oil and Gas Industry,” *Journal of Petroleum Technology,* vol. 65, no. 09, 2013.

[5] G. Heiken, D. Vaniman and B. French, Lunar Sourcebook: A User's Guide to the Moon, Cambridge University Press, 1991.

[6] S. P. Gorevan, T. Myrick, K. Davis, J. J. Chau and P. Bartlett et al, “Rock Abrasion Tool: Mars Exploration Rover Mission,” *Journal of Geophysical Research,* vol. 108, 2003.

[7] M. T. Mellon, W. V. Boynton, W. C. Feldman, R. E. Ardvison and T. N. Titus et al, “A Prelanding Assessment of the Ice Table Depth and Ground Ice Characteristics in Martian Permafrost at the Phoenix Landing Site,” *Journal of Geophysical Research,* vol. 114, no. 3, pp. 1-14, 2009.

[8] P. Chu, J. Wilson, K. Davis, L. Shiraishi and K. Burke, “Icy Soil Acquisition Device for the 2007 Phoenix Mars Lander,” in *39th Aerospace Mechanisms Symposium* , NASA Marchall Space Flight Center, 2008.

[9] G. H. Peters, J. A. Smith, G. S. Mungas, G. H. Bearman and L. Shiraishi et al, “RASP-based Sample Acquisition of Analogue Martian Permafrost Samples: Implications for NASA's Phoenix Scout Mission,” *Planetary and Space Science,* vol. 56, no. 3, pp. 303-309, 2008.

[10] R. E. Ardvison, R. G. Bonitz, M. L. Robinson, J. L. Carsten and R. A. Volpe et al, “Results from the Mars Phoenix Lander Robotic Arm Experiment,” *Journal of Geophysical Research*, vol. 114, no. 10, pp. 1-21, 2009.

[11] A. B. Okon, “Mars Science Laboratory Drill,” in *40th Aerospace Mechanisms Symposium* , NASA Kennedy Space Center, 2010.

[12] A. E. Finzi, F. B. Zazzera, C. Dainese, F. Malnati and P. G. Magnani et al, “SD2 - How to Sample a Comet,” *Space Science Reviews*, vol. 128, no. 1, pp. 281-299, 2006.

[13] P. Magnani, P. Bologna, A. E. Finzi, F. B. Zazzera and A. Nista et al, “Rosetta Philae SD2 Drill System and its Operation on 67P/Churyumov-Gerasimenko,” in *ASTRA 2015*, Leiden, The Netherlands., 2015.

[14] R. Lichtenheldt, B Schafer and O. Kromer, “Hammering Beneath the Surface of Mars: Modelling and Simulation of the Impact-driven Locomotion of the HP3 Mole by Coupling enhanced Multi-body Dynamics,” in *58th Ilmenau Scientific Colloqium 2014*, 2014.

[15] J. Vago, O. Witasse, H. Svedhem, P. Baglioni and A. Haldemann et al, “ESA ExoMars Program: The Next Step in Exploring Mars,” *Solar System Research*, vol. 49, no. 7, pp. 518-528, 2015.

[16] Selex ES, “ExoMars Drill System Corporate Brochure”.

[17] L. Chu, K. M. Brown and K. Kriechbaum, “Mars 2020 Sampling and Caching Subsystem Environmental Development Testing and Preliminary Results,” in *IEE Aerospace Conference*, 2017.

[18] J. Mustard, “Report of the Mars 2020 Science Definition Team,” 2013.

[19] K. A. Farley and K. H. Williford, “Scientific Rationale for Depot Caching on Mars 2020,” NASA JPL, 2017.

[20] R. Trautner, S. J. Barber, J. Carpenter, R. Fisackerly and B. Houdou et al, “PROSPECT: A Novel Package for Subsurface Sample Acquisition and Analysis of Lunar Volatiles,” in *69th International Astronomical Congress (IAC)* , Bremen, Germany , 2018.

[21] B. W. Johansen, P. Lee, W. Lekens, H. Sorensen and O. Wetteland et al, “A New Plasma Drilling Technology with Applications for Moon, Asteroid and Mars Exploration and ISRU,” in *45th Lunar and Planetary Science Conference*, 2014.

[22] C. Hoftun, B. W. Johansen, K. Naesje, P. S. Adl and D. Paulsen et al, “Plasma Drill for Mars Exploration,” in *ASCE Earth and Space 2016*, Orlando, FL, USA., 2016.

[23] S. Maurice, R. Wiens, M. Saccoccio and D. Vaniman et al, “The ChemCam Instrument Suite on the Mars Science Laboratory (MSL) Rover: Science Objectives and Mast Unit Description,” *Space Science Review*, vol. 170, 2012.

[24] J. Wang, P. Cao, C. Liu and P. G. Talalay, “Comparison and Analysis of Subglacial Bedrock Core Drilling Technology in Polar Regions,” *Polar Science*, vol. 9, pp. 208-220, 2015.

[25] K. Zacny, Y. Bar-Cohen, M. Brennan, G. Briggs and G. Cooper et al, “Drilling Systems for Extraterrestrial Subsurface Exploration,” *Asrobiology*, vol. 8, no. 3, pp. 665-706, 2008.

[26] W. C. Feldman, S. Maurice, D. J. Lawrence, R. C. Litle and S. L. Lawson et al, “Evidence for Water Ice near the Lunar Poles,” *Journal of Geophysical Research*, vol. 106, pp. 22231-23252, 2001.

[27] W. C. Feldman, T. H. Prettyman, S. Maurice, J. J. Plaut and D. L. Bish et al, “Global Distribution of Near-Surface Hydrogen on Mars,” *Journal of Geophysical Research*, vol. 109, no. 9, 2004.

[28] T. Szwarc, Thermal Modelling of Coring and Drilling Operations for Solar System Exploration Applications - Thesis, 2013.

[29] J. Conrad Jaeger, N. GW Cook and R. Zimmerman, Fundamentals of Rock Mechanics, Wiley-Blackwell, 2008.

[30] K. Zacny, G. Paulsen, C. P. McKay, B. Glass and A. Dave et al, “Reaching 1 m Deep on Mars: The Icebreaker Drill,” *Astrobiology*, vol. 12, no. 12, pp. 1166-1198, 2013.

[31] Y. Malamed, A. Kiselev, M. Gelfgat, D. Dreesen and J. Blacic, “Hydraulic Hammer Drilling Technology: Developments and Capabilities,” *Journal of Energy Resources Technology*, vol. 122, no. 1, pp. 1-8, 2000.

[32] K. Zacny and G. A. Cooper, “Methods for Cuttings Removal from Holes Drilled on Mars,” *The International Journal of Mars Science and Exploration*, vol. 3, pp. 42-56, 2007.

[33] K. Zacny and G. A. Cooper, “Friction of Drill Bits under Martian Pressure,” *Journal of Geophysical Research: Planets*, vol. 112, no. 3, pp. 1-9, 2007.

[34] K. Zacny, M. C. Quayle and G. A. Cooper, “Enhancing Cuttings Removal with Gas Blasts While Drilling on Mars,” *Journal of Geophysical Research - Planets,* vol. 110, pp. 1-16, 2005.

[35] Y. Bar-Cohen, S. Sherrit, B. P. Dolgin, X. Bao, Z. Chang et al, “Ultrasonic/Sonic Drilling/Coring (USDC) for Planetary Applications,” in *8th Annual International Symposium on Smart Structures and Materials*, Newport, CA, USA., 2001.

[36] M. Badescu, S. Stroescu, S. Sherrit, J. Aldrich and X. Bao et al, “Rotary-Hammer Ultrasonic-Sonic Drill System,” in *IEEE International Conference on Robotics and Automation*, Pasadena, CA, USA., 2008.

[37] D. Firstbrook, “Ultrasonically Assisted Penetration Through Granual Materials for Planetary Exploration,” University of Glasgow, Glasgow, Scotland, UK., 2017.

[38] X. Li, P. Harkness, K. Worrall, R. Timoney and M. Lucas, “A Parametric Study for the Design of an Optimized Ultrasonic Percussive Planetary Drill Tool,” *IEEE Transactions on Ultrasonics, Ferroelectrics and Frequency Control,* vol. 64, no. 3, pp. 577-589, 2017.

[39] P. Harkness, M. McRobb, Y. W. Loh, M. Hyde and M. Lucas, “A Rock-Coring Campaign in an Analogue Environment,” in *AIAA Space 2015*, San Diego, CA, USA., 2014.

[40] R. Timoney, P. Harkness, K. Worrall, X. Li, A. Bolhovitins and M. Lucas, “The Development of the European Ultrasonic Planetary Core Drill (UPCD),” in *AIAA Space 2015*, Pasadena, CA, USA., 2015.

[41] X. Li, M. Lucas and P. Harkness, “Full and half-wavelength Ultrasonic Percussive Drills,” *IEEE Transactions on Ultrasonics, Ferroelectrics and Frequency Control,* vol. 65, no. 11, pp. 2150-2159, 2018.

[42] P. Magnani, E. Re, S. Senese, F. Rizzi, A. Gily and P. Baglioni, “The Drill and Sampling System for the ExoMars Rover,” in *i-SAIRAS*, Sapporo, Japan, 2010.

[43] R. Timoney, X. Li, K. Worrall, P. Harkness and M. Lucas, “Push and Twist Drillstring Assemblies,” in *ASCE Earth and Space 2016*, Orlando, FL, USA., 2016.

[44] M. Badescu, S. Kassab, S. Sherrit, J. Aldrich, X. Bao and Y. Bar-Cohen et al, “Ultrasonic/Sonic Driller/Corer as a Hammer-Rotary Drill,” in *SPIE 6529*, 2007.

[45] X. Li, K. Worrall, P. Harkness, R. Timoney, A. Bolhovitins and M. Lucas, “A Motion Control System Design for an Ultrasonic Percussive Coring/Drilling (UPCD) unit,” in *AIAA Space 2015*, Pasadena, CA, USA., 2015.

[46] L. Preston, M. Grady and S. Barber, “Concepts for Activities in the Field for Exploration - TN2: The Catalogue of Planetary Analogues,” The Open University, Milton Keynes, UK. , 2012.

[47] K. Zacny, D. Glaser, P. Bartlett, K. Davis and S. Gorevan, “Drilling Results in Ice-Bound Simulated Lunar Regolith,” in *AIP Conference Proceedings 880*, 2007.

[48] M. Savoia, P. Magnani, D. Hazan, M. Molina and A. Fumagalli et al, “Lunar Icy Soil Sampling,” in *66th International Astronautical Congress* , Jerusalem, Israel, 2015.

[49] R. Timoney, K. Worrall and P. Harkness, “Preliminary Testing of the European Ultrasonic Planetary Core Drill (UPCD) in Simulated Permafrost Terrain,” in *13th International Planetary Probe Workshop*, Laurel, MY, USA., 2016.

[50] B Myers, “Adhesion of Freezing Particulates to Aircraft Surfaces,” Transp. Dev. Cent. Transport Canada, Quebec, Montreal, Canada., 1996.

[51] K. Zacny and G. A. Cooper, “Investigation of the Performance of a Coring Bit in Frozen Mud under Martian Conditions of Low Temperture and Pressure,” *Journal of Geophysical Research: Planets*, vol. 110, no. 4, 2005.

[52] M. H. Hecht, S. P. Kounaves, R. C. Quinn, S. J. West and S. M. M. Young et al, “Detection of Perchlorate and the Solube Chemistry of Martian Soil at the Phoenix Lander Site,” *Science*, vol. 325, pp. 64-67, 2009.

[53] G. D. Clow and B. Koci, “A Fast Mechanical-Access Drill for Polar Glaciology, Paleoclimatatology, Geology, Tectonics and Biology,” *Mem. Natl. Polar Res. Spec. Issue*, vol. 56, pp. 1-30, 2002.

[54] M. J. Flowerdew S. Tyrrell, T. R. Riley and M. J. Whitehouse et al, “Distringuishing East and West Antarctic Sediment Sources using the Pb Isotope Composition of detrital K-feldspar,” *Chemical Geology*, Vols. 292-293, pp. 88-102, 2012.

[55] P. Spector, J. Stone, D. Pollard, T. Hillebrand, C. Lewis and J. Gombiner, “West Antarctic Sites for Subglacial Drilling to Test for Past Ice-sheet Collapse,” *The Cryosphere*, vol. 12, pp. 2741-2757, 2018.

[56] D. E. Sugden, M. J. Bentley and C. O. Cofaigh, “Geological and Geomorphological Insights into Antarctic Ice Sheet Evolution,” *Phil. Trans. R. Soc. A.*, vol. 364, pp. 1607-1625, 2012.

[57] A. Dutto, A. E. Carlson, A. J. Long and G. A. Milne et al, “Sea-level Rise Due to Polar Ice-sheet Mass Loss During Past Warm Periods,” *Science*, vol. 349, p. 153, 2015.

[58] A. Church, “Sea Level Change in Climate Change 2013: The Physical Science Basis,” Firth Assessment Report of the Intergovernmental Panel on Climate Change - Cambridge University Press, Cambridge, UK and New York, NY, USA, 2013.

[59] I. W. Paper, “Ice Core Drilling Technical Challenges”.

[60] M. Orosei, S. E. Lauro, E. Pettinelli , A. Cicchetti and M. Coradini et al, “Radar Evidence of Subglacial Liquid Water on Mars,” Science, 2018.

[61] J. Triest, R. Mulvaney and O. Alemany, “Technical Innovations and Optimization for Intermediate Ice-core Drilling Operations,” *Ana. Glacio.*, vol. 55, no. 68, pp. 243-252, 2014.

[62] P. G. Talalay, “Subglacial Till and Bedrock Drilling,” *Cold Regions Science and Technology*, vol. 86, pp. 142-166, 2013.

[63] National Research Council, “Future Scientific Opportunities in Antarctica and the Southern Ocean,” National Academies Press, Washington DC, USA., 2011.

[64] R. Mulvaney, O. Alemany and P. Possneti, “The Berkner Island (Antarctica) Ice-core Drilling Project,” *Ana. Glacio.*, vol. 55, no. 68, 2014.

[65] R. Mulvaney, K. Triest and O. Alemany , “The James Ross Island and the Fletcher Promontory Ice-core Drilling Projects,” *Ana. Glacio. ,* vol. 55, no. 68, 2014.

[66] P. Fretwell, H. D. Pritchard, D. G. Vaughan, J. L. Bamber and N. E. Barrand et al, “Bedmap2: Improved Ice Bed, Surface and Thickness Datasets for Antarctica,” *The Cryosphere*, vol. 7, pp. 375-393, 2013.

[67] J. W. Goodge and J. P. Severinghaus, “Rapid Access Ice Drill: A New Tool for Exploration of the Deep Antarctic Ice Sheets and Subglacial Geology,” *Journal of Glaciology*, pp. 1-6, 2016.

[68] IDDO, “Agile Sub-Ice Geological Drill System Design Review,” IDDO, 2015.

[69] R. Mulvaney, S. Bremner, A. Tait and N. Audley, “A Medium-depth Ice Core Drill,” in *Fifth International Workshop on Ice Drilling Technologies,* Tokyo, Japan, 2002.

[70] J. Rix, R. Mulvaney, J. Hong and D. Ashurst, “Development of the British Antarctic Survey Rapid Access Isotope Drill,” *Journal of Glaciology,* no. In Press, 2019.

[71] P. Cao, C. Yang and Z. Zheng et al, “Low-load Diamond Drill Bits for Subglacial Bedrock Sampling,” *Ana. Glacio.,* vol. 55, no. 68, pp. 124-130, 2014.

[72] J. Wang, P. Cao, C. Lio and P. G. Talalay, “Comparison and Analysis of Subglacial Bedrock Core Drilling Technology in Polar Regions,” *Polar Science ,* vol. 9, pp. 208-220, 2015.

[73] P. G. Talalay, “Subglacial Till and Bedrock Drilling,” *Cold Regions Science and Technology,* vol. 86, pp. 142-166, 2013.

[74] P. Chu, J. Spring and K. Zacny, “ROPEC - ROtary PErcussive Coring Drill for Mars Sample Return,” in *42nd Aerospace Mechanisms Symposium*, NASA Goddard Space Flight Center, Washington DC. USA., 2014.

[75] Q. Quan , “Development of a Rotary-percussive Drilling Mechanism (RPDM),” in *IEEE International Conference on Robotics and Biomimetics ,* Guangzhou, China, 2012.

[76] G. Han and M. Dusseault, “Dynamically Modelling Rock Failure in Percussion Drilling,” in *40th Symposium on Rock Mechanics,* Alaska Rock, AL, USA., 2005.

[77] A. Okon, “Mars Science Laboratory Drill,” in *40th Aerospace Mechanisms Symposium*, Kennedy Space Center, FL, USA., 2010.

[78] K. Worrall, R. Timoney, P. Harkness, X. Li and M. Lucas, “UPCD: Field Trial Results and Further Work,” in *ASCE Earth and Space 2018,* Cleveland, OH, USA., 2018.

[79] R. L. Norton, Cam Design and Manufacturing Handbook, New York, NY, USA: Industrial Press, 2009.

[80] R. Timoney, K. Worrall, D. Firstbrook, P. Harkness and J. Rix et al, “The Development of a Low Resource Subglacial Bedrock Sampler Inspired by Planetary Drilling Technologies: The Percussive Rapid Access Isotope Drill (P-RAID),” *Astrobiology,* 2019.

[81] A. P. Zent, M. H. Hecht, D. R. Cobos, S. E. Wood and T. L. Hudson et al, "Initial Results from the Thermal and Electrical Conductivity Probe (TECP) on Phoenix," *Journal of Geophysical Research: Planets,* vol. 115, pp. 1-23, 2010.

[82] M. H. Hecht, S. P. Kounaves, R. C. Quinn, S. J. West and S. M. M. Young et al, "Detection of Perchlorate and the Soluble Chemistry of Martian Soil at the Phoenix Lander Site," *Science,* vol. 325, pp. 64-67, 2009.

[83] V. F. Chevrier, J. Hanley and T. S. Altheide, "Stability of Perchlorate Hydrates and their Liquid Solutions at the Phoenix Landing Site, Mars," *Geophysical Research Letters,* vol. 36, no. 10, pp. 1-6, 2009.

[84] S. Cull, R. E. Ardvison, J. G. Catalano, D. W. Ming and R. V. Morris, "Concentrated Perchlorate at the Mars Phoenix Landing Site: Evidence for Thin Film Liquid Water on Mars," *Geophysical Research Letters,* vol. 37, no. 22, 2010.

[85] M. Savoia, A. Rusconi, A. Fumagalli, C. Panza and R. Fisackerly et al, "PROSPECT: Sampling Tool Approaches for Lunar Icy Regolith," in *68th International Astronautical Congress,* Adelaide, Australia., 2017.

[86] R. Phillips, M. Palladino and C. Courtois, "Development of Brushed and Brushless DC Motors for Use in the ExoMars Drlling and Sampling Mechanism," in *41st Aerospace Mechanisms Symposium,* NASA Jet Propulsion Laboratory, Pasadena, CA, USA, 2012.

[87] P. Magnani, E. Re, S. Senese, G. Cherubini and A. Olivieri, "Different Drill Tool Concepts," *Acta Astronautica,* vol. 59, no. 8-11, pp. 1014-1019, 2006.

[88] K. Zacny, M. Quayle and G. Cooper, "Enhancing cuttings removal with gas blasts while drilling on Mars," *Journal of Geophysical Research,* vol. 3, no. 110, pp. 42-56, 2005.